

Maryanna E. Lanning

20 North Pine Street, PHN706
Baltimore, MD 21201

(410)-706-4718 (Work)
mlanning@umaryland.edu
melanning@gmail.com

EDUCATION

University of Maryland Baltimore
School of Pharmacy
Department of Pharmaceutical Sciences
Baltimore, MD

PhD Pharmaceutical Sciences
Focus: Medicinal and Organic Chemistry
August 2012 – June 2017
GPA – 3.81

University of North Carolina, Greensboro.
Greensboro, NC

Major in Chemistry, Minor in Biochemistry
Undergraduate Research Assistant
Chemistry Club

Bachelors of Science
August 2005 – May 2009
GPA - 3.01
2007-2009
2006-2009

RESEARCH EXPERIENCE

GRADUATE RESEARCH ASSISTANT

University of Maryland, Baltimore, MD

August 2012 – June 2017

- The design, synthesis and biological evaluation of amphipathic/two-faced synthetic α -helix mimetics as disruptors of helix-mediated protein-protein interactions involved in disease, specifically cancer. Synthetic agents will be developed to mimic the helical BH3 domain of pro-apoptotic proteins and inhibit Mcl-1 and Bcl-x_L (cancer). To test for Polypharmacological properties, molecules will be tested against p53-HDM2.
- Characterize compounds by NMR, Column Chromatography, and HPLC.
- Biological testing using Fluorescence Polarization Competition Assay (FPCA) and Anisotropy.

LERNER RESEARCH INSTITUTE-LAB TECHNICIAN

Cleveland Clinic Foundation, Cleveland, OH

August 2009 – August 2012

- Alloreactive T Cell Immunity in Human Transplant Candidates Study- Studied the frequency of IFN- γ production in leukocytes as an independent contributor to human allograft injury.
- Clinical Trials in Organ Transplantation- A noninvasive multi-center study focused on long and short-term effects of graft injury in immunosuppressed kidney and heart recipients.
- Performed ELISAs on urine supernatant to measure chemokine and cytokine production
- Executed flow cytometry for a phenotypic analysis of patient samples and analyze data for Th1, Th17 cell subsets
- Performed ELISPOTS on given patient samples looking at IFN- γ production in response to stimulators
- Extracted RNA from urine pellets and whole blood; reverse transcribe into cDNA for real time-PCR analysis

- Isolated peripheral blood mononuclear cells, urine supernatant and sediment for future experiments

INTERN/LEVEL 1 SCIENTIST

Targacept, INC, Winston – Salem, NC

June 2007 – November 2007

- Created a library of compounds from a lead compound for future research and testing
- Worked on small and large scales of compound synthesis
- Reinforced and expanded knowledge of organic chemistry and biochemistry
- LCMS, Column Chromatography, TLC to determine compound purity

RESEARCH ASSISTANT

University of North Carolina, Greensboro

January 2007 - May 2009

- Synthesized aldimines to test as a substrate for aldehyde oxidase.
- NMR technician for lab.
- Skilled in characterizing compounds using, UV-Vis, IR, NMR, Chromatography
- Prepared all solutions and enzymes needed for experiments and research.
- Set up and ran experiments for multiple results to validate and verify process.
- Read and analyzed data to verify and validate results.
- Characterized compounds

PUBLICATIONS

1. Yap, J.L., Chen, L., **Lanning, M.E.**, and Fletcher, S. “Expanding the Cancer Arsenal with Targeted Therapies: Disarmament of the Anti-Apoptotic Bcl-2 Proteins by Small-Molecules” *J. Med. Chem.* **2017**, *60*(3), 821-838.
2. **Lanning, M.E.**, Yu, W., Yap, J.L., Chauhan, J., Chen, L., Whiting, E., Pidugu, L.S., Atkinson, T., Bailey, H., Roth, B.M., Toth, E.A., MacKerell, Jr., A.D., Wilder, P.T., and Fletcher, S. “Structure-Based Design of *N*-Substituted 1-Hydroxy-4-Sulfamoyl-2-Naphthoates as Potent Inhibitors of the Mcl-1 Oncoprotein” *Eur. J. Med. Chem.* **2016**, *113*, 273–292.
3. Drennen, B., Scheenstra J.A., Yap, J.L., Chen L., **Lanning, M.E.**, Wilder, P.T., Fletcher, S. “Structural Re-Engineering of the α -Helix Mimetic JY-1-106 into Small Molecules: Disruption of the Mcl-1 – Bak-BH3 Protein-Protein Interaction with 2,6-Disubstituted Nicotinates.” *ChemMedChem* **2015**, *11*(8), 827–833.
4. **Lanning, M.E.**, and Fletcher, S. “Multi-Facial, Non-Peptidic α -Helix Mimetics” *Biology* **2015**, *4*(3), 540–555.
5. Chen, L., Yap, J.L., Yoshioka, M., **Lanning, M.E.**, Fountain, R.N. Scheenstra, J.A. Raje, M., Stovel, J.W. and Fletcher, S. “BRD4 Structure–Activity Relationships of Dual PLK1 Kinase–BRD4 Bromodomain Inhibitor BI-2536” *ACS Med. Chem. Lett.* **2015**, *6*(7), 764–769.

6. **Lanning, M.E.**, Wilder, P.T., Bailey, H., Chen, L., and Fletcher, S. "Towards More Drug-Like Proteomimetics: Two-Faced, Synthetic α -Helix Mimetics Based on a Purine Scaffold" *Org. Biomol. Chem.* **2015**, *13*, 8642–8646.
7. Jung, K.Y., Wang, H., Teriete, P., Yap, J. L., Chen, L., **Lanning, M.E.**, Hu, A., Lambert, L., Cosford, N., Prochownik, E., and Fletcher, S. "Perturbation of the c-Myc–Max Protein–Protein Interaction via Synthetic α -Helix Mimetics" *J. Med. Chem.* **2015**, *58*(7), 3002–3024.
8. **Lanning, M.E.**, Whiting, E., Scheenstra, J.A., and Fletcher S. "Chromatography-Free Entry to Substituted Salicylonitriles: Mitsunobu-Triggered Domino Reaction of Salicylaldoximes" *J. Org. Chem.* **2015**, *80*(2), 1229–1234. (co-first author).
9. Chen, L., **Lanning, M.E.**, and Fletcher, S. "Small Molecule Inhibitors of the Mcl-1 Oncoprotein" *Austin J. Anal. Pharm. Chem.* **2014**, *1*(3), 1015-
10. **Lanning, M.E.**, and Fletcher, S. "Recent Advances in the Design of Small Molecule, Non-Peptidic, α -Helix Mimetics for the Modulation of Protein–Protein Interactions." *Future Med. Chem.* **2013**, *5*(18), 2157-2174.
11. **Lanning, M. E.**, and Fletcher, S. "Azodicarbonyl dimorpholide (ADDM): An efficient, versatile and water-soluble Mitsunobu reagent." *Tetrahedron Lett.* **2013**, *54* (11), 4624-4628.
12. Jung, K.-Y., Samadani, R., Chauhan, J., Nevels, K., Yap, J. L., Zhang, J., Worlikar, S., **Lanning, M. E.**, Chen, L., Ensey, M., Shukla, S., Salmo, R., Heinzl, G., Gordon, C., Dukes, T., MacKerell, Jr., A. D., Shapiro, P. and Fletcher, S. "Structural Modifications of (Z)-3-(2-aminoethyl)-5-(4-ethoxybenzylidene)thiazolidine-2,4-dione that Improve Selectivity for the Inhibition of Melanoma Cells Containing Active ERK Signaling." *Org. Biomol. Chem.* **2013**, *11*, 3706–3732.
13. Jung, K.-Y., Vanommeslaeghe, K., **Lanning, M. E.**, Yap, J. L., Gordon, C., MacKerell, Jr., A. D. and Fletcher, S. "Amphipathic α -Helix Mimetics Based on a 1,2-Diphenylacetylene Scaffold." *Org. Lett.* **2013**, *15*(13), 3234-3237.
14. Cherkassky, L., M.D., **Lanning, M.**, Lalli, P. N., Czerr, J., Siegel, H., Danziger-Isakov, L., Srinivas, T., Valujskikh, A., Shoskes, D. A., Baldwin, W., Fairchild, R. L., Poggio, E. D., "Evaluation of alloreactivity in kidney transplant recipients treated with anti-thymocyte globulin versus IL-2 receptor blocker" *Am. J. of Transplantation*, **2011**, *11*(7), 1388-1396.

CONFERENCE PRESENTATIONS

- **Lanning, M.E.**, Pritts, J. D., MacKerell Jr., A. D., and Fletcher, S. “Substituted acylsulfonamides as surrogates of a terminal carboxylic acid: More effective small-molecule blockade of the Mcl-1 oncoprotein.” Presented at the 253rd ACS National Meeting, San Francisco, CA April 2-6, 2017.
- **Lanning, M.E.**, Moore, K., and Fletcher, S. “Synthetic α -helix mimetics based on a 2,6,9-Tri-Substituted Purine Disrupts the Mcl-1–BH3 Protein-Protein Interaction” Presented at the Frontiers at the Chemical Biology Interface Symposium, Baltimore, MD May 14, 2016.
- **Lanning, M.E.**, and Fletcher, S. “Second-Generation Synthetic α -Helix mimetics based on a 2,6,9-Tri-Substituted Purine Disrupts the Mcl-1–BH3 Protein-Protein Interaction” Presented at the 250th ACS National Meeting, Boston, MA August 16-20, 2015.
- **Lanning, M.E.**, Chen, L., MacKerell, Jr., A. D., Wilder, P.T., and Fletcher, S. “Structure-Based Design of Inhibitors of the Mcl-1 Oncoprotein” Abstract for poster presentation. 2015 AACP Annual Meeting in National Harbor, MD July 11-15, 2015.
- **Lanning, M.E.**, Chen, L., MacKerell, Jr., A. D., Wilder, P.T., and Fletcher, S. “Structure-Based Design of Inhibitors of the Mcl-1 Oncoprotein” Presented at the 2015 AACP Annual Meeting in National Harbor, MD July 11-15, 2015.
- **Lanning, M.E.**, Wilder, P.T., and Fletcher, S. “Two-faced, biphenyl-based synthetic α -helix mimetics are effective inhibitors of the Mcl-1 oncoprotein.” Presented at the 249th ACS National Meeting, Denver, CO March 22-26, 2015. Poster
- **Lanning, M.E.**, Bailey, H., Wilder, P.T., and Fletcher, S. “2,6,9-Tri-Substituted Purines as Amphipathic α -Helix Mimetics to Inhibit the Anti-Apoptotic Bcl-2 Proteins.” Presented at the 247th ACS National Meeting, Dallas, TX March 16-20, 2014. Poster
- **Lanning, M.E.**, and Fletcher, S. “Azodicarbonyl dimorpholide (ADDM): An efficient, versatile and water-soluble Mitsunobu reagent.” Presented at the 246th ACS National Meeting, Indianapolis, IN September 8–12, 2013. Poster
- **Lanning, M.**, Czerr J., Lalli, P.N., Siegel, H., Hricik, D.E., Fairchild R.L., Poggio E.D., and Augustine, J.J. “Terminally Differentiated Effector T Cells Correlate with Longer Dialysis Vintage and Alloimmune Reactivity in Patients Awaiting Kidney Transplantation.” Presented at the American Transplant Congress 2011, Philadelphia, Pa, May 1-4, 2011. Poster
- Kombo, D.C., Strachan, J.P., Chewning, J., **Lanning, M.**, Hammond, P.S., Yohannes,

D, Woodward, C, Frey, D.F., Breining, S.F, Miller, C.H., and Gatto, G.J. "Predicting ligand binding affinity to the rat $\alpha 4\beta 2$ neuronal nicotinic receptor: Lessons from bayesian categorization modeling." Presented at the 235th ACS National Meeting, New Orleans, LA, April 6-10, 2008. Poster

AWARDS & FELLOWSHIPS

- Department of Pharmaceutical Sciences Merit Award (\$2000) 2015 – 2016
- American Foundation for Pharmaceutical Education (AFPE) Fellowship (\$10,000/year) 2015 – 2017
- Chemical Biology Interface Training Grant Member (\$2500/year) 2014 – 2016
- ACS Travel Award (\$400/year) Spring 2015
Spring 2014
- Undergraduate Research Assistantship (\$1000/semester) 2008 – 2009

LEADERSHIP & AFFILIATIONS

- Graduate School Steering Committee
Graduate Student Member 2013 – 2014
- Pharmacy Graduate Student Association
President 2012 – 2017
Vice President 2013 – 2014
2012 – 2013
- Rho Chi Member 2014 – 2017
- American Chemical Society Member 2010 – Present
- Chi Omega Sorority 2006 – 2009

Abstract

Dissertation Title: Towards Targeted Antineoplastics: The Disruption of Aberrant Protein–Protein Interactions with Low Molecular-Weight Proteomimetics

Maryanna E. Lanning, Doctor of Philosophy, 2017

Dissertation Directed By: Dr. Steven Fletcher, Associate Professor, Pharmaceutical Sciences

Protein–protein interactions (PPIs) play pivotal roles in a range of cellular processes including proliferation, differentiation, metabolism and apoptosis. Dysregulations of certain PPIs can lead to the development and progression of human cancers. In particular, the overexpression of the anti-apoptotic BCL-2 family members, specifically Mcl-1, have been linked to pancreatic, colorectal and lung cancers as well as leukemia and lymphoma. When over-expressed, MCL-1 prevents cell death by binding and sequestering the BH3 “death” domain of its pro-apoptotic counterpart, such as Bim. Mcl-1 has become an important target for the development of novel antineoplastics. As with many, helix-mediated PPIs, several key residues are hydrophobic and located on one face of the BH3 α -helix, specifically at the i , $i + 3/4$, $i + 7$ residues. In addition to exhibiting a hydrophobic face, Asp67 on the “other” face of the Bim-BH3 helix forms a salt bridge with the protein (Arg263). In an improved effort to develop more potent and more selective agents to disrupt the MCL-1-BH3 PPI, we used structure-based design, and developed two complementary strategies: synthetic α -helix (purine based) and BH3 mimetics (naphthoate based). Both scaffolds yielded molecules that disrupted the MCL-1–BIM PPI consistently, and subsequent studies were undertaken towards second-generation molecules. The designed molecules were subjected to biological assays and further structure–activity

relationship (SAR) studies to increase affinity and potency in an effort to translate *in vitro* activity to on target cell activity. It is anticipated that the SAR developed in the present study will facilitate the development of novel therapeutics capable of inhibiting Mcl-1 will be identified, which can be advanced to preclinical evaluation.

Towards Targeted Anti-Neoplastics: The Disruption of Aberrant Protein–Protein
Interactions with Low Molecular-Weight Proteomimetics

by
Maryanna E. Lanning

Dissertation submitted to the Faculty of the Graduate School of the
University of Maryland, Baltimore in partial fulfillment
of the requirements for the degree of
Doctor of Philosophy
2017

For my parents
Who always told me I could do anything
I set my mind to.

Thank you for always
believing in me.

Acknowledgements

It has been a long and challenging road to reach this point in my graduate career, and not without some difficult times. However, the rewards and accomplishments have definitely outweighed everything; as have the friendships I have made, which will last a life time. It is these experiences that have made me the independent scientist I have become today. All the work presented within has not been a sole accomplishment, but has been a collaborative effort. It has been long discussions of thoughts and ideas with mentors and friends to gain outside perspective and designs, which ultimately helped me pursue this PhD.

First and foremost, I want to thank my advisor, mentor and friend Steven Fletcher. If not for him, I would not be where I am today as a chemist or as a scientist. I honestly could not have hoped for a better mentor to train and learn from when joining this program. I sincerely appreciate all the guidance and support he has given me, from discussions in lab to bouncing ideas off him. If not for his encouragement and backing I would not have been able to attend the conferences, where I gained valuable insight into our field, and to pursue learning new techniques and skills. Thank you for believing in me and not giving up on me when times were rough and I seemed quite impossible. I will forever be grateful for everything you have done for me and consider it an honor and privilege to have worked with and learned from you.

I would also like to thank my committee members Andy Coop, Alex MacKerell, and Angela Wilks for their guidance and insightful discussions over the past several years, as well as Dr. Amy Newman for agreeing to sit on my committee. Their support has been vital to the success of finishing my PhD. There have been many collaborators who have

helped with the research presented herein. Dr. Wenbo Yu has been extremely helpful and essential with the molecular modeling performed for my projects and helped give shape to future work. Dr. Paul Wilder, who performed some of the fluorescence polarization competition assay used to test our molecules and allowed me to shadow and learn the assay, so I could independently run the experiments. I would like to thank the labs of Andy Coop, and Fengtian Xue and their lab members who were helpful during group meetings: Thank you for the advice and ideas you shared. I also want to thank my current lab members Jay, Branden and Ivie, as well as past lab members, Jerry, Lee, Kwan-Young, Ellis, and Danny. I could not have asked for better lab mates and we have had a blast in and out of lab.

I especially would like to thank Lindsay, and Aaron. Aaron has been a constant source of support and level headedness, through the 4 years we have known each other. He has made an enormous impact on my life and I would not have made it through this process without him. Thank you for all of your love and unending encouragement! I cannot wait to see what the world has in store for us and I look forward to many more adventures with you! Lindsay was the very first person I met when I came to interview and we have been friends ever since. She has always been a sounding board and partner in crime when I needed one. We have had many Starb runs and wine nights to get us through the past five years and I know we will be friends for a long time to come and can't thank you enough for everything you have been through with me! I also need to thank Geoff Shimberg, Bennett, who along with Lindsay and Aaron have made graduate school quite the adventure. From our first two weeks in Baltimore through all the ups and downs of the past five years, we have survived. I cannot wait to see what lies ahead.

Last, but not least, I have been tremendously fortunate to have an amazing support

system and unending encouragement from my family. I know I would not be the person I am today nor where I am today without you. Mom, Dad, Jacqueline, and John – Thank you for believing in me and encouraging me to pursue my dreams and shaping me into the person I am today.

Table of Contents

Chapter	Page
List of Tables.....	xii
List of Figures.....	xiv
List of Abbreviations.....	xx
Chapter 1 Protein-Protein Interactions: Approaches for Targeted Disruption of BCL-2 Anti-Apoptotic Family.	1
1.1 Introduction.....	1
1.2 The BCL-2 Family: Apoptotic Regulators in the Mitochondria.....	3
1.3 Structure of the BCL-2 family of proteins.....	9
1.4 Approaches for Targeted Disruption	13
1.4.1 Bis-Benzamides	17
1.4.2 Benzoylureas.....	20
1.4.3 1,2-Diphenylacetylenes.....	20
1.4.4 Anthraquinones and Acridines.....	22
1.4.5 2,6,9-Tri-Substituted Purines	23
1.4.6 Tetrahydro-1H-benzo[e][1,4]diazepines.....	24
1.4.7 Phenyl-Piperazine-Triazine.....	25
1.5 Targeting the BCL-2 Family: BCL-2 and BCL-x _L	27

1.5.1 Abbott Laboratories	28
1.5.2 Genetech	33
1.5.3 Pan-BCL-1 Inhibitors.....	36
1.6 Targeting the BCL-2 Family: MCL-1.....	38
1.6.1 Abbvie.....	38
1.6.2 Vanderbilt University (Fesik's Laboratory).....	42
1.6.3 Servier Research Laboratories	45
1.6.4 University of Michigan (Nikolovska Coleska's Laboratory)	47
1.6.5 Amgen.....	47
1.7 Conclusions.....	48
Chapter 2 Structure-Based Design of N-Substituted 1-Hydroxy-4-Sulfamoyl-2-Naphthoates as Selective Inhibitors of the MCL-1 Oncoprotein.....	50
2.1 Design strategy towards 1-hydroxy-4-sulfamoyl-2-naphthoate	51
2.2 Results and Discussion	55
2.3 Comprehensive SILCS SAR analysis of Mcl-1 binding.....	70
2.4 SILCS quantitatively captures the binding specificity of compounds for Mcl-1 over Bcl-x _L	74
2.5 Cellular activity of Mcl-1 inhibitors.	78
2.6 Conclusions.....	79
2.7 Experimental.....	80

2.7.1 Computational.....	80
2.7.2 Chemistry.....	84
2.7.3 Biology.....	125
Chapter 3 Towards More Drug-Like Proteomimetics: Two-Faced Synthetic α-Helix Mimetics Based on a Purine Scaffold.....	129
3.1 Design and Strategy Towards the Purine Scaffold.....	129
3.2 Results and Discussion.....	135
3.3 Conclusions.....	141
3.4 Experimental.....	141
3.4.1 Chemistry.....	141
3.4.2 Biology.....	154
Chapter 4 Azodicarbonyl Dimorpholide (ADDM): An Efficient, Versatile and Water-Soluble Mitsunobu Reagent.....	163
4.1 Azodicarbonyl Dimorpholide (ADDM).....	164
4.2 Scope of ADDM: Results and Discussion.....	165
4.3 Conclusions.....	171
4.4 Experimental.....	171
4.4.1 Chemistry.....	171
Chapter 5 Chromatography-Free Entry to Substituted Salicylonitriles: Mitsunobu-Triggered Domino Reactions of Salicylaldoximes.....	174

5.1 Synthetic Strategy	176
5.2 Conclusions.....	183
5.3 Experimental.....	184
5.3.1 Chemistry.....	184
Chapter 6 Ongoing and Future Synthetic α-Helix and BH3 Mimetics	195
6.1 Ongoing and Future Small Molecule BH3 Mimetics	195
6.1.1 Design Strategy for Acyl-sulfonamides based on a Naphthoic Acid Core....	195
6.1.2 Synthesis of Acyl-Sulfonamides.....	198
6.1.3 Future Directions	199
6.2 Ongoing and Future Synthetic α -Helix Mimetics	199
6.2.1 Design of Second-Generation Purines.....	199
6.2.2 Synthesis of Purines.....	202
6.2.3 Results and Discussion	203
6.2.4 Future Directions	207
6.2.5 Design of Pyrrolopyrimidines.....	207
6.2.6 Synthesis of Pyrrolopyrimidines.....	211
6.2.7 Future Directions	212
6.3 Experimental.....	213
6.3.1 Chemistry.....	213

6.3.2 Biology.....	244
Chapter 7 References.....	246

List of Tables

Table 1.1: Protein–protein interaction classifications with key examples and crystal structures.....	2
Table 2.1: Experimental and computational Mcl-1 and Bcl-xL inhibitory profiles of first generation inhibitors. Experimental data determined by a fluorescence polarization competition assay. ^a K _i values determined by Nikolovska-Coleska equation from IC ₅₀ values. ¹⁷⁰ Data represent the average of at least two independent assays; errors are standard deviations. ^b Selectivity is defined as the K _i (Bcl-x _L) divided by the K _i (Mcl-1). NA, no activity.....	59
Table 2.2: Experimental and computational Mcl-1 and Bcl-xL inhibitory profiles of second-generation inhibitors. Experimental data determined by a fluorescence polarization competition assay. ^a K _i values determined by Nikolovska-Coleska equation from IC ₅₀ values. ¹⁷⁰ Data represent the average of at least two independent assays; errors are standard deviations. ^b Selectivity is defined as the K _i (Bcl-x _L) divided by the K _i (Mcl-1). ND, not determined.	65
Table 2.3: Investigation into the significance of the inhibitor’s carboxylic acid and hydroxyl group towards the inhibition of Mcl-1. Experimental data determined by a fluorescence polarization competition assay. ^a K _i values determined by Nikolovska-Coleska equation from IC ₅₀ values. ¹⁷⁰ Data represent the average of at least two independent assays; errors are standard deviations.	68
Table 2.4: Inhibition of cell proliferation by select compounds, as determined by a cell titer blue assay.....	79
Table 3.1: Binding affinities of purine-based, amphipathic α-helix mimetics to MCL-1, BCL-x _L , HDM2 that were prepared for this study	137
Table 4.1: Alcohol substrate scope for Mitsunobu coupling to phenol with ADDM. ^a	165
Table 4.2: Alcohol substrate scope for Mitsunobu coupling to phenol with ADDM. ^a ...	167
Table 4.3: Pro-nucleophile substrate scope for Mitsunobu coupling to benzyl alcohol with ADDM. ^a	169
Table 5.1: Screening of reaction conditions. ^a	177
Table 5.2: Salicylaldehyde substrate scope. ^a	181
Table 5.3: Alternative azodicarbonyl and phosphine species. ^a	183
Table 6.1: Experimental FPCA data for second generation purines based on a 2,6-dichloropurine scaffold. K _i values determined by Nikolovska-Coleska equation from IC ₅₀	

values.¹⁷⁰ Data represent the average of at least two independent assays; errors are standard deviations. NA, no activity. 205

List of Figures

- Figure 1.1:** MCL-1 (grey, red and blue) bound to BH3 pro-apoptotic protein BIM (green). Key binding residues are highlighted on the truncated BIM peptide: Phe69, Ile65, Leu62, Leu58..... 3
- Figure 1.2:** Pro-apoptotic proteins binding the anti-apoptotic family of proteins. (A) BH3-only or initiator pro-apoptotic proteins BIM, PUMA, and tBID bind all the BCL-2 family proteins, while BAD and NOXA only interact with some. (B) Pro-apoptotic effector proteins BAX binds all the anti-apoptotic BCL-2 proteins, while BAK only binds BCL-x_L, MCL-1, and A1. 4
- Figure 1.3:** Intrinsic or Mitochondrial apoptosis pathway regulated by the BCL-2 family. 6
- Figure 1.4:** Extrinsic apoptosis pathway, which can initiate the intrinsic pathway through cleavage of BID..... 8
- Figure 1.5:** The BCL-2 Homology Domains of the BCL-2 family of proteins. 10
- Figure 1.6:** Pro-apoptotic proteins BIM and BAK with labeled key binding residues representing the i , $i + 3/4$, $i + 5$ and $i + 7$ 11
- Figure 1.7:** The anti-apoptotic proteins labeled with conserved Arginine residue. 12
- Figure 1.8:** Peptidomimicry of an α -helix with modified side chains to undergo ring closing metathesis using a ruthenium catalyst. 13
- Figure 1.9:** BIM BH3 scaffold with labeled side chains to mimic. 15
- Figure 1.10:** Generic scaffolds of single and amphipathic α -helix mimetics. 16
- Figure 1.11:** Oligoarylamides as single-faced helix mimetics. 18
- Figure 1.12:** Two-faced bis-benzamide helix mimetics. Dashed lines represent hydrogen bonds. 19
- Figure 1.13:** A two-faced helix mimetic centered on a benzoylurea scaffold. Dashed lines represent a bifurcated hydrogen bond. 20
- Figure 1.14:** An intramolecular hydrogen bond (dashed line) influences the projection of side-chains from opposing faces of a diphenylacetylene scaffold. 21
- Figure 1.15:** Appropriately functionalized anthraquinones (left) and acridines (right) have disrupted the Bim–Mcl-1 PPI through two-faced mimicry of the Bim-BH3 α -helix..... 23

Figure 1.16: 2,6,9-Tri-substitution of a purine scaffold permits the mimicry of two faces of an α -helix, according to the disruption of the Mcl-1–Bak-BH3 PPI.	24
Figure 1.17: In addition to their ability to mimic the epitopes of β -turns and one face of an α -helix, benzodiazepines have been introduced as scaffolds to reproduce functionality displayed from two faces of an α -helix.	25
Figure 1.18: A phenyl-piperazine-triazine helix mimetic disrupts the Bim–Mcl-1 PPI. Synthetic strategies to vary the ethyl group should allow the additional mimicry of the $i + 5$ position on the opposing face.	27
Figure 1.19: (A) ABT-737 a de novo small molecule inhibitor of BCL-2 and BCL-x _L . (B) Crystal Structure of ABT-737 with BCL-x _L . (PDBID 2YXJ).	29
Figure 1.20: (A) ABT-263 (Navitoclax) an orally bioavailable small molecule BH3 mimetic of the BCL-2 pro-apoptotic family to inhibit BCL-2 and BCL-x _L . (B) Crystal Structure of ABT-737 with BCL-x _L . (PDBID 4LVT).	30
Figure 1.21: (A) ABT-199 a BCL-2 selective inhibitor. Recently approved by the FDA for treatment of CLL. (B)	32
Figure 1.22: (A) WEHI-539: A potent BCL-x _L inhibitor found through SAR. (B) Crystal Structure of WEHI-539 bound to BCL-x _L . (PDBID 3ZLR).	34
Figure 1.23: Abbvie and Genetech further developed a selective and potent BCL-x _L inhibitor.	35
Figure 1.24: Structures of gossypol and analogues.	37
Figure 1.25: A pan-BCL-2 inhibitor from GeminX Pharmaceutical.	38
Figure 1.26: Abbvie's MCL-1 selective inhibitor that binds the p2 pocket and interacts with Arg263.	39
Figure 1.27: Crystal structure of 36 bound in the p2 pocket of MCL-1. (PDBID 4OQ5)	40
Figure 1.28: Abbvie's potent and selective MCL-1 inhibitors.	41
Figure 1.29: Fesik and co-workers MCL-1 selective inhibitor with submicromolar inhibition. Individual classes and then merged to final potent inhibitor.	43
Figure 1.30: Fesik's second-generation indole inhibitors extend into the p4 pocket utilizing acylsulfonamides.	44
Figure 1.31: MCL-1 small molecule inhibitors with picomolar activity, cell activity, and low serum binding from the Fesik group.	45

Figure 1.32: Servier Research Institutes MCL-1 selective inhibitor with sub-nanomolar affinity and cell activity..... 46

Figure 1.33: University of Michigan MCL-1 selective inhibitors based on a 1-hydroxy-naphthalene core..... 47

Figure 1.34: Amgen's MCL-1 selective inhibitors entering phase I clinical trials. 48

Figure 2.1: Structure-based design of novel 1-hydroxy-4-sulfamoyl-2-naphthoates as Mcl-1 inhibitors.: Structure-based design of novel 1-hydroxy-4-sulfamoyl-2-naphthoates as Mcl-1 inhibitors. 52

Figure 2.2: (a) ClSO₃H, 0 °C, 1 h; (b) ArNH₂, pyr, acetone, 50 °C, 3 h or R₁NH₂/R₁R₂NH, DIPEA, acetone, RT, 5 h. 53

Figure 2.3: (A) Predicted binding orientation (cyan carbons) of 1 overlaid on its crystal orientation (pink carbons). FragMaps are shown as wire mesh in the following colors and GFE cutoff for generic nonpolar (APOLAR, green, -1.2 kcal/mol), neutral donor (HBDON, blue, -1.0 kcal/mol), neutral acceptor (HBACC, red, -1.0 kcal/mol), and negative acceptor (NEG, orange, -1.3 kcal/mol). (B & C) The crystallographic orientation of the inhibitor 1 (from PDB ID: 4HW3) overlaid (B) on the crystal protein surface of the Mcl-1-BH3 peptide complex structure (PDB ID: 4HW4) used to initiate the SILCS simulations and (C) on the SILCS exclusion map..... 55

Figure 2.4: (A) The binding mode of 3a, as predicted by SILCS. Important residues within the p2 binding pocket are shown in stick representation with the carbon atoms colored in green. (B) Compound 3a and 2 are shown in stick representation with the carbon atoms colored in cyan and pink, respectively. Colors and cutoffs used to show the FragMaps are the same as in Figure 2.3. (C) 2D chemical structure of 3a. 56

Figure 2.5: (a) ArOH, K₂CO₃, 100 °C, 16 h; (b) SnCl₂•2H₂O, EtOAc, 50 °C, 16 h; (c) isobutyraldehyde, benzaldehyde or cyclopentanone, NaBH(OAc)₃, 1,2-dichloroethane, RT, 16 h..... 64

Figure 2.6: (a) ArNH₂, pyr, acetone, 50 °C, 3 h; (b) MeI, K₂CO₃, DMF, rt, 16 h; (c) NaOH, MeOH/THF/H₂O, 3:1:1, rt, 16 h. 67

Figure 2.7: The NMR HSQC spectra shows chemical shift perturbations caused by the direct interaction of compound 3ba with Mcl-1. The spectrum of the control sample (black) is overlaid with the spectrum of Mcl-1 bound to 3ba (red). Inset is enlargement of boxed region. 69

Figure 2.8: Mcl-1 residues (blue) whose chemical shifts are perturbed or lost in the presence of compound 3ba..... 70

Figure 2.9: The orientations of the four compounds binding to Mcl-1 predicted by SILCS. (A) 3b; (B) 3a; (C) 3bi; (D) 3bl. Compounds shown in stick format with atom-based

coloring. The compound, **2**, from the previously reported complex structure 4HW3 is also shown, with the carbon atoms colored in pink. Mcl-1 residue R263 is shown. Same color and GFE cutoff is used as in **Figure 2.3**..... 72

Figure 2.10: Atom GFE contributions for the most LGFE favorable binding conformation of the four compounds. (A) **3b**; (B) **3a**; (C) **3bi**; (D) **3bl**. 74

Figure 2.11: (A) Difference FragMaps (Δ FragMaps) between Mcl-1 and Bcl-xL showing the favorable binding patterns for Mcl-1. Hydrophobic and neutral donor Δ FragMaps are shown in green and blue, respectively. The atom GFE contributions to the binding affinity difference are also shown. (B) Experimental structures of Mcl-1 (blue, 4HW4) and Bcl-xL (red, 1BXL) shows that the binding pocket between helix α 4 (upper right) and α 5 (bottom left) is larger for Mcl-1 than Bcl-xL. The predicted binding modes of **3a** for Mcl-1 (blue) and Bcl-xL (red) differs due to this p2 pocket difference. The 4-bromophenyl ring of **3a** binds deeply to the opened pocket for Mcl-1 while it binds on the protein surface for Bcl-xL. (C) Binding orientations of **3bl** to Mcl-1 (blue, 4HW4) and Bcl-xL (red, 1BXL) along with the Δ FragMaps. (D) Binding orientations of **3bl** to Bcl-xL (1BXL) along with the Bcl-xL APOLAR and NEG FragMaps at the contour levels specified in **Figure 2.3**. 77

Figure 2.12: (a) SOCl₂, MeOH, rt, 48 h; (b) BrCH₂OCOCH₃, K₂CO₃, MeCN, 0 °C, 16 h. 78

Figure 3.1: Substitution of the 2, 6 and 9 positions of the purine scaffold putatively permits mimicry of two faces of an α -helix..... 131

Figure 3.2: (A) Key residues of the Bak-BH3 α -helix. (B) A purine-based α -helix mimetic designed to imitate Leu78, Ile81, Ile85 and Asp83. (C) Superimposition of an MM2 energy-minimized conformation of the molecule in B on the Bak-BH3 α -helix. (D) Simplified Bak-BH3 α -helix mimetic where R¹ and R² are proposed to imitate the i + 3 and i + 7 side chains, respectively, whilst the Asp83 mimetic is fixed as CH₂COOH, and the Leu78 mimetic constrained as tert-butyl..... 134

Figure 3.3: (a) Boc₂O, cat. DMAP, DMSO, 0 °C to RT; (b) NaH, THF, 0 °C to RT; (c) R¹OH, DIAD, PPh₃, THF, RT; (d) R²OH, DIAD, PPh₃, THF, 35 °C; (e) glycine, K₂CO₃, iPrOH, reflux. 136

Figure 3.4: The FITC-BAK⁷¹⁻⁸⁹ was competed off Mcl-1¹⁷²⁻³²⁷ with 5db giving an estimated IC₅₀ of 72.3 ± 21.2 μ M. Data are an average of biological triplicates and errors are standard deviations. mA = milli-anisotropy. An absolute anisotropy of 40 mA indicates complete competition. For further details, please see the Supporting Information. 138

Figure 3.5: GOLD docking of 5db to Mcl-1 (PDB ID: 2PQK). Colored by atom type: grey = carbon, red = oxygen; blue = nitrogen; yellow = sulfur). A. Superimposition of 5db (yellow, colored by atom type) with the Bim-BH3 α -helix (green, key side chains shown in stick format, labeled in green). B. Predicted binding mode of 5db from A with BH3 α -helix removed: Arg263 and p1 – p4 subpockets on Mcl-1 labeled in black. 140

Figure 4.1: Reaction scheme to make ADDM from DEAD and morpholine.	165
Figure 4.2: Yields for the Mitsunobu reaction with (a) ADDM prepared from DEAD and (b) recycled ADDM prepared by re-oxidation of ADDM-H ₂	170
Figure 4.3: A chromatography-free Mitsunobu reaction.	171
Figure 5.1: Existing methods to prepare salicylonitriles.	175
Figure 5.2: Proposed mechanism for the two step, one-pot conversion of salicylaldoximes to their corresponding salicylonitriles.	179
Figure 6.1: SILCS modeling of MCL-1 and compound 3ba (blue). FragMaps (green) indicate areas of general hydrophobicity. Arg263 and Met231 are highlighted (cyan) to orient protein and show key interactions. PDBID: 4HW4.	196
Figure 6.2: (A) Example of scaffolds being taken forward based on K _i from Chapter 2. (B) Example of acyl sulfonamide groups to target p4 pocket. (Right, sulfonamide Nikolovska-Coleska and co-workers utilized. Left, sulfonamide used by Abbvie in the development of ABT-199) ^{65, 94}	197
Figure 6.3: Synthetic scheme to acquire acyl-sulfonamides. (a) ClSO ₃ H, 0 °C, 30 min; (b) R ₁ NH ₂ /R ₁ R ₂ NH, pyridine, Acetone, 50 °C, o.n.; (c) BnBr, K ₂ CO ₃ , DMF, 60 °C, o.n.; (d) NaOH, THF/H ₂ O, 60 °C, o.n.; (e) RSO ₂ NH ₂ , EDCl, DMAP, CH ₂ Cl ₂ , rt, o.n.; (f) CH ₂ Cl ₂ /TFA, rt, 3d	198
Figure 6.4: Schematic of moving from original purine scaffold to the second-generation purine scaffold utilizing substituted piperazines.....	201
Figure 6.5: Synthesis of di-substituted (2-(piperazin-1-yl)-9H-purin-6-yl)glycine (a) Aryl-Br, K ₂ CO ₃ , DMF, rt, 16 h; (b) t-Butyl glycine, K ₂ CO ₃ , n-BuOH, 60°C, 12 h; (c) 1-substituted piperazines, K ₂ CO ₃ , pyridine, 180°C, 18 h; (d) TFA/ CH ₂ Cl ₂ , rt, 3 h.....	203
Figure 6.6: SILCS Molecular Modeling renderings of the binding orientation of compound 8. A: Surface representation of MCL-1 (silver) and compound 8 binding to the p2 and p1 pockets (cyan) B: Exclusion FragMap indicating protein flexibility around compound 8 FragMaps: Green represent general hydrophobic residues, Orange represents the functional group acetic acid. Silver represents carbon atoms, blue: nitrogens, and red: oxygens.....	204
Figure 6.7: Transforming the purine core to a pyrrolopyrimidine core.....	208
Figure 6.8: Servier Research Laboratories S63845 (cyan) molecule bound into MCL-1 (white = carbon, blue = basic, red = acid) PDBID: 5LOF.....	209

Figure 6.9: Schematic functionalizing pyrrolopyrimidine molecule at the 4, 5, and 7 positions to bind into the MCL-1 hydrophobic groove (left). Fully functionalized proof of concept scaffold (right)..... 210

Figure 6.10: (A) MCL-1 bound to proof of concept molecule with one of the higher scoring Gold docking solutions. The acid connected to the 4C position interacts with Arg263 and the morpholine moiety extends into the p4 pocket. (B) Another higher scoring solution with the 7N pointing into the p2 pocket, the Phe acid forming a salt bridge with Arg263. PDBID: 4HW2. Molecule constrained to Arg263 in a 10Å radius.....211

Figure 6.11: Synthesis of tri-substituted pyrrolopyrimidine: (a) NIS, DMF, rt, 16 h; (b) alkylation, K₂CO₃, DMF, rt, 16 h; (c) protected amino acid, Et₃N, EtOH, DABCO 100°C, 2d; (d) Suzuki: 4-substituted-phenylboronic acid, CsF, tetrakis, DME/MeOH, 80°C, 18 h; (e) alkylation, K₂CO₃, DMF, rt, 16 h; (f) LiOH·H₂O, THF/MeOH/H₂O, rt, 1-2 h..... 212

List of Abbreviations

Acquired Immunodeficiency Syndrome	AIDS
Acute Myeloid Leukemia	AML
Apoptotic Protease Activating Factor 1	APAF1
Area Under the Curve	AUC
Azodicarbonyl Dimorpholide	ADDM
B-Cell Homology	BH
B-Cell Lymphoma 2	BCL-2
B-Cell Lymphoma Extra Large	BCL-x _L
BCL-2 Antagonist Killer	BAK
BCL-2 Associated Death Promoter	BAD
BCL-2 Associated Protein X	BAX
BCL-2 Like Protein 11	BIM
BCL-2 Like Protein 2	BCL-W
Benzyl Bromide	BnBr
BH3 Interacting Death Domain Agonist	BIM
Cesium Fluoride	CsF
Chloroform	CHCl ₃
Chlorosulfonic Acid	ClSO ₃ H
Chronic Lymphocytic Leukemia	CLL
Chronic Myeloid Leukemia	CML
Computer Aided Drug Design	CADD
Cytochrome c	cyt-c

Death Receptor 4	DR4
Death Receptor 5	DR5
2'-Deoxyadenosine 5' Triphosphate	dATP
Di-Tert-Butyl Dicarboxylate	BOC ₂ O
Dichloromethane	CH ₂ Cl ₂
Diethyl Azodicarboxylate	DEAD
1,2-Dichloroethane	1,2-DCE
Diethyl Ether	Et ₂ O
1,4-diazabicyclo[2.2.2]octane	DABCO
Diisopropyl Azodicarboxylate	DIAD
Diisopropyl Ethylamine	DIPEA
Dimethoxy Ethane	DME
Dimethoxyethyl Azodicarboxylate	DMEAD
Dimethyl Sulfoxide	DMSO
Dimethylaminopyridine	DMAP
Dimethylformamide	DMF
1-Ethyl-3-(3-Dimethylaminopropyl)carbodiimide	EDCI
Ethanol	EtOH
Ethyl Acetate	EtOAc
Fas Associated Death Domain	FADD
Fas Ligand	FasL
Fluorescein Isothiocyanate	FITC
Fluorescence Polarization Competition Assay	FPCA

Fragment Based Drug Design	FBDD
Grid Free Energy	GFE
Heteronuclear Single Quantum Coherence	HSQC
High Throughput Screen	HTS
Human Double Minute 2	HDM-2
Human Immunodeficiency Virus	HIV
Hydrogen Bond Acceptor	HBACC
Hydrogen Bond Donor	HBDON
Isopropanol	i-PrOH
Ligand Grid Free Energy	LGFE
Lithium Hydroxide Monohydrate	LiOH·H ₂ O
Mantle Cell Lymphoma	MCL
Methanol	MeOH
Methyl Iodide	MeI
Mitochondria Outer Membrane Permeabilization	MOMP
Molecular Dynamics	MD
Monte Carlo – SILCS	MC–SILCS
Mouse Double Minute-2	MDM-2
Multiple Myeloma	MM
Myeloid Cell Leukemia 1	MCL-1
<i>N</i> -Iodosuccinimide	NIS
<i>N</i> -Methylmorpholine	NMM
Non-Small Cell Lung Cancer	NSCLC

Nuclear Magnetic Resonance	NMR
Nuclear Overhauser Effect	NOE
Outer Mitochondrial Membrane	OMM
p53 Upregulated Modulator Apoptosis	PUMA
Pharmacodynamics	PD
Pharmacokinetics	PK
Potassium Carbonate	K_2CO_3
Protein Database	PDB
Protein-Protein Interactions	PPI
Pyridine	pyr
Reactive Oxygen Species	ROS
Silver Oxide	Ag_2O
Site Identification Ligand Competition Saturation	SILCS
Sodium Hydride	NaH
Sodium Hydroxide	NaOH
Sodium triacetoxyborohydride	$NaBH(OAc)_3$
Structure Activity Relationship	SAR
Tetrahydro-1H-benzo[e][1,4]diazepines	BZD
Tetrahydrofuran	THF
Thin Layer Chromatography	TLC
Thionyl Chloride	$SOCl_2$
Tin Chloride Dihydrate	$SnCl_2 \cdot 2H_2O$

TNF-Related Apoptosis Inducing Ligand	TRAIL
TNFR Associated Death Domain	TRADD
Transmembrane	TM
Tributyl Phosphine	PBu ₃
Triethylamine	Et ₃ N
Trifluoroacetic Acid	TFA
Triphenyl Phosphine	PPh ₃
Truncated BID	t-BID
Tumor Necrosis Factor	TNF
Tumor Necrosis Factor Receptor	TNFR
Tumor Necrosis Factor Receptor 1	TNFR1
Vascular Endothelial Growth Factor	VEGF

Chapter 1 Protein-Protein Interactions: Approaches for Targeted Disruption of BCL-2 Anti-Apoptotic Family.

1.1 Introduction

Protein–protein interactions (PPIs) are involved in a variety of vital cellular processes that include differentiation, apoptosis, signal transduction and transcription.¹⁻³ Their dysregulation, therefore, render them attractive therapeutic targets for the treatment of a variety of diseases, including cancer, diabetes, neurodegenerative disorders and HIV/AIDS, among others.⁴⁻⁸ There are several classes of PPIs that are grouped based on how their interactions occur, such as the BCL-2 family, which are globular proteins that interact with a peptide through a discontinuous epitope.⁹ Other important interactions that our lab has focused on occur between a globular protein and a peptide with anchor residue owing to a post-translational modification binding into the pocket, and peptide-peptide interactions, where a pair of α -helices bind with an elongated interaction (**Table 1.1**).⁹ Long considered an insurmountable challenge, the scientific literature is now rife with synthetic strategies to disrupt aberrant PPIs, and, whilst the number of such small-molecules that have reached the clinic remains low, e.g., ABT-737/263/199, the development of chemical probes en route to drug candidates has assisted in the delineation of PPI-mediated cellular processes.¹⁰⁻¹¹ PPIs boast solvent-exposed, large, hydrophobic binding grooves.¹ These features are in stark contrast to enzyme active sites where small-molecules can be fashioned after the enzyme’s substrate or designed de novo to recognize the well-defined cavity. Furthermore, hydrophilic groups can be more readily exploited,

which directly aids in compound solubility and, ultimately may facilitate bioavailability.


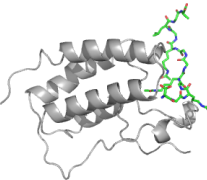
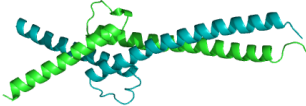
PPI Class	Description	Key Examples	Representative Crystal Structure
Globular protein binding helical peptide	Helix with a discontinuous epitope binding into a hydrophobic groove	MCL-1-BIM BCL-x _L -BAK HDM2-p53	 PDB ID: 2PQK
Globular protein binding peptide; post-translational modification (PTM)	Peptide binding to a protein with a PTM binding into a pocket	Bromodomains L3MBTL3	 PDB ID: 3UVW
Peptide interacting with a peptide	A pair of peptides interacting in an elongated fashion	MYC-MAX	 PDB ID: 1NKP

Table 1.1: Protein-protein interaction classifications with key examples and crystal structures

Despite the large interfacial areas involved in PPIs, much of the free energy of binding is attributed to “hot spots”, smaller regions within the PPI that are more tractable to low-molecular-weight ligand design.¹² One such subset of PPIs is described by those that are mediated by α -helices, such as the MCL-1-BIM interaction (**Figure 1.1**), wherein key residues projected from the helix recognize hot spots in the target protein.¹³⁻¹⁵ α -Helices are found at the interfaces of almost two-thirds of the PPIs found in the Protein Data Bank (PDB), demonstrating their significance in protein-protein recognition, and around half of these involve the helix utilizing a single recognition face.¹³

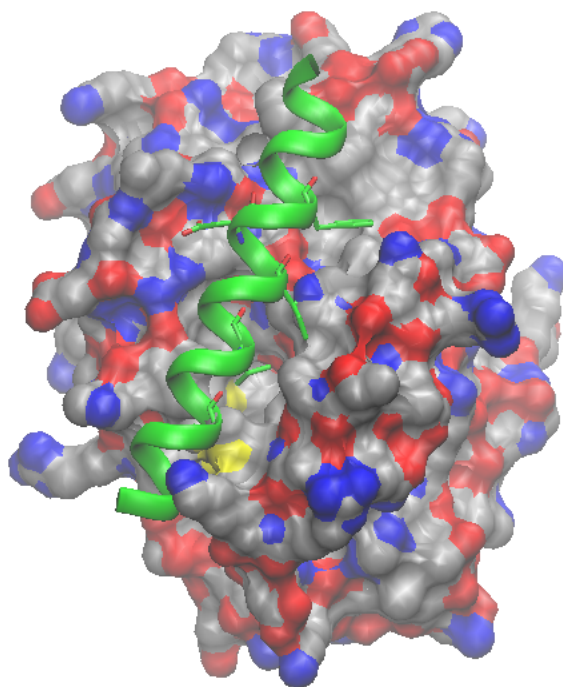


Figure 1.1: *MCL-1 (grey, red and blue) bound to BH3 pro-apoptotic protein BIM (green). Key binding residues are highlighted on the truncated BIM peptide: Phe69, Ile65, Leu62, Leu58.*

1.2 The BCL-2 Family: Apoptotic Regulators in the Mitochondria

One main class of PPIs, as previously mentioned, that are main contributors in the progression of cancer are the globular protein-helical peptide interaction.⁹ This class encompasses the BCL-2 family of proteins, which are involved in the regulation of apoptosis. Apoptosis is a highly-conserved process of programmed cell death and its evasion allows for the development and growth of tumors and can occur through two pathways, intrinsic or extrinsic and both converge to activate downstream caspases. The intrinsic pathway, in which mitochondria play an essential role in activating the caspase proteases, is also called the BCL-2 regulated or mitochondrial pathway, and relies strictly on the BCL-2 family.¹⁶⁻²⁴ As mentioned above, the B-Cell Lymphoma 2 (BCL-2) family of proteins are key regulators of this pathway and are characterized by the Bcl-2 homology

(BH) domains BH1, BH2, BH3 and BH4, of which they share one or more of.²¹ They are comprised of the multi-domain anti-apoptotic proteins or guardians (BCL-2, BCL-X_L, MCL-1, BCL-W, and BCL2A1 (or A1)) and multi-domain pro-apoptotic proteins or effectors (BAX, and BAK) and the BH3 only pro-apoptotic proteins or initiators (e.g. BIM, BAD, BID, NOXA, and PUMA).²⁰⁻²² The interaction between the anti- and pro-apoptotic proteins constitutes a tight regulation of apoptosis. Not all pro-apoptotic proteins bind the anti-apoptotic proteins due to the subtle differences in structure, however some BH3 only proteins do bind all of the anti-apoptotic proteins as depicted in **Figure 1.2**. It is well documented that the BCL-2 anti-apoptotic family members, i.e BCL-2 or BCL-x_L sequester and inhibit BAX and BAK to prevent apoptosis and that the BH3 only pro-apoptotic proteins can alleviate BAX and BAK by directly binding to the anti-apoptotic members.

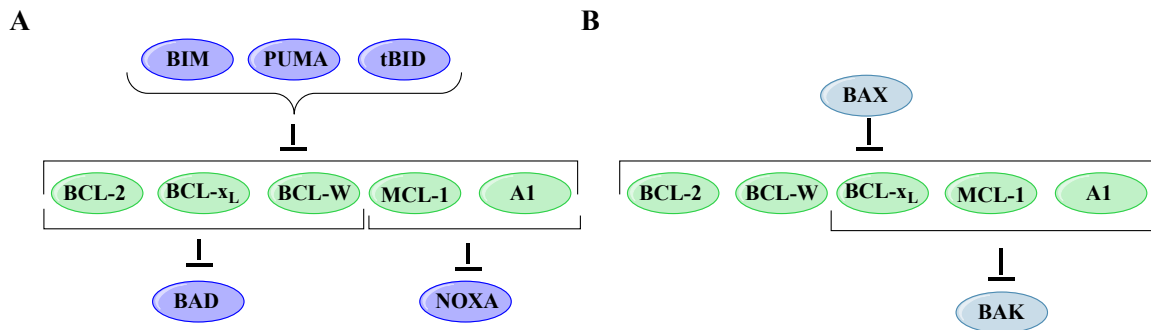


Figure 1.2: Pro-apoptotic proteins binding the anti-apoptotic family of proteins. (A) BH3-only or initiator pro-apoptotic proteins BIM, PUMA, and tBID bind all the BCL-2 family proteins, while BAD and NOXA only interact with some. (B) Pro-apoptotic effector proteins BAX binds all the anti-apoptotic BCL-2 proteins, while BAK only binds BCL-x_L, MCL-1, and A1.

The activation of intrinsic apoptosis occurs through various developmental or environmental cues, such as viral infection, DNA damage, and growth-factor deprivation.

These cues result in the upregulation of BH3-only proteins until the apoptotic threshold has been achieved. The initiators, such as BIM and PUMA, directly activate BAX and BAK by binding²⁵ directly or through release from the anti-apoptotic protein, such as BCL-2 or BCL-x_L.²⁶ This process activates BAX and BAK to form oligomers, or homodimers, which translocate to the outer mitochondrial membrane (OMM).²² This allows the oligomers to form pores within the membrane that permits the release of cytochrome *c* (cyt-*c*), an apoptogenic molecule that leads to caspase activation. BAX and BAK either directly or indirectly stimulate the release of proteins from the space between the inner and outer mitochondrial membranes in a process known as mitochondrial outer membrane permeabilization (MOMP) and results in the release of not only cyt-*c*, but other soluble proteins into the cytosol. Cytochrome *c* binds to apoptotic protease-activating factor 1 (APAF1) and with dATP (2'-deoxyadenosine 5'-triphosphate) forms the protein ring called an apoptosome, which recruits and activates caspase 9, that activates downstream caspases and ultimately cell death (**Figure 1.3**).¹⁸

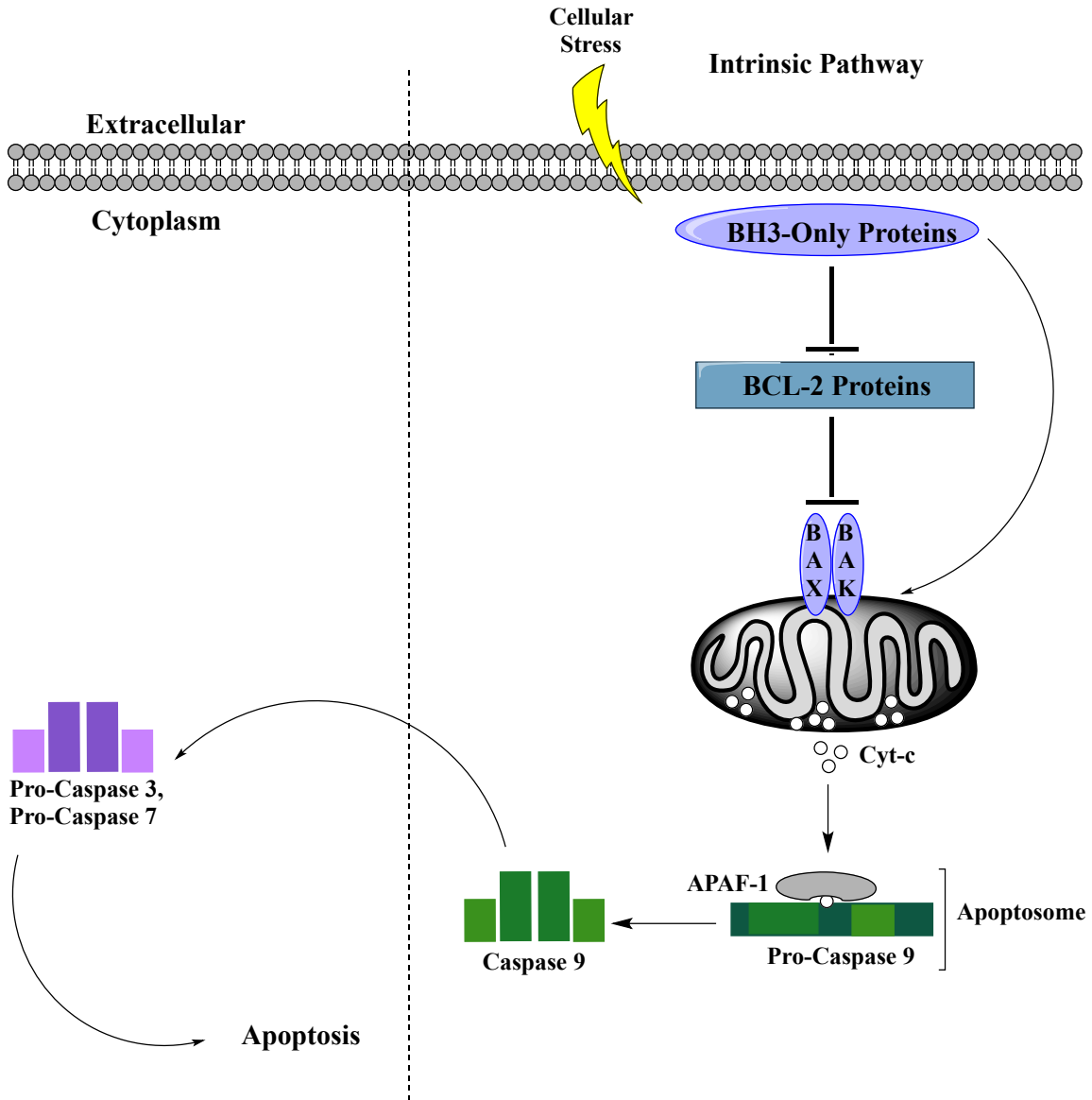


Figure 1.3: Intrinsic or Mitochondrial apoptosis pathway regulated by the BCL-2 family.

The extrinsic or death-receptor pathway, can ultimately activate the intrinsic pathway through truncation of BID. This pathway is activated by the binding of “death receptors”, which belong to the tumor necrosis factor (TNF) receptor family: Fas ligand (FasL), TNF, or TNF-related apoptosis-inducing ligand (TRAIL). These ligands contain an intracellular death domain, that can recruit and activate caspase-8 through the binding

of their respective receptors, i.e. Fas, TNF receptor 1 (TNFR1), death receptor 4 (DR4), or DR5 at the cell surface. These interactions lead to the recruitment of Fas-associated death domain (FADD) and TNFR-associated death domain protein (TRADD) and the subsequent activation of caspase 8. This activation leads to downstream activation of effector caspases -3, -6, or -7 without involving the BCL-2 family.^{16, 18} In some types of cells the extrinsic and intrinsic pathways cross. Caspase-8 activates the intrinsic pathway through cleavage of the pro-apoptotic protein BID to the C-terminal truncated form of BID (t-BID). t-BID translocates to the mitochondria to activate the intrinsic apoptosis pathway (**Figure 1.4**).¹⁶

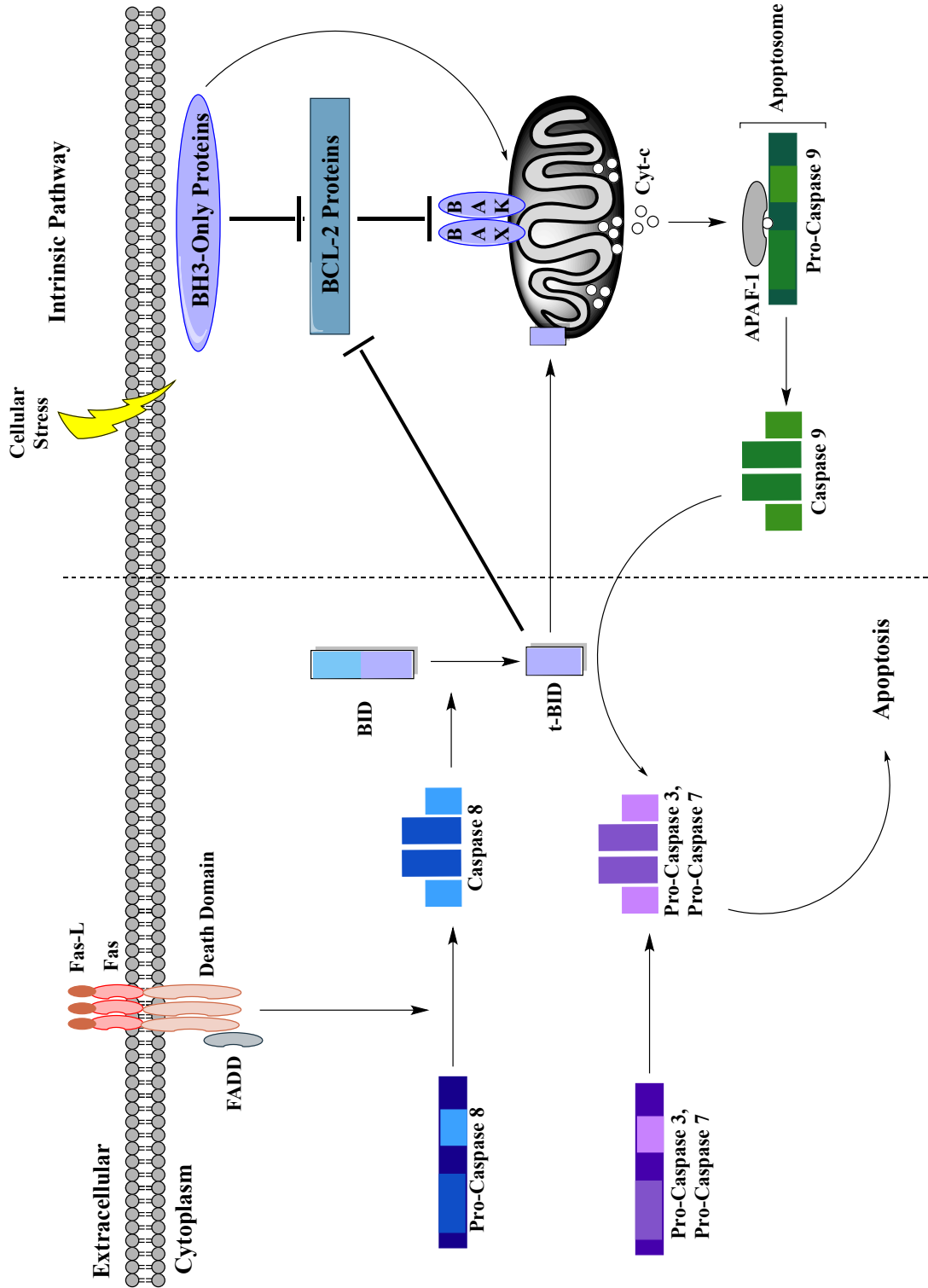


Figure 1.4: Extrinsic apoptosis pathway, which can initiate the intrinsic pathway through cleavage of BID.

1.3 Structure of the BCL-2 family of proteins

As mentioned, within the pro-apoptotic proteins of Bcl-2, there are two subsets of proteins: the BH3-only domain proteins or initiators, and BH multi-domain proteins or effectors. The BH3-only proteins have only the conserved homologous BH3 α -helix, where the BH multi-domain proteins exhibit structural similarities to the anti-apoptotic proteins having BH1-BH4 domains (**Figure 1.5**). The shared sequence homology of the BCL-2 family is quite low and ranges from 3-40%, but is typically around 20%. The anti-apoptotic proteins BCL-2 and BCL-x_L share 40% identity, while Bim, a BH3-only protein, has 20% shared identity. BAX, one of the BH multi-domain proteins share a mere 3% identity.²⁷ While the sequence identity shared is low among the BCL-2 family; they all have conserved sequence regions (BH domains) that translates to the secondary and tertiary structures and the overall functionality of the proteins.^{19, 27} Not only do the BCL-2 proteins have conserved BH domains, they frequently share a trans-membrane (TM) region located at the C-terminus, which is important for localization to the OMM.

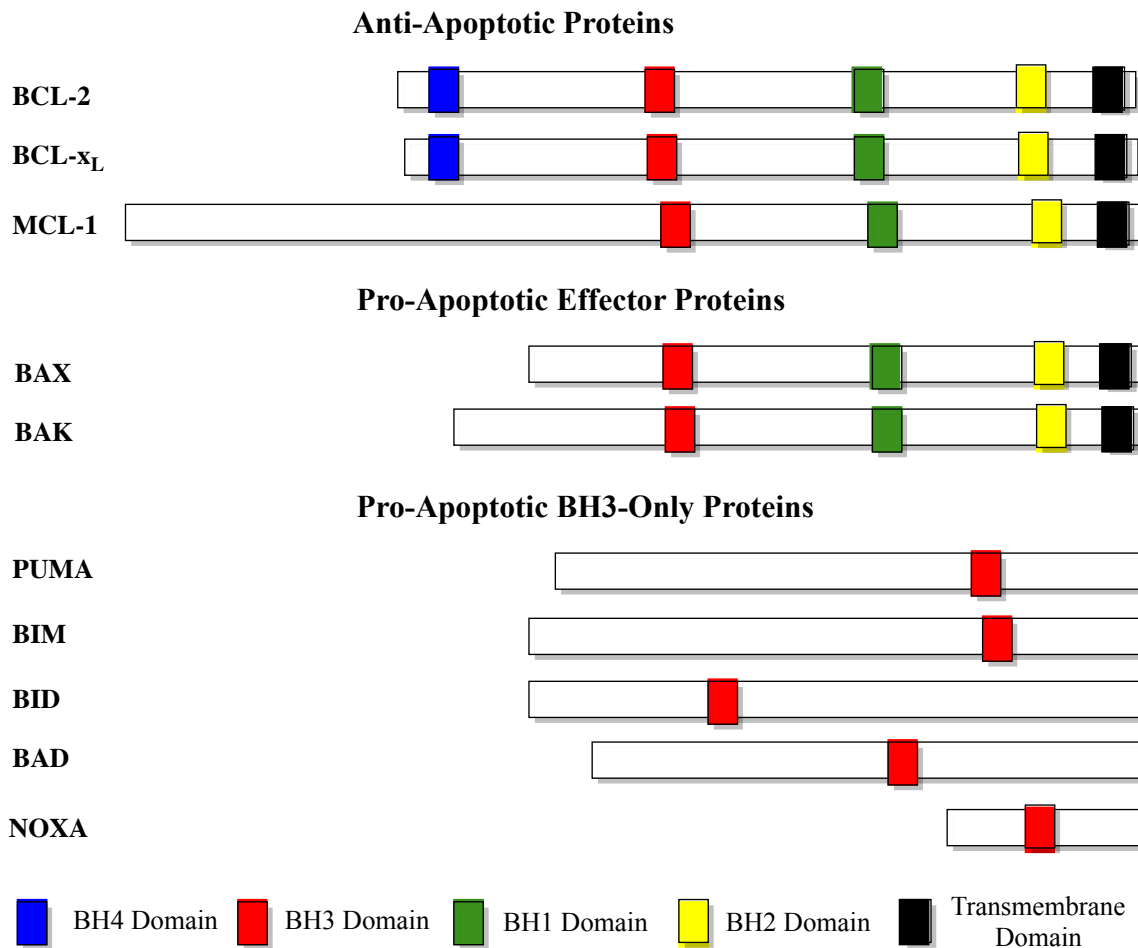


Figure 1.5: The BCL-2 Homology Domains of the BCL-2 family of proteins.

Sattler et al. showed through NMR studies that apoptotic activation primarily occurs by the BH3 only α -helices that bind the BCL-2 family anti-apoptotic proteins.^{16, 22, 28} To confirm what was seen in the NMR solution experiments, alanine scanning mutagenesis was performed to show that helices BH1, BH2, and BH4 are not involved in apoptotic activation.²⁸ Interestingly all the pro-apoptotic proteins, both multi-domain and BH3 only have conserved hydrophobic residues on one face of the helix at the i , $i + 3/4$, and $i + 7$ positions and an Asp residue on the other face at the $i + 5$ position.^{1, 29-30} BH3 proteins that will be addressed in this dissertation: BAK with key residues Leu78, Ile81, Asp83, and

Ile85; BIM with residues Leu62, Ile65, Asp67, and Phe69 at the i , $i + 3/4$, $i + 5$ and $i + 7$ respectively (**Figure 1.6**).

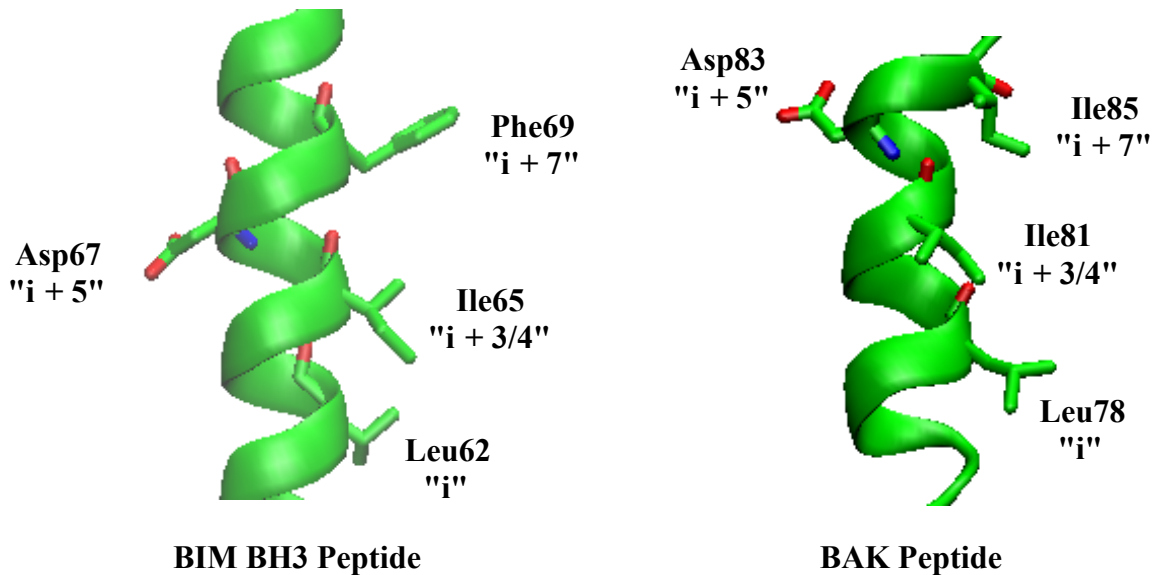


Figure 1.6: Pro-apoptotic proteins BIM and BAK with labeled key binding residues representing the i , $i + 3/4$, $i + 5$ and $i + 7$.

These residues have been identified as key binding residues within the helix and have been noted as critical for binding through alanine scanning mutagenesis experiments.^{28, 31-32} Both BAK and BIM have similar amino acids on the BH3 helix resulting in conserved intermolecular interactions within the hydrophobic binding grooves of the BCL-2 anti-apoptotic proteins.³¹⁻³² Fairlie et al further confirmed Sattler's experiments showing that the key binding residues in BIM are vital for BCL-x_L and MCL-1 inhibition.³¹

As previously mentioned, the pro-apoptotic BCL-2 proteins (BH3 helix) bind into the anti-apoptotic protein (BH1-BH3 helices) hydrophobic groove, which consists of 4 pockets (p1, p2, p3, and p4).^{22, 27-28} There are important electrostatic interactions that occur

opposite the p3 pocket between aspartic acid residues of the pro-apoptotic proteins (Asp83 on BAK or Asp67 on BIM) and the arginine residues of the anti-apoptotic proteins (R146 (BCL-2), R139 (BCL-x_L), and R263 (MCL-1)) **Figure 1.7**. These residues interact to form a salt-bridge, but when mutated to alanine there is a loss of binding.³¹⁻³²

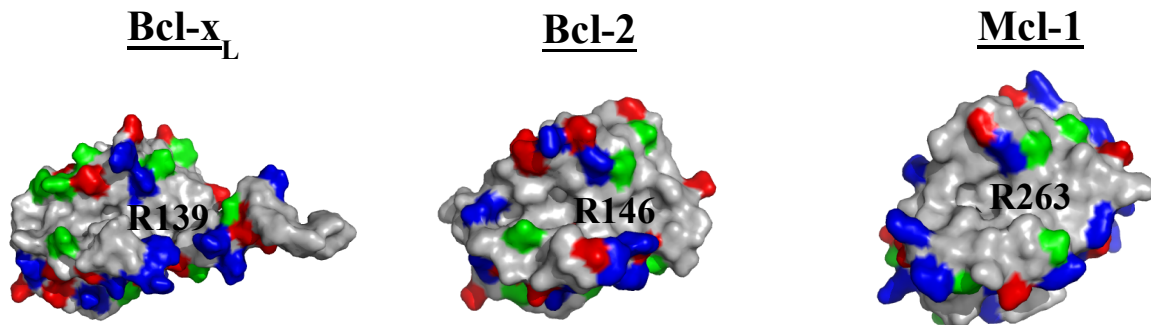


Figure 1.7: The anti-apoptotic proteins labeled with conserved Arginine residue.

As mentioned previously, the anti-apoptotic proteins share sequence homology, which translates into structural similarities. However, MCL-1 has a relatively different topology, which pictorially looks flat and shallow compared to BCL-2 and BCL-x_L. This difference can be attributed to a poorly defined p4 region that is ordered in the other anti-apoptotic proteins. BCL-2 and BCL-x_L have well defined p4 regions that form an organized binding crevice that interacts with either Ile85 of BAK or Phe69 of BIM, while the p4 pocket of MCL-1 is unstructured and solvent exposed.³³⁻³⁵ The topological differences in the structure of MCL-1 could explain the previous difficulties in targeting this protein. As will be seen below in this thesis, targeting this family of proteins has been fruitful, yielding several clinical trials and monumental leaps towards a selective MCL-1 inhibitor.^{22, 35}

1.4 Approaches for Targeted Disruption

Broadly speaking, synthetic strategies to disrupt helix-mediated PPIs fall into two categories: peptidic and non-peptidic. In the former category, Cabezas¹⁴ and Arora¹⁵ have independently enforced helical conformations of peptides by replacing internal hydrogen bonds with covalent linkages; this approach has led to the discovery of a novel inhibitor of the HIF1 α -p300 PPI.³⁶ Meanwhile, as a follow-up to Grubbs's earlier report that a ring-closing metathesis reaction between two unnatural amino acids carrying alkenyl-based side chains promoted helicity (**Figure 1.8**), Verdine later demonstrated that such "stapled" peptides can inhibit the Bid-Bcl-2 PPI, amongst others, and, despite the highly peptidic nature of the inhibitor, was biologically active in vivo, reducing the growth of human leukemia xenografts.³⁷⁻³⁸ Other chemical conformational constraints between amino acid side chains include lactams,³⁹ disulfide bridges,⁴⁰ intramolecular salts,⁴¹ and triazoles⁴².

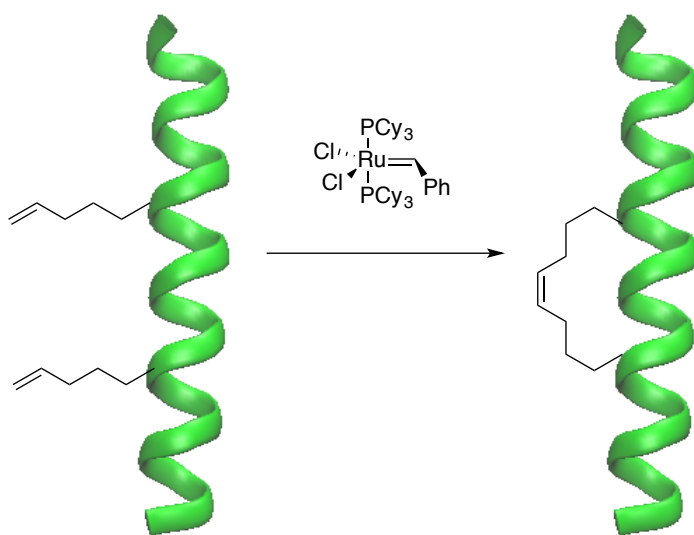


Figure 1.8: Peptidomimicry of an α -helix with modified side chains to undergo ring closing metathesis using a ruthenium catalyst.

Some drawbacks of the peptidic strategy to mimic α -helices include potential metabolic instability through digestion of peptide bonds, as well as limited cell penetrating properties due to the presence of charged side chains and the cumulative effect of the polar peptide bonds. The second category of targeting helix mimetics, encompasses structures of non-peptidic design, and so aims to address the limitations of the previous category. Synthetic, non-peptidic agents that can accurately project functional groups from a scaffold in an orientation similar to the native α -helix have effectively disrupted helix-mediated PPIs within cells.⁴³⁻⁴⁴ Although the first report on helix mimicry with synthetic agents was published by Howson and co-workers,⁴⁵⁻⁴⁶ it was Hamilton's laboratory that pioneered the field of helix mimicry with low-molecular-weight ligands covering a wide range of synthetic scaffolds including terphenyls (**1**),⁴⁷⁻⁴⁸ terpyridines,⁴⁹ trispicolinamides (**2**),⁵⁰ terephthalamides,⁵¹⁻⁵² benzoylureas (**3**),⁵³⁻⁵⁵ and enamines.⁵⁶⁻⁵⁷ Since many α -helices utilize only one face to recognize their partner proteins, specifically through the side chains of the i , $i + 3/4$ and $i + 7$ residues (**Figure 1.9**), the development of helix surrogates has traditionally focused on the mimicry of these residues and hence on only one face of an α -helix. In addition to excellent reproduction of the relative distances between the side chain mimics, it is important to note that the subunits within the terphenyls are staggered due to steric interactions, which further promotes helix mimicry since the i , $i + 3/4$ and $i + 7$ residues are likewise staggered. Increasingly, two- and three-sided helix-mediated PPIs are being discovered at therapeutically important interfaces.¹³

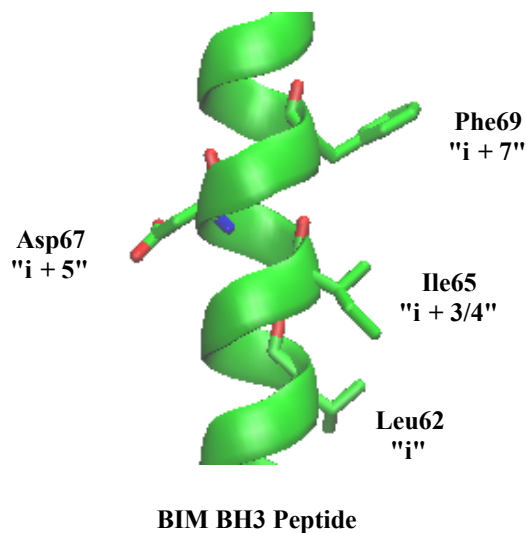


Figure 1.9: BIM BH3 scaffold with labeled side chains to mimic.

Many of the conformationally flexible Hamilton and Hamilton-type scaffolds, such as the pioneering terphenyls, that were designed to mimic the residues on only one face of an α -helix may be capable of mimicking residues on multiple faces or turns of the requisite helix. Mimicking multiple faces has come to the realization through the 1,2-diphenylacetylenes (**4**)⁵⁸ ($i, i + 2, i + 5, i + 7$), benzoylureas (**5**)⁵³⁻⁵⁴ ($i, i + 1, i + 4, i + 6, i + 7$), and 2,6,9-tri-substituted purines⁵⁹ ($i, i + 3/4, i + 5, i + 7$) to name a few (**Figure 1.10**). To this end, our group has pursued this synthetic strategy to target the BCL-2 family and this pattern of replicating the spatial orientation of an α -helix will be further discussed in this section, and **Chapters 3** and **6**.

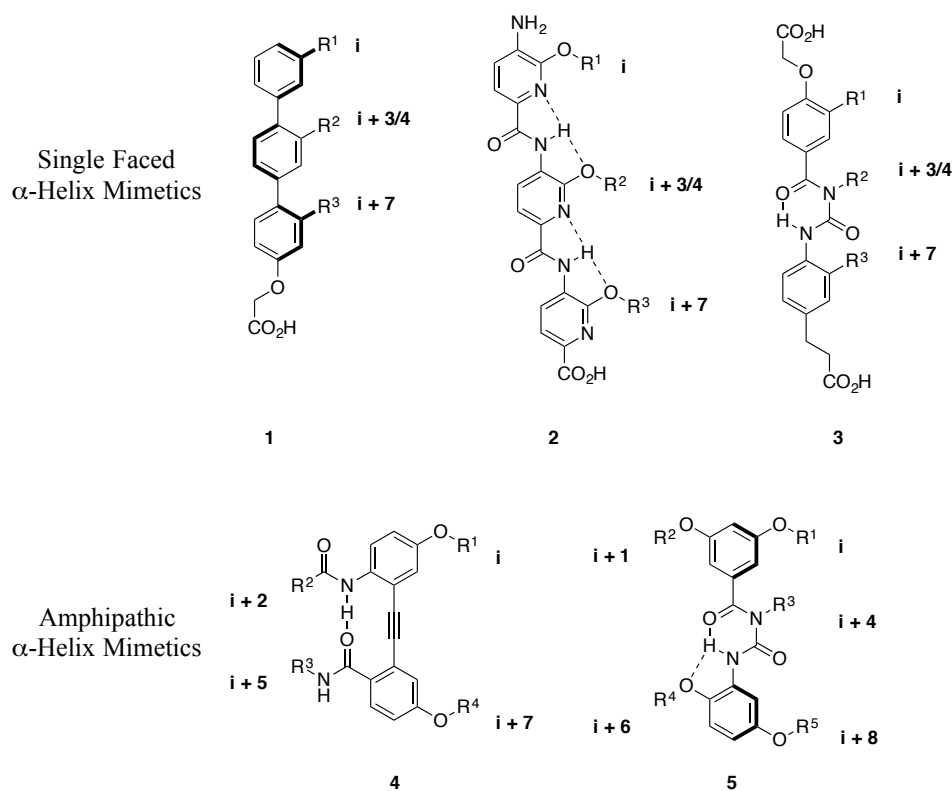


Figure 1.10: Generic scaffolds of single and amphipathic α -helix mimetics.

Another non-peptidic approach to the disruption of PPIs that has gained significantly more traction in the past four years is small molecule inhibitors. This approach utilizes fragment-based or structure-based drug design to develop molecules for the binding groove of proteins, such as the anti-apoptotic BCL-2 family or HDM2/MDM2.⁶⁰⁻⁶² Fragment-based drug design utilizes an NMR based screen with a library of fragments to develop classes of compounds that can be categorized as “hits”, meaning they bind a certain position on the protein. In cases where the hits bind into multiple sites, the fragments were merged to develop a more potent inhibitor than the individual moieties.^{33, 60, 63} The Abbott, Abbvie, and Fesik laboratories have developed inhibitors using these methods against the BCL-2 family targeting their conserved pockets. Structure-based design utilizes the 3D

structure of the protein in question interacting with a small molecule or multiple small molecules to inspire future drug discovery. This de novo strategy is usually supported with molecular modeling or crystal structures.^{61, 64} The Fletcher,⁶⁴ Nikolovska-Coleska,⁶⁵ and Lessene⁶¹ laboratories have developed lead molecules with low nM inhibition using this strategy. Both fragment-based and structure-based drug design as methods to inhibit the BCL-2 family will be further examined in sections **1.6**, **1.7** and **Chapters 2** and **6** below.

1.4.1 Bis-Benzamides

An alternative and synthetically more accessible helix mimetic to the terphenyls are the tris-picolinamides⁵³, which have formed the basis for two-faced helix mimicry (see below). However, given their rich contribution to single-faced helix mimicry, we first begin with a summary of the simpler oligoarylamides. Through mimicry of the *i* (V74), *i* + 4 (L78) and *i* + 7 (L81) side chains of the Bak-BH3 α -helix with alkoxy groups, representative trispicolinamide **7** (**Figure 1.11**) disrupted the Bak–Bcl-xL PPI with a K_i of 1.6 μ M. The anti-apoptotic Bcl-2 proteins, which include Bcl-xL, Bcl-2 and Mcl-1, neutralize the pro-apoptotic Bcl-2 proteins, such as Bak and Bim, by capturing their BH3 α -helical “death domains”⁴. Since the upregulation of the anti-apoptotic Bcl-2 proteins has been associated with the development and progression of various cancers⁴, compound **7** provides a starting point from which new antineoplastics might be realized. The role of the pyridine nitrogens was to promote the projection of the three side chains from the same face of the mimetic through bifurcated hydrogen bonds. Oligomerization of the picolinamide core generated an inhibitor of islet amyloid polypeptide aggregation (compound **8**, **Figure 1.11**)⁶⁶⁻⁶⁷, whilst Wilson replaced the pyridine rings with benzene rings, which afforded potent inhibitors, such as **9**, of the p53–HDM2 PPI through accurate

mimicry of F19 (i), W23 (i + 4), L26 (i + 7) of the p53 helix.⁶⁸ The therapeutic significance of Wilson's work lies in the potential discovery of new anti-cancer drugs since the tumor suppressor role of p53 is inactivated by HDM2.⁶⁹ Using the Bak–Bcl-xL PPI as a tool, the Fletcher group interrogated the role of the preorganizing pyridine nitrogen atoms of a trispiconlinamide through systematically replacing the pyridine nitrogens with CH groups (i.e., benzene rings), resulting in the potent and cell-active compound **10** (JY-1-106).^{29, 70}

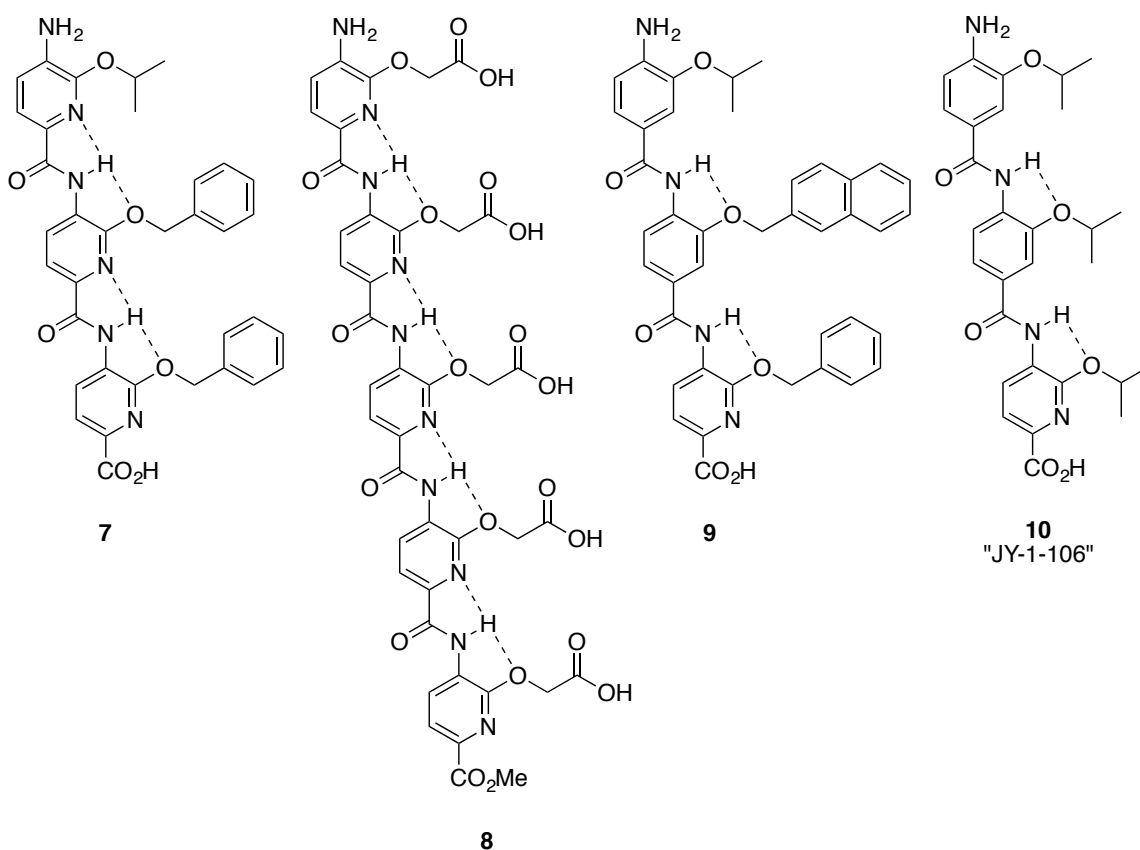


Figure 1.11: Oligoarylamides as single-faced helix mimetics.

As alluded to earlier, the oligoamides, which present simpler syntheses than their terphenyl predecessors, are attractive candidates for accomplishing the mimicry of two faces of an α -helix. Accordingly, two groups independently converted single-faced bis-

benzamides into two-faced helix mimetics. Hamilton's laboratory introduced amides opposite the alkoxy-decorated face to allow for the additional mimicry of the $i + 2$ and $i + 6$ side chains; the generic structure is illustrated by compound **11** (**Figure 1.12**).⁵⁵ The desired conformational constraints hinged on the formation of six-membered intramolecular hydrogen bonds, which were confirmed by X-ray crystallography. In a complementary strategy, Anh's group developed synthetic chemistry to introduce additional alkoxy functionality into the opposing face that, through a bifurcated hydrogen bond, also permits mimicry of two opposing recognition faces of an α -helix (compound **12**, **Figure 1.12**).⁷¹ A crystal structure revealed five- and six-membered, intramolecular hydrogen bonds between the amide NH and the ether oxygens, resulting in excellent spatial mimicry of the i , $i + 7$ and $i + 2$, $i + 5$ side chains from opposite faces. No biological data has been reported on these new, multi-facial bis-benzamides. It is anticipated that both types of bis-benzamide will allow the introduction of hydrophobic and hydrophilic groups.

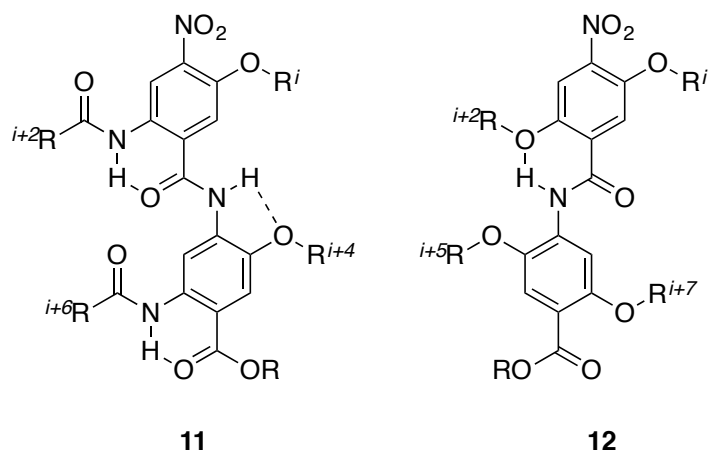


Figure 1.12: Two-faced bis-benzamide helix mimetics. Dashed lines represent hydrogen bonds.

1.4.2 Benzoylureas

Hamilton demonstrated that five residues (i , $i + 1$, $i + 4$, $i + 6$ and $i + 8$) spanning two turns and opposing faces of an α -helix could be effectively reproduced through the elaboration of a benzoylurea scaffold that was previously reported by the group.⁵³⁻⁵⁴ Confirmation that the two-faced benzoylurea **13** (**Figure 1.13**) folds into a helical-type structure through a bifurcated hydrogen bond was provided by X-ray crystallography, although whether this organized structure can be attained under physiological conditions is unknown. Unlike the bis-benzamides, the “upper” phenyl ring of the benzoylureas is not subjected to non-covalent interactions, providing a two-faced helix mimetic with greater conformational flexibility, as well as the ability to emulate a fifth side chain.

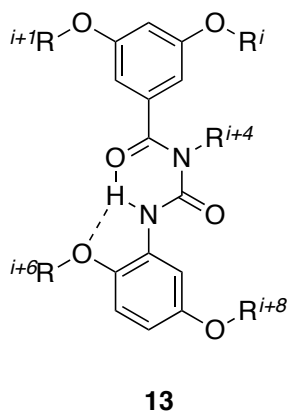


Figure 1.13: A two-faced helix mimetic centered on a benzoylurea scaffold. Dashed lines represent a bifurcated hydrogen bond.

1.4.3 1,2-Diphenylacetylenes

Functionalized 1,2-diphenylacetylenes have recapitulated the epitopes of β -turns and β -strands by virtue of strategically fashioned intramolecular hydrogen bonds.⁷²⁻⁷⁵ The

Fletcher group considered that this framework might also be exploited to elicit two-faced α -helix mimicry.⁷⁶ The prototypical compound **14** (**Figure 1.14**) was prepared, which, according to computational modeling, reproduced the spatial and angular projections of the i and $i + 7$ side chains on one face and the $i + 2$ and $i + 5$ on the opposite face. The presence of the key intramolecular hydrogen bond to influence the projection of specific side chains from opposing faces of the scaffold was then ratified in the solution state by ^1H NMR titration experiments. As stated earlier, the oncoprotein Mcl-1 neutralizes the pro-apoptotic Bcl-2 proteins, which include Bim and Bak, through binding their BH3 domains. Elaboration of the design, as in the amphipathic helix mimetic **15**, allowed for the mimicry of five residues of the Bim-BH3 α -helix located across two faces and within two turns of the helix: i , $i + 1$, $i + 3$, $i + 5$ and $i + 7$. In addition to structurally mimicking the Bim-BH3 α -helix, the group demonstrated that **15** was also a functional helix mimetic, inhibiting Mcl-1 with a K_i of 3.24 μM , as determined by a fluorescence polarization competition assay (FPCA).

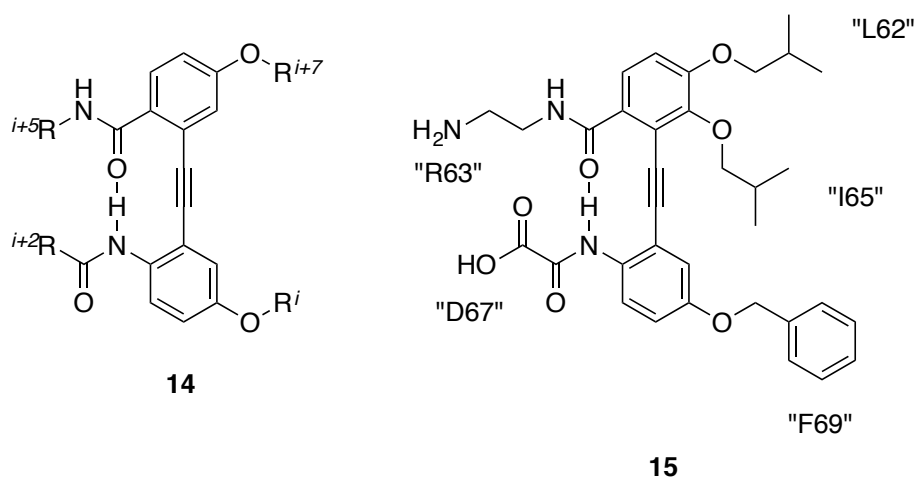


Figure 1.14: An intramolecular hydrogen bond (dashed line) influences the projection of side-chains from opposing faces of a diphenylacetylene scaffold.

1.4.4 Anthraquinones and Acridines

Zhang and colleagues designed and evaluated anthraquinones as two-faced helix mimetics wherein substitution of opposite sides of the rigid scaffold affords reasonable mimicry of side chains located on opposing faces of an α -helix.³² The width of the anthraquinone core (4.8 Å) is similar to the diameter of an α -helix, and so it was postulated that appropriate functionalization of the two edges of the scaffold would allow for mimicry of D67 and I65 of the Bim-BH3 α -helix. Pleasingly, the group identified nanomolar dual inhibitors of the Bim-Mcl-1 and Bim-Bcl-2 PPIs, with their most potent compound, **16** (**Figure 1.15**), exhibiting K_i 's of 13 and 24 nM for Mcl-1 and Bcl-2, respectively, according to FPC assays. HSQC NMR experiments with **16** resulted in significant chemical shift perturbations of many residues in the hydrophobic groove of ¹⁵N-labeled Mcl-1, most particularly those of R263/N260 and V220/H224/V274/F228, corresponding to hotspots recognized by D67 and I65 of the Bim-BH3 α -helix, respectively. Taken together, these data suggest anthraquinone **16** inhibits Mcl-1 and Bcl-2 through structural and functional mimicry of opposing faces of the Bim-BH3 α -helix. The same group developed their anthraquinone into an elaborate acridine scaffold that could accomplish additional mimicry of two more residues.⁷⁷ Acridine **17** bound Mcl-1 and Bcl-2 with K_i values of 79 and 56 nM, respectively, through proposed mimicry of the i , $i + 3$, $i + 5$ and $i + 7$ side chains of the Bim-BH3 α -helix. Once again, HSQC NMR spectroscopy corroborated Zhang's design, indicating that **17** accurately mimicked the side chains of L62, I65, F69 and D67 of Bim. Direct binding of **17** to Mcl-1 was confirmed by isothermal titration calorimetry (ITC) ($K_d = 107$ nM), substantiating the affinity determined in the FPCA assay. Finally,

since some acridines are DNA intercalators, **17** was evaluated for its effect on DNA: no significant differences in superhelical content or band shape in agarose gel electrophoresis was detected indicating this acridine does not interact with DNA.

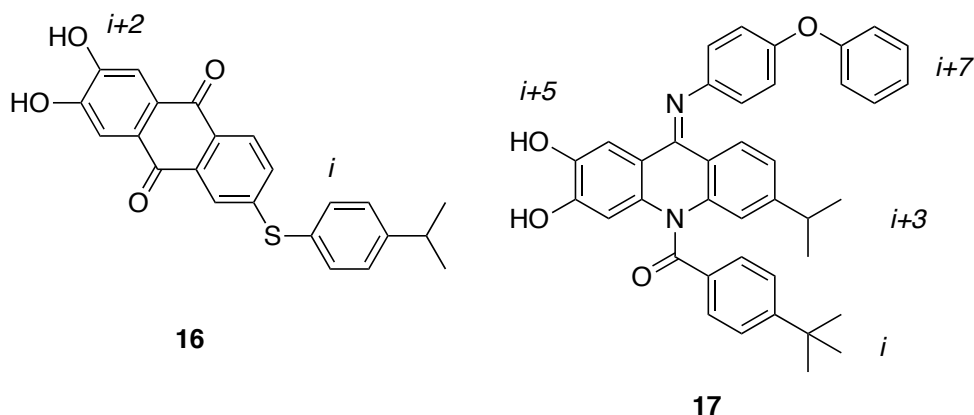


Figure 1.15: Appropriately functionalized anthraquinones (left) and acridines (right) have disrupted the Bim–Mcl-1 PPI through two-faced mimicry of the Bim-BH3 α -helix.

1.4.5 2,6,9-Tri-Substituted Purines

Towards the disruption of the p53–HDM2 PPI, the Lim group recently developed single-faced helix mimetics of the p53 α -helix, based on a pyrrolopyrimidine core, and, despite its rigidity, several potent inhibitors of HDM2 were discovered.⁷⁸ Their research thus highlighted that a flexible scaffold for helix mimicry is not crucial, presumably provided the side chains are sufficiently flexible that mimicry of staggered side chains can be accomplished. Inspired by this work, and having previously developed synthetic chemistry to control the N9-regioselective alkylation of the purine nucleus,⁷⁹ the Fletcher group introduced 2,6,9-tri-substituted purines as two-faced helix mimetics.⁵⁹ On the simplest level, this scaffold was proposed to mimic the i , $i + 2$ and $i + 3/4$ side chains across opposing faces within one turn (compound **18**, **Figure 1.16**). Elaboration of their design

allowed for the additional mimicry of a fourth residue: i , $i + 3/4$, $i + 5$ and $i + 7$, corresponding to L78, I81, D83 and I85 of the Bak-BH3 α -helix. A small library of compounds was prepared, the most potent member of which, **19**, disrupted the Bak-BH3–Mcl-1 PPI with an estimated IC_{50} of 72 μ M. It was hypothesized that the rigid tert-butyl of the Boc group would be a poor mimetic of the i side chain, and this may account for the moderate inhibition, but was incorporated into the design to facilitate the synthetic chemistry and allow the rapid evaluation of such functionalized purines as helix surrogates. Thus, to address this caveat, the group is presently focusing on the replacement of the Boc group with more flexible carbamates and sulfonamides to realize better helix mimicry. This scaffold will be discussed further in **Chapter 3**.

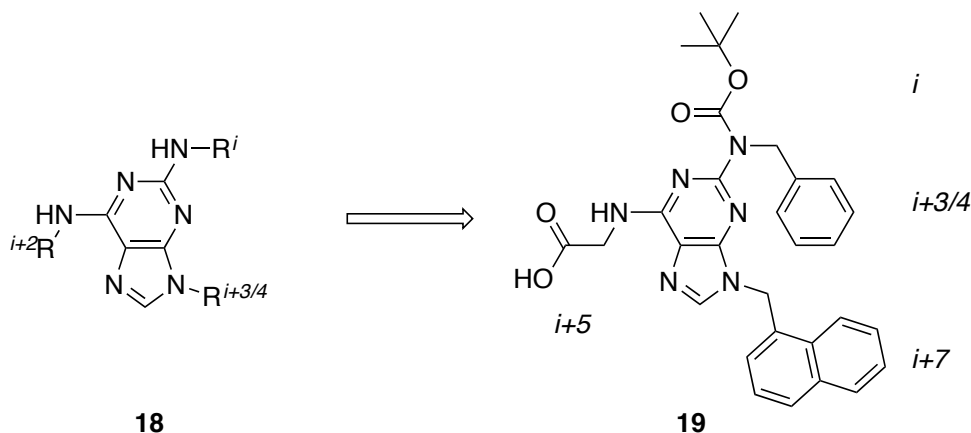


Figure 1.16: 2,6,9-Tri-substitution of a purine scaffold permits the mimicry of two faces of an α -helix, according to the disruption of the Mcl-1–Bak-BH3 PPI.

1.4.6 Tetrahydro-1H-benzo[e][1,4]diazepines

Benzodiazepines have a rich and privileged history in medicinal chemistry, including in proteomimicry, where they have featured as scaffolds for the mimicry of β -

turns and one face of an α -helix.^{66, 80} Due to the rigid framework and projection of substitutable nitrogen atoms from opposite sides, the Fletcher group considered that tetrahydro-1H-benzo[e][1,4]diazepines (BZDs) could also lend itself to two-faced helix mimicry, reproducing the i , $i + 3/4$ and $i + 7$ side chains on one face, and the $i + 5$ residue on the other (generic structure **20**, **Figure 1.17**).⁶⁷ A small library of appropriately functionalized BZDs was prepared and then assessed for their abilities to disrupt the Bak-BH3-Mcl-1 PPI. The most potent compound was the amphipathic helix mimetic **21**, which inhibited Mcl-1 with a $K_i = 6.67 \mu\text{M}$. The group is currently streamlining the synthetic chemistry to facilitate the assembly of a large BZD library to further interrogate the Bak-BH3-Mcl-1 PPI, as well as other helix-mediated PPIs.

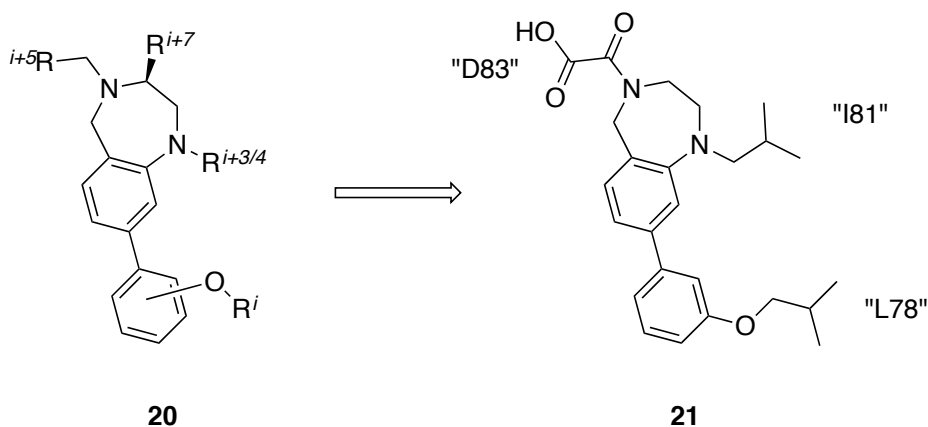


Figure 1.17: In addition to their ability to mimic the epitopes of β -turns and one face of an α -helix, benzodiazepines have been introduced as scaffolds to reproduce functionality displayed from two faces of an α -helix.

1.4.7 Phenyl-Piperazine-Triazine

Towards improving the physicochemical properties of traditional helix mimetics, Lim and co-workers devised a unique helix mimetic constructed from a phenyl-piperazine-

triazine core (generic structure **22**) to target the Bim-BH3 –Mcl-1 PPI.⁶⁸ The authors exploited solid phase chemistry to accomplish rapid diversification, creating a library of 36 compounds. For prototypical compounds in which all three side chains are methyls, the phenyl-piperazine-triazine helix surrogate sports a cLog P of 0.96, which contrasts considerably with the analogous terphenyl scaffold (cLog P = 6.02). The library members were tested for their abilities to inhibit Mcl-1 using an FPCA assay; their most potent compound, **23** (**Figure 1.18**), with $R^1 = R^2 = R^3 = \text{Bn}$, had a K_i of 7.3 μM based on the FP data. Lim's group also evaluated the specificity for Mcl-1 over the related anti-apoptotic Bcl-2 protein Bcl-xL, both of which have similar BH3-binding grooves.^{68, 81} Interestingly, **23** exhibited no affinity to Bcl-xL up to 100 μM , indicating this new helix mimetic is capable of discriminating between the two Bcl-2 proteins. It is unclear if the Mcl-1 selectivity can be attributed to the specific side chains or the scaffold itself since only one library member was evaluated in the selectivity assay. Retrosynthetic analysis of the triazine moiety reveals its origin to be cyanuric trichloride, which may be triply-functionalized, allowing side chains on opposing faces of an α -helix to be emulated. Thus, although this scaffold presently has been used to realize the imitation of only one face of an α -helix, Lim's work inherently provides a platform to achieve two-faced helix mimicry ($i + 5$ position). Finally, the stereogenic center in the piperazine ring (**24**), will permit the investigation into the effect of helix mimetic chirality on protein recognition.

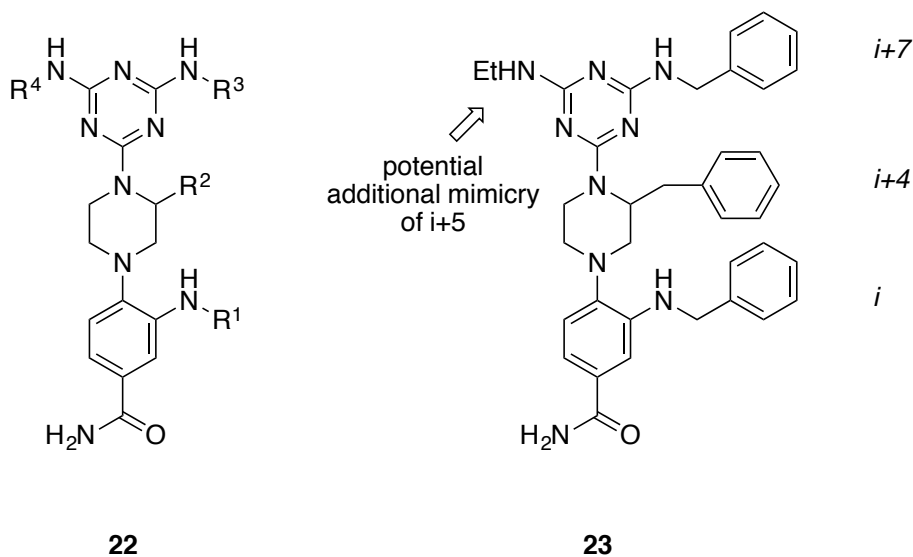


Figure 1.18: A phenyl-piperazine-triazine helix mimetic disrupts the Bim–Mcl-1 PPI. Synthetic strategies to vary the ethyl group should allow the additional mimicry of the $i + 5$ position on the opposing face.

The mimicry of one face of an α -helix with non-peptidic scaffolds is now a well-established field of research, although clinical candidates to disrupt aberrant helix-mediated PPIs remain elusive. Since α -helices often recognize their target proteins through multiple recognition faces, it is considered that the reproduction of functionality from multiple faces of an α -helix might afford more potent and more selective agents. In turn, it is reasoned that such multi-facial helix mimetics might result in the discovery of potential therapeutic agents suitable for advancement into preclinical development. Further discussion of this field will be given in **Chapter 3** and **6**.

1.5 Targeting the BCL-2 Family: BCL-2 and BCL-x_L

Targeting BCL-2 and BCL-x_L with a potent, selective inhibitor has long been a goal of cancer research, especially since the BCL-2 family's role in apoptosis was elucidated as a major contributor in cancer progression. The BCL-2 protein plays a dominant role in the

survival of lymphoid tumors when overexpressed, however, the overexpression of BCL-x_L has been correlated with drug resistance and disease progression of multiple solid tumors and hematological malignancies.^{21, 82} Several laboratories undertook this task to develop small molecule mimetics of the pro-apoptotic proteins, dubbed BH3 mimetics.

1.5.1 Abbott Laboratories

The first of its class was ABT-737 (**24**) from the Abbott laboratory. First developed in 2005, and found by using structure activity relationship (SAR) by NMR (high-throughput fragment-based NMR screen using a chemical library).^{60, 83} This method identified small molecules that bound to BCL-x_L, and through several rounds of SAR found ABT-737 (**Figure 1.19**).^{60, 83} This compound binds with high affinity for BCL-x_L, and BCL-2 ($K_i \leq 1\text{nM}$), which as previously mentioned have high sequence homology, but binds MCL-1 (a less homologous protein of the BCL-2 family) with a $K_i > 1\ \mu\text{M}$.⁶⁰ They found that the molecule bound in the p2 and p4 pocket of BCL-2 and BCL-x_L and the acyl sulfonamide, was designed to engage R146 or R139 respectively.^{60, 84} Fairlie and co-workers later crystalized (PDBID: 2YXJ) **24** bound to BCL-x_L, which showed that the acyl sulfonamide did not form an hydrogen bond interaction with Arg139.³⁴ **24** initiated apoptosis through the intrinsic pathway and was shown to inhibit the BCL-2 proteins as the initiator BH3 pro-apoptotic proteins (i.e. BAD) do. However, while **24** was a potent inhibitor of various cancer cell lines, it depleted platelets in the RBC causing rapid thrombocytopenia. In the presence of 10% serum, ABT-737 maintained potency for BCL-2 and BCL-x_L with IC₅₀'s of 103 nM and 35 nM respectively. As use as a single agent, **24** was tested in a subset of cancer cell lines representing lymphoid malignancies and SCLC.^{60, 85-86} Next they tested against primary patient derived follicular lymphoma cells (IC₅₀ 10-

100 nM).^{60, 85-86} In an established SCLC tumor xenograft model, when treated with ABT-737 ($EC_{50} < 1 \mu M$) the tumors did not grow back.⁶⁰ A correlation was found that cells resistant to **24** had higher MCL-1 protein levels.⁸⁵ Resistant cells with high levels of MCL-1 were re-sensitized to **24** through downregulation, destabilization, or inactivation of MCL-1.⁸⁷

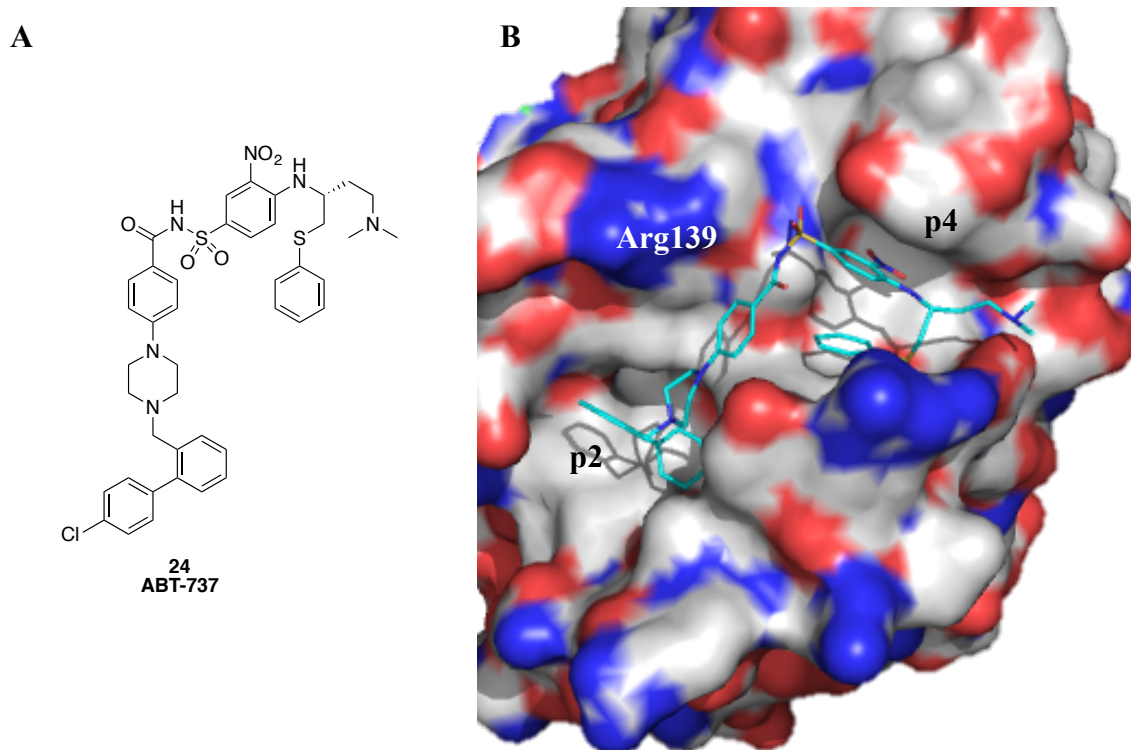


Figure 1.19: (A) ABT-737 a *de novo* small molecule inhibitor of BCL-2 and BCL-x_L. (B) Crystal Structure of ABT-737 with BCL-x_L. (PDBID 2YXJ).

Ultimately ABT-737 was not orally bioavailable and had low aqueous solubility, which limited the formulation of the drug. This led Abbott to discover ABT-263 (**25**), an orally bioavailable version of ABT-737.

After a thorough SAR of **24**, an orally bioavailable molecule was discovered (ABT-263, **Figure 1.20**). According to Lipinski's rule of five, small molecules that have a high molecular weight (>500), high number of hydrogen bond donors or acceptors (>5 and >10

respectively), and high lipophilicity (clogP) are predicted to have poor oral absorption and low permeability. However, while this made **24** an unlikely drug-candidate, its features were important for its pharmacological activity, i.e. inhibiting a large protein surface area.

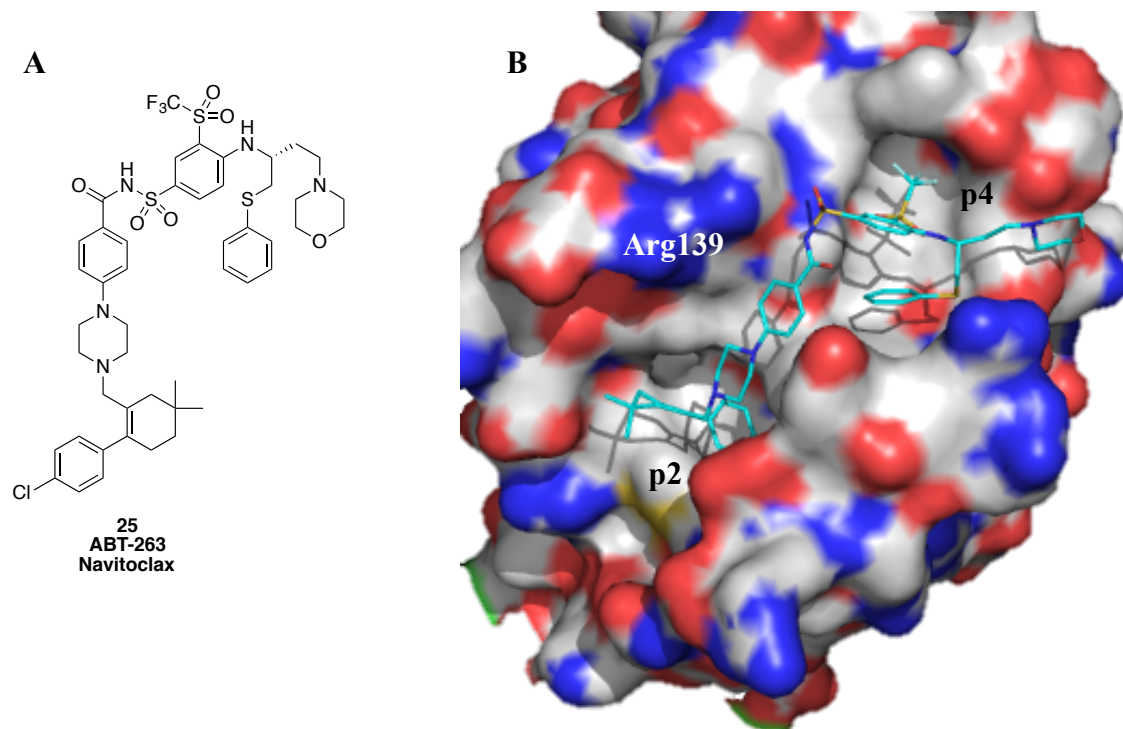


Figure 1.20: (A) ABT-263 (Navitoclax) an orally bioavailable small molecule BH3 mimetic of the BCL-2 pro-apoptotic family to inhibit BCL-2 and BCL-x_L. (B) Crystal Structure of ABT-737 with BCL-x_L. (PDBID 4LVT).

Elmore and co-workers discovered that making small changes to pK_a values would enhance oral absorption, such as replacing the nitro group for a trifluoromethylsulfonyl group increased oral absorption by 16-fold. They then looked at replacing the dimethylamino group from ABT-737, which was found to be a major route for metabolism and ultimately was replaced by a morpholino group and finally the 4-chlorobiphenyl moiety was modified to a 4'-chloro-4,4-dimethyl-2,3,4,5-tetrahydro-1,1'-biphenyl group. In total, they made three substantial changes to identify ABT-263 (**25**) or Navitoclax, which

has a similar binding profile to ABT-737, but has a 20-fold improvement in oral absorption.⁸⁴ The SAR helped improve the PK/PD profile, which is represented by the ratio of AUC/EC₅₀ *in vivo* and avoided toxic metabolites associated with nitro functional groups.⁸⁸ Elmore and co-workers showed that Navitoclax induced apoptosis through the inhibition of the BCL-2 family proteins. Both **24** and **25** enhanced the activity of chemotherapeutic agents, such as carboplatin/etoposide and ABT-737 or rituximab and ABT-263, but also are robust single agent therapies.^{85, 88} ABT-263 (**25**) induced a rapid onset of thrombocytopenia in a dose dependent manner that was reversible.⁸⁸ In the last decade it has been shown that both **24** and **25** are very potent inhibitors in chronic lymphocytic leukemia (CLL) and induce rapid and extensive apoptosis in primary CLL cell lines.⁸⁹

Early signs of thrombocytopenia occurred while ABT-263 (**25**) was in phase II clinical trials⁹⁰⁻⁹¹, so Souers and co-workers hypothesized a BCL-2 selective inhibitor would reduce platelet depletion, while maintaining efficacy. They concluded a selective BCL-2 inhibitor would improve toxicity because BCL-x_L is required for platelet survival.⁹²⁻
⁹³ Using a BCL-2-small molecule co-crystal structure to guide rational design, they discovered compound **26 (Figure 1.21)**.⁹⁴ Souers and co-workers modified the trifluoromethylsulfonyl moiety back to the nitro group of ABT-737 (**24**), shifting the 4,4-dimethyl group on the 1-chloro-4-(4,4-dimethylcyclohex-1-enyl)benzene moiety to the 5 position. These changes led to an inhibitor that remarkably crystallized with two proteins as a dimer. The Trp30 of one BCL-2 protein interacts through pi-stacking with the nitro-aryl functional group, and the nitrogen from the indole on the Trp30 forms a hydrogen bond with Asp103, which is Glu96 in BCL-x_L one of the few residue differences between

the BH3 binding domains of the two proteins.

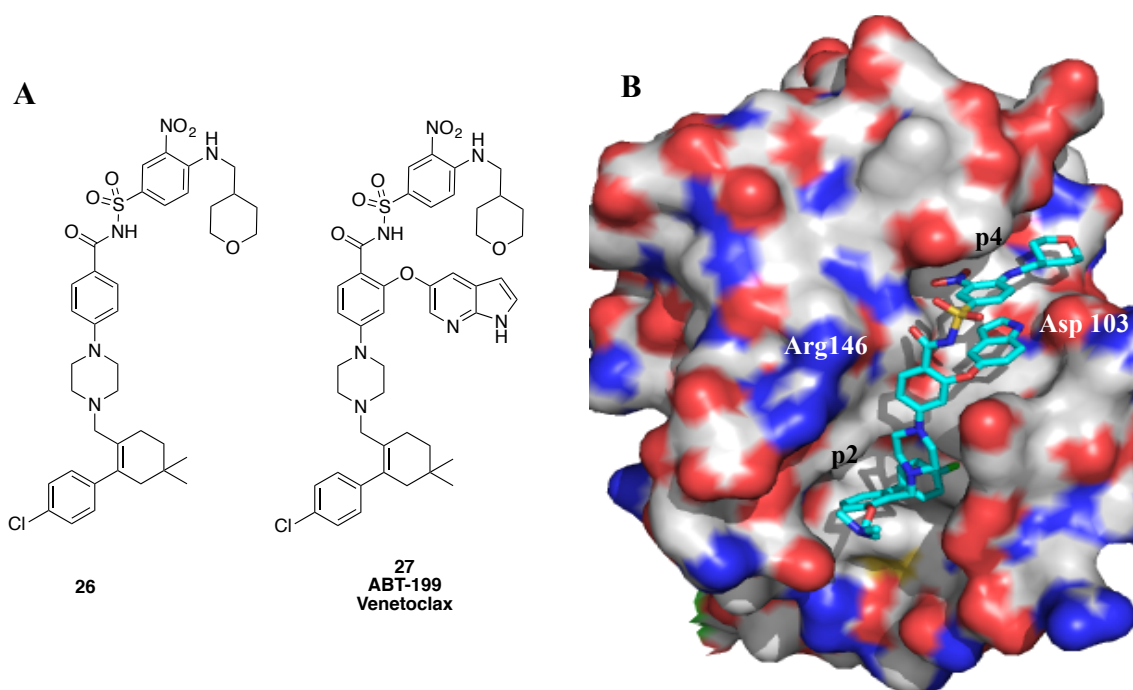


Figure 1.21: (A) ABT-199 a BCL-2 selective inhibitor. Recently approved by the FDA for treatment of CLL. (B)

To mimic the interactions they were seeing from the tryptophan in their crystal structure, they introduced an azaindole ether linkage, and thus ABT-199 (**27**) was developed as a highly potent and selective BCL-2 inhibitor.⁹⁴ **27** binds and inhibits BCL-2 with sub-nanomolar affinity ($K_i < 0.010$ nM) in a time-resolved fluorescence resonance energy transfer (tr-FRET)⁹⁴, but binds BCL-x_L less with a $K_i = 48$ nM and has little affinity for MCL-a ($K_i > 444$ nM). They showed **27** induces intrinsic apoptosis as its mechanism of action in a dose dependent manner *in vitro* and in tumor regression *in vivo* using xenograft mice models.⁹⁴⁻⁹⁶ To test their original hypothesis that a selective BCL-2 inhibitor will alleviate the effects of thrombocytopenia, they evaluated both Venetoclax (**25**) and **27** on human platelets *ex vivo* and saw that **27** was much less active with an EC₅₀

= 5.5 μ M versus an average EC_{50} = 0.083 μ M for **25**. Given orally *in vivo*, **27** has minimal effects on circulating platelets. Ultimately, **27** was shown to induce apoptosis in primary CLL cell lines and in 3 patients in a clinical trial, effectively establishing BCL-2 inhibition as a valid cancer therapy. ABT-199/Venetoclax (**27**) was recently FDA approved as a treatment for CLL.^{21, 94}

1.5.2 Genetech

Abbott has well defined inhibitors for the BCL-2/BCL-x_L binding pocket, which has led several other labs to develop selective inhibitors for these proteins. First, a collaboration between Genetech and several Universities in Australia led to the development of a potent and specific BCL-x_L inhibitor, and has a higher specificity as compared to MCL-1 and BCL-2 as it is overexpressed in several cancers and a potential mode of resistance.⁶¹ However, there is no naturally occurring pro-apoptotic protein that exclusively binds BCL-x_L and they devised a new scaffold through a high throughput screen (HTS). They used these compounds in crystal structures with BCL-x_L to develop and give insight into the mechanism of binding. The HTS was performed and the hits were screened against both MCL-1 and BCL-x_L to identify lead compounds, which contained a benzothiazole-hydrazone core. It was found like MCL-1, BCL-x_L has a high degree of plasticity around the p2 pocket that can be targeted by small molecules, that the BH3 pro-apoptotic peptides cannot interact.⁶¹ Through several thorough SARs they developed WEHI-539 (**Figure 1.22**), and from a co-crystal structure showed that **28** binds to the p2 and p4 pocket,⁶¹ while forming a salt bridge with Arg139 through the acid and nitrogen atom on the thiazole ring. WEHI-539 forms key binding interactions with Leu108, Ser106, Arg139, and Glu96.⁶¹ These interactions were confirmed through the crystal structure of

28 bound to BCL-x_L.

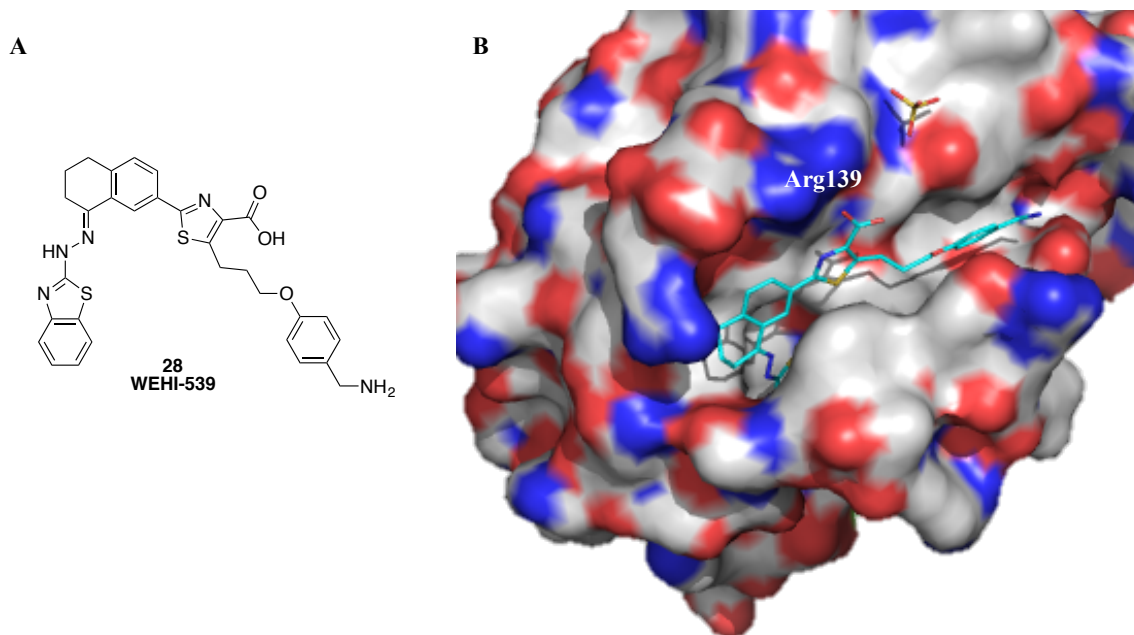


Figure 1.22: (A) WEHI-539: A potent BCL-x_L inhibitor found through SAR. (B) Crystal Structure of WEHI-539 bound to BCL-x_L. (PDBID 3ZLR).

It was determined that **28** binds BCL-x_L with an IC₅₀ = 1.1 nM and exhibits superior cellular activity compared to previous molecules in the series.⁶¹ **28** binds to BCL-2, BCL-x_L, and MCL-1 with K_{DS} of > 750 nM, 55 nM, and >550 nM respectively. It was determined that their molecules trigger apoptosis through the intrinsic pathway by the release of cyt-c and downstream activation of caspase-3. As with previous BCL-2/BCL-x_L inhibitors the presence or overexpression of MCL-1 prevents apoptosis in the presence of **28**, and causes thrombocytopenia *in vitro*. While further biological studies for WEHI-539 will not be pursued, this compound will be valuable tool to study the effects of inhibiting BCL-x_L.⁶¹

A derivative of WEHI-539 (**28**), A-1155463 (**29**) from Abbvie (a subsidiary of Abbott), Genetech and the laboratories in Australia developed a new potent BCL-x_L inhibitor. They replaced the toxic hydrazone moiety with an amide functional group and

improved the physiochemical properties so dosing would be possible. To replace the p4 binder they performed SAR by NMR fragment-based design and discovered A-1155463 (**Figure 1.23**) that binds to BCL-x_L with a K_i of < 0.01 nM and BCL-2 with a K_i of 88 nM, which is over a 1000 fold decrease in binding affinity for BCL-2. They ultimately, were able to show different dependencies towards BCL-2 and BCL-x_L from a panel of SCLC and AML cell lines.⁹⁷ Within 6 h of dosing platelet counts dropped drastically, but recovered fully within 72 h, likely owing to inhibition of BCL-x_L in platelets.

A-1155463 was optimized further to develop an orally bioavailable analogue A-1331852. As a BCL-x_L selective inhibitor, it caused reversible thrombocytopenia *in vivo*, which corroborates the previously mentioned pharmacological contributions from such inhibition.⁹⁷ When co-administered *in vivo*, the response in strength and longevity helped improve docetaxel. It has been previously shown that BCL-2 inhibition was responsible for the adverse effect associated with neutropenia when Navitoclax was dosed with docetaxel. From this information there might be a clinical opportunity to use A-1331852 in combination with docetaxel without causing neutropenia⁹⁷

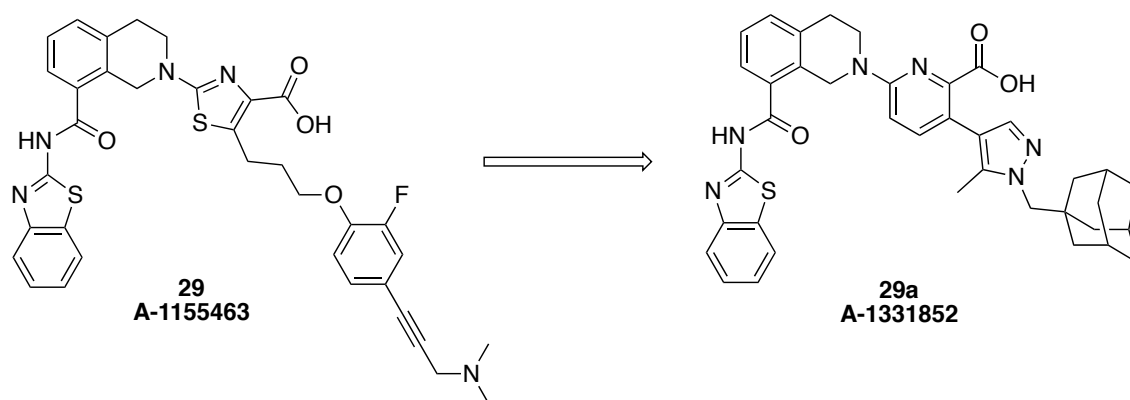


Figure 1.23: Abbvie and Genetech further developed a selective and potent BCL-x_L inhibitor.

1.5.3 Pan-BCL-1 Inhibitors

Gossypol (**30**), a natural product, was first isolated from *Gossipium sp.*, but until recently, its use as a cancer therapeutic had not been established.⁹⁸ It was discovered that (-)-gossypol exhibited *in vitro* cell growth inhibition against various cancer cell lines,⁹⁹⁻¹⁰² and *in vivo* tumor regression activity.¹⁰³⁻¹⁰⁴ The inhibition of the BCL-2 family of proteins by **30** (**Figure 1.24**) played a significant role in triggering the apoptosis pathway in cancer cells. It is known that more complicated mechanisms are responsible for the anti-tumor activity both *in vitro* and *in vivo*. This includes causing DNA degradation,¹⁰⁵ generating reactive oxygen species (ROS),¹⁰⁶ and modifying VEGF signaling-mediated angiogenesis.¹⁰⁷

Since the initial isolation of gossypol, several laboratories have undertaken designing and synthesizing analogues including apogossypol (**31**) and apogossypolone (**32**, **Figure 1.24**). Apogossypolone was found experimentally to be a pan-BCL-2 inhibitor with K_i 's for BCL-2 = 76 nM, BCL-x_L = 1.27 μM, and MCL-1 = 51 nM.¹⁰⁸ When tested in cells, **32** exhibited cell growth inhibition against hepatocellular carcinoma, and diffuse large cell lymphoma cells; it also demonstrated tumor regression in their xenograft mice model *in vivo*.¹⁰⁹⁻¹¹¹ Apogossypolone was shown to be less toxic than parent compound **30** and displayed stronger single agent activity, which suggests that removing the aldehyde functional group was beneficial.¹¹²

There have been several reports in the literature about structure-based designs of small molecules to mimic the interaction between gossypol and the BCL-2 proteins, which is represented by TW-37 (**33**, **Figure 1.24**) from Wang and colleagues. TW-37 was shown to interact with BCL-2, BCL-x_L, and MCL-1 with K_i 's = 290 nM, 1.11 mM and 260 nM,

respectively. From molecular modeling simulations, the polyphenol group was predicted to form polar interactions with R146, and N143 of BCL-2, with the tert-butyl benzene sulfonyl moiety occupying the p2 pocket. **33** inhibited growth of PC-3 cancer cells *in vitro* with evidence suggesting the apoptosis pathway is becoming activated.¹¹³

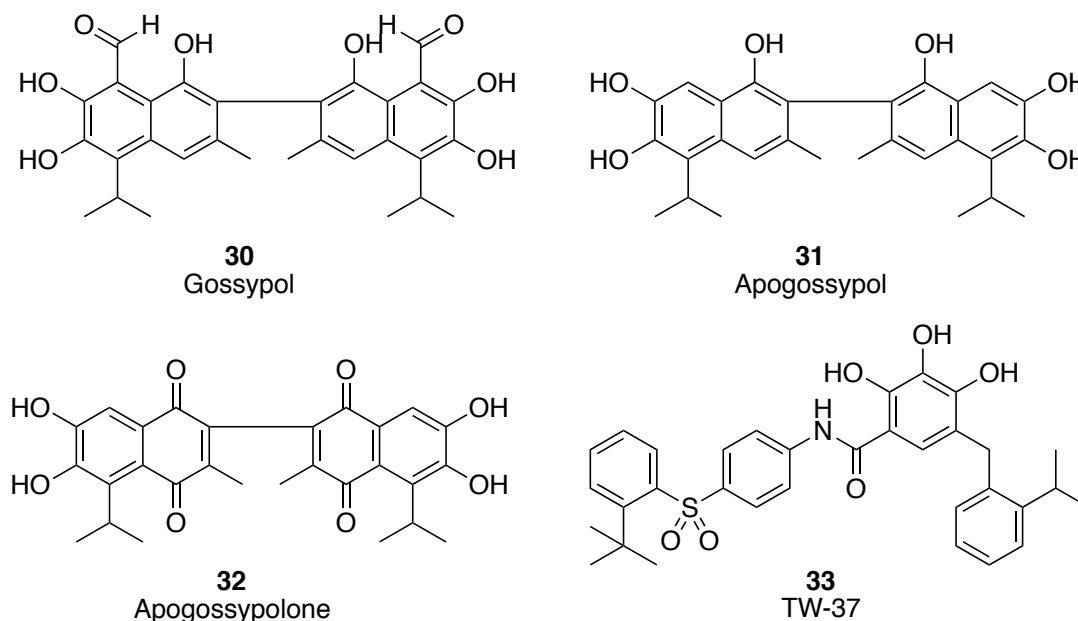
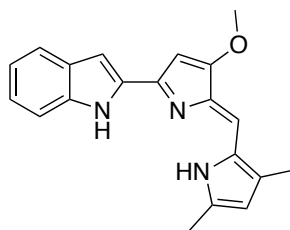


Figure 1.24: Structures of gossypol and analogues.

GeminX Pharmaceutical's developed a pan-BCL-2 (**34**) inhibitor, that was determined to bind BCL-2, BCL-x_L, and MCL-1 in the FPCA with IC₅₀s = 1.11 μM, 4.69 μM, and 2.90 μM respectively (**Figure 1.25**).¹¹⁴ It was shown *in vitro* that Obatoclax (**34**) inhibits cells growth activity in various pre-clinical studies against mantle cell lymphoma (MCL), non-small cell lung cancer (NSCLC) and multiple myeloma (MM).¹¹⁵⁻¹¹⁷ Some evidence suggested that the mechanism of action was not only through the intrinsic pathway.¹¹⁸⁻¹¹⁹ The uncertainty of the mechanism of action increased its toxicity risk during clinical development. Obatoclax has been investigated in several clinical trials targeting

advanced hematologic malignancies and solid tumors.¹²⁰⁻¹²¹ Currently, obatoclax is no longer in clinical trials due to dose limiting toxicity.¹²²



34
GX15-070
Obatoclax

Figure 1.25: A pan-BCL-2 inhibitor from GeminX Pharmaceutical.

1.6 Targeting the BCL-2 Family: MCL-1

Since the early 2000s there has been significant advancement made in targeting BCL-2 and BCL-x_L by small molecule BH3 mimetics. However, limited progress had been made towards inhibition of MCL-1, which was shown to be a major mechanism of resistance against numerous anticancer therapies when upregulated or overexpressed.¹²³ The amplification of MCL-1 is the one most common genetic aberrations observed in human cancer, and a lack of inhibitors in clinical trials has subsequently made it an attractive target for inhibition.¹²⁴⁻¹²⁵ Recently, focus has shifted towards MCL-1 and groups started developing inhibitors through both structure and fragment-based drug design.

1.6.1 Abbvie

Abbvie has been a pioneer in the BCL-2 family since the early 2000's so after developing potent inhibitors against BCL-2 and BCL-x_L, the next logical target was MCL-

1. From their 2008 patent, they used the same process as with the other proteins in the family, by employing a NMR-based fragment screen.¹²⁶ They tested 17,000 molecules in batches of 30 and the top NMR binders were classified by FPCA affinity, synthetic feasibility, and for binding efficiency.^{62, 127} Based on the classifications, aryl sulfonamides and salicylic acids were moved into SAR studies. They were able to obtain a crystal structure (**Figure 1.27**) with both lead fragments, but also determined the binding mode through NMR NOE studies.¹²⁸⁻¹²⁹ From the proposed binding mode, they modified the para-position on the aryl sulfonamide first followed by modifications to the salicylic acid. They synthesized a small library with the most potent compound (**35**) having an $IC_{50} = 0.4 \mu M$, and subsequent changes to the sulfonamide moiety yielded compound **36** with an $IC_{50} = 0.03 \mu M$ (**Figure 1.26**). Next making changes to the salicylic acid yielded a lead compound (**37**) with an $IC_{50} = 3.3 \mu M$. Several novel scaffolds were discovered from this NMR-based screen, indicating that inhibiting MCL-1 with a small molecule is possible.¹²⁷⁻

129

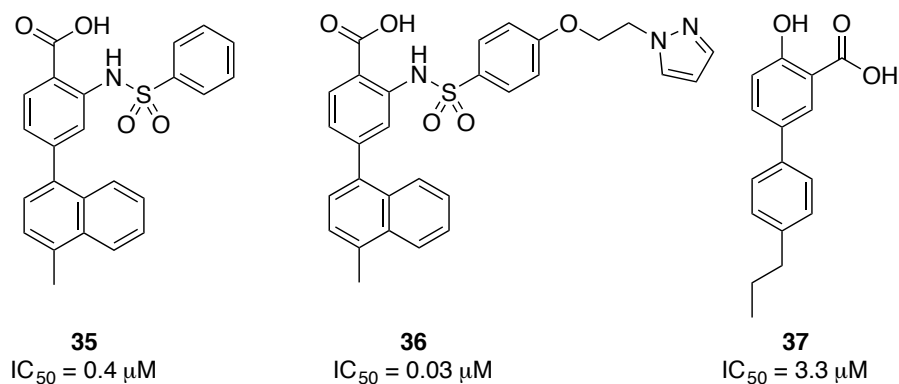


Figure 1.26: Abbvie's MCL-1 selective inhibitor that binds the p2 pocket and interacts with Arg263.

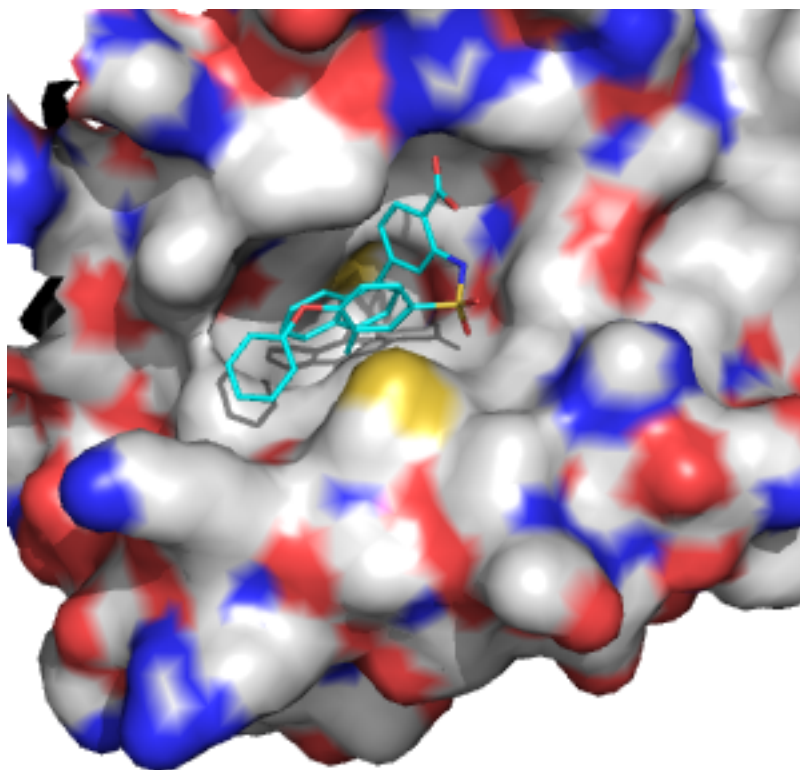


Figure 1.27: Crystal structure of **36** bound in the p2 pocket of MCL-1. (PDBID 4OQ5)

Abbvie has continued to further develop MCL-1 inhibitors derived from a HTS. The parent compound (**38**) has low micromolar affinity, a clogP of 2.13, and after subsequent SAR developed the final compound (**39**).¹²⁸⁻¹²⁹ With the core having a low clogP, it makes it a good candidate to be delivered orally. As seen in **Figure 1.28**, the core molecule is prime to build off at multiple positions, so Souers and co-workers started at the C3 position and optimized linker length and hydrophobic moiety. Crystal structures showed that the moiety off the C3 position binds into the p2 pocket with the indole NH pointing towards the p3 pocket and the carboxylic acid interacts forming a salt bridge with Arg263.¹²⁷⁻¹²⁹ With increased binding affinity they looked to extend the interactions within the binding groove and optimized the C7 position with tolyl groups moving the methyl group to garner increased affinity. However, they also attached trisubstituted pyrazoles,

which increased the binding affinity more than the o-tolyl group. The final step in optimization was transforming the N1 of the indole by adding a solubilizing group off a three-carbon linker. Their completely optimized compounds (**39**, **40**) have K_i 's of 0.43 nM and 0.45 nM respectively.¹²⁷⁻¹²⁹ While they have a higher molecular weight (> 500), this is no longer a major concern as ABT-199 was FDA approved for CLL. They moved compound **39** into cell assays and the most potent compound has an IC₅₀ of 6.0 nM.

Compound **39** is selective for MCL-1 over the other anti-apoptotic proteins ($K_i > 0.66 \mu\text{M}$) in a tr-FRET assay and inhibits cell growth as a single agent (EC₅₀ = 917 nM in BxPc-3 cell lines), but can synergize with ABT-263 (EC₅₀ = 19.2 nM in BxPc-3 cell lines). Compound **40** demonstrated on-target effects to trigger apoptosis intrinsically. Differences *in vitro* vs cell growth inhibition were attributed to serum binding coupled with the zwitterionic nature of the molecule and likely limited cell penetration.¹²⁷⁻¹²⁹

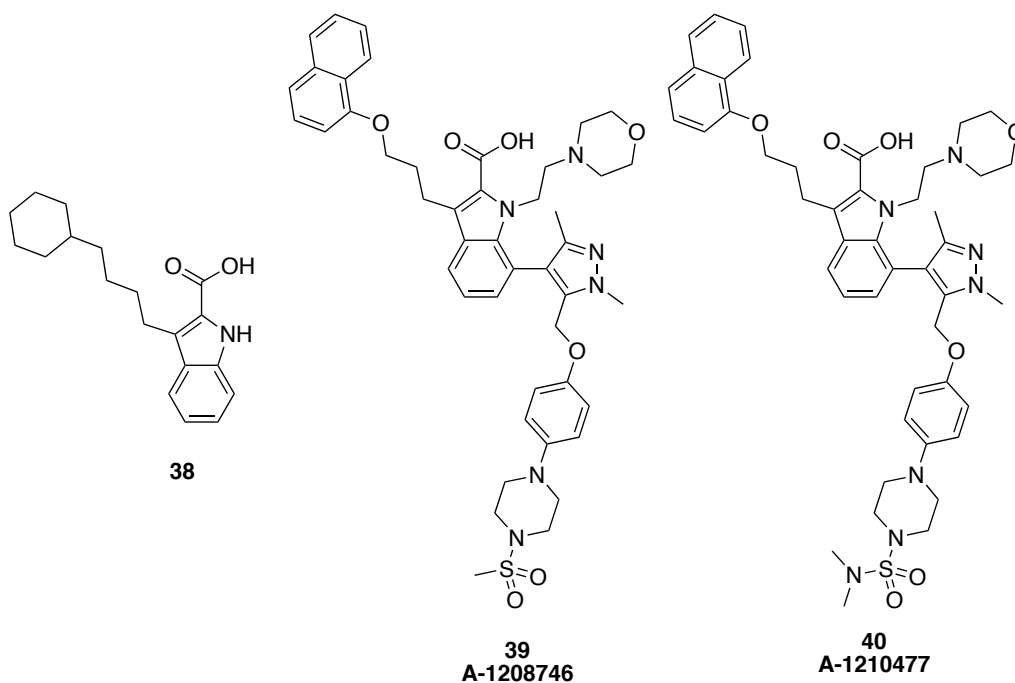


Figure 1.28: Abbvie's potent and selective MCL-1 inhibitors.

1.6.2 Vanderbilt University (Fesik's Laboratory)

Fesik and co-workers took a similar approach as with the development of ABT-263, using a NMR-based fragment screen, discovered two distinct classes of molecules that bound MCL-1 in two different pockets.³³ However, their work is very similar to that from Abbott who utilized an indole core.^{62, 127-129} They determined that class I bound above class II which occupied a deeper position within the p2 pocket. They merged the two classes of molecules to obtain a potent inhibitor with greater binding affinity than the two moieties separately (**Figure 1.29**).³³ Aided by crystal structures and NMR binding data, a complete SAR was utilized to optimize each fragment class individually and then merged fragments were adjusted. From the SAR, it was found that the size, substitution pattern and hydrophobicity of the aromatic groups are essential when binding MCL-1.³³ The optimized merged fragments and the best compound **43** binds into the p2 and p3 pockets with submicromolar affinity (320 nM) and have selectivity for MCL-1 over BCL-2 and BCL-x_L. For future work, expansion into unoccupied pockets is hypothesized to give better binding affinity.³³

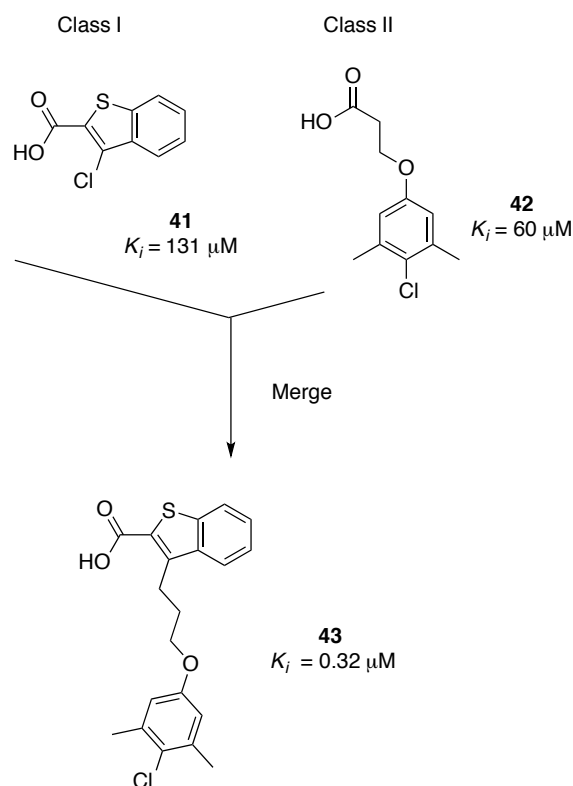


Figure 1.29: Fesik and co-workers MCL-1 selective inhibitor with submicromolar inhibition. Individual classes and then merged to final potent inhibitor.

As a follow-up to the initial class of MCL-1 selective inhibitors, Fesik and co-workers used a fragment-based approach and blocked the p2 pocket with their previous molecule, while interrogating fragments that would bind into the p4 pocket. A small library of fragments was identified that occupied the p4 pockets and linking to the initial compound was proposed through a acylsulfonamide linker.¹³⁰ They in fact showed an ability to link the p2 and p4 pockets to create an initial lead molecule (**44**) that has increased affinity for MCL-1 and the sulfonamide was able to replicate the hydrogen bonding that carboxylic acid formed with Arg263 (**Figure 1.30**).¹³⁰ To optimize the sulfonamide moiety they used phenyl and pyridyl moieties. They developed picomolar inhibitors, which

they determined through development of a fluorescein label incorporated into their molecules and then tested by tr-FRET.^{33, 130} The most potent molecule (**45**) has a $K_i = 0.36$ nM when it competed off the molecule with the fluorescein incorporated into it. They obtained a crystal structure of **45** bound to MCL-1 to confirm the binding mode and interactions with Arg263, the p2 and p4 pocket. The compounds had a high serum binding, however to circumvent this issue, they replaced in the furan ring with a 4-pyridyl moiety.¹³⁰ This had a desired effect of reducing serum binding, but compounds still had low cell permeability. All of the compounds had a selectivity profile of >500 for MCL-1 versus BCL-xL.¹³⁰ The ability to correlate *in vitro* data to cell data requires picomolar MCL-1 inhibition, which Fesik et al. exhibited, but also requires low serum binding. They showed that using a more rigid linker to reach the p4 pocket reduced the number of rotatable bonds and therefore the entropic penalty upon binding to the MCL-1 protein.¹³⁰⁻¹³¹

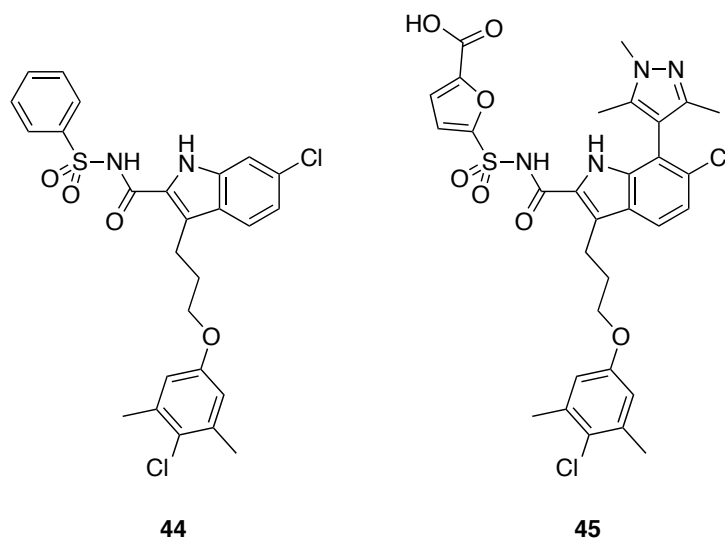


Figure 1.30: Fesik's second-generation indole inhibitors extend into the p4 pocket utilizing acylsulfonamides.

The culmination of Fesik's work expanded upon their previous substituted indoles

through rigorous SAR studies to develop (**46**, **Figure 1.31**), which was 20-fold more potent than previously mentioned **45** in the presence of 1% FBS, indicating this molecule has lower non-specific serum binding.¹³¹ After obtaining a crystal structure of **46**, the molecule carboxylic acid interacts with Arg263. **46** binds MCL-1 with an $K_i = 23$ nM and in the presence of 1% FBS 108 nM.¹³¹ After some SAR, Fesik and co-workers reduced the number of rotatable bonds within the substituted indoles, which yielded potent molecules that have cell activity and low serum binding (**47**, **48**). Compounds **47** and **48** bind MCL-1 with a $K_i = < 1$ nM as determined by a tr-FRET assay, and in the presence of 1% FBS maintained low nanomolar inhibition (2.3 and 2.8 nM respectively).¹³² In cells, both compounds inhibit H929 cells with low μ M inhibition ($GI_{50} = 1.4$ and 2.0 μ M respectively). When the authors removed the acid from their compounds, a ten to a 100-fold decrease in affinity was observed, but they did not show the data.¹³¹

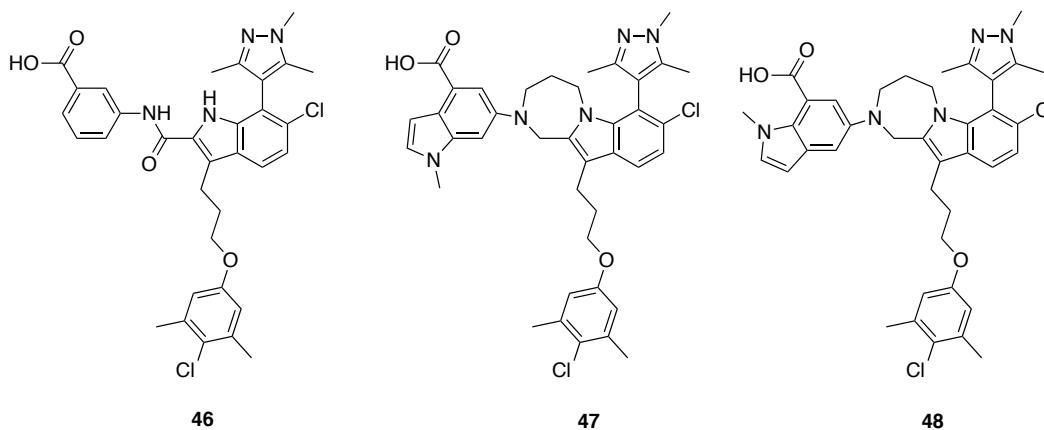


Figure 1.31: MCL-1 small molecule inhibitors with picomolar activity, cell activity, and low serum binding from the Fesik group.

1.6.3 Servier Research Laboratories

Recently, Servier Laboratories developed S63845 (**49**, **Figure 1.32**) that is well

tolerated in several cancer models. They found that compound **49** binds MCL-1 with a K_d of 190 pM.⁶³ They tested to see their molecule would induce apoptosis through the intrinsic pathway of BCL-2 dependent cell lines. **49** killed H929 cells, which are dependent on MCL-1 and is 1,000-fold more potent than A-1210477 (**40**), an Abbvie compound.⁶³ Selectivity towards MCL-1 was confirmed through co-immunoprecipitation (Co-IP) experiments and showed the compound had no impact on BCL-2 or BCL-x_L. They tested **49** in hematological cancers, 25 MM cell lines and found 17 were highly sensitive with an $IC_{50} = <0.1 \mu\text{M}$. High selectivity for 5 CML cell lines were obtained with an $IC_{50} = <0.1 \mu\text{M}$ and in AML cell lines with an $IC_{50} = 4\text{-}233 \text{ nM}$.⁶³ In AML patient samples it was shown that compound **49** could be used as a single agent and in solid tumors was moderately effective. *In vivo* models looked at the effects on several organs and multiple blood-cell subsets at a dose of 25 mg/kg, which is highly efficacious against mouse tumors.⁶³ Since this data was published S63845 or MIK665 is entering Phase I clinical trials, but not yet accepting patients.

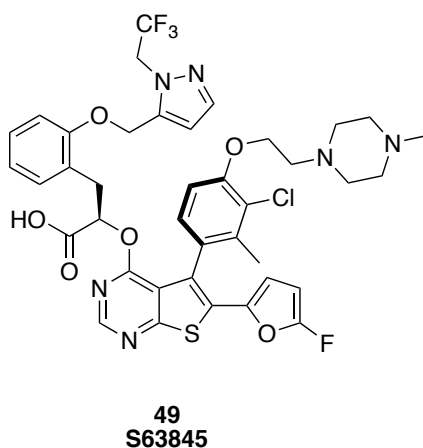


Figure 1.32: Servier Research Institutes MCL-1 selective inhibitor with sub-nanomolar affinity and cell activity.

1.6.4 University of Michigan (Nikolovska Coleska's Laboratory)

Nikolovska-Coleska at the University Michigan has developed MCL-1 inhibitors based on a hydroxyl-naphthalene core. Using a HTS of 53.5K small molecules in a FPCA assay. The lead compound **50** has a K_i of $1.55 \pm 0.18 \mu\text{M}$ and is primed to undergo an SAR (Figure 1.33).^{65, 133} They synthesized 46 molecules optimizing the sulfonamide and then the 2C position. The most potent compound **51** has a $K_i = 0.18 \pm 0.05 \mu\text{M}$ from the FPCA assay and an $\text{IC}_{50} = 1.45 \pm 0.29 \mu\text{M}$ in the SPR assay.^{65, 133} They next moved the optimized lead into biological assays first using a pull down and showed that their molecule disrupted the Noxa-MCL-1 interaction. After they tested for cell viability, which **51** showed potent cell killing ability.^{65, 133} Future work has shown that an analogue (**52**), has efficacy in a BxPC-3 xenograft model of pancreatic cancer.^{65, 133}

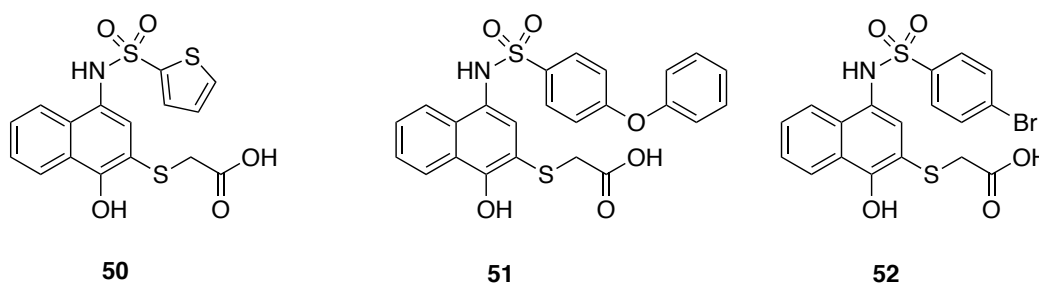


Figure 1.33: University of Michigan MCL-1 selective inhibitors based on a 1-hydroxynaphthalene core.

1.6.5 Amgen

Amgen recently disclosed their MCL-1 selective inhibitor that is based on a tetrahydronaphthalene scaffold (Figure 1.34). In the patent covering this class of molecules they synthesized 83 molecules and subjected them to biological evaluation *in vitro* and in

cellular assays (luciferase) and human MM cells (OPM2).¹³⁴ To obtain **53**'s binding affinity for MCL-1 they used a TR-FRET assay ($IC_{50} = 0.25$ nM). In cells they test the compound and then in the presence of 10% FBS.¹³⁴ Compound **53** was found to bind MCL-1 with an $IC_{50} = 31.2$ nM in the luciferase assay, and $IC_{50} = 259.9$ nM in OPM2 cells. Lastly, they evaluated **53** *in vivo* using an OPM2 xenograft mice model and it was found to have a dose dependent effect on tumor regression with a 10 day course.¹³⁴ **53** was administered IP and PO (25 mg/kg) and showed more shrinkage than Bortezomib (1 mg/kg).¹³⁴ Currently AMG-176 has entered clinical trials and is currently accepting patients.

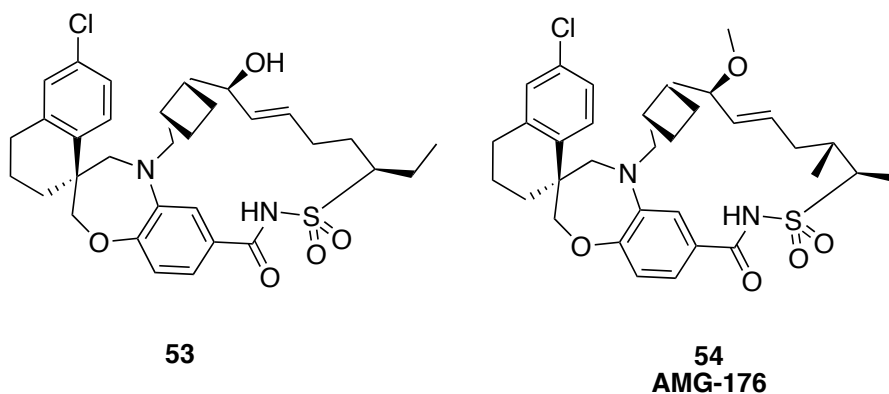


Figure 1.34: Amgen's MCL-1 selective inhibitors entering phase I clinical trials.

1.7 Conclusions

There has been significant progress made in targeting MCL-1, and a lot has been learned about what is needed to make a selective and potent MCL-1 inhibitor. Abbvie, Fesik, Servier, Amgen and U of Michigan have elucidated that to have cellular activity, picomolar *in vitro* activity is required.^{63, 128, 131, 135} These groups have made significant strides towards this goal, but as yet only Servier and Amgen have progressed a compound to Phase I clinical trials. This shows how difficult MCL-1 inhibition is and how more research is

needed in this area. Inhibition of the BCL-2 family of proteins has been a long road with nominal successes. Over the past several decades a lot of progress has been made in targeting this family, with several BCL-2 and BCL-x_L inhibitors making it to clinical trials and FDA approval. The Fletcher lab has undertaken targeting this family of proteins and herein my work towards inhibition of this family will be presented.

Chapter 2 Structure-Based Design of N-Substituted 1-Hydroxy-4-Sulfamoyl-2-Naphthoates as Selective Inhibitors of the MCL-1 Oncoprotein

The B-cell lymphoma-2 (Bcl-2) family of proteins regulates the intrinsic apoptosis pathway that is responsible for programmed cell death, or apoptosis. The pathway involves protein–protein interactions (PPIs) between pro-apoptotic members of the Bcl-2 family, such as Bim, Bak and Bad, and anti-apoptotic members, such as Bcl-x_L and myeloid cell leukemia-1 (Mcl-1).^{16, 141} More specifically, through conserved hydrophobic crevices, the anti-apoptotic Bcl-2 proteins capture the BH3 α -helical domains of their pro-apoptotic counterparts, effectively “neutralizing” their cell killing functions. Evasion of apoptosis is a hallmark of cancer, and is also one culprit for the development of resistance to current chemo- and radiotherapies.¹⁴² More than a decade of research has seen the emergence of potent inhibitors of Bcl-x_L, including the prototypical BH3 mimetic ABT-737.^{60, 89, 143} In particular ABT263, or Navitoclax, which is a dual inhibitor of Bcl-x_L and Bcl-2, but not of Mcl-1,⁴ has performed well in phase I/II clinical trials for several malignancies, validating the inhibition of the anti-apoptotic Bcl-2 proteins as a strategy to treat cancer.^{90-91, 144-145}

Mcl-1 overexpression and/or amplification of the *Mcl-1* gene immortalizes cells, and has been observed in many human solid tumors, including pancreatic, prostate, cervical, lung and breast cancers,¹⁴⁶⁻¹⁵² as well as B-cell lymphomas and hematological cancers, including acute myeloid leukemia (AML).¹⁵³⁻¹⁵⁴ While Navitoclax continues to perform well in clinical trials, its low affinity for Mcl-1 is a contributing factor to the observed resistance of several tumor cell lines.^{85-87, 127, 155} Moreover, the upregulation of Mcl-1 has been directly linked to the reduced efficacy of several FDA-approved anti-cancer chemotherapies. Meanwhile, Zhang and colleagues demonstrated that RNAi-

mediated downregulation of Mcl-1 decreased tumorigenicity of a mouse xenograft model.¹⁵⁶ Taken together, these findings indicate that the pharmacologic inhibition of Mcl-1 is an attractive, complementary and/or adjuvant strategy towards the execution of cancer cells by re-activating apoptosis.

In a similar vein to the inhibition of Bcl-x_L, it is envisaged that the development of synthetic agents capable of disrupting the interaction between Mcl-1 and the BH3 α -helical “death” domains of pro-apoptotic Bcl-2 proteins will “neutralize” Mcl-1’s cell survival role. Indeed, several groups have implemented this stratagem and successfully developed effective inhibitors of Mcl-1.^{29, 33, 62, 65, 70, 76, 127-128, 157-162} We herein report a structure-based design approach that has led to the discovery of potent inhibitors of Mcl-1 based on a novel 1-hydroxy-2-naphthoate scaffold.

2.1 Design strategy towards 1-hydroxy-4-sulfamoyl-2-naphthoate

Fesik and co-workers recently reported the identification of potent and selective inhibitors of Mcl-1 through fragment-based drug design (FBDD).^{33, 132} Their inhibitor design, for example **1 (Figure 2.1)**, encompasses a hydrophobic bi-aryl scaffold, projected from which is a carboxylic acid that recognizes R263 (bound by D67 of Bim-BH3), and also a hydrophobic linker and “tail” that probes into the p2 pocket (bound by L62 of Bim-BH3).

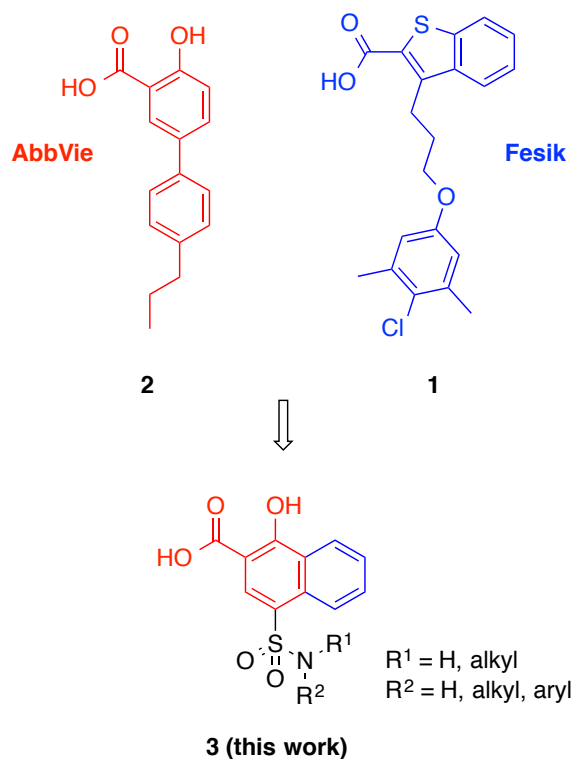


Figure 2.1: Structure-based design of novel 1-hydroxy-4-sulfamoyl-2-naphthoates as Mcl-1 inhibitors.: Structure-based design of novel 1-hydroxy-4-sulfamoyl-2-naphthoates as Mcl-1 inhibitors.

Meanwhile, researchers at AbbVie discovered 5-substituted salicylates, such as **2**, as potent inhibitors of Mcl-1 wherein the carboxylic acid also binds R263 and the 5-substituent delves into the p2 and/or p1 pockets.⁶² Inspired by these reports, we considered that merging the two scaffolds to afford a 1-hydroxy-2-naphthoic acid core would provide a novel and alternate platform from which to inhibit Mcl-1, wherein the carboxylic acid was predicted to bind R263, and the distal phenyl ring towards and/or in the p3 pocket. Further engineering to gain access to the p2 pocket was driven by the hydroxyl group and the carboxylic acid whose *ortho*- and *meta*-directing effects, respectively, synergize to promote the regioselective 4-chlorosulfonylation of the scaffold;¹⁶³ subsequent amination of this readily introduced functional group is expected to facilitate occupancy of the p2

pocket. In addition, although not discussed by Abbvie, we reasoned that the hydroxyl group of their salicylate moiety might promote cell permeability through an intramolecular hydrogen bond that serves to mask the negative charge of the carboxylic acid. Whilst this work was in progress, similar small-molecules derived from 2-((1-hydroxynaphthalen-2-yl)thio)acetic acid were reported to inhibit Mcl-1,^{65, 133} although the present work differs in that the bicycle core is unique and the synthetic route to access target molecules is simpler and shorter (**Figure 2.2**).

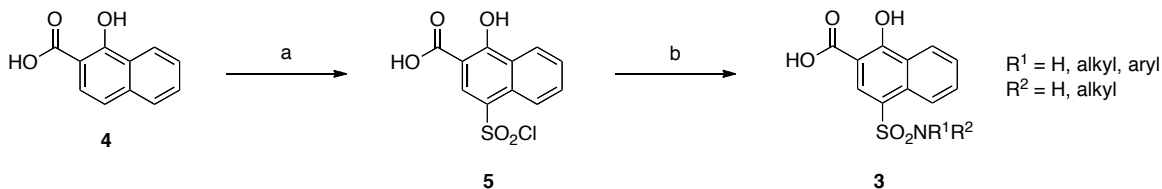


Figure 2.2: (a) ClSO_3H , 0 °C, 1 h; (b) ArNH_2 , pyr, acetone, 50 °C, 3 h or $\text{R}_1\text{NH}_2/\text{R}_1\text{R}_2\text{NH}$, DIPEA, acetone, RT, 5 h.

To facilitate ligand design, the Site Identification by Ligand Competitive Saturation (SILCS) method¹⁶⁴⁻¹⁶⁷ was used. SILCS FragMaps represent the 3D free energy functional group requirements for different types of functional groups in and around the protein. The FragMaps include contributions from solute-protein interactions and both solute and protein desolvation in the context of protein flexibility.¹⁶⁵⁻¹⁶⁶ In addition, to assure that all regions accessible to solute atoms can be occupied by the studied ligands, the protein surface is defined based on SILCS exclusion maps.¹⁶⁸ Notably, the information content of SILCS may be used to qualitatively direct ligand design as well as to rapidly make quantitative estimates of relative ligand affinities.¹⁶⁶

As motivation for the present ligand design was in part based on the compound

reported by Fesik and coworkers (**1**), initial analysis of the SILCS maps on Mcl-1 was performed with respect to this compound. **Figure 2.3** shows the generic FragMaps overlaid on Mcl-1 along with the crystallographic and docked orientations of **1**. The docked orientation closely mimics the crystallographic orientation of the ligand. The ligand occupies nonpolar FragMaps, including a region in the upper left of panel A that is occupied by the chlorine of **1**. In addition, a negative (NEG) FragMap (orange) is occupied by the acid moiety of the ligand. While these features largely directed the docked orientation of **1**, the inclusion of protein flexibility in the SILCS method is essential. Shown in **Figure 2.3B** is a surface representation of the crystal structure of Mcl-1 used to initiate the SILCS simulations onto which the crystallographic orientation of **1** is overlaid. As can be seen, the inhibitor structure overlaps with the protein surface, such that if the protein surface from the crystal structure was used for docking, it would not be possible to attain the experimental binding orientation. However, as the SILCS method includes protein flexibility allowing for solutes in the SILCS simulations to penetrate the initial protein surface the surface may alternatively be defined based on the region not sampled by the solutes or water during the simulations. This allows the protein surface to be defined in terms of an exclusion map that, as shown in **Figure 2.3C**, accounts for the structural changes in the protein required to properly dock **1**. A notable feature of the bound orientation of **1** and the SILCS FragMaps is the pocket into which the 4-chloro-3,5-dimethylphenyl moiety binds. This is occupied by a nonpolar FragMap, which extends beyond the 4-chloro-3,5-dimethylphenyl ring, suggesting that larger nonpolar groups could facilitate binding in that region consistent with the ligand design strategy.

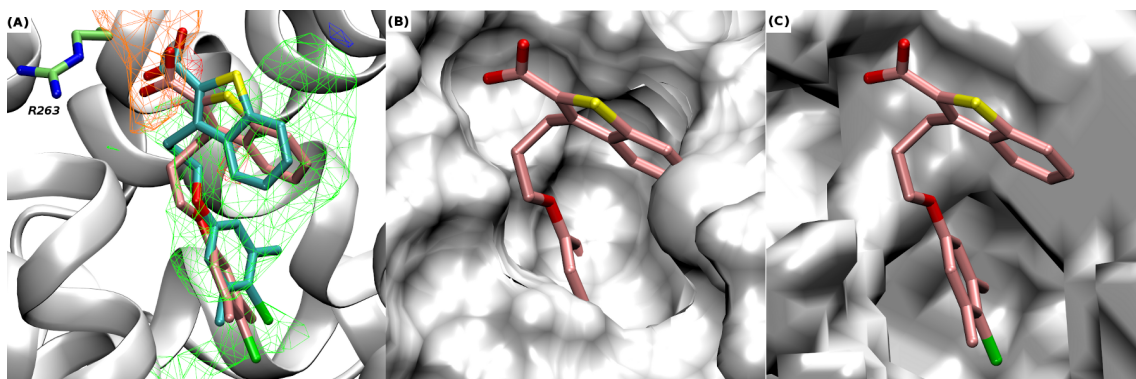


Figure 2.3: (A) Predicted binding orientation (cyan carbons) of **1** overlaid on its crystal orientation (pink carbons). FragMaps are shown as wire mesh in the following colors and GFE cutoff for generic nonpolar (APOLAR, green, -1.2 kcal/mol), neutral donor (HBDON, blue, -1.0 kcal/mol), neutral acceptor (HBACC, red, -1.0 kcal/mol), and negative acceptor (NEG, orange, -1.3 kcal/mol). (B & C) The crystallographic orientation of the inhibitor **1** (from PDB ID: 4HW3) overlaid (B) on the crystal protein surface of the Mcl-1-BH3 peptide complex structure (PDB ID: 4HW4) used to initiate the SILCS simulations and (C) on the SILCS exclusion map.

2.2 Results and Discussion

Molecular modeling and SILCS functional group affinity mapping (FragMaps)¹⁶⁴⁻¹⁶⁷ of the Mcl-1 binding site indicated that the carboxylic acid of designed molecule **3a** (Figure 2.4) would occupy an energetically favorable region indicated by a negative FragMap, associated with a salt bridge interaction with R263, while the distal ring of the naphthyl core is close to the p3 pocket demarcated by a favorable non-polar FragMap, consistent with the published studies.^{33, 62, 65} As anticipated, the aniline was directed into the hydrophobic p2 pocket, which is also demarcated by a nonpolar FragMap. With the molecular modeling data in hand, compound **3a** was then synthesized according to Figure 2.2. Briefly, commercially available 1-hydroxy-2-naphthoic acid (**4**) was regioselectively 4-chlorosulfonylated to yield **5**, which was isolated by pouring over ice and used without further purification. Sulfonyl chloride **5** was next reacted with 4-bromoaniline to furnish

the target molecule **3a** in excellent overall yield (83%). This convenient and simple 2-step synthesis allowed us to access the range of ligands presented below, resulting in the discovery of a low-nanomolar binder, and is in sharp contrast to the more lengthier synthesis of other families of Mcl-1 inhibitors.⁶⁵

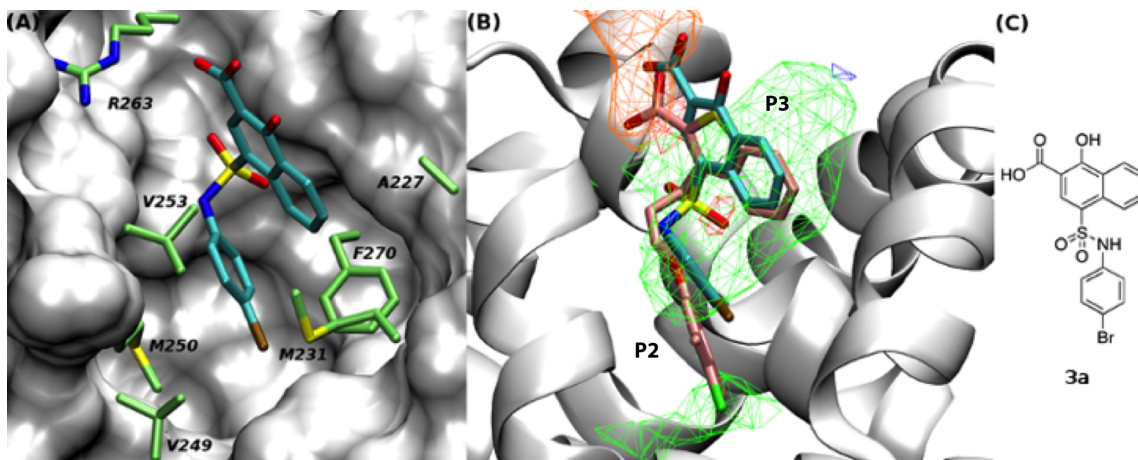


Figure 2.4: (A) The binding mode of **3a**, as predicted by SILCS. Important residues within the p2 binding pocket are shown in stick representation with the carbon atoms colored in green. (B) Compound **3a** and **2** are shown in stick representation with the carbon atoms colored in cyan and pink, respectively. Colors and cutoffs used to show the FragMaps are the same as in Figure 2.3. (C) 2D chemical structure of **3a**.

Evaluation of **3a** in a fluorescence polarization competition assay (FPCA)¹⁶⁹ indicated that it disrupted the Mcl-1–Bak-BH3 PPI with an IC_{50} of 10.9 μ M, corresponding to a K_i of 2.76 μ M. Given the ability of **3a** to inhibit Mcl-1, we embarked on a structure-activity relationship (SAR) campaign, the results of which are presented in **Tables 2.1-2.3**. The target molecules in **Table 2.1** were all prepared according to the concise synthetic route depicted in **Figure 2.2**, those in **Table 2.2** were synthesized using anilines prepared (or purchased) as described in **Figure 2.5**, whilst those in **Table 2.3** were generated by following the synthetic route in **Figure 2.6**. SAR model development was based on visual

inspection of predicted binding orientations based on the SILCS modeling, with quantitative analysis based on the SILCS ligand grid free energy (LGFE) scores, as described in more detail below.

Fluorescence Anisotropy and Polarization

Polarization and anisotropy both measure the orientation and motion of a fluorophore in regard to a particular axis in solution.¹³⁶ This depends on the excited state lifetime from absorption to emission of light. Unpolarized or natural light when in an electric field can oscillate in any direction perpendicular to the light propagation direction.¹³⁷⁻¹⁴⁰ However, when a polarizer is inserted in the path of excited light beam, one can isolate a unique direction of the light in the electric field. Only the population of fluorophores oriented within the same axis of the polarized light become excited. In solution these molecules tumble and change their axis in regards to incident polarized light resulting in emissions at a different axis.¹³⁷⁻¹⁴⁰ This rotational lifetime constant is dependent upon the size of the fluorescent molecule where smaller molecules tumble more quickly than larger molecules (or proteins).¹³⁶ Therefore, fluorescence anisotropy polarized light is used to measure the binding constants that cause a change in the rotational time of the molecules.¹³⁶⁻¹⁴⁰ If the fluorophore is bound to a small molecule, the rate at which it tumbles can decrease significantly when it is bound tightly to a large protein.¹³⁷⁻¹⁴⁰ If the fluorophore is attached to the larger protein in a binding pair, the difference in polarization between bound and unbound states will be smaller (because the unbound protein will already be fairly stable and tumble slowly to begin with) and the measurement will be less accurate.¹³⁷⁻¹³⁹ The degree of binding is calculated by using the difference in anisotropy of the partially bound, free and fully bound (large excess of protein) states measured by

titrating the two binding partners.¹³⁷⁻¹⁴⁰

First the K_d is determined based on: $K_d = [P][L]/[PL]$, where $[P]$ is the concentration of the protein (MCL-1 or BCL-x_L), $[L]$ is the fluorescently labeled ligand molecule (BAK), and $[PL]$ is the protein ligand complex. This gives the dissociation constant and can be used in further equations to determine K_i .¹⁷⁰

To determine the IC_{50} of the protein-ligand interaction depends on the dose response curve. This curve is determined by the titration of the drug plate (varying concentrations from 25 mM to 0) into the assay plate.^{137-140,170} The IC_{50} can be calculated from the concentration of the ligand needed to inhibit 50% of the protein concentration. In equation form, $IC_{50} = (FP_0 + FP_{100})/2$ where FP_0 is the fluorescence signal detected at 0% inhibition, and FP_{100} is the fluorescence signal at 100% inhibition. The pitfall of using an IC_{50} depends on the assay used and the conditions of the measurement. From the IC_{50} , the inhibitory constant (K_i) of the molecule can be determined using the Cheng-Prusoff equation for one.^{138-140,170}

$$K_i = IC_{50}/(1 + [L]/K_d)$$

where $[L]$ = is the concentration of the unbound, K_d = the dissociation constant.

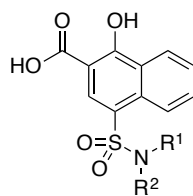
Alternatively, Nikolovska-Coleska and co-workers developed an equation to determine K_i .¹⁷⁰ They determined that the assumptions made by the Cheng-Prusoff equation did not hold up; meaning that the required concentration of the unbound reference ligand could not be measured and therefore the equation uses the total concentration of the reference ligand.¹⁷⁰ Second, they noticed that using higher concentrations of the receptor/protein resulted in higher IC_{50} values for one inhibitor.¹⁷⁰ Nikolovska-Coleska and co-workers demonstrated that the Cheng-Prusoff equation will yield higher K_i values when

the total receptor/protein concentration is higher. They have thus independently developed an equation that computes the K_i based on the following:¹⁷⁰

$$K_i = [I]_{50}/([L]_{50}/K_d + [P]_0/K_d + 1)$$

where $[I]_{50}$ is the concentration of the free inhibitor at 50% inhibition, $[L]_{50}$ is the concentration of the free labeled ligand (Bak in our FP assay) at 50% inhibition, $[P]_0$ is the free protein concentration at 0% inhibition and K_d is the dissociation constant of the protein-ligand complex.¹⁷⁰ Ultimately, the Nikolovska-Coleska equation is utilized over the Cheng-Prusoff because it is a more accurate depiction of the ligand-protein complex and takes into account more precise factors than the aforementioned equation.

Table 2.1: *Experimental and computational Mcl-1 and Bcl-xL inhibitory profiles of first generation inhibitors. Experimental data determined by a fluorescence polarization competition assay. ^a K_i values determined by Nikolovska-Coleska equation from IC50 values.¹⁷⁰ Data represent the average of at least two independent assays; errors are standard deviations. ^bSelectivity is defined as the K_i (Bcl-x_L) divided by the K_i (Mcl-1). NA, no activity.*



Compound	R ¹	R ²	MCL-1 <i>K_i</i> (μM) ^a	BCL-x _L <i>K_i</i> (μM) ^a	Selectivity ^b	MCL-1 LGFE (kcal/mol)	BCL-x _L LGFE (kcal/mol)
3a	4-Br-C ₆ H ₄	H	2.76 ± 1.26	51.4 ± 31.3	19	-39	-36
3b	H	H	99.0 ± 11.2	NA	-	-31	-
3c	Bn	H	56.3 ± 2.1	NA	-	-39	-
3d	CH ₂ -(2-Cl-C ₆ H ₄)	H	50.3 ± 11.8	-	-	-37	-
3e	CH ₂ -(3-Cl-C ₆ H ₄)	H	5.3 ± 2.78	-	-	-39	-
3f	CH ₂ -(4-Cl-C ₆ H ₄)	H	21.0 ± 3.9	338 ± 203	16	-41	-39
3g	CH ₂ -C ₆ H ₁₁	H	7.31 ± 1.42	77.6 ± 14.3	11	-42	-41
3h	Me	Me	25.7 ± 4.86	NA	-	-36	-
3i	-CH ₂ CH ₂ CH ₂ CH ₂ CH ₂ -		2.95 ± 0.43	-	-	-43	-
3j	-CH ₂ CH ₂ N(Ph)CH ₂ CH ₂ -		4.54 ± 3.86	-	-	-45	-
3k	-CH ₂ CH ₂ N(Bn)CH ₂ CH ₂ -		3.41 ± 0.37	-	-	-34	-
3l	Ph	H	106 ± 26	NA	-	-37	-
3m	2-Br-C ₆ H ₅	H	6.84 ± 2.23	-	-	-37	-
3n	3-Br-C ₆ H ₅	H	5.64 ± 1.76	-	-	-39	-

Table 2.1: Continued

3o	2,4-di-Br-C ₆ H ₅	H	0.420 ± 0.163	2.31 ± 1.35	5.5	-39	-38
3p	1-Naphthyl	H	11.2 ± 2.0	110 ± 45	10	-40	-38
3q	2-Naphthyl	H	4.58 ± 1.56	68.5 ± 36.3	15	-39	-37
3r	2-Ph-C ₆ H ₄	H	8.50 ± 1.34	-	-	-43	-
3s	3-Ph-C ₆ H ₄	H	1.88 ± 0.62	-	-	-41	-
3t	4-Ph-C ₆ H ₄	H	1.54 ± 0.46	-	-	-44	-
3u	2-CF ₃ -C ₆ H ₄	H	4.05 ± 2.11	19.3 ± 9.0	4.8	-42	-41
3v	4-Cl-C ₆ H ₄	H	1.91 ± 0.26	-	-	-40	-
3w	4-CF ₃ -C ₆ H ₄	H	2.50 ± 0.65	-	-	-43	-
3x	4-Me-C ₆ H ₄	H	34.3 ± 1.0	-	-	-39	-
3y	4-(iPr)-C ₆ H ₄	H	3.86 ± 1.53	-	-	-42	-
3z	4-OMe-C ₆ H ₄	H	11.9 ± 2.5	71.9 ± 21.0	6	-38	-36
3aa	4-(OiPr)-C ₆ H ₄	H	54.0 ± 4.6	NA	-	-41	-
3ab	4-CN-C ₆ H ₄	H	22.2 ± 1.6	-	-	-37	-
3ac	4-NO ₂ -C ₆ H ₄	H	4.49 ± 1.20	23.3 ± 2.5	5.2	-39	-38
3ad	3-CN-C ₆ H ₄	H	26.9 ± 0.6	-	-	-36	-

Unsubstituted sulfonamide **3b** was the weakest Mcl-1 inhibitor with a K_i of 99.0 μ M, consistent with the less favourable LGFE score as compared to **1** (Table 1, see supporting information). Replacement of the NH₂ group with benzylic amines and anilines improved Mcl-1 inhibitory activity in every case, which is attributed to the occupancy of the apolar FragMaps with the apolar FragMap in the p2 pocket yielding more favourable LGFE scores. In addition, the FragMaps extend further towards the interior of the protein, a region partially occupied by the 4-chloro-3,5-dimethylphenyl of **2**, suggesting that further hydrophobic extension of benzylic amines would improve activity. Indeed, chlorobenzylic

amine derivatives **3d–3f** were more potent than unsubstituted benzylic amine derivative **3c** by up to 8-fold. Replacement of the benzyl group in **3c** with a cyclohexylmethyl group (**3g**) also afforded an 8-fold improvement in inhibitory activity with a K_i of 7.31 μM . Piperidine derivative **3i** achieved good inhibition ($K_i = 2.95 \mu\text{M}$), as did the neutral and basic piperazines **3j** and **3k**, respectively, indicating a positively-charged group here is not detrimental to binding. Substitution of the aniline ring in **3l** with bromine atoms afforded between 10 to 54-fold improvement in activity, with the most profound effect observed with *para*-substituted derivative **3a** ($K_i = 2.76 \mu\text{M}$ cf 83.8 μM for **3l**). Introduction of an additional bromine atom into the *ortho* position of **3a** to afford 2,4-dibromo derivative **3o** led to an even more potent inhibitor with a K_i of 420 nM. Concomitantly, however, this change also led to an erosion in selectivity of more than ten-fold for Mcl-1 over Bcl-x_L. Naphthalene derivatives **3p** and **3q** were also more active than unsubstituted **3l**. Functionalization of the aniline ring in **3l** with additional phenyl rings to afford biphenyls **3r–3t** resulted in improved inhibition in each case due to occupancy of the apolar map adjacent to residues in the p2 pocket, which include V249 and M250, as well as residues in a non-peptide-binding sub-pocket (A227 and M231) in the vicinity of the p3 pocket. Once again, the *para*-substituted derivative **3u** proved the most potent of the series ($K_i = 1.54 \mu\text{M}$). It is noteworthy that this sub-pocket was recently shown to be important in the recognition of Fesik's inhibitor **1**.³³ For the remainder of the compounds in **Table 2.1**, substitution of the aniline ring in **3l** with hydrophobic and polar groups resulted in enhanced activities in all instances with the greatest improvements observed with hydrophobic groups in the *para* position.

Motivated by the improved activity of extended hydrophobic substituents on the sulfonamide phenyl ring (e.g. **3o** and **3s**) along with the extended apolar FragMap in the p2 pocket (**Figure 2.4b**), we chose to expand our library of *para*-substituted anilines by introduction of various aryloxy groups into the *para* position. Requisite anilines were synthesized according to **Figure 2.5**, and then coupled to sulfonyl chloride **5** according to **Figure 2.2**. As shown in **Table 2.2**, compounds **3ba–3bi** afforded potent inhibition of Mcl-1 with the tightest binder delivering a K_i of 79 nM. This ~1000-fold enhancement in inhibitory activity relative to unsubstituted aniline **3l** is associated with the increased overlap of the nonpolar groups with the second apolar FragMaps in the p2 pocket, as quantified by the systematically more favourable LGFE scores (**Table 2.2**). Simultaneously, these modifications also greatly increased affinity of the compounds to Bcl-x_L, which is associated with a change in the predicted binding orientation with Bcl-x_L as discussed below. The sulfonamide NH group in **3bi** offers an additional position from which further inhibitory activity might be acquired associated with occupancy of the apolar FragMap in the vicinity of residue V253, as shown in **Figure 2.4B** for **3a**. Indeed, alkylation of this nitrogen atom with cyclopentyl (**3bk**) and benzyl (**3bl**) resulted in our most potent inhibitors yet with K_i 's of 33 nM and 31 nM, respectively. Pleasingly, these alkylations also led to a recovery of selectivity for Mcl-1 over Bcl-x_L of up to eleven-fold.

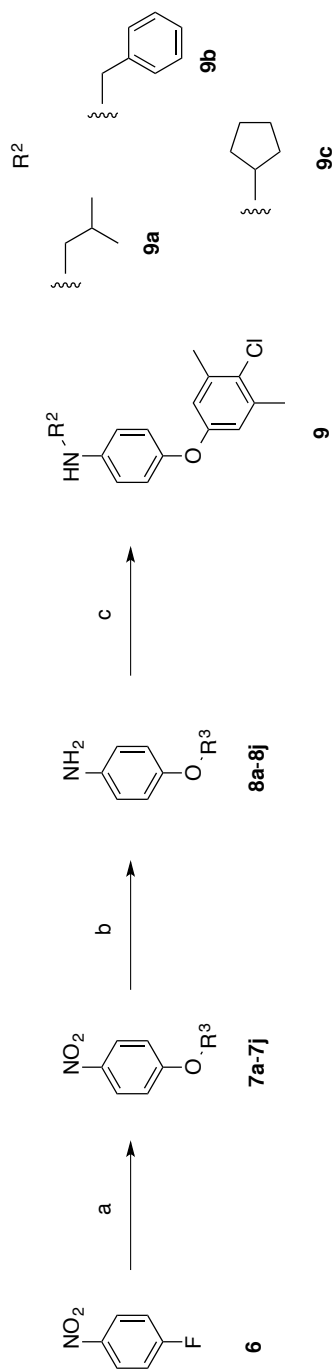
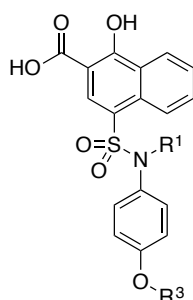


Figure 2.5: (a) $ArOH$, K_2CO_3 , $100\text{ }^\circ\text{C}$, 16 h ; (b) $SnCl_2 \cdot 2H_2O$, $EtOAc$, $50\text{ }^\circ\text{C}$, 16 h ; (c) isobutyraldehyde, benzaldehyde or cyclopentanone, $NaBH(OAc)_3$, 1,2-dichloroethane, RT , 16 h .



Compound	R ¹	R ³	MCL-1 K _i (μM) ^a	BCL-x _L K _i (μM) ^a	Selectivity ^b	MCL-1 LGFE (kcal/mol)	BCL-x _L LGFE (kcal/mol)
3ba	iBu	iPr	0.487 ± 0.035	6.08 ± 0.81	12	-39	-36
3bb	H	Ph	1.15 ± 0.28	ND	-	-44	-
3bc	H	4-Me-C ₆ H ₄	0.335 ± 0.027	0.84 ± 0.05	2.5	-44	-43
3bd	H	1-Naphthyl	0.082 ± 0.012	0.22 ± 0.06	3.7	-47	-48
3be	H	3-Br-C ₆ H ₄	0.114 ± 0.017	0.30 ± 0.04	3.8	-45	-44
3bf	H	3,5-di-Me-C ₆ H ₃	0.284 ± 0.125	0.39 ± 0.10	1.4	-46	-46
3bg	H	2,4-di-Cl-C ₆ H ₃	0.079 ± 0.010	0.19 ± 0.02	2.4	-47	-46
3bh	H	4-Cl-C ₆ H ₄	0.173 ± 0.070	ND	-	-46	-
3bi	H	4-Cl-3,5-di-Me-C ₆ H ₂	0.117 ± 0.060	0.48 ± 0.05	4.1	-47	-47
3bj	iBu	4-Cl-3,5-di-Me-C ₆ H ₂	0.080 ± 0.019	0.17 ± 0.06	2.1	-48	-47
3bk	Cp	4-Cl-3,5-di-Me-C ₆ H ₂	0.033 ± 0.025	0.29 ± 0.05	8.8	-40	-39
3bl	Bn	4-Cl-3,5-di-Me-C ₆ H ₂	0.031 ± 0.017	0.34 ± 0.13	11	-52	-51

Table 2.2: Experimental and computational Mcl-1 and Bcl-x_L inhibitory profiles of second-generation inhibitors. Experimental data determined by a fluorescence polarization competition assay. ^aK_i values determined by Nikolovska-Coleska equation from IC₅₀ values.¹⁷⁰ Data represent the average of at least two independent assays; errors are standard deviations. ^bSelectivity is defined as the K_i (Bcl-x_L) divided by the K_i (Mcl-1). ND, not determined.

Finally, we wanted to verify the importance of the carboxylic acid and hydroxyl groups of the inhibitor scaffold. Analysis of **Figure 2.4B** showing overlap of the negative FragMaps with the acid moiety indicate the importance of that group to binding while analysis of the acceptor FragMaps at a lower contour level of -0.3 kcal/mol (not shown)

indicated small, but favourable contributions from the alcohol moiety. Accordingly, we synthesized the compounds shown in **Figure 2.6**. As seen in **Table 2.3**, the carboxylic acid is critical to activity, which is consistent with its likelihood of forming a salt bridge with R263. Methylation of the hydroxyl group to deliver compound **12** resulted in around a 40-fold reduction in activity indicating its importance, too. Although SILCS predicted the methoxy derivative **12** (LGFE = -42 kcal/mol) to bind with similar affinity than its hydroxy counterpart **3ca** (LGFE = -42 kcal/mol), the observed disparity may be explained by an anticipated greater acidity for the latter through a six-membered intramolecular hydrogen bond between the hydroxyl and the carboxylate that affords a stronger salt bridge with R263.

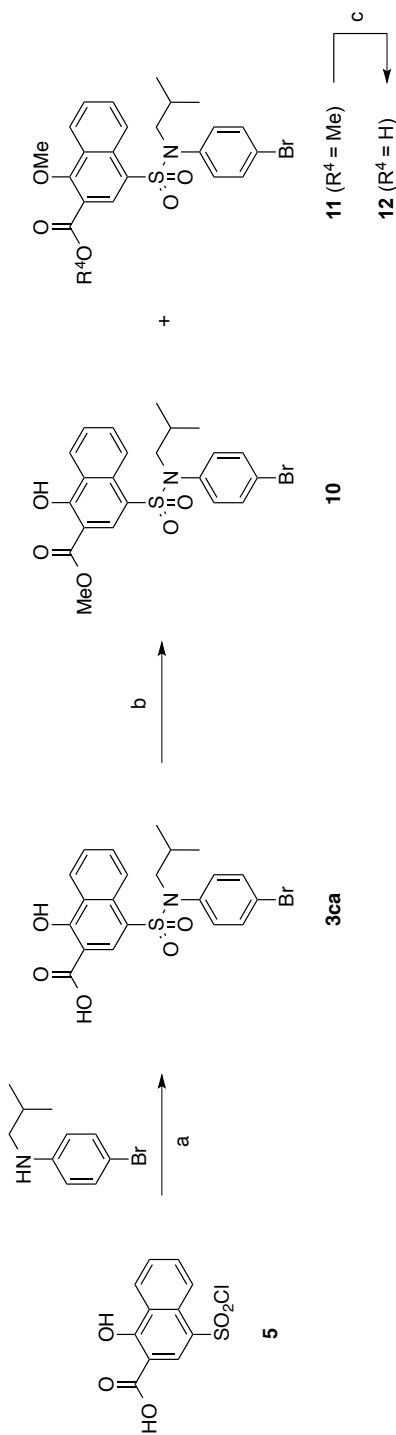
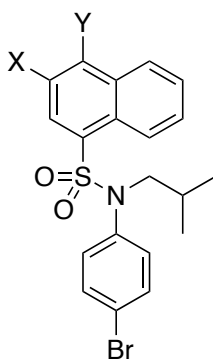


Figure 2.6: (a) $ArNH_2$, pyr, acetone, 50 °C, 3 h; (b) MeI, K_2CO_3 , DMF, rt, 16 h; (c) NaOH, MeOH/THF/ H_2O , 3:1:1, rt, 16 h.



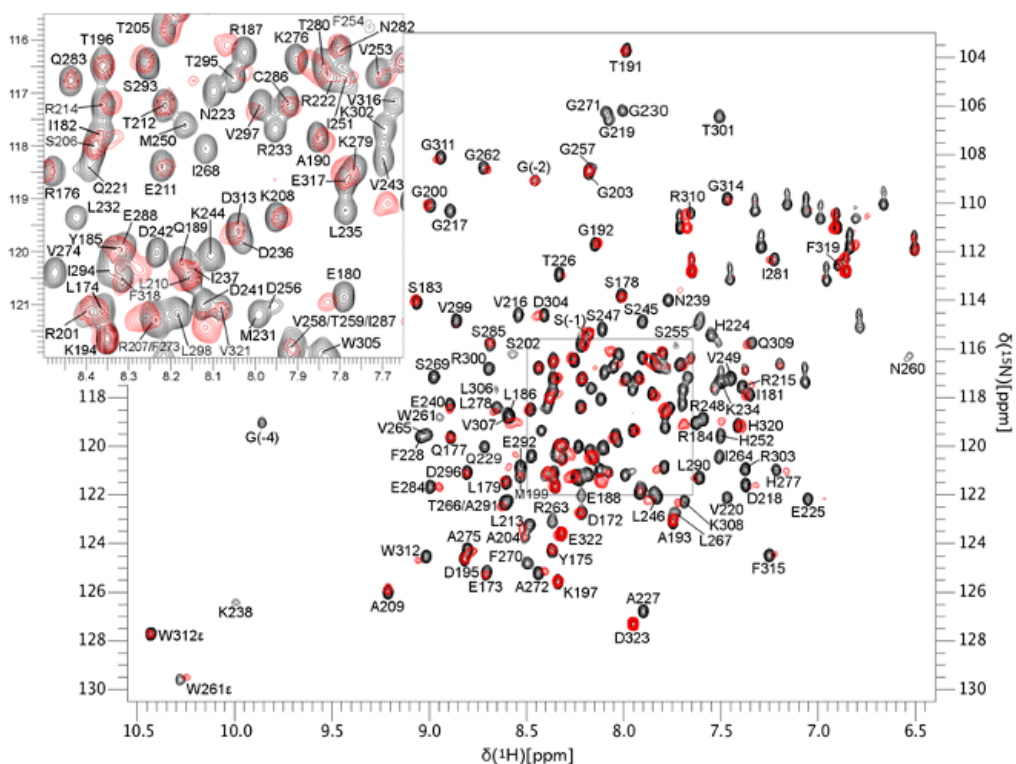
Compound	X	Y	MCL-1 K_i (μM) ^a	MCL-1 LGFE (kcal/mol)
3ca	CO ₂ H	OH	0.566 ± 0.031	-42
10	CO ₂ Me	OH	> 500	-34
11	CO ₂ Me	OMe	> 500	-35
12	CO ₂ H	OMe	23.4 ± 2.6	-42

Table 2.3: Investigation into the significance of the inhibitor's carboxylic acid and hydroxyl group towards the inhibition of Mcl-1. Experimental data determined by a fluorescence polarization competition assay. ^a K_i values determined by Nikolovska-Coleska equation from IC_{50} values.¹⁷⁰ Data represent the average of at least two independent assays; errors are standard deviations.

NMR HSQC experiments using ¹⁵N-labeled Mcl-1¹⁷²⁻³²⁷ (recombinant human Mcl-1 residues 172 to 327) confirmed the direct interaction of this class of compounds with the protein. Specifically, the HSQC spectra of ¹⁵N-labeled Mcl-1¹⁷²⁻³²⁷ (**Figure 2.7**: black = Mcl-1; red = Mcl-1 and inhibitor) shows the addition of compound **3ba** causes perturbations in the chemical shifts or loss of Mcl-1 backbone ¹H-¹⁵N correlations due to chemical exchange broadening in amino acids consistent with the predicted binding mode of **3a** shown in **Figure 2.4**. When the residues that are perturbed or lost due to chemical exchange broadening are mapped onto the 3D structure of Mcl-1 (**Figure 2.8**) their

positions support the model shown in **Figure 2.4**. The majority of the changes occur in residues near the predicted binding mode of the compound including R263 and N260, and residues in the p2 pocket (V249, M250, and F270). There are also chemical shift perturbations near the p3 pocket (A227 and M231), although these may be associated with indirect effects. The residues undergoing chemical shift changes are also consistent with the X-ray crystal structure of **1** bound to Mcl-1 (PDB ID: 4HW3)³³ with most changes located on the end of helix 2 (residues 204 to 224) and in most of helices 3 (residues 226 to 236), 4 (residues 239 to 255), and 5 (residues 260 to 280) that form the BH3-binding groove.

Figure 2.7: The NMR HSQC spectra shows chemical shift perturbations caused by the direct interaction of compound 3ba with Mcl-1. The spectrum of the control sample (black) is overlaid with the spectrum of Mcl-1 bound to 3ba (red). Inset is enlargement of boxed region.



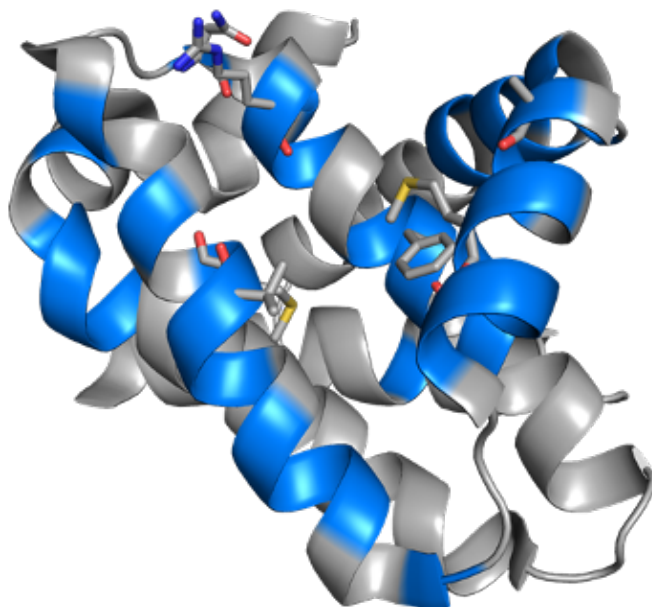


Figure 2.8: *Mcl-1* residues (blue) whose chemical shifts are perturbed or lost in the presence of compound **3ba**.

2.3 Comprehensive SILCS SAR analysis of Mcl-1 binding

Additional SILCS based modeling was undertaken to predict the bound orientation of the active ligands, to quantitatively predict the relative affinities of the ligands as well as the contributions of the different regions of the ligands to binding to Mcl-1 and Bcl-x_L and to develop a quantitative model of differential binding of the compounds to Mcl-1 versus Bcl-x_L. This information would be of utility in designing ligands with improved potency and selectivity for Mcl-1. Thus, subsequent modeling involved docking of each studied compound using the SILCS-Pharm approach as described in the supporting information (Figure S1).¹⁶⁷⁻¹⁶⁸ The docked orientation of each compound was then subjected to MC-SILCS sampling to allow the molecules to conformationally sample the local binding region as defined by the FragMaps and the exclusion maps, with the LGFE

scores calculated from the MC SILCS conformational sampling. Comparison of the LGFE values for all the tested compounds with the experimental affinities converted to free energies ($\Delta G = -RT\ln K_i$, where R is the Boltzmann constant and T is the temperature) for Mcl-1 yields a correlation of $R^2 = 0.53$ and a high predictive index¹⁷¹ of 0.70, (Figure S2, supporting information). Thus, the LGFE scores correlate with the Mcl-1 experimental data, indicating the quality of the bound orientations from the SILCS-Pharm-MC-SILCS protocol.¹⁶⁶⁻¹⁶⁸

Given the predictive capabilities of the LGFE scores, further analysis was undertaken to use the SILCS modeling to further interpret the experimental SAR data. This analysis focused on four compounds: **3b**, **3a**, **3bi** and **3bl**. These compounds differ in the number of phenyl rings attached to the sulfonamide moiety going from 0 to 3 rings, in that order, with the binding affinities varying from 99 μ M down to 31 nM. For these compounds, a correlation of $R^2 = 0.99$ between the LGFE and experimental G values is obtained.

The predicted conformation of the four compounds is presented in **Figure 2.9** along with the crystallographic orientation of **1**.³³ For all four compounds, the carboxylic acid overlaps with the negative FragMap (orange arrows), associated with its interaction with R263 of Mcl-1 and the aromatic rings suitably overlap with hydrophobic FragMaps (green arrows), binding within the hydrophobic groove. For **3b**, the sulfonamide group is placed outside of the hydrophobic binding pocket corresponding to an H-bond donor FragMap (blue arrow in (A)) indicating its possible H-bonding interaction with residue H224. The hydroxyl group on the naphthalene ring overlaps with an H-bond acceptor FragMap (red arrow in (A)), possibly making an H-bond to residue T266. For the other three compounds,

the naphthalene group flipped over relative to **3b**, maintaining the position of the carboxylic acid while allowing the additional aromatic groups to interact with the hydrophobic binding pocket, consistent with that observed with **1**. Notably the sulfonamide oxygen atoms in this orientation overlap with an acceptor FragMap associated with interactions with residue T266 (red arrows).

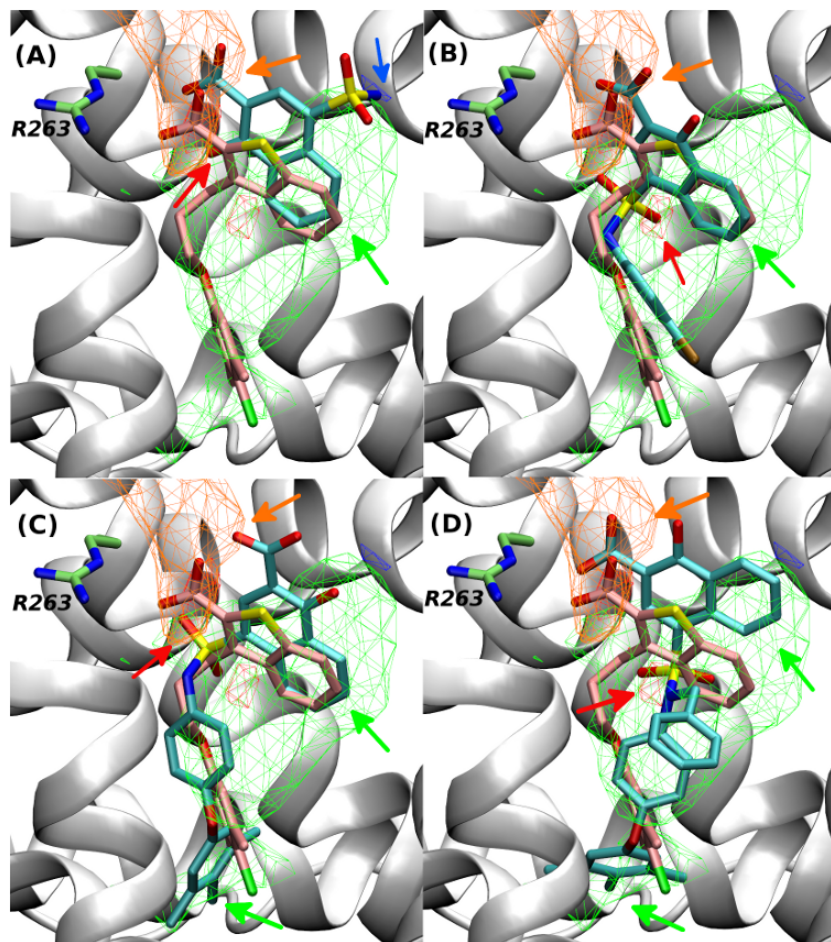


Figure 2.9: The orientations of the four compounds binding to Mcl-1 predicted by SILCS. (A) **3b**; (B) **3a**; (C) **3bi**; (D) **3bl**. Compounds shown in stick format with atom-based coloring. The compound, **2**, from the previously reported complex structure 4HW3 is also shown, with the carbon atoms colored in pink. Mcl-1 residue R263 is shown. Same color and GFE cutoff is used as in **Figure 2.3**.

Additional analysis of the contribution of individual atoms and functional groups on the compounds to binding was performed by analyzing the atom-based GFE contributions of the individual atoms to the overall LGFEs. Presented in **Figure 2.10** are the atom-based GFE contributions for the most favorable binding conformations of the four compounds. For all compounds, the naphthyl and acid moieties make favorable contributions to binding. With **3b**, significant favorable contributions occur with both the sulfonamide and hydroxyl moieties. In the remaining three compounds with the naphthyl moiety flipped; the sulfonamide and hydroxyl moieties still make favorable contributions to binding though the magnitude is generally less than that of **3b**. For example, while some of the sulfonamide oxygens make more favorable contributions with the larger compounds, the amide NH makes a very unfavorable contribution. However, the less favorable interactions of the hydroxyl and sulfonamide moieties are overcome by favorable contributions from the additional aromatic groups, which lead to the improved binding of the larger inhibitors. Interestingly, the quite favorable contributions from the second phenyl ring coming off the sulfonamide at the R² position was counter-balanced by decreased contributions from the aromatics group at the R¹ position upon going from **3bi** to **3bl**. This is consistent with the experimental free energy of binding changing by only -0.8 kcal/mol versus **3bi** while differences going from **3b** to **3a** and **3a** to **3bi** are -2.1 and -1.9 kcal/mol, respectively. This atomic detailed interpretation of the experimental SAR data is anticipated to facilitate further improvements in the compounds.

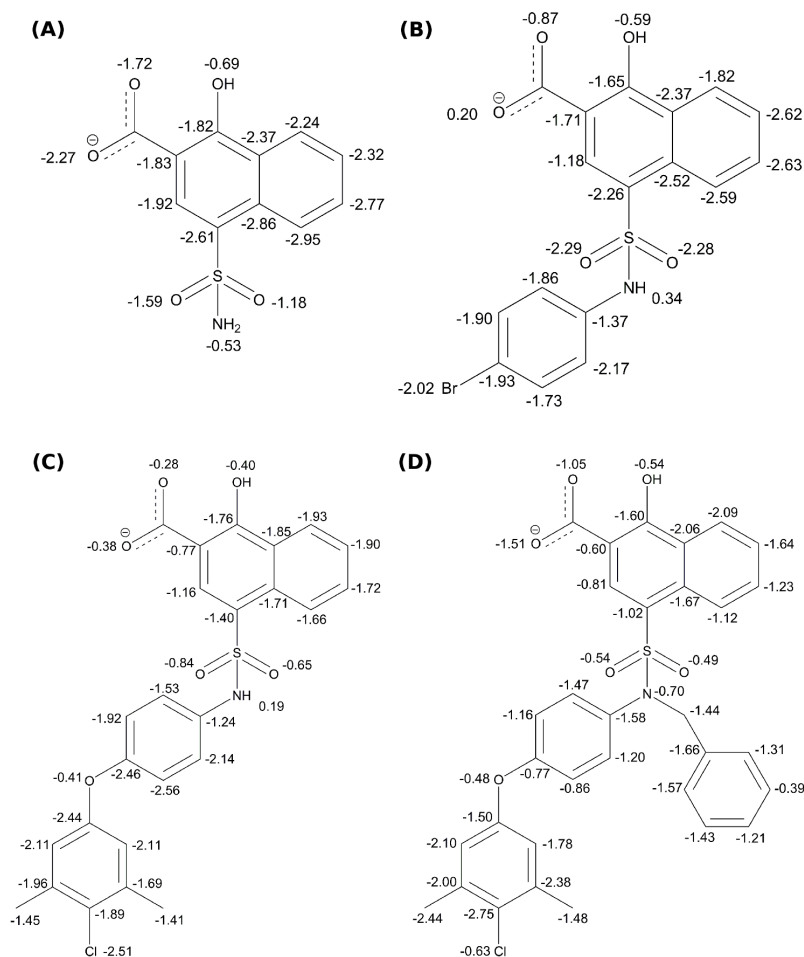


Figure 2.10: Atom GFE contributions for the most LGFE favorable binding conformation of the four compounds. (A) **3b**; (B) **3a**; (C) **3bi**; (D) **3bl**.

2.4 SILCS quantitatively captures the binding specificity of compounds for Mcl-1 over Bcl-x_L

A long-standing challenge in targeting the anti-apoptotic Bcl-2 proteins is achieving family member specificity, particularly Mcl-1 specificity, although selective ligands are beginning to emerge.^{17, 33, 89, 128, 132, 172} To investigate the binding specificity of compounds for Mcl-1 versus Bcl-x_L, SILCS simulations and GFE FragMap generation

followed by LGFE scoring were also done for Bcl-x_L (Table S1 of the supporting information). A correlation of $R^2 = 0.58$ and a high predictive index of 0.76 was found between the LGFE and experimental binding data for Bcl-x_L (Figure S3 of the supporting information). Difference FragMaps, Δ FragMaps, were then calculated as $GFE_{Bcl-x_L} - GFE_{Mcl-1}$ such that positive Δ FragMaps favor Mcl-1 over Bcl-x_L. The Δ FragMaps may then be used to qualitatively understand the contributions driving specificity as well as quantitatively obtain difference LGFE scores (Δ LGFE). Correlation analysis between the Δ LGFE scores and the experimental differences in the binding affinities for Mcl-1 and Bcl-x_L yielded an $R^2 = 0.57$ and predictive index of 0.83 (Figure S4 in supporting information), indicating the quality of the SILCS Δ FragMaps in modeling the relative affinities for Mcl-1 versus Bcl-x_L. Additional analysis was therefore undertaken on **3a** as this compound showed the largest specificity for Mcl-1 over Bcl-x_L. **Figure 2.11A** shows the Δ FragMaps between Mcl-1 and Bcl-x_L, and includes the docked orientation of **3a** with the atom contributions to the Δ LGFE between Mcl-1 and Bcl-x_L mapped onto this orientation. The *p*-bromophenyl group (green arrow) that binds deeply in the p2 pocket between helices α_4 and α_5 is in a Mcl-1 positive Δ FragMap indicating that region to favor binding to Mcl-1. Similarly, the sulfonamide oxygen (red arrow) contributes to the binding of **3a** to Mcl-1 over Bcl-x_L. Alternatively, the NH moiety of the sulfonamide contributes to more favorable binding to Bcl-x_L over Mcl-1. The acid moiety in the lower right of the figure is also predicted to favor binding to Bcl-x_L over Mcl-1. Summing over the different Δ FragMap classes showed the overall Δ LGFE score of 3.0 kcal/mol favoring binding to Mcl-1 to have favorable contributions from the hydrophobic and neutral acceptor terms, 4.4 and 1.6 kcal/mol, respectively, while the neutral donor, negatively charged acceptor and hydroxyl

groups favor Bcl-x_L binding, with values of -1.8, -0.7 and -0.5 kcal/mol, respectively. Similar trends are observed for the other compounds for which a selectivity of Mcl-1 over Bcl-x_L was found, as shown in Table S2 in the supporting information. Indeed, given that all the tested compounds favored Mcl-1 binding over Bcl-x_L, these results indicate that the exploitation of the binding pocket inherently favors Mcl-1 binding, as previously discussed by Fesik.³³ The docked orientation of **3a** to the two proteins in **Figure 2.11B** shows that this pocket is not being exploited with Bcl-x_L. This is consistent with the fact that Mcl-1 shows more opening at the p2 pocket as compared to Bcl-x_L as illustrated in **Figure 2.11B**,³³ disallowing access of **3a** deep into the hydrophobic pocket in the p2 site of Bcl-x_L.

However, further extension of the ligands (e.g. **3bl**) leads to improved binding affinity, but not improved specificity. This may be explained by different predicted binding orientations of the compound to the two proteins. As seen in **Figure 2.11C**, **3bl** binds with its additional 4-chloro-3,5-dimethylphenyl R³ group deep in the p2 pocket of Mcl-1, and with the R² benzyl group occupying the upper region of the p2 pocket. In contrast, the orientation of **3bl** bound to Bcl-x_L shows the 4-chloro-3,5-dimethylphenyl still interacting with the p2 site, though not as deep as that occurring with Mcl-1. This leads to a shift in the location of the naphthyl ring as well as the R² phenyl group into the p3 site where they can exploit the hydrophobic character of that sub-pocket as well as interactions with R263, as indicated by the apolar and negative Bcl-x_L FragMaps in **Figure 2.11D**, respectively. Thus, the significant increase in the size of **3bl** leads to increased affinity with respect to both Mcl-1 and Bcl-x_L, with that larger size predicted to change the binding orientation with Bcl-x_L such that further increased specificity for Mcl-1 is not gained over **3a**.

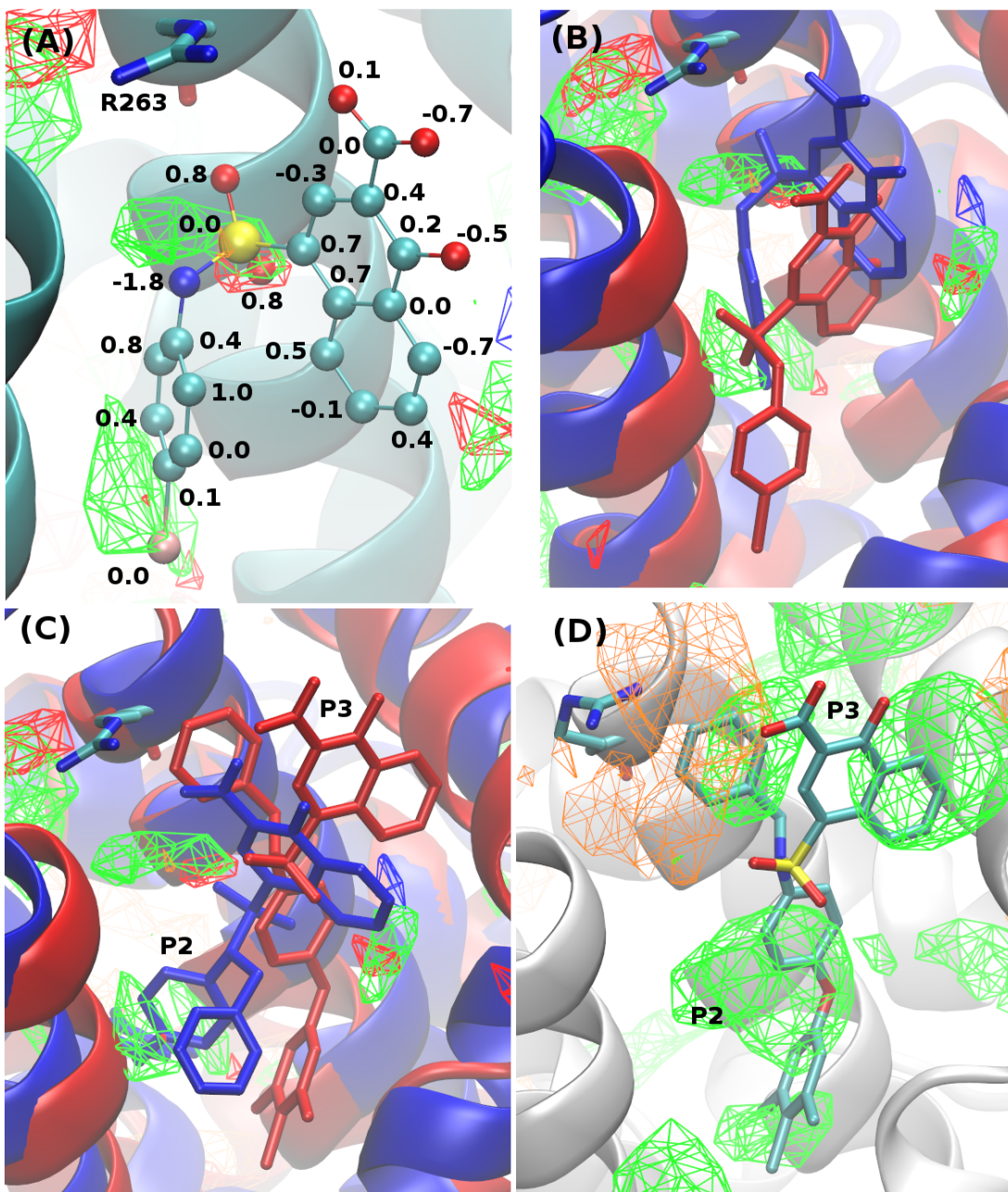


Figure 2.11: (A) Difference FragMaps (Δ FragMaps) between Mcl-1 and Bcl-xL showing the favorable binding patterns for Mcl-1. Hydrophobic and neutral donor Δ FragMaps are shown in green and blue, respectively. The atom GFE contributions to the binding affinity difference are also shown. (B) Experimental structures of Mcl-1 (blue, 4HW4) and Bcl-xL (red, 1BXL) shows that the binding pocket between helix α 4 (upper right) and α 5 (bottom left) is larger for Mcl-1 than Bcl-xL. The predicted binding modes of **3a** for Mcl-1 (blue) and Bcl-xL (red) differs due to this p2 pocket difference. The 4-bromophenyl ring of **3a** binds deeply to the opened pocket for Mcl-1 while it binds on the protein surface for Bcl-xL. (C) Binding orientations of **3bl** to Mcl-1 (blue, 4HW4) and Bcl-xL (red, 1BXL) along with the Δ FragMaps. (D) Binding orientations of **3bl** to Bcl-xL (1BXL) along with the Bcl-xL APOLAR and NEG FragMaps at the contour levels specified in **Figure 2.3**.

2.5 Cellular activity of Mcl-1 inhibitors.

To investigate the cellular activity of our Mcl-1 inhibitors, the most potent compound **3bl** was evaluated for its ability to inhibit the proliferation of A375 and SK-MEL-5 melanoma cells, both of which express high levels of Mcl-1.¹⁷³ Unfortunately, the IC₅₀ for **3bl** was 50 μ M and 90 μ M in A375 and SK-MEL-5 cells, respectively (**Table 2.4**). We attributed the poor efficacy in cells to the charged carboxylic acid of **3bl**. To test this hypothesis, we prepared two ester prodrugs of the potent, but more hydrophilic, inhibitor **3ba**, methyl ester **13** and acetoxymethyl ester **14**, according to **Figure 2.12**. As expected, both prodrugs **13** and **14** demonstrated no binding affinity to Mcl-1 *in vitro*. (data not shown). Naphthoate derivative **3ba** exhibited worse activity than **3bl** in cells, consistent with its weaker affinity to Mcl-1 (**Table 2.3**). However, the acetoxymethyl ester **14** displayed an IC₅₀ of 15 μ M in both A375 and SK-MEL-5 cells, presumably due to improved cell penetration and then intracellular hydrolysis to the active metabolite **3ba** (**Table 2.4**).

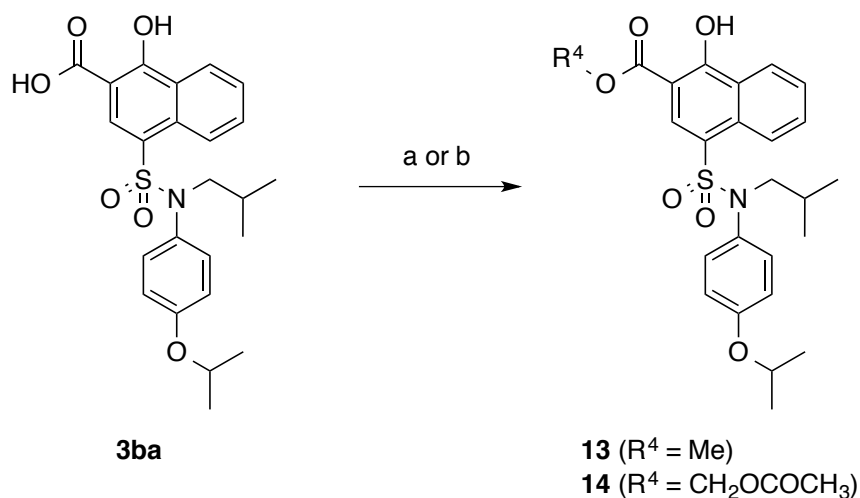


Figure 2.12: (a) SOCl_2 , MeOH, rt, 48 h; (b) $\text{BrCH}_2\text{OCOCH}_3$, K_2CO_3 , MeCN, 0 $^\circ\text{C}$, 16 h.

We postulate that the lack of cellular activity for methyl ester **13** might be due to limited hydrolysis to **3ba**, as we have observed elsewhere.¹⁷⁴ These results suggest a path forward with respect to rationally improving the cell penetration capabilities of this class of compounds based on a prodrug strategy.

Compound	IC ₅₀ (μM)	
	A375	SK-MEL-5
3a	~300	~300
3bl	50	90
3ba	150	~300
13	~300	~300
14	15	15

Table 2.4: Inhibition of cell proliferation by select compounds, as determined by a cell titer blue assay.

2.6 Conclusions

Presented is a novel class of Mcl-1 inhibitors that target R263 and the p2 and p3 pockets within the hydrophobic BH3-binding crevice on the surface of the protein. Inhibitor design was motivated by compounds reported by Fesik and coworkers and by AbbVie that are known to exploit the p2 pocket and interactions with R263. SILCS analysis of this region of the BH3 binding site supported this strategy, with the use of the SILCS exclusion maps indicating significant additional opening of the p2 pocket that could be exploited in ligand design. Accordingly, a series of compounds were designed, synthesized and subjected to experimental evaluation using a FP assay with binding of **3ba** to targeted pocket of Mcl-1 verified using NMR. From this strategy, **3bl** was identified with a $K_i = 31$ nM for Mcl-1 with a specificity of 11-fold over Bcl-x_L. Although only moderate cell activity was observed with the 2-hydroxynaphthoate-based Mcl-1 inhibitors, this was

enhanced by the preparation of an acetoxymethyl ester prodrug of the critical carboxylic acid.

The two-step synthesis developed in this study allowed us to rapidly synthesize and test over 40 analogs, with the selected compounds based, in part, on commercially available starting materials. These synthetic capabilities allowed us to readily synthesize compounds that would be able to reach into and complement the hydrophobic p2 pocket. This yielded compounds with affinities spanning over a 10,000-fold range. Detailed SILCS analysis of all of these compounds quantified the contributions of the different moieties leading to improved affinity. These results suggest that fine tuning of interactions with the p2 pocket via appropriate modifications of the R³ ring (**Table 2.2**) as well as of the R¹ ring will likely lead to improved affinity. Additional SILCS analysis on the differential binding of selected compounds to Mcl-1 versus Bcl-x_L indicates that fine tuning of the R³ ring occupying the p2 pocket may also improve specificity. Further modifications that may contribute to improved specificity include alkylation of the NH moiety of the sulfonamide moiety and additions of both hydrogen bond acceptor (e.g. OMe) or hydrophobic (e.g. Cl) functional groups to the naphthyl ring as indicated by the differential FragMaps in the top, central region of **Figure 2.11A**. Future studies will involve the design of new compounds using the validated SILCS affinity and specificity models for quantitative analysis of synthetically accessible compounds.

2.7 Experimental

2.7.1 Computational

Molecular modeling studies were initiated with the crystal structure of the Mcl-1-

BH3 peptide complex (PDB ID: 4HW4),³³ following removal of the 16mer BH3 peptide, and with the Bcl-x_L-Bak complex structure (PDB ID: 1BXL), following removal of the Bak peptide. For both proteins, the Reduce software¹⁷⁵ was used to choose optimal Asn, Gln, and His side-chain orientations and determine the optimal protonation states of His residues. The protein was immersed in a box of an aqueous solution containing eight small probe molecules at approximately 0.25 M each with water at ~55 M. The size of the simulation box was chosen so as to have the protein extrema separated from the edges by a minimum of 8 Å based on non-hydrogen atoms. The small molecules, or solutes, include benzene, propane, methanol, formamide, acetaldehyde, methylammonium and acetate, as previously used,¹⁶⁶ along with imidazole. Ten such protein-small molecule aqueous systems were generated for each protein with each simulation system differing in the initial positions and orientations of the small molecules and water. The SILCS¹⁶⁴⁻¹⁶⁷ molecular dynamics (MD) simulations were performed using the GROMACS¹⁷⁶ simulation program with the CHARMM36 force field,¹⁷⁷ CHARMM general force field (CGenFF)¹⁷⁸⁻¹⁷⁹ and TIP3P water model¹⁸⁰ to describe the protein, small molecules and water, respectively. The simulations were each extended for 40 ns, yielding a total of 400 ns of simulation time for each protein. Additional MD simulation details can be found in Reference 9.¹⁶⁶

From the simulation, 3D probability distributions of selected atoms from the small molecules were constructed to form the FragMaps, yielding a total of ten different FragMaps. The final FragMaps are converted to free energies, termed grid free energies (GFE), by normalizing the distributions with respect to the distributions of the solutes in an aqueous solution in the absence of the proteins followed by Boltzmann transformation to yield the GFE values.¹⁶⁶ As the GFE FragMaps are normalized with respect to the

fragment probabilities in solution, they contain both favorable regions as well as unfavorable regions. The unfavorable regions typically range from 0 to 3 kcal/mol, with the upper limit based on sampling issues. In addition to the FragMaps, exclusion maps were constructed by calculating the 3D probability distributions of all non-hydrogen atoms of the water and solutes together and identifying those voxels with zero occupancies, which defines the exclusion maps. This exclusion map represents regions forbidden to the small molecules and water and may be considered an alternate to more traditional representations of the protein surface. For quantitative analysis, these voxels were assigned a very high energetic penalty (1000 kcal/mol) while the remaining voxels were assigned energies associated with the specific FragMaps. The availability of the GFE FragMaps and the exclusion maps allows for quantitative estimates of binding affinities to be made, referred to as ligand grid free energies (LGFE). These are a simple summation of the GFE energy contribution of all the atoms in each ligand that are classified with respect to the FragMap types followed by normalization of the summed energies by the number of classified ligands atoms and subsequent multiplication by the total number of non-hydrogen atoms, yielding the final LGFE values. Note that the LGFE scores are not directly equivalent to experimental free energies due to the additive approximation of the LGFE scores (i.e. the individual atom-based GFEs are summed to yield the LGFE), the lack of accounting for the energy cost of connecting the fragments that comprise the full compounds and issues associated with the standard state in the experimental and computational conditions.

In the present study, the specific FragMaps were used for calculation of GFE and LGFE scores, while generic FragMaps are used for visualization. The specific and generic FragMap types that were used include: (1) aromatic, AROM (benzene carbons); (2)

aliphatic, ALIP (propane carbons); (3) dual role hydrogen bonding atom, MEOO (methanol oxygens); (4) FORN, (formamide nitrogen); (5) FORO, (formamide oxygen); (6) IMIN, (imidazole acceptor nitrogen); (7) IMIH, (imidazole donor nitrogen); (8) AALO, (acetaldehyde oxygen); (9) positive donor, POS (methylammonium nitrogen); (10) negative acceptor, NEG (acetate oxygens); (11) generic nonpolar, APOLAR (benzene and propane carbons); (12) generic neutral hydrogen-bond donor, HBDON (formamide and imidazole donor nitrogen); and (13) generic neutral hydrogen-hydrogen acceptor, HBACC (formamide, acetaldehyde oxygens and imidazole acceptor nitrogen). The convergence of the FragMaps was examined by calculating the overlap coefficient between two sections of the simulations (trajectories 1–5 and trajectories 6–10), as previously described.¹⁶⁶ All the generic FragMaps show an overlap coefficient of greater than 0.6, indicating satisfactory convergence.

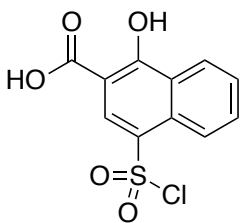
To identify the binding modes of the tested compounds with Mcl-1, the SILCS-Pharm protocol¹⁶⁷⁻¹⁶⁸ was used in which the FragMaps are used to define the pharmacophore features. This involved identifying all possible pharmacophore features in the peptide binding pocket based on the region close to inhibitor **2** (PDB ID: 4HW3).³³ The selected pharmacophore was used to direct docking of the studied compounds in the Mcl-1 binding pocket. Generation of 250 conformations of each compound and pharmacophore docking were conducted using MOE.¹⁸¹ For each compound, the best conformation, based on the smallest RMSD with the pharmacophore was retained for SILCS ligand grid free energy (LGFE) scoring. The compounds were locally relaxed and minimized using FragMap-based Monte Carlo (MC) sampling in the field of the GFE FragMaps (MC-SILCS) from which the LGFE scores were obtained.¹⁶⁶ The MC-SILCS was conducted for

50000 steps under slow cooling mode and was repeated 20 times for each conformation with different random seeds to get a Boltzmann averaged LGFE value, along with the corresponding standard deviation. The lowest energy LGFE conformation for each compound was chosen for visual presentation and analysis. The SILCS-MC was also performed in the same way using FragMaps of Bcl-x_L to calculate Bcl-x_L related LGFEs for the compounds that have available Bcl-x_L experimental data. Bcl-x_L SILCS-MC calculations were initiated from the Mcl-1 SILCS-PHARM orientations in the context of the Bcl-x_L FragMaps and exclusion maps.

2.7.2 Chemistry

General. Unless otherwise stated, all reactions were performed under an inert atmosphere (N₂). Reagents and solvents were ACS grade, and purchased from Sigma-Aldrich, Alfa Aesar, Oakwood and TCI America. Anhydrous solvents were used as provided without further purification. Reactions were monitored by thin-layer chromatography (TLC), visualizing with a UV lamp and/or KMnO₄ stain. Flash column chromatography was performed with silica gel 60 Å (70-230 mesh, Merck). ¹H and ¹³C NMR spectra were recorded on a Varian INOVA 400 MHz NMR spectrometer at 25 °C. Chemical shifts are reported in parts per million (ppm). Data for ¹H NMR are reported as follows: chemical shift (δ ppm) (multiplicity, coupling constant (Hz), integration), where multiplicities are: s = singlet, d = doublet, t = triplet, sep = septet, m = multiplet. The residual solvent peak was used as an internal reference: CDCl₃ (δ_H 7.26; δ_C 77.21) and d₆-DMSO (δ_H 2.50; δ_C 39.51). Mass spectra were obtained on an Electrospray TOF (ESI-TOF) mass spectrometer (Bruker AmaZon X). All final molecules were deemed to be >95% pure by reversed-phased HPLC

using a Waters 1525 analytical/preparative HPLC fitted with a C18 reversed-phase column (Atlantis T3: 4.6 mm x 150 mm) according to the following conditions with solvents (A) H₂O/0.1% TFA, (B) CH₃CN–H₂O, 9:1 with 0.1% TFA at 1 ml min⁻¹: (I) a gradient of 100% A to 100% B over 22 min; (II) a gradient of 50% A to 100% B over 22 min; (III) a gradient of 25% A to 100% B over 22 min; (IV) an isocratic gradient of 100% B over 22 min; (V) a gradient of 100% A to 100% B over 22 min, then 100% B for 13 min. Data are presented as retention time (*t_R* (min)), purity (%), condition (I or II).



4-Chlorosulfonyl-1-hydroxy-2-naphthoic acid (5). 1-Hydroxy-2-naphthoic acid (**4**; 5 g, 26.6 mmol) was added portionwise with stirring over the course of 1 h to chlorosulfonic acid (25 mL) at -10 °C. Once the addition was complete, TLC of the reaction mixture confirmed all starting material had been consumed (Acetone/EtOAc, 1:1). The reaction mixture was carefully poured over ice. The resulting pinkish-grey solid was collected by vacuum filtration, washing several times with ice-cold water. After the product was allowed to dry on the filter for 1 h, it was transferred to a vacuum oven where it was dried further at 50 °C for 16 h.

General Procedure A: Amination with Anilines. 4-Chlorosulfonyl-1-hydroxy-2-naphthoic acid (**5**; 1 eq) was suspended in anhydrous acetone (0.2 M), and then the requisite aniline (1.2 eq) and pyridine (3 eq) were added under an inert (N₂) atmosphere. The reaction mixture was stirred at 50 °C for 3 h, by which time TLC (acetone/EtOAc, 1:1)

indicated that the reaction was complete. The reaction was concentrated to dryness and then suspended in a 1:1 mixture of EtOAc and 1 M HCl and was vigorously stirred for 5 min. The mixture was transferred to a separatory funnel, then partitioned between EtOAc and 1 M HCl. The organic layer was washed three times with 1 M HCl, dried over Na₂SO₄, filtered, concentrated to deliver a residue that was purified by column chromatography over silica gel using an eluent of CH₂Cl₂/MeOH/AcOH 92:7:1 to provide the title compound.

General Procedure B: Amination with Primary Aliphatic Amines. 4-Chlorosulfonyl-1-hydroxy-2-naphthoic acid (**5**; 1 eq) was suspended in anhydrous acetone (0.2 M). The requisite benzylic amine (1.2 eq) and DIPEA (2.5 eq) were added under an inert (N₂) atmosphere at room temperature (RT). The reaction was stirred at RT for 16 h. TLC (acetone/EtOAc, 1:1) indicated that reaction was complete. The reaction was concentrated to dryness and then suspended in a 1:1 mixture of EtOAc and 1 M HCl and was vigorously stirred for 5 min. The mixture was transferred to a separatory funnel, then partitioned between EtOAc and 1 M HCl. The organic layer was washed three times with 1 M HCl, dried over Na₂SO₄, filtered, concentrated to deliver a residue that was purified by column chromatography over silica gel using an eluent of CH₂Cl₂/MeOH/AcOH 92:7:1 to provide the title compound.

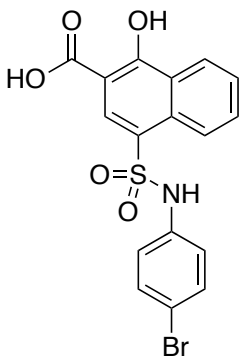
General Procedure C: Amination with Secondary Aliphatic Amines. 4-Chlorosulfonyl-1-hydroxy-2-naphthoic acid (**5**; 1 eq) was suspended in anhydrous acetone (0.2 M), and then the requisite secondary amine (3 eq) was added under an inert (N₂) atmosphere at room temperature. After 1 h, TLC (acetone/EtOAc, 1:1) indicated that the

reaction was complete. The reaction was concentrated to dryness and then suspended in a 1:1 mixture of EtOAc and 1 M HCl and was vigorously stirred for 5 min. The mixture was transferred to a separatory funnel, then partitioned between EtOAc and 1 M HCl. The organic layer was washed three times with 1 M HCl, dried over Na₂SO₄, filtered, concentrated to deliver a residue that was purified by column chromatography over silica gel using an eluent of CH₂Cl₂/MeOH/AcOH 92:7:1 to provide the title compound.

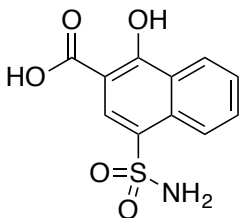
General Procedure D: Nucleophilic aromatic substitution (S_NAr). 4-Fluoronitrobenzene (1 eq) and the requisite phenol (1 eq) were dissolved in anhydrous DMSO (0.3 M). K₂CO₃ (2 eq) was added, and then the reaction was stirred at 120 °C for 16 h. The next day, TLC (Hex/EtOAc, 9:1) indicated the reaction was complete. The reaction was quenched with water and ice, which resulted in precipitation. The precipitate was collected by vacuum filtration and then dried overnight in a vacuum oven at 50 °C to furnish compounds **7** that were sufficiently pure to be advanced to the next step.

General Procedure E: Reduction of Nitro Group with SnCl₂·2H₂O. The appropriate nitroarene **7** was dissolved in EtOAc (0.1 M), and then SnCl₂·2H₂O (5 eq) was added. The reaction mixture was stirred at 50 °C for 16 h, by which time TLC confirmed reaction completion. The reaction mixture was partitioned between EtOAc and sat. NaHCO₃. The organic layer was collected and the aqueous layer was extracted two times with EtOAc. The organics were combined, washed with sat. NaHCO₃, brine, dried with Na₂SO₄, filtered and concentrated. No further purification was required.

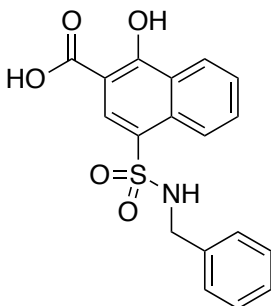
General Procedure F: Reductive Amination. The aniline (1 eq) was dissolved in 1,2-dichloroethane (0.1 M) and the required aldehyde (1 eq) was added, followed by NaBH(OAc)₃ (2 eq). The reaction mixture stirred for 16 h at room temperature. TLC (Hex/EtOAc, 1:1) indicated that the reaction was complete. The reaction mixture was diluted with CH₂Cl₂ and then partitioned with sat. NaHCO₃. The aqueous layer was extracted with further CH₂Cl₂ (x2), and then the organic layers were combined, washed with brine, dried (Na₂SO₄) filtered and concentrated. The crude material was purified by flash column chromatography over silica gel using an eluent of Hex/EtOAc, 1:1 to provide the title compound.



4-(N-(4-bromophenyl)sulfamoyl)-1-hydroxy-2-naphthoic acid (3a). 4-Chlorosulfonyl-1-hydroxy-2-naphthoic acid (**5**) was coupled to 4-bromoaniline according to General Procedure A on a 1 mmol scale to yield the title compound as an off-white solid (300 mg, 71%); δ_{H} (400 MHz, *d*₆-DMSO) 10.47 (s, 1H, SO₂NH), 8.48 – 8.45 (m, 2H, Ar), 8.32 (d, 1H, Ar, *J* = 8.0 Hz), 7.67 (t, 1H, Ar, *J* = 7.4 Hz), 7.49 (t, 1H, Ar, *J* = 7.4 Hz), 7.31 (d, 2H, Ph, *J* = 8.4 Hz), 6.93 (d, 2H, Ph, *J* = 8.8 Hz); δ_{C} (100 MHz, *d*₆-DMSO) 171.0, 138.0, 133.8, 132.2, 131.5, 130.0, 128.1, 125.4, 125.2, 124.5, 120.7, 117.5, 115.3, 107.3, 95.9; Calcd (M⁺): 421.0, Found: 420.0 ([M-H]⁻); *t*_R = 8.1 min (100%, III).

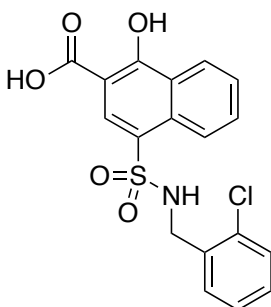


1-Hydroxy-4-sulfamoyl-2-naphthoic acid (3b). 4-Chlorosulfonyl-1-hydroxy-2-naphthoic acid (**5**; 287 mg, 1 eq) was suspended in dioxane (5 mL) at 0 °C, then NH₄OH (1 mL) was added dropwise. After 1 h, TLC (Acetone/EtOAc 1:1) confirmed the reaction was complete. The reaction mixture was concentrated to dryness, then partitioned between EtOAc (50 mL) and 1 M HCl (25 mL). The aqueous layer was extracted with further EtOAc (50 mL), then the organic layers were washed with brine, dried (Na₂SO₄), filtered and concentration to afford the title compound light orange solid (160 mg, 60%): δ_{H} (400 MHz, *d*₆-DMSO) 8.43 – 8.40 (m, 2H, Ar), 8.34 (d, 1H, Ar, *J* = 8.4 Hz), 7.60 (t, 1H, Ar, *J* = 7.4 Hz), 7.46 (t, 1H, Ar, *J* = 8.0 Hz), 7.13 (s, 2H, SO₂NH₂); δ_{C} (100 MHz, *d*₆-DMSO) 171.3, 170.6, 131.5, 130.6, 128.9, 128.4, 125.3, 125.0, 124.6, 122.6, 107.9; Calcd (M⁺): 267.0, Found: 266.0 ([M-H]⁻).

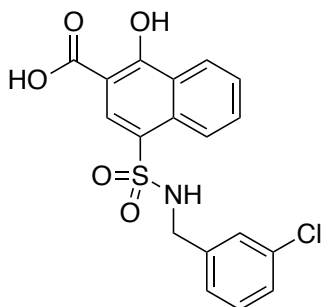


4-(N-Benzylsulfamoyl)-1-hydroxy-2-naphthoic acid (3c). 4-Chlorosulfonyl-1-hydroxy-2-naphthoic acid (**5**) was coupled to benzylamine according to General Procedure B on a 1

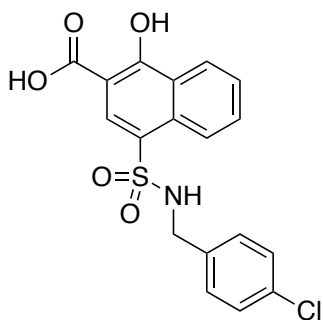
mmol scale to yield the title compound as a dark yellow solid (232 mg, 65%): δ_{H} (400 MHz, d_6 -DMSO) 8.45 (d, $J = 8.0$, 1 H, *Ar*), 8.43 (s, 1 H, *Ar*), 8.36 (d, $J = 8.0$, 1 H, *Ar*), 7.95 (t, $J = 6.4$, 1 H, *NH*), 7.62 (t, $J = 8.0$, 1 H, *Ar*), 7.48 (t, $J = 8.0$, 1 H, *Ar*), 7.22-7.10 (m, 5 H, *Ar*), 3.89 (d, $J = 6.4$, 2 H, CH_2); δ_{C} (100 MHz, d_6 -DMSO) 171.2, 138.6, 132.9, 131.7, 129.3, 128.4, 127.8, 127.3, 125.1, 125.0, 124.8, 46.2; Calcd (M^+): 357.1, Found: 356.0 ($[\text{M}-\text{H}]^-$); $t_{\text{R}} = 11.5$ min (98.9%, II).



4-(N-(2-Chlorobenzyl)sulfamoyl)-1-hydroxy-2-naphthoic acid (3d). 4-Chlorosulfonyl-1-hydroxy-2-naphthoic acid (**5**) was coupled to 2-chlorobenzylamine according to General Procedure B on a 1 mmol scale to yield the title compound as a light purple solid (274 mg, 70%): δ_{H} (400 MHz, d_6 -DMSO) 8.45-8.33 (m, 2 H, *Ar*), 8.35 (d, $J = 7.6$, 1 H, *Ar*), 7.99 (t, $J = 6.0$, 1 H, *NH*), 7.61 (t, $J = 7.6$, 1 H, *Ar*), 7.46 (t, $J = 7.6$, 1 H, *Ar*), 7.40-7.37 (m, 1 H, *Ar*), 7.32-7.29 (m, 1 H, *Ar*), 7.22-7.17 (m, 2 H, *Ar*), 3.98 (d, $J = 6.0$, 2 H, CH_2); δ_{C} (100 MHz, d_6 -DMSO) 171.0, 135.7, 133.1, 132.2, 131.7, 129.9, 129.3, 129.1, 128.6, 127.2, 125.1, 125.0, 124.7, 107.8, 43.6; Calcd (M^+): 391.0, Found: 414.1 ($[\text{M}+\text{Na}]^+$); $t_{\text{R}} = 10.2$ min (97.2%, II).

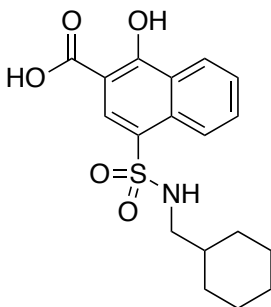


4-(N-(3-Chlorobenzyl)sulfamoyl)-1-hydroxy-2-naphthoic acid (3e). 4-Chlorosulfonyl-1-hydroxy-2-naphthoic acid (**5**) was coupled to 3-chlorobenzylamine according to General Procedure B on a 1 mmol scale to yield the title compound as a dark purple solid (286 mg, 73%): δ_{H} (400 MHz, d_6 -DMSO) 8.43-8.39 (m, 2 H, *Ar*), 8.35 (d, $J = 7.6$, 1 H, *Ar*), 8.04 (t, $J = 6.4$, 1 H, *NH*), 7.63 (t, $J = 7.6$, 1 H, *Ar*), 7.47 (t, $J = 7.6$, 1 H, *Ar*), 7.21-7.15 (m, 3 H, *Ar*), 7.13-7.09 (m, 1 H, *Ar*), 3.91 (d, $J = 6.4$, 2 H, *CH*₂); δ_{C} (100 MHz, d_6 -DMSO) 171.2, 141.2, 133.1, 132.8, 131.6, 130.1, 129.4, 128.3, 127.6, 127.1, 126.4, 125.1, 125.0, 124.9, 107.6, 45.5; Calcd (M^+): 391.0, Found: 414.1 ($[\text{M}+\text{Na}]^+$); $t_{\text{R}} = 21.5$ min (98.8%, I).

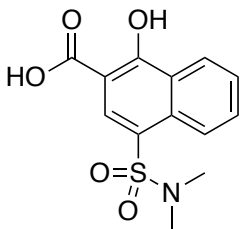


4-(N-(4-Chlorobenzyl)sulfamoyl)-1-hydroxy-2-naphthoic acid (3f). 4-Chlorosulfonyl-1-hydroxy-2-naphthoic acid (**5**) was coupled to 4-chlorobenzylamine according to General Procedure B on a 1 mmol scale to yield the title compound as a light brown solid (294 mg, 75%): δ_{H} (400 MHz, d_6 -DMSO) 8.56 (d, 1H, *Ar*, $J = 8.4$ Hz), 8.46 (t, 1H, SO_2NH , $J = 5.8$ Hz), 8.39 (d, 1H, *Ar*, $J = 8.8$ Hz), 8.32 (s, 1H, *Ar*), 7.84 (t, 1H, *Ar*, $J = 7.6$ Hz), 7.71 (t,

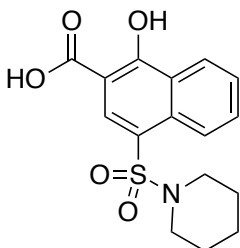
1H, Ar, $J = 7.4$ Hz), 7.11, 7.06 (ABq, 4H, Ar, $J_{AB} = 8.8$ Hz), 3.97 (d, 2H, Ar, $J = 6.4$ Hz); δ_C (100 MHz, $CDCl_3$) 177.1, 169.4, 141.6, 136.7, 136.1, 136.0, 134.6, 134.4, 134.2, 132.3, 131.9, 130.6, 130.1, 129.1, 109.8, 50.3; Calcd (M^+): 391.0, Found: 392.0 ($[M+H]^+$); $t_R = 12.8$ min (100%, II).



4-(N-(Cyclohexylmethyl)sulfonyl)-1-hydroxy-2-naphthoic acid (3g). 4-Chlorosulfonyl-1-hydroxy-2-naphthoic acid (**5**) was coupled to cyclohexylmethylamine according to General Procedure B on a 1 mmol scale to yield the title compound as a brown solid (218 mg, 60%): δ_H (400 MHz, d_6 -DMSO) 8.61 (d, 1H, Ar, $J = 8.8$ Hz), 8.42 – 8.39 (m, 3H, Ar), 7.86 – 7.81 (m, 2H, Ar, SO_2NH), 7.71 (t, 1H, Ar, $J = 7.4$ Hz), 2.56 (t, 1H, $CHCH_2$, $J = 5.8$ Hz), 1.55 – 1.45 (m, 5H, cyclohexyl), 1.30 – 1.18 (m, 1H, $CHCH_2$), 1.05 – 0.90 (m, 3H, cyclohexyl), 0.62 – 0.74 (m, 2H, cyclohexyl); δ_C (100 MHz, d_6 -DMSO) 172.1, 164.1, 131.2, 130.8, 129.1, 126.8, 125.8, 125.2, 125.1, 124.0, 104.5, 48.6, 37.2, 30.1, 25.9, 25.3; Calcd (M^+): 363.1, Found: 386.3 ($[M+Na]^+$); $t_R = 13.7$ min (98.2%, II).

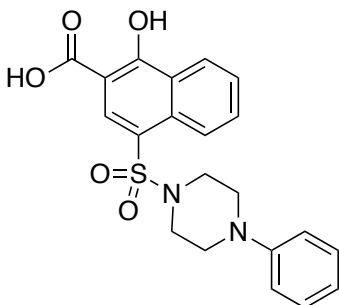


4-(N,N-Dimethylsulfonyl)-1-hydroxy-2-naphthoic acid (3h). 4-Chlorosulfonyl-1-hydroxy-2-naphthoic acid (**5**) was coupled to dimethylamine hydrochloride according to General Procedure B on a 1 mmol scale to yield the title compound as a dark purple solid (170 mg, 58%): δ_{H} (400 MHz, d_6 -DMSO) 8.58 (d, 1H, Ar, $J = 8.4$ Hz), 8.43 (d, 1H, Ar, $J = 8.0$ Hz), 8.40 (s, 1H, Ar), 7.86 (t, 1H, Ar, $J = 7.8$ Hz), 7.71 (t, 1H, Ar, $J = 7.4$ Hz), 2.70 (s, 6H, $\text{N}(\text{CH}_3)_2$); δ_{C} (100 MHz, d_6 -DMSO) 172.2, 165.3, 132.3, 131.5, 127.3, 127.2, 125.7, 125.5, 124.5, 121.7, 105.6, 37.4; Calcd (M^+): 295.1, Found: 296.2 ($[\text{M}+\text{H}]^+$); $t_{\text{R}} = 20.5$ min (98.3%, I).

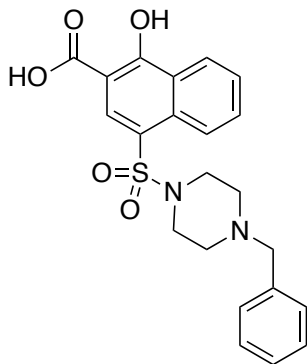


1-Hydroxy-4-(piperidin-1-ylsulfonyl)-2-naphthoic acid (3i). 4-Chlorosulfonyl-1-hydroxy-2-naphthoic acid (**5**) was coupled to piperidine according to General Procedure C on a 0.8 mmol scale to yield the title compound as a light brown solid (265 mg, 79%): δ_{H} (400 MHz, d_6 -DMSO) 8.58 (d, 1H, Ar, $J = 8.4$ Hz), 8.43 (d, 1H, Ar, $J = 8.8$ Hz), 8.40 (s, 1H, Ar), 7.88 (t, 1H, Ar, $J = 7.8$ Hz), 7.73 (t, 1H, Ar, $J = 7.6$ Hz), 3.05 – 3.03 (m, 4H, CH_2NCH_2), 1.50 – 1.32 (m, 6H, piperidinyl); δ_{C} (100 MHz, d_6 -DMSO) 172.3, 164.7, 132.1, 131.5, 131.2,

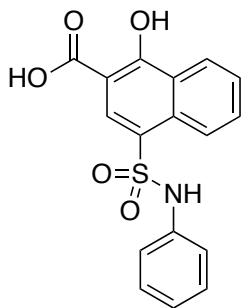
127.4, 125.5, 125.4, 124.5, 122.9, 105.4, 46.2, 25.4, 23.3; Calcd (M^+): 335.1, Found: 336.2 ($[M+H]^+$); $t_R = 16.5$ min (95.1%, II).



1-Hydroxy-4-((4-phenylpiperazin-1-yl)sulfonyl)-2-naphthoic acid (3j). 4-Chlorosulfonyl-1-hydroxy-2-naphthoic acid (**5**) was coupled to 1-phenylpiperazine according to General Procedure C on a 0.8 mmol scale to yield the title compound as a brown-orange solid (264 mg, 64%): δ_H (400 MHz, d_6 -DMSO) 8.70 (d, 1H, Ar, $J = 8.8$ Hz), 8.46 – 8.43 (m, 2H, Ar), 7.88 (t, 1H, Ar, $J = 8.0$ Hz), 7.73 (t, 1H, Ar, $J = 7.4$ Hz), 7.17 (t, 2H, Ph, $J = 7.8$ Hz), 6.86 (d, 2H, Ph, $J = 8.0$ Hz), 6.78 (d, 1H, Ph, $J = 7.2$ Hz) 3.19 – 3.12 (m, 8H, piperazinyl); δ_C (100 MHz, d_6 -DMSO) 171.9, 165.0, 150.4, 131.8, 131.5, 131.3, 129.0, 127.0, 125.3, 125.1, 124.2, 121.3, 119.8, 116.2, 105.3, 48.3, 45.2; Calcd (M^+): 412.1, Found: 413.3 ($[M+H]^+$); $t_R = 19.4$ min (100%, II).

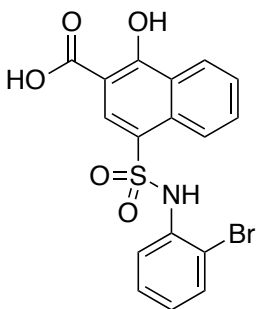


4-((4-Benzylpiperazin-1-yl)sulfonyl)-1-hydroxy-2-naphthoic acid (3k). 4-Chlorosulfonyl-1-hydroxy-2-naphthoic acid (**5**) was coupled to *N*-benzylpiperazine according to General Procedure C on a 1 mmol scale to yield the title compound as a light yellow solid (303 mg, 71%): δ_{H} (400 MHz, d_6 -DMSO) 8.41 – 8.37 (m, 3H, Ar), 7.62 (t, 1H, Ar, $J = 7.6$ Hz), 7.47 (t, 1H, Ar, $J = 7.6$ Hz), 7.43 – 7.36 (m, 5H, Ph), 4.22 (br s, 2H, CH_2Ph), 3.70 – 2.80 (m, 8H, piperazinyl); δ_{C} (100 MHz, d_6 -DMSO) 173.4, 170.4, 158.7, 135.3, 132.6, 131.3, 131.0, 129.9, 129.2, 129.1, 125.6, 125.5, 124.9, 124.8, 107.9; Calcd (M^+): 426.1, Found: 427.2 ($[\text{M}+\text{H}]^+$); $t_{\text{R}} = 6.5$ min (95.3%, II).

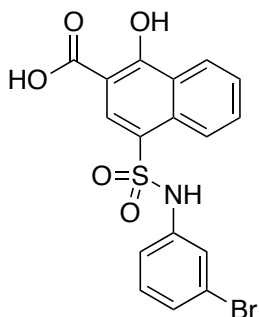


1-Hydroxy-4-(N-phenylsulfamoyl)-2-naphthoic acid (3l). 4-Chlorosulfonyl-1-hydroxy-2-naphthoic acid (**5**) was coupled to aniline according to General Procedure A on a 1 mmol scale to yield the title compound as a cream solid (275 mg, 80%): δ_{H} (400 MHz, d_6 -DMSO)

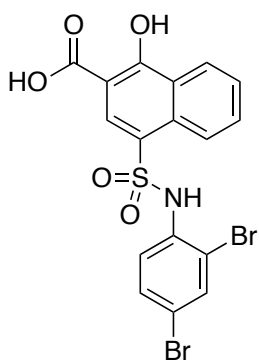
10.58 (s, 1H, SO₂NH), 8.66 (d, 1H, Ar, $J = 8.4$ Hz), 8.47 (s, 1H, Ar), 8.38 (d, 1H, Ar, $J = 8.8$ Hz), 7.87 (t, 1H, Ar, $J = 8.0$ Hz), 7.71 (t, 1H, Ar, $J = 7.8$ Hz), 7.15 (t, 2H, Ph, $J = 7.8$ Hz), 6.99 (d, 2H, Ph, $J = 8.0$ Hz), 6.92 (t, 1H, Ph, $J = 7.0$ Hz); δ_C (100 MHz, *d*₆-DMSO) 172.2, 164.9, 137.9, 131.6, 131.3, 130.9, 129.5, 127.4, 125.3, 125.0, 124.7, 124.6, 124.1, 119.7, 105.2; Calcd (M⁺): 343.1, Found: 344.1 ([M+H]⁺); $t_R = 3.9$ min (100%, II).



4-(N-(2-bromophenyl)sulfamoyl)-1-hydroxy-2-naphthoic acid (3m). 4-Chlorosulfonyl-1-hydroxy-2-naphthoic acid (**5**) was coupled to 2-bromoaniline according to General Procedure A on a 1 mmol scale to yield the title compound as a pink solid (287 mg, 68%): δ_H (400 MHz, *d*₆-DMSO) 10.07 (s, 1H, SO₂NH), 8.60 (d, 1H, Ar, $J = 8.4$ Hz), 8.41 (d, 1H, Ar, $J = 8.4$ Hz), 8.31 (s, 1H, Ar), 7.78 (t, 1H, Ar, $J = 7.4$ Hz), 7.69 (t, 1H, Ar, $J = 7.4$ Hz), 7.48 (d, 1H, Ar, $J = 7.6$ Hz), 7.23 (t, 1H, Ar, $J = 7.4$ Hz), 7.15 (d, 1H, Ar, $J = 8.0$ Hz), 7.09 (t, 1H, Ar, $J = 7.4$ Hz); δ_C (100 MHz, *d*₆-DMSO) 172.2, 165.2, 135.4, 133.5, 131.7, 131.1, 130.2, 128.9, 128.8, 128.7, 128.6, 127.2, 125.8, 125.6, 124.4, 120.9, 105.3; Calcd (M⁺): Calcd (M⁺): 421.0, Found: 420.2 ([M-H]⁻); $t_R = 12.0$ min (98.6 %, II).

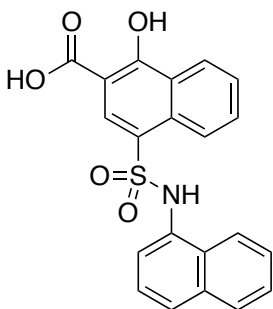


4-(N-(3-Bromophenyl)sulfonyl)-1-hydroxy-2-naphthoic acid (3n). 4-Chlorosulfonyl-1-hydroxy-2-naphthoic acid (**5**) was coupled to 3-bromoaniline according to General Procedure A on a 1 mmol scale to yield the title compound as a light pink solid (300 mg, 71%): δ_{H} (400 MHz, d_6 -DMSO) 11.86 (s, 1H, SO_2NH), 8.61 (d, 1H, Ar, $J = 8.8$ Hz), 8.51 (s, 1H, Ar), 8.38 (d, 1H, Ar, $J = 8.4$ Hz), 7.87 (t, 1H, Ar, $J = 7.4$ Hz), 7.69 (t, 1H, Ar, $J = 7.4$ Hz), 7.18 (s, 1H, Ar), 7.14 – 7.00 (m, 3H, Ar); δ_{C} (100 MHz, d_6 -DMSO) 172.1, 165.5, 139.7, 131.6, 131.5, 131.4, 131.2, 127.4, 126.5, 125.6, 125.5, 124.7, 123.5, 122.2, 121.4, 117.8, 105.4; Calcd (M^+): 421.0, Found: 420.2 ($[\text{M}-\text{H}]^-$); $t_{\text{R}} = 12.3$ min (98.5%, II).

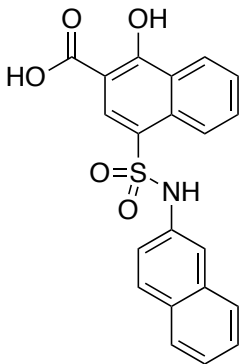


4-(N-(2,4-Dibromophenyl)sulfonyl)-1-hydroxy-2-naphthoic acid (3o). 4-Chlorosulfonyl-1-hydroxy-2-naphthoic acid (**5**) was coupled to 2,4-dibromoaniline according to General Procedure A on a 1 mmol scale to yield the title compound as a dark beige solid (291 mg, 58%): δ_{H} (400 MHz, d_6 -DMSO) 10.15 (s, 1H, SO_2NH), 8.56 (d, 1H, Ar, $J = 8.4$ Hz), 8.41

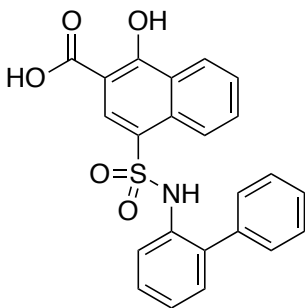
(d, 1H, Ar, $J = 8.4$ Hz), 8.30 (s, 1H, Ar), 7.80 – 7.75 (m, 2H, Ar), 7.69 (t, 1H, Ar, $J = 7.4$ Hz), 7.50 (dd, 1H, Ar, $J = 8.8, 1.6$ Hz), 7.09 (d, 1H, Ar, $J = 8.4$ Hz); δ_C (100 MHz, d_6 -DMSO) 172.2, 165.3, 135.4, 135.1, 131.8, 131.6, 131.2, 130.3, 129.8, 127.3, 125.6, 125.5, 125.4, 124.5, 121.8, 120.0, 105.3; Calcd (M^+): 498.9, Found: 498.1 ($[M-H]^-$); $t_R = 18.2$ min (97.0%, II).



1-Hydroxy-4-(N-(naphthalen-1-yl)sulfamoyl)-2-naphthoic acid (3p). 4-Chlorosulfonyl-1-hydroxy-2-naphthoic acid (**5**) was coupled to 1-naphthylamine according to General Procedure A on a 1 mmol scale to yield the title compound as a dark purple solid (283 mg, 72%): δ_H (400 MHz, d_6 -DMSO) 10.46 (s, 1H, SO_2NH), 8.74 (d, 1H, Ar, $J = 8.8$ Hz), 8.38 (d, 1H, Ar, $J = 8.8$ Hz), 8.26 (s, 1H, Ar), 7.96 (d, 1H, Ar, $J = 8.8$ Hz), 7.85 – 7.83 (m, 2H, Ar), 7.73 – 7.68 (m, 2H, Ar), 7.41 (t, 1H, Ar, $J = 7.6$ Hz), 7.34 (t, 1H, Ar, $J = 7.8$ Hz), 7.28 (t, 1H, Ar, $J = 7.4$ Hz), 7.12 (d, 1H, Ar, $J = 8.0$ Hz); δ_C (100 MHz, d_6 -DMSO) 171.8, 164.6, 134.7, 133.8, 132.2, 131.3, 130.9, 130.0, 129.4, 128.5, 128.0, 126.9, 126.7, 126.2, 125.9, 125.6, 125.0, 124.9, 124.1, 123.0, 104.8; Calcd (M^+): 393.1, Found: 416.2 ($[M+Na]^+$); $t_R = 9.7$ min (100%, II).

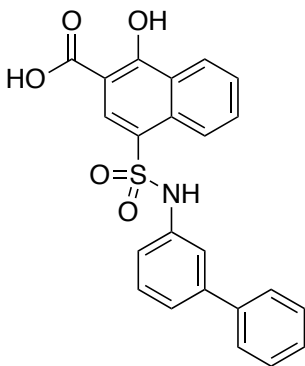


1-Hydroxy-4-(N-(naphthalen-2-yl)sulfamoyl)-2-naphthoic acid (3q). 4-Chlorosulfonyl-1-hydroxy-2-naphthoic acid (**5**) was coupled to 2-naphthylamine according to General Procedure A on a 1 mmol scale to yield the title compound as a grey-purple solid (303 mg, 77%): δ_{H} (400 MHz, d_6 -DMSO) 10.83 (s, 1H, SO₂NH), 8.72 (d, 1H, Ar, $J = 7.6$ Hz), 8.57 (s, 1H, Ar), 8.35 (d, 1H, Ar, $J = 8.4$ Hz), 7.87 (t, 1H, Ar, $J = 8.0$ Hz), 7.72 – 7.65 (m, 4H, Ar), 7.47 (s, 1H, Ar), 7.38 (t, 1H, $J = 7.0$ Hz), 7.32 (t, 1H, Ar, $J = 7.0$ Hz), 7.22 (d, 1H, Ar, $J = 8.8$ Hz); δ_{C} (100 MHz, d_6 -DMSO) 171.8, 164.9, 135.3, 133.2, 131.2, 131.0, 130.9, 129.8, 129.1, 127.5, 127.0, 126.9, 126.8, 125.2, 124.9, 124.6, 124.3, 123.7, 119.7, 115.0, 105.0; Calcd (M^+): 393.1, Found: 392.2 ($[M-H]^+$); $t_{\text{R}} = 12.7$ min (94.5%, II).

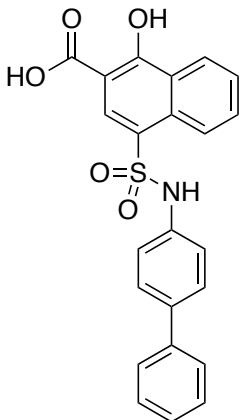


4-(N-([1,1'-Biphenyl]-2-yl)sulfamoyl)-1-hydroxy-2-naphthoic acid (3r). 4-Chlorosulfonyl-1-hydroxy-2-naphthoic acid (**5**) was coupled to 2-aminobiphenyl according to General Procedure A on a 1 mmol scale to yield the title compound as a beige solid (252 mg, 60%):

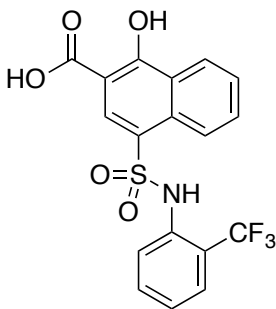
δ_{H} (400 MHz, d_6 -DMSO) 9.60 (s, 1H), 8.33-8.28 (m, 2H), 8.07 (s, 1H), 7.62-7.58 (m, 2H), 7.23 (t, $J=4.8$ Hz, 2H), 7.11 (t, $J=4.8$ Hz, 1H), 7.03-7.00 (m, 6H). δ_{C} (100 MHz, d_6 -DMSO) 172.3, 164.9, 139.9, 138.6, 133.5, 131.4, 131.3, 130.9, 129.5, 129.1, 128.5, 127.8, 127.7, 126.9, 126.8, 126.4, 125.5, 125.4, 124.3, 105.1; Calcd (M^+): 419.1, Found: 442.2 ($[\text{M}+\text{Na}]^+$); $t_{\text{R}} = 14.6$ min (98.7%, II).



4-(N-([1,1'-Biphenyl]-3-yl)sulfamoyl)-1-hydroxy-2-naphthoic acid (3s). 4-Chlorosulfonyl-1-hydroxy-2-naphthoic acid (**5**) was coupled to 3-aminobiphenyl according to General Procedure A on a 1 mmol scale to yield the title compound as a dark brown solid (239 mg, 58%): δ_{H} (400 MHz, d_6 -DMSO) 10.45 (s, 1H), 8.61 (s, 1H), 8.53 (d, $J=8.8$ Hz, 1H), 8.32 (d, $J=8.8$ Hz, 1H), 7.68 (t, $J=8$ Hz, 1H), 7.49 (t, $J=7.6$ Hz, 1H), 7.40 (m, 4H), 7.34 (m, 1H), 7.28 (s, 1H), 7.20 (t, $J=7.6$ Hz, 1H), 7.13 (d, $J=8$ Hz, 1H), 6.95 (d, $J=8$ Hz, 1H). δ_{C} (100 MHz, d_6 -DMSO) 171.1, 141.3, 140.2, 139.2, 134.1, 131.6, 130.1, 129.9, 129.4, 128.0, 126.9, 125.4, 125.2, 124.6, 121.5, 117.7, 116.6, 107.1; Calcd (M^+): 419.1, Found: 418.3 ($[\text{M}-\text{H}]^-$); $t_{\text{R}} = 13.9$ min (100%, II).

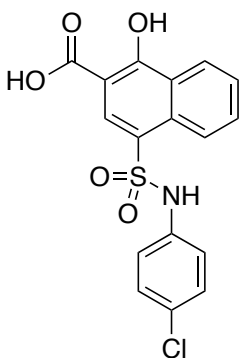


4-(N-([1,1'-Biphenyl]-4-yl)sulfamoyl)-1-hydroxy-2-naphthoic acid (3t). 4-Chlorosulfonyl-1-hydroxy-2-naphthoic acid (**5**) was coupled to 4-aminobiphenyl according to General Procedure A on a 1 mmol scale to yield the title compound as a brown solid (260 mg, 62%): δ_{H} (400 MHz, d_6 -DMSO) 10.37 (s, 1H), 8.54 (s, 1H), 8.47 (d, $J=8$ Hz, 1H), 8.31 (d, $J=7.6$ Hz, 1H), 7.62 (t, $J=8$ Hz, 1H), 7.51 (d, $J=8$ Hz, 2H), 7.44 (d, $J=8.4$ Hz, 3H), 7.35 (t, $J=8$ Hz, 2H), 7.25 (t, $J=7.6$ Hz, 1H), 7.05 (d, $J=7.6$ Hz, 2H). δ_{C} (100 MHz, d_6 -DMSO) 172.5, 170.8, 139.9, 138.2, 134.8, 134.3, 131.6, 129.6, 129.2, 128.7, 127.6, 127.3, 126.6, 125.3, 124.8, 124.5, 118.8, 116.3, 107.9; Calcd (M^+): 419.5, Found: 418.3 ($[M-H]^-$); $t_{\text{R}} = 13.9$ min (98.3%, II).

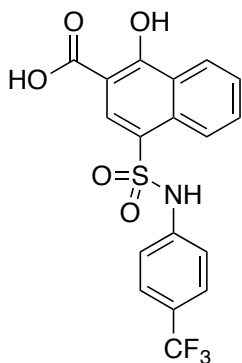


1-Hydroxy-4-(N-(2-(trifluoromethyl)phenyl)sulfamoyl)-2-naphthoic acid (3u). 4-Chlorosulfonyl-1-hydroxy-2-naphthoic acid (**5**) was coupled to 2-trifluoromethylaniline

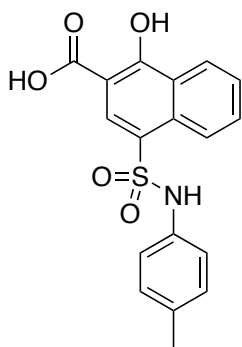
according to General Procedure A on a 1 mmol scale to yield the title compound as a dark pink solid (222 mg, 54%): δ_{H} (400 MHz, d_6 -DMSO) 10.06 (s, 1H, SO₂NH), 8.62 (d, 1H, Ar, J = 8.0 Hz), 8.44 (d, 1H, Ar, J = 8.8 Hz), 8.32 (s, 1H, Ar), 7.80 (t, 1H, Ar, J = 7.4 Hz), 7.71 – 7.66 (m, 2H, Ar), 7.52 (t, 1H, Ar, J = 7.2 Hz), 7.41 (t, 1H, Ar, J = 7.0 Hz), 6.99 (d, 1H, Ar, J = 7.6 Hz); δ_{C} (100 MHz, d_6 -DMSO) 172.1, 166.2, 134.5, 133.8, 133.7, 131.5, 131.0, 130.6, 129.5, 127.8, 127.4, 126.9, 126.4, 126.2 (q, $^2J_{\text{CF}}$ = 40 Hz), 125.5 (q, $^1J_{\text{CF}}$ = 108 Hz), 124.9, 124.6, 105.6; Calcd (M^+): 411.0, Found: 410.2 ($[M-H]^+$); t_{R} = 10.7 min (96.7%, II).



4-(N-(4-Chlorophenyl)sulfamoyl)-1-hydroxy-2-naphthoic acid (3v). 4-Chlorosulfonyl-1-hydroxy-2-naphthoic acid (**5**) was coupled to 4-chloroaniline according to General Procedure A on a 1 mmol scale to yield the title compound as a light brown solid (189 mg, 50%): δ_{H} (400 MHz, d_6 -DMSO) 10.74 (s, 1 H, NH), 8.62 (d, J = 8.8, 1 H, Ar), 8.46 (s, 1 H, Ar), 8.39 (d, J = 8.8, 1 H, Ar), 7.86 (t, J = 8.8, 1 H, Ar), 7.71 (t, J = 8.8, 1 H, Ar), 7.22 (d, J = 8.4, 2 H, Ar), 7.00 (d, J = 8.4, 2 H, Ar); δ_{C} (100 MHz, d_6 -DMSO) 172.2, 165.0, 136.9, 131.7, 131.2, 131.1, 129.5, 128.1, 127.4, 125.4, 124.9, 124.6, 124.2, 121.1, 105.3; Calcd (M^+): 377.0, Found: 376.2 ($[M-H]^+$); t_{R} = 12.2 min (95.7%, II).

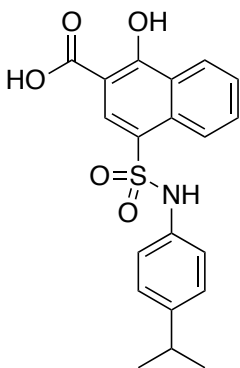


1-Hydroxy-4-(N-(4-(trifluoromethyl)phenyl)sulfamoyl)-2-naphthoic acid (3w). 4-Chlorosulfonyl-1-hydroxy-2-naphthoic acid (**5**) was coupled to 4-trifluoromethylaniline according to General Procedure A on a 1 mmol scale to yield the title compound as a light pink solid (218 mg, 53%): δ_{H} (400 MHz, d_6 -DMSO) 11.13 (s, 1 H, *NH*), 8.60 (d, $J = 8.8$, 1 H, *Ar*), 8.57 (s, 1 H, *Ar*), 8.39 (d, $J = 8.8$, 1 H, *Ar*), 7.85 (t, $J = 8.8$, 1 H, *Ar*), 7.68 (t, $J = 8.8$, 1 H, *Ar*), 7.55 (d, $J = 8.8$, 2 H, *Ar*), 7.19 (d, $J = 8.8$, 2 H, *Ar*); δ_{C} (100 MHz, d_6 -DMSO) 172.0, 165.7, 141.8, 131.7, 131.5, 131.2, 127.4, 127.0, 125.9, 125.7, 124.8, 124.7, 123.6, 118.2, 105.5; Calcd (M^+): 411.0, Found: 434.2 ($[M+Na]^+$); $t_{\text{R}} = 15.6$ min (95.4%, II).

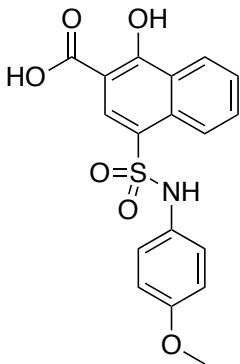


1-Hydroxy-4-(N-(p-tolyl)sulfamoyl)-2-naphthoic acid (3x). 4-Chlorosulfonyl-1-hydroxy-2-naphthoic acid (**5**) was coupled to *p*-toluidine according to General Procedure A on a 1 mmol scale to yield the title compound as a beige solid (225 mg, 63%): δ_{H} (400 MHz, d_6 -

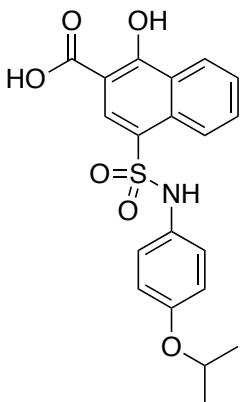
DMSO) 10.39 (s, 1 H, *NH*), 8.65 (d, *J* = 8.8, 1 H, *Ar*), 8.43 (s, 1 H, *Ar*), 8.38 (d, *J* = 8.8, 1 H, *Ar*), 7.86 (t, *J* = 8.8, 1 H, *Ar*), 7.70 (t, *J* = 8.8, 1 H, *Ar*), 6.95 (d, *J* = 8.0, 2 H, *Ar*), 6.87 (d, *J* = 8.0, 2 H, *Ar*), 2.11 (s, 3 H, *CH*₃); δ_{C} (100 MHz, *d*₆-DMSO) 172.2, 165.0, 135.2, 133.4, 131.5, 131.4, 131.0, 129.9, 127.3, 125.4, 125.1, 124.5, 120.2, 105.3, 20.6; Calcd (*M*⁺): 357.1, Found: 380.2 (*[M+Na]*⁺); *t*_R = 9.0 min (95.5%, II).



1-Hydroxy-4-(N-(4-isopropylphenyl)sulfamoyl)-2-naphthoic acid (3y). 4-Chlorosulfonyl-1-hydroxy-2-naphthoic acid (**5**) was coupled to *p*-isopropylaniline according to General Procedure A on a 1 mmol scale to yield the title compound as a beige solid (235 mg, 61%): δ_{H} (400 MHz, *d*₆-DMSO) 10.42 (s, 1 H, *NH*), 8.63 (d, *J* = 8.4, 1 H, *Ar*), 8.46 (s, 1 H, *Ar*), 8.39 (d, *J* = 8.4, 1 H, *Ar*), 7.84 (t, *J* = 8.4, 1 H, *Ar*), 7.70 (t, *J* = 8.4, 1 H, *Ar*), 7.02 (d, *J* = 8.4, 2 H, *Ar*), 6.90 (d, *J* = 8.0, 2 H, *Ar*), 2.71 (sept, *J* = 7.2, 1 H, *CH*), 1.06 (d, *J* = 7.2, 6 H, 2 x *CH*₃); δ_{C} (100 MHz, *d*₆-DMSO) 172.2, 164.8, 144.3, 135.5, 131.5, 131.4, 130.8, 127.3, 125.3, 125.1, 124.5, 120.0, 105.2, 33.1, 24.2; Calcd (*M*⁺): 385.1, Found: 408.3 (*[M+Na]*⁺); *t*_R = 15.3 min (95.9%, II).

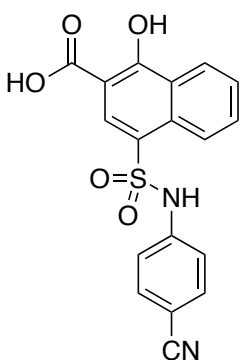


1-Hydroxy-4-(N-(4-methoxyphenyl)sulfamoyl)-2-naphthoic acid (3z). 4-Chlorosulfonyl-1-hydroxy-2-naphthoic acid (**5**) was coupled to *p*-anisidine according to General Procedure A on a 1 mmol scale to yield the title compound as a light brown solid (281 mg, 75%): δ_{H} (400 MHz, d_6 -DMSO) 10.18 (s, 1H, SO₂NH), 8.64 (d, 1H, Ar, $J = 8.8$ Hz), 8.38 (d, 1H, Ar, $J = 8.4$ Hz), 8.36 (s, 1H, Ar), 7.86 (t, 1H, Ar, $J = 7.4$ Hz), 7.71 (t, 2H, Ar, $J = 7.6$ Hz), 6.85 (d, 2H, Ar, $J = 9.2$ Hz), 6.71 (d, 2H, Ar, $J = 8.8$ Hz), 3.59 (s, 3H, OMe); δ_{C} (100 MHz, d_6 -DMSO): 172.2, 164.7, 156.8, 131.5, 131.4, 130.7, 130.3, 127.3, 125.3, 125.2, 124.8, 124.5, 123.3, 114.7, 105.2, 55.5; Calcd (M⁺): 373.1, Found: 372.3 ([M-H⁻]; $t_{\text{R}} = 8.7$ min (99.6%, III).

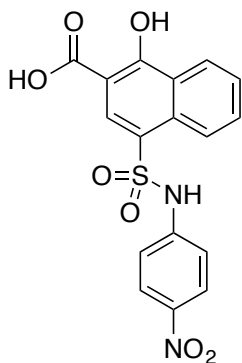


1-Hydroxy-4-(N-(4-isopropoxyphenyl)sulfamoyl)-2-naphthoic acid (3aa). 4-Chlorosulfonyl-1-hydroxy-2-naphthoic acid (**5**) was coupled to 4-isopropoxyaniline

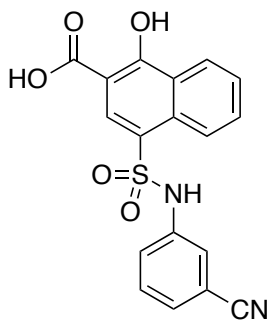
according to General Procedure A on a 1 mmol scale to yield the title compound as a white solid (289 mg, 72%): δ_{H} (400 MHz, d_6 -DMSO) 10.15 (s, 1H, SO₂NH), 8.63 (d, 1H, Ar, J = 8.8 Hz), 8.39 (d, 1H, Ar, J = 8.0 Hz), 8.35 (s, 1H, Ar), 7.85 (t, 1H, Ar, J = 7.4 Hz), 7.71 (t, 1H, Ar, J = 7.8 Hz), 6.83 (d, 2H, Ar, J = 9.6 Hz), 6.69 (d, 2H, Ar, J = 8.8 Hz), 4.41 (hep, 1H, CH(CH₃)₂, J = 5.8 Hz), 1.14 (d, 6H, CH(CH₃)₂, J = 5.2 Hz); δ_{C} (100 MHz, d_6 -DMSO) 172.2, 164.7, 155.0, 131.5, 131.4, 130.7, 130.1, 127.3, 125.3, 125.2, 124.9, 124.5, 123.4, 116.5, 105.2, 69.7, 22.1; Calcd (M⁺): 401.1, Found: 402.0 ([M+H]⁺); t_{R} = 10.2 min (98.6%, II).



4-(N-(4-Cyanophenyl)sulfamoyl)-1-hydroxy-2-naphthoic acid (3ab). Chlorosulfonyl-1-hydroxy-2-naphthoic acid (**5**) was coupled to 4-aminobenzonitrile according to General Procedure A on a 1 mmol scale to yield the title compound as a light pink solid (254 mg, 69%): δ_{H} (400 MHz, d_6 -DMSO) 11.32 (s, 1H, SO₂NH), 8.60 – 8.57 (m, 2H, Ar), 8.39 (d, 1H, Ar, J = 8.8 Hz), 7.87 (t, 1H, Ar, J = 7.4 Hz), 7.69 (t, 1H, Ar, J = 7.8 Hz), 7.63 (d, 2H, Ar, J = 8.4 Hz), 7.15 (d, 2H, Ar, J = 8.8 Hz); δ_{C} (100 MHz, d_6 -DMSO) 172.0, 166.1, 142.5, 134.1, 131.8, 131.7, 131.1, 127.3, 125.8, 124.8, 124.6, 122.9, 119.1, 118.1, 105.9, 105.3; Calcd (M⁺): 368.1, Found: 367.1 ([M-H]⁻); t_{R} = 5.5 min (98.3%, II).

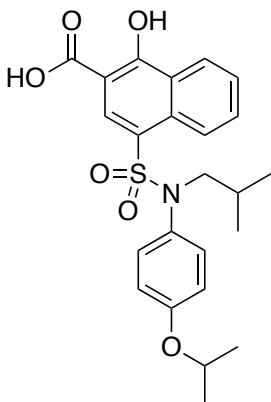


1-Hydroxy-4-(N-(4-nitrophenyl)sulfamoyl)-2-naphthoic acid (3ac). 4-Chlorosulfonyl-1-hydroxy-2-naphthoic acid (**5**) was coupled to 4-nitroaniline according to General Procedure A on a 2 mmol scale to yield the title compound as a dark yellow solid (249 mg, 64%): δ_{H} (400 MHz, d_6 -DMSO) 11.54 (s, 1H, SO_2NH), 8.61 – 8.58 (m, 2H, Ar), 8.38 (d, 1H, Ar, $J = 8.0$ Hz), 8.07 (d, 2H, Ar, $J = 8.4$ Hz), 7.86 (t, 1H, Ar, $J = 7.6$ Hz), 7.68 (t, 1H, Ar, $J = 7.6$ Hz), 7.20 (d, 2H, Ar, $J = 9.2$ Hz); δ_{C} (100 MHz, d_6 -DMSO) 171.5, 166.2, 144.1, 142.2, 131.8, 131.3, 130.8, 126.9, 125.6, 125.5, 124.5, 124.1, 121.9, 117.2, 105.4; Calcd (M^+): 388.0, Found: 387.3 ($[\text{M}-\text{H}]^-$); $t_{\text{R}} = 4.8$ min (97.4%, I).

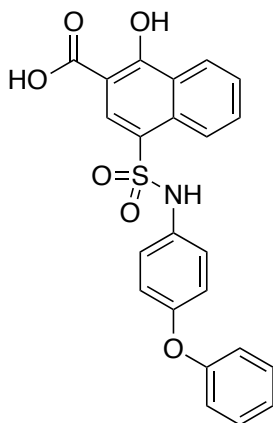


4-(N-(3-Cyanophenyl)sulfamoyl)-1-hydroxy-2-naphthoic acid (3ad) 4-Chlorosulfonyl-1-hydroxy-2-naphthoic acid (**5**) was coupled to 3-aminobenzonitrile according to General Procedure A on a 1 mmol scale to yield the title compound as a reddish-purple solid (188 mg, 61%): δ_{H} (400 MHz, d_6 -DMSO) 10.71 (s, 1H, NH), 8.54 (s, 1H, Ar), 8.40 (d, $J = 8.4$,

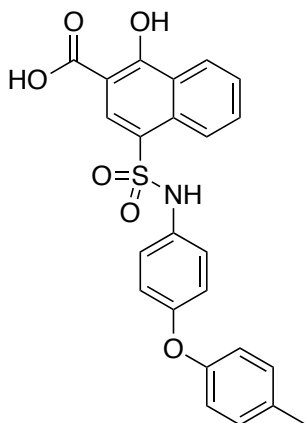
1 H, *Ar*), 8.32 (d, $J = 8.4$, 1 H, *Ar*), 7.63 (t, $J = 8.4$, 1 H, *Ar*), 7.44 (t, $J = 8.4$, 1 H, *Ar*), 7.39-7.27 (m, 4 H, *Ar*); δ_C (100 MHz, d_6 -DMSO) 173.3, 170.5, 139.9, 134.7, 131.5, 130.9, 129.7, 129.0, 126.5, 125.5, 124.9, 124.2, 122.7, 120.7, 118.8, 114.8, 112.1, 107.8; Calcd (M^+): 368.1, Found: 367.1 ($[M-H]^+$); $t_R = 7.4$ min (97.2%, II).



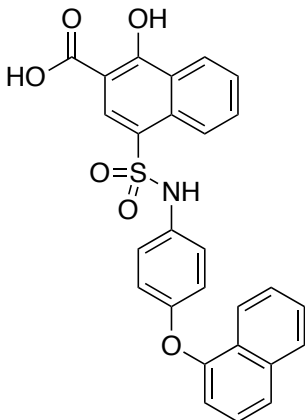
1-Hydroxy-4-(N-isobutyl-N-(4-isopropoxyphenyl)sulfamoyl)-2-naphthoic acid (3ba). 4-Chlorosulfonyl-1-hydroxy-2-naphthoic acid (**5**) was coupled to 4-isopropoxyaniline (**8a**) according to General Procedure A on a 1 mmol scale to yield the title compound as a beige solid (350 mg, 69%): δ_H (400 MHz, d_6 -DMSO) 8.32 (d, 1H, *Ar*, $J = 8.4$ Hz), 8.30 (s, 1H, *Ar*), 8.10 (d, 1H, *Ar*, $J = 7.6$ Hz), 7.49 – 8.39 (m, 2H, *Ar*), 6.96 (d, 2H, Ph, $J = 8.8$ Hz), 6.77 (d, 2H, Ph, $J = 8.8$ Hz), 4.56 – 4.50 (m, 1H, OCH), 3.25 (d, 2H, CH₂CH, $J = 6.8$ Hz), 1.39 – 1.34 (m, 1H, CH₂CH), 1.22 (d, 6H, OCH(CH₃)₂, $J = 6.4$ Hz), 0.73 (d, 6H, CH₂CH(CH₃)₂, $J = 6.8$ Hz); δ_C (100 MHz, d_6 -DMSO) 172.4, 170.8, 156.9, 134.7, 132.3, 131.9, 130.2, 128.9, 128.6, 125.1, 125.0, 124.6, 115.9, 115.4, 108.0, 69.7, 57.5, 26.7, 22.2, 20.1; Calcd (M^+): 457.2, Found: 456.2 ($[M-H]^-$); $t_R = 16.7$ min (99.5%, III).



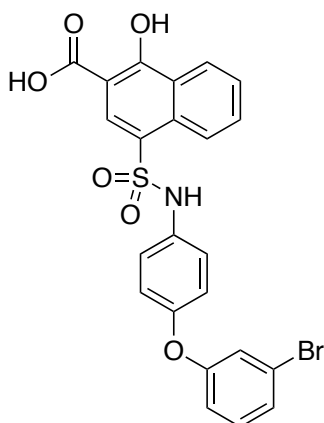
1-Hydroxy-4-(N-(4-phenoxyphenyl)sulfamoyl)-2-naphthoic acid (3bb). 4-Chlorosulfonyl-1-hydroxy-2-naphthoic acid (**5**) was coupled to 4-phenoxyaniline (**8b**) according to General Procedure A on a 1 mmol scale to yield the title compound as a beige solid (340 mg, 78%): δ_{H} (400 MHz, d_6 -DMSO) 10.41 (s, 1H, SO_2NH), 8.63 (d, 1H, Ar, $J = 8.8$ Hz), 8.40 – 8.38 (m, 2H, Ar), 7.85 (t, 1H, Ar, $J = 7.6$ Hz), 7.71 (t, 1H, Ar, $J = 7.6$ Hz), 7.31 (t, 2H, Ar, $J = 8.0$ Hz), 7.06 (t, 1H, Ar, $J = 7.4$ Hz), 6.96 (d, 2H, Ar, $J = 8.8$ Hz), 6.84 – 6.81 (m, 4H, Ar); δ_{C} (100 MHz, d_6 -DMSO) 172.2, 165.1, 158.2, 157.4, 133.5, 131.5, 131.0, 130.4, 127.3, 125.4, 125.1, 124.6, 123.5, 122.8, 120.2, 118.3, 116.0, 114.9, 105.3; Calcd (M^+): 435.1, Found: 436.0 ($[\text{M}+\text{H}]^+$); $t_{\text{R}} = 14.4$ min (100%, II).



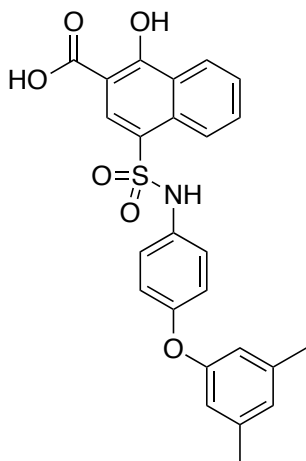
1-Hydroxy-4-(N-(4-(p-tolyloxy)phenyl)sulfonyl)-2-naphthoic acid (3bc). 4-Chlorosulfonyl-1-hydroxy-2-naphthoic acid (**5**) was coupled to 4-(*p*-tolylloxy)aniline (**8c**) according to General Procedure A on a 1 mmol scale to yield the title compound as a beige solid (342 mg, 76%): δ_{H} (400 MHz, d_6 -DMSO) 10.37 (s, 1H, SO₂NH), 8.63 (d, 1H, Ar, $J = 8.8$ Hz), 8.41 – 8.39 (m, 2H, Ar), 7.85 (t, 1H, Ar, $J = 7.4$ Hz), 7.71 (t, 1H, Ar, $J = 7.8$ Hz), 7.11 (d, 2H, Ar, $J = 8.8$ Hz), 6.94 (d, 2H, Ar, $J = 8.4$ Hz), 6.78 (d, 2H, Ar, $J = 8.8$ Hz), 6.74 (d, 1H, Ar, $J = 8.0$ Hz), 2.24 (s, 3H, CH₃); δ_{C} (100 MHz, d_6 -DMSO) 172.2, 164.5, 154.9, 153.9, 133.0, 132.7, 131.5, 130.9, 130.7, 127.3, 125.3, 125.1, 124.6, 122.8, 119.6, 118.6, 105.2, 20.6; Calcd (M⁺): 449.1, Found: 472.3 ([M+Na]⁺); $t_{\text{R}} = 9.3$ min (100%, III).



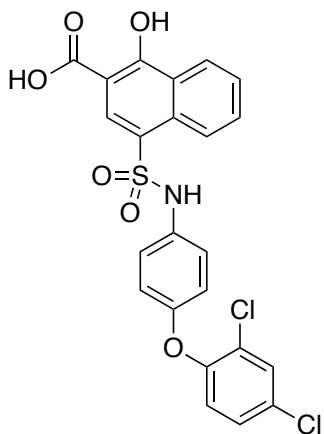
1-Hydroxy-4-(N-(4-(naphthalen-1-yloxy)phenyl)sulfamoyl)-2-naphthoic acid (3bd). 4-Chlorosulfonyl-1-hydroxy-2-naphthoic acid (**5**) was coupled to 4-(naphthalen-1-yloxy)aniline¹⁸² (**8d**) according to General Procedure A on a 1 mmol scale to yield the title compound as a light purple solid (351 mg, 70%): δ_{H} (400 MHz, d_6 -DMSO) 10.42 (s, 1H, SO₂NH), 8.63 (d, 1H, Ar, $J = 8.8$ Hz), 8.42 – 8.39 (m, 2H, Ar), 7.99 (d, 1H, Ar, $J = 8.8$ Hz), 7.94 (d, 1H, Ar, $J = 8.0$ Hz), 7.86 (t, 1H, Ar, $J = 7.4$ Hz), 7.72 (t, 1H, Ar, $J = 7.8$ Hz), 7.66 (d, 1H, Ar, $J = 8.8$ Hz), 7.55 (t, 1H, Ar, $J = 7.4$ Hz), 7.49 (t, 1H, Ar, $J = 7.0$ Hz), 7.38 (t, 1H, Ar, $J = 7.8$ Hz), 6.98, 6.88 (ABq, 4H, Ar, $J_{\text{AB}} = 8.4$ Hz), 6.73 (d, 1H, Ar, $J = 8.0$ Hz); δ_{C} (100 MHz, d_6 -DMSO) 172.2, 165.2, 153.9, 153.0, 147.4, 134.9, 133.5, 131.4, 131.3, 131.0, 128.3, 127.3, 127.2, 126.6, 126.5, 125.5, 125.1, 124.6, 124.3, 123.5, 122.8, 121.7, 119.8, 113.1, 105.3; Calcd (M^+): 485.1, Found: 508.3 ($[M+\text{Na}]^+$); $t_{\text{R}} = 11.2$ min (100%, III).



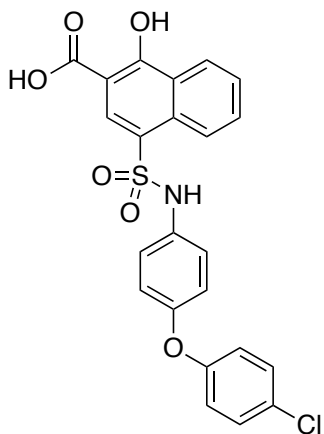
4-(N-(4-(3-Bromophenoxy)phenyl)sulfamoyl)-1-hydroxy-2-naphthoic acid (3be). 4-Chlorosulfonyl-1-hydroxy-2-naphthoic acid (**5**) was coupled to 4-(3-bromophenoxy)aniline¹⁸³ (**8e**) according to General Procedure A on a 1 mmol scale to yield the title compound as a beige solid (334 mg, 65%): δ_{H} (400 MHz, d_6 -DMSO) 10.45 (s, 1H, SO₂NH), 8.62 (d, 1H, Ar, $J = 8.8$ Hz), 8.43 (s, 1H, Ar), 8.40 (d, 1H, Ar, $J = 8.8$ Hz), 7.86 (t, 1H, Ar, $J = 7.4$ Hz), 7.71 (t, 1H, Ar, $J = 7.4$ Hz), 7.26 – 7.25 (m, 2H, Ar), 7.01 – 6.99 (m, 3H, Ar), 6.90 (d, 2H, Ar, $J = 8.4$ Hz), 6.83 – 6.80 (m, 1H, Ar); δ_{C} (100 MHz, d_6 -DMSO) 172.2, 165.2, 158.7, 152.2, 134.2, 132.1, 131.4, 131.0, 127.3, 126.2, 125.6, 125.1, 124.6, 122.6, 122.5, 120.9, 120.8, 117.0, 115.9, 112.5, 105.3; Calcd (M^+): 513.0, Found: 513.9 ($[M+H]^+$); $t_{\text{R}} = 10.7$ min (99.6%, III).



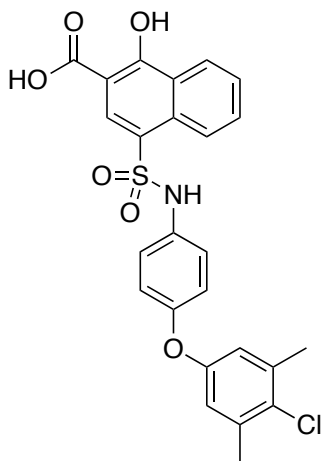
4-(N-(4-(3,5-Dimethylphenoxy)phenyl)sulfamoyl)-1-hydroxy-2-naphthoic acid (3bf). 4-Chlorosulfonyl-1-hydroxy-2-naphthoic acid (**5**) was coupled to 4-(3,5-dimethylphenoxy)aniline (**8f**) according to General Procedure A on a 1 mmol scale to yield the title compound as a cream solid (306 mg, 66%): δ_{H} (400 MHz, d_6 -DMSO) 10.40 (s, 1H, SO₂NH), 8.62 (d, 1H, Ar, $J = 8.8$ Hz), 8.41 – 8.39 (m, 3H, Ar), 7.85 (t, 1H, Ar, $J = 7.4$ Hz), 7.71 (t, 1H, Ar, $J = 7.4$ Hz), 6.95, 6.79 (ABq, 4H, Ar, $J_{\text{AB}} = 9.0$ Hz), 6.70 (s, 1H, Ar), 6.43 (s, 2H, Ar), 2.18 (s, 6H, 2xCH₃); δ_{C} (100 MHz, d_6 -DMSO) 172.2, 157.4, 153.4, 139.7, 133.3, 131.6, 131.4, 130.9, 129.9, 127.4, 127.3, 125.5, 125.1, 124.6, 124.5, 122.7, 120.1, 116.1, 105.3, 21.3; Calcd (M⁺): 463.1, Found: 463.91 ([M+H]⁺); $t_{\text{R}} = 19.8$ min (98.9%, II).



4-(N-(4-(2,4-Dichlorophenoxy)phenyl)sulfamoyl)-1-hydroxy-2-naphthoic acid (3bg). 4-Chlorosulfonyl-1-hydroxy-2-naphthoic acid (**5**) was coupled to 4-(2,4-dichlorophenoxy)aniline¹⁸⁴ (**8g**) according to General Procedure A on a 1 mmol scale to yield the title compound as a beige solid (297 mg, 66%): δ_{H} (400 MHz, d_6 -DMSO) 10.46 (s, 1H, SO₂NH), 8.62 (d, 1H, Ar, $J = 8.8$ Hz), 8.41 – 8.39 (m, 2H, Ar), 7.85 (t, 1H, Ar, $J = 7.4$ Hz), 7.73 – 7.70 (m, 2H, Ar), 7.34 (dd, 1H, Ar, $J = 8.8, 2.4$ Hz), 6.97 (d, 2H, Ar, $J = 8.8$ Hz), 6.88 – 6.82 (m, 3H, Ar); δ_{C} (100 MHz, d_6 -DMSO) 172.1, 165.3, 151.6, 148.8, 133.9, 131.4, 131.0, 130.5, 129.1, 127.4, 127.3, 125.5, 125.0, 124.2, 124.1, 122.6, 121.6, 119.3, 105.3; Calcd (M^+): 503.0, Found: 503.9 ($[M+H]^+$); $t_{\text{R}} = 12.3$ min (100%, III).

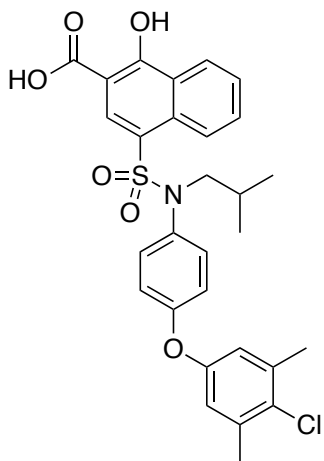


4-(N-(4-(4-Chlorophenoxy)phenyl)sulfamoyl)-1-hydroxy-2-naphthoic acid (3bh). 4-Chlorosulfonyl-1-hydroxy-2-naphthoic acid (**5**) was coupled to 4-(4-chlorophenoxy)aniline (**8h**) according to General Procedure A on a 1 mmol scale to yield the title compound as a beige solid (291 mg, 62%): δ_{H} (400 MHz, d_6 -DMSO) 10.45 (s, 1H, SO_2NH), 8.63 (d, 1H, Ar, $J = 8.8$ Hz), 8.41 – 8.39 (m, 2H, Ar), 7.86 (t, 1H, Ar, $J = 7.4$ Hz), 7.72 (t, 1H, Ar, $J = 7.4$ Hz), 7.35 (d, 1H, Ar, $J = 9.2$ Hz), 6.98 (d, 1H, Ar, $J = 8.4$ Hz), 6.85 (app t, 4H, Ar, $J = 8.6$ Hz); δ_{C} (100 MHz, d_6 -DMSO) 172.2, 165.0, 156.4, 152.8, 133.9, 131.5, 131.4, 130.9, 130.2, 127.4, 127.2, 125.4, 125.1, 124.6, 124.5, 122.7, 120.4, 119.9, 105.2; Calcd (M^+): 469.0, Found: 469.91 ($[\text{M}+\text{H}]^+$); $t_{\text{R}} = 19.5$ min (98.8%, II).

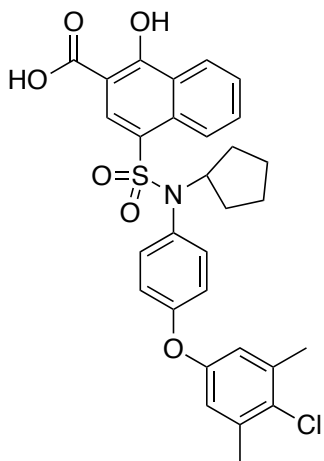


4-(N-(4-(4-Chloro-3,5-dimethylphenoxy)phenyl)sulfamoyl)-1-hydroxy-2-naphthoic acid

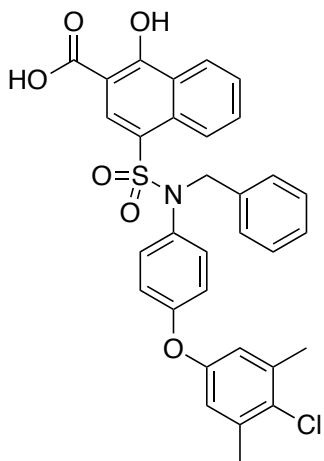
(3bi). 4-Chlorosulfonyl-1-hydroxy-2-naphthoic acid (**5**) was coupled to 4-(4-chloro-3,5-dimethylphenoxy)aniline (**8i**) according to General Procedure A on a 1 mmol scale to yield the title compound as an off-white solid (374 mg, 75%): δ_{H} (400 MHz, d_6 -DMSO, TMS) δ_{H} 10.41 (s, 1H, NH), 8.61 (d, 1H, Ar-H, $J = 8.8$ Hz), 8.42 (s, 1H, Ar-H), 8.39 (d, 1H, Ar-H, $J = 8.4$ Hz), 7.84 (t, 1H, Ar-H, $J = 7.6$ Hz), 7.69 (t, 1H, Ar-H, $J = 7.6$ Hz), 6.96 (d, 2H, Ar-H, $J = 8.8$ Hz), 6.82 (d, 2H, Ar-H, $J = 8.8$ Hz), 6.70 (s, 2H, Ar-H), 2.24 (s, 6H, Ar-CH₃). δ_{C} (100 MHz, d_6 -DMSO) 172.2, 164.8, 155.2, 153.2, 137.6, 133.4, 131.5, 130.8, 128.2, 127.3, 125.3, 125.1, 124.7, 124.5, 122.5, 119.9, 118.6, 105.2, 20.7; Calcd (M⁺): 497.1, Found: 496.2 ([M-H]⁻); $t_{\text{R}} = 4.0$ min (95.0%, IV).



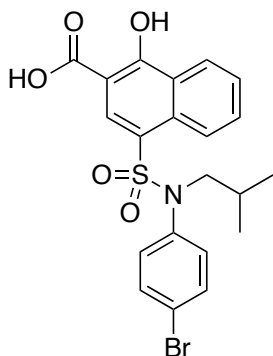
4-(*N*-(4-(4-Chloro-3,5-dimethylphenoxy)phenyl)-*N*-isobutylsulfamoyl)-1-hydroxy-2-naphthoic acid (**3bj**). 4-Chlorosulfonyl-1-hydroxy-2-naphthoic acid (**5**) was coupled to 4-(4-chloro-3,5-dimethylphenoxy)-*N*-isobutylaniline (**9a**) according to General Procedure A on a 1 mmol scale to yield the title compound as a cream solid (399 mg, 72%): δ_{H} (400 MHz, d_6 -DMSO, TMS) δ_{H} 8.37 (d, 1H, Ar-H, $J = 8$ Hz), 8.27 (s, 1H, Ar-H), 8.14 (d, 1H, Ar-H, $J = 8$ Hz), 7.62 (t, 1H, Ar-H, $J = 7.4$ Hz), 7.56 (t, 1H, Ar-H, $J = 7.4$ Hz), 7.06 (d, 2H, Ar-H, $J = 8.8$ Hz), 6.86 (s, 2H, Ar-H), 6.85 (d, 2H, Ar-H, $J = 8.8$ Hz), 3.32 (d, 2H, NCH₂, $J = 7.2$ Hz), 2.31 (s, 6H, Ar-CH₃), 1.42 (m, 1H, CH₂CH(CH₃)₂), 0.78 (d, 6H, CH(CH₃)₂, $J = 6.4$ Hz) δ_{C} (100 MHz, d_6 -DMSO) 156.3, 154.3, 137.9, 134.2, 132.9, 132.2, 130.6, 130.2, 128.9, 126.7, 126.1, 125.2, 124.7, 119.7, 118.7, 57.3, 26.8, 20.7, 20.2; Calcd (M^+): 553.1, Found: 552.2 ($[M-H]^-$); $t_{\text{R}} = 8.0$ min (96.8%, IV).



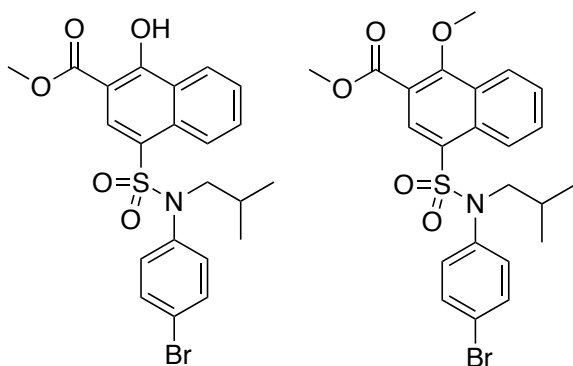
4-(*N*-(4-(4-Chloro-3,5-dimethylphenoxy)phenyl)-*N*-cyclopentylsulfamoyl)-1-hydroxy-2-naphthoic acid (**3bk**). 4-Chlorosulfonyl-1-hydroxy-2-naphthoic acid (**5**) was coupled to 4-(4-chloro-3,5-dimethylphenoxy)-*N*-isobutylaniline (**9b**) according to General Procedure A on a 1 mmol scale to yield the title compound as a white solid (396 mg, 70%): δ_{H} (400 MHz, d_6 -DMSO, TMS) δ_{H} 8.44 (app. t, 2H, Ar-H, $J = 7.2$ Hz), 8.27 (s, 1H, Ar-H), 7.90 (t, 1H, Ar-H, $J = 7.8$ Hz), 7.74 (t, 1H, Ar-H, $J = 7.6$ Hz), 6.94 (d, 2H, Ar-H, $J = 8.8$ Hz), 6.88 (d, 4H, Ar-H, $J = 8.4$ Hz), 4.54 (m, 1H, NCH(CH₂)₂, $J = 8.2$ Hz), 2.30 (s, 6H, Ar-CH₃), 1.80-1.68 (m, 2H, (CHCH₂CH₂)), 1.50-1.17 (m, 6H, 3(CHCH₂CH₂)) δ_{C} (100 MHz, d_6 -DMSO) 172.2, 165, 157.3, 153.9, 138, 134, 131.6, 131.5, 130.2, 129.2, 127.3, 125.4, 125.2, 124.6, 124.4, 119.9, 118.3, 105.3, 59.9, 30.3, 22.4, 20.7; Calcd (M⁺): 565.1, Found: 564.3 ([M-H]⁻); $t_{\text{R}} = 8.5$ min (95.4%, IV).



4-(*N*-Benzyl-*N*-(4-(4-chloro-3,5-dimethylphenoxy))phenyl)sulfamoyl)-1-hydroxy-2-naphthoic acid (**3bl**). 4-Chlorosulfonyl-1-hydroxy-2-naphthoic acid (**5**) was coupled to 4-(4-chloro-3,5-dimethylphenoxy)-*N*-isobutylaniline (**9c**) according to General Procedure A on a 1 mmol scale to yield the title compound as a white solid (423 mg, 72%): δ_{H} (400 MHz, d_6 -DMSO, TMS) δ_{H} 8.43 (d, 1H, Ar-H, $J = 8$ Hz), 8.39 (s, 1H, Ar-H), 8.26 (d, 1H, Ar-H, $J = 8$ Hz), 7.73 (m, 2H, Ar-H, $J = 7.2$ Hz), 7.24-7.17 (m, 5H, Ph), 7.02 (d, 2H, Ar-H, $J = 8.8$ Hz), 6.77 (m, 3H, Ar-H), 4.78 (s, 2H, NCH₂), 2.28 (s, 6H, (Ar-CH₃)₂) δ_{C} (100 MHz, d_6 -DMSO) 172.2, 165.2, 156.3, 154.2, 137.9, 136.5, 133.6, 132, 131.9, 131.2, 130.9, 128.9, 128.6, 127.8, 127.2, 125.5, 125.4, 124.5, 123.1, 119.6, 118.5, 105.5, 53.8, 20.7; Calcd (M⁺): 587.1, Found: 586.2 ([M-H]⁻); $t_{\text{R}} = 5.7$ min (95.9%, IV).

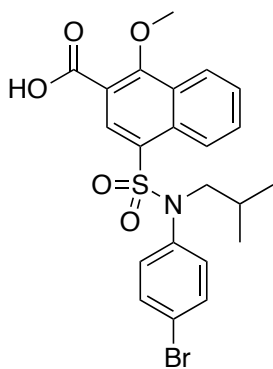


4-(N-(4-Bromophenyl)-N-isobutylsulfamoyl)-1-hydroxy-2-naphthoic acid (3ca). 4-chlorosulfonyl-1-hydroxy-2-naphthoic acid (**5**) was coupled to 4-bromo-*N*-isobutylaniline (**8j**) according to General Procedure A on a 6 mmol scale to yield the title compound as a light pink solid (393 mg, 68%): δ_{H} (400 MHz, d_6 -DMSO, TMS) δ_{H} 8.41 – 8.39 (m, 1H, Ar), 8.29 (s, 1H, Ar), 8.15 – 8.13 (m, 1H, Ar), 7.68 – 7.65 (m, 2H, Ar), 7.48 (d, 2H, Ph, $J = 8.8$ Hz), 7.07 (d, 2H, Ph, $J = 8.4$ Hz), 3.36 (d, 2H, NCH_2 , $J = 7.2$ Hz), 1.44 – 1.37 (m, 1H, CH_2CH), 0.77 (d, 6H, $\text{CH}(\text{CH}_3)_2$, $J = 6$ Hz) δ_{C} (100 MHz, d_6 -DMSO) 172.0, 165.8, 138.5, 132.4, 132.1, 131.9, 131.1, 130.8, 127.1, 125.7, 125.2, 124.5, 122.8, 120.9, 105.6, 57.1, 26.9, 19.9; Calcd (M^+): 477.0, Found: 476.0 ($[\text{M}-\text{H}]^-$); $t_{\text{R}} = 16.3$ min (99.5%, III).



Methyl 4-(N-(4-bromophenyl)-N-isobutylsulfamoyl)-1-hydroxy-2-naphthoate (3cb) and *Methyl 4-(N-(4-bromophenyl)-N-isobutylsulfamoyl)-1-methoxy-2-naphthoate (3cc)*.

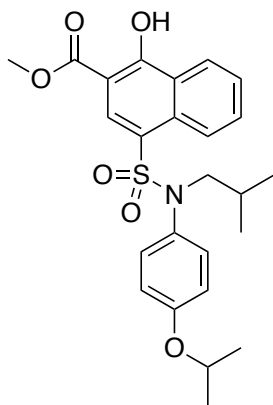
Compound **3ca** (752 mg, 1.3 mmol, 1 eq) was treated with MeI (2.2 eq) and K₂CO₃ (3 eq) in DMF (13 mL) at RT. After 16 h, the reaction was incomplete, yielding two products. Water (150 mL) was added to the reaction mixture, which was subsequently extracted with EtOAc (30 mL x 3). The EtOAc extractions were combined, washed with water (100 mL x 3), brine, dried (Na₂SO₄), filtered and concentrated. The residue was adsorbed onto silica gel and purified by flash column chromatography, eluting with a gradient of EtOAc in hexanes to deliver first **3cc** (395 mg, 60%) and second **3cb** (211 mg, 33%) as cream-colored solids. **3cb**: δ_{H} (400 MHz, *d*₆-DMSO) 12.28 (s, 1H, OH), 8.40 (d, 2H, Ar, *J* = 8.4 Hz), 8.27 (s, 1H, Ar), 8.11 (d, 2H, Ar, *J* = 8.4 Hz), 7.70 – 7.45 (m, 2H, Ar), 7.46 (d, 2H, Ar, *J* = 8.4 Hz), 7.05 (d, 2H, Ar, *J* = 8.4 Hz), 3.96 (s, 3H, CO₂CH₃), 3.34 (d, 1H, CH₂CH(CH₃)₂), *J* = 7.6 Hz), 1.38 (hep, 1H, CH(CH₃)₂), *J* = 6.9 Hz), 0.75 (d, 6H, CH(CH₃)₂), *J* = 6.0 Hz); δ_{C} (100 MHz, *d*₆-DMSO) 174.3, 168.2, 143.1, 137.2, 136.5, 136.3, 135.7, 135.6, 132.5, 130.0, 129.9, 129.3, 129.2, 125.9, 109.8, 61.9, 58.4, 31.6, 24.7; Calcd (M⁺): 491.0, Found: 514.0 ([M+Na]⁺); *t*_R = 9.5 min (95.1%, IV). **3cc**: δ_{H} (400 MHz, *d*₆-DMSO) 8.37 (d, 1H, Ar, *J* = 7.6 Hz), 8.31 (s, 1H, Ar), 8.15 (d, 1H, Ar, *J* = 8.8 Hz), 7.75 (t, 1H, Ar, *J* = 7.6 Hz), 7.67 (t, 1H, Ar, *J* = 7.4 Hz), 7.50 (d, 2H, Ar, *J* = 8.4 Hz), 7.08 (d, 2H, Ar, *J* = 8.4 Hz), 4.05 (s, 3H, CH₃), 3.93 (s, 3H, CH₃), 3.39 (d, 1H, CH₂CH(CH₃)₂), *J* = 6.8 Hz), 1.43 (hep, 1H, CH(CH₃)₂), *J* = 6.7 Hz), 0.79 (d, 6H, CH(CH₃)₂), *J* = 5.2 Hz); δ_{C} (100 MHz, *d*₆-DMSO) 165.1, 162.1, 138.2, 132.5, 132.2, 131.3, 130.9, 130.7, 129.3, 128.8, 128.3, 125.3, 124.7, 121.2, 117.1, 64.2, 57.2, 53.2, 26.9, 19.9; Calcd (M⁺): 505.1, Found: 528.1 ([M+Na]⁺).



4-(*N*-(4-Bromophenyl)-*N*-isobutylsulfamoyl)-1-methoxy-2-naphthoic acid (**3cd**).

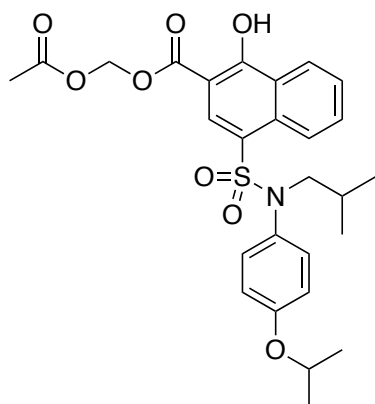
Compound **3cc** was saponified using LiOH.H₂O (3eq) in a mixture of THF/H₂O/MeOH (3:1:1) on a 0.2 mmol scale to deliver the title compound as a white solid (79 mg, 80%):

δ_{H} (400 MHz, *d*₆-DMSO) 13.5 (br s, 1H, CO₂H), 8.36 (d, 1H, Ar, *J* = 8.4 Hz), 8.32 (s, 1H, Ar), 8.15 (d, 1H, Ar, *J* = 8.0 Hz), 7.73 (t, 1H, Ar, *J* = 7.8 Hz), 7.65 (t, 1H, Ar, *J* = 7.6 Hz), 7.49 (d, 2H, Ar, *J* = 8.4 Hz), 7.07 (d, 2H, Ar, *J* = 8.4 Hz), 4.06 (s, 3H, OMe), 3.40 (d, 2H, CH₂CH(CH₃)₂, *J* = 6.8 Hz), 1.43 (hep, 1H, CH(CH₃)₂, *J* = 6.8 Hz), 0.80 (d, 6H, CH(CH₃)₂, *J* = 6.4 Hz); δ_{C} (100 MHz, *d*₆-DMSO) 166.0, 161.6, 137.9, 132.5, 132.1, 130.8, 130.6, 130.0, 129.0, 128.2, 127.8, 124.9, 124.3, 120.8, 117.9, 63.6, 56.8, 26.5, 19.6; Calcd (M⁺): 491.0, Found: 490.0 ([M-H]⁻); *t*_R = 15.3 min (98.5%, III).



Methyl 1-hydroxy-4-(N-isobutyl-N-(4-isopropoxyphenyl)sulfamoyl)-2-naphthoate (**13**).

3ba (458 mg, 1 mmol, 1 eq) was dissolved in MeOH (4 mL) at 0 °C. Thionyl chloride (1 mL, 12 mmol, 12 eq) was added dropwise to the stirred solution. The reaction was allowed to warm to room temperature, overnight. TLC (CH₂Cl₂/MeOH/AcOH, 92:7:1) indicated that reaction was complete, and was concentrated to dryness. The residue was azeotroped with CHCl₃ (4 x 100 mL) to remove residual thionyl chloride. The resulting compound yielded the title compound as an off-white solid in quantitative yield, 472 mg: δ_{H} (400 MHz, CDCl₃) 12.46 (s, 1H, OH), 8.46-8.42 (m, 2H Ar), 8.32-8.30 (m, 2H, Ar), 7.57-7.55 (m, 2H, Ar), 6.91 (d, 2H, Ph, J = 8.8 Hz), 6.67 (d, 2H, Ph, J = 8.4 Hz), 4.49-4.43 (m, 1H, OCH), 3.98 (s, 3H, MeO), 3.36 (d, 2H, CH₂CH, J = 6.8 Hz), 1.60-1.53 (m, 1H, CH₂CH), 1.29 (d, 6H, OCH(CH₃)₂, J = 6 Hz), 0.86 (d, 6H, CH₂CH(CH₃)₂, J = 7.2 Hz); δ_{C} (100 MHz, CDCl₃) 170.6, 164.4, 157.2, 132.4, 131.1, 130.8, 130.7, 130.2, 126.5, 125.7, 125.1, 125.0, 124.3, 115.9, 104.0, 70.0, 58.1, 52.7, 29.7, 26.7, 21.9, 19.9; Calcd (M⁺): 471.17, Found: 472.0 ([M+H]⁺); t_{R} = 11.98 min (100%; IV).



Acetoxymethyl 1-hydroxy-4-(N-isobutyl-N-(4-isopropoxyphenyl)sulfamoyl)-2-naphthoate (**14**). **3ba** (200 mg, 0.437 mmol, 1 eq) and K_2CO_3 (66.5 mg, 0.481 mmol, 1.1 eq) were dissolved in acetonitrile (4.4 mL) at 0 °C and stirred for 1 h. Bromomethyl acetate (43 μ L, 0.437 mmol, 1 eq) was then added dropwise. The reaction was allowed to warm to RT and stirred overnight. The next day, TLC indicated the reaction was incomplete, so another 1.1 eq of K_2CO_3 and 1 eq of bromomethyl acetate were added and the reaction was stirred at RT for another 16 h. The reaction was quenched with water and extracted with EtOAc (3 x 25 mL). The organics were collected washed with brine, dried with Na_2SO_4 , and concentrated to dryness. The crude material was purified by flash chromatography over silica gel using an eluent of Hex/EtOAc 3:1 to produce the title compound as a pale pink solid (116 mg, 50%): δ_H (400 MHz, $CDCl_3$) 12.14 (s, 1H, OH), 8.48-8.46 (m, 1H, Ar), 8.43 (s, 1H, Ar), 8.33-8.30 (m, 1H, Ar), 7.59-7.57 (m, 2H, Ar), 6.93 (d, 2H, Ph, J = 8.8 Hz), 6.68 (d, 2H, Ph, J = 8.4 Hz), 6.04 (s, 2H, OCH_2O), 4.49-4.44 (m, 1H, OCH), 3.37 (d, 2H, CH_2CH , J = 6.8 Hz), 2.17 (s, 3H, $CH_3C=O$), 1.61-1.54 (m, 1H, CH_2CH), 1.30 (d, 6H, $OCH(CH_3)_2$, J = 6.4 Hz), 0.87 (d, 6H, $CH_2CH(CH_3)_2$, J = 6 Hz); δ_C (100 MHz, $CDCl_3$) 169.1, 165.0, 157.3, 132.6, 131.1, 131.0, 130.3, 130.1, 126.8, 125.8, 125.6, 125.1, 124.4, 115.9, 103.2, 79.9, 70.0, 58.1, 31.6, 26.7, 21.9, 20.7, 19.9; Calcd (M⁺): 529.18, Found:

530.0 ([M+H]⁺); $t_R = 26.99$ min (100%; V).

2.7.3 Biology

General. All chemical reagents were ACS grade or higher unless otherwise indicated. All buffers were passed through Chelex-100 (Bio-Rad, Hercules, CA) to remove trace metals. The D₂O, d₆-DMSO, ¹⁵NH₄Cl, and ¹³C-labeled glucose were purchased from Cambridge Isotope Laboratories, Inc. (Andover, MA).

Protein Production

A His6-MBP tagged recombinant human Mcl-1 residues 172 to 327 was produced in *E. coli* in either LB or minimal media supplemented with ¹⁵NH₄Cl to produce unlabeled or ¹⁵N-labeled Mcl-1. The tagged protein was initially purified from the crude cell lysate by Immobilized Metal Affinity Chromatography (IMAC) chromatography (GE Healthcare Life Sciences), and after dialysis to remove the imidazole the affinity tag was cleaved using PreScission Protease (GE Healthcare Life Sciences). A Sephacryl S-200 size exclusion column was used as a final purification step before the protein was concentrated with a 10,000 MWCO centrifugal filter concentrator (Millipore). The protein purity was shown to be >98% by Coomassie Brilliant Blue (Bio-Rad) stained SDS-PAGE gel and the final concentration was determined using the Bradford protein assay (Bio-Rad) with BSA standards (Pierce).

Peptide

A 6-aminohexanoic acid linker was conjugated to the N-terminus of the Bak BH3 peptide (GQVGRQLAIIGDDINR), capped with fluorescein (on the amino group of the linker), and the peptide was amidated on the C-terminus to give FITC-Ahx-GQVGRQLAIIGDDINR-CONH₂, hereafter referred to as “FITC-Bak” (synthesized by

Neo BioScience in >95% purity).

Fluorescence polarization experiments

Fluorescence polarization experiments were conducted using a BMG PHERAstar FS multimode microplate reader equipped with two PMTs for simultaneous measurements of the perpendicular and parallel fluorescence emission. The assays were performed in black polypropylene 384-well microplate (Costar) with a final volume of 20 μ L. Initially the affinity (K_D) of the FITC-Bak peptide was determined by titrating Mcl-1¹⁷²⁻³²⁷ into 10 nM FITC-Bak peptide in 20 mM HEPES, pH 6.8, 50 mM NaCl, 3 mM DTT, 0.01% Triton X-100 and 5% DMSO at room temperature while monitoring the perpendicular and parallel fluorescence emission with a 485 nm excitation and 520 nm emission filters. The fluorescence polarization competition assay (FPCA) was performed using 100 nM Mcl-1¹⁷²⁻³²⁷ in the same buffer (thus, 15 nM FITC-Bak) with varying concentrations of either unlabeled peptide or experimental. Regression analysis was carried out using Origin (OriginLab, Northampton, MA) to fit the data to the Hill equation (1) to determine the initial binding affinity (K_D) and the IC_{50} in the FPCA. For the fluorescence polarization competition titrations, an equation derived by Nikolovska-Coleska et al. was used to calculate the K_i from the IC_{50} data.¹⁷⁰ The affinity of FITC-Bak for Mcl-1¹⁷²⁻³²⁷ was determined to be 33.8 ± 0.50 nM in the assay conditions used.

Nuclear magnetic resonance spectroscopy

NMR spectra was collected at 25 °C with a Bruker AVANCE 800 NMR spectrometer (800.27 MHz for protons) equipped with pulsed-field gradients, four frequency channels, and triple resonance, z-axis gradient cryogenic probes. A one-second relaxation delay was used, and quadrature detection in the indirect dimensions was obtained with states-TPPI

phase cycling; initial delays in the indirect dimensions were set to give zero- and first-order phase corrections of 90° and -180° , respectively.¹⁸⁵⁻¹⁸⁶ Data were processed using the processing program nmrPipe on Linux workstations.¹⁸⁷ All proton chemical shifts are reported with respect to the H₂O or HDO signal, taken to be 4.658 ppm relative to external TSP (0.0 ppm) at 37°C. The ¹⁵N chemical shifts were indirectly referenced using the zero-point frequency at 37°C of 0.10132905 for ¹⁵N-¹H, as previously described.¹⁸⁸⁻¹⁸⁹ Uniformly ¹⁵N-labeled Mcl-1 was used to collect two-dimensional ¹H,¹⁵N-fast HSQC (heteronuclear single quantum coherence) spectra of Mcl-1 with and without compound to detect changes in the backbone ¹⁵N and ¹H resonances of Mcl-1 due to the direct interaction with the compound.¹⁹⁰ All compounds used for NMR were initially suspended in 100% d₆-DMSO. The NMR samples contained 131 μM ¹⁵N-labeled Mcl-1, 182 μM compound, 20 mM HEPES, pH 6.8, 50 mM NaCl, 3 mM DTT, 20% D₂O, and 5% d₆-DMSO.

Cell titer-blue viability assay

A375 cells were plated at 5,000 cells/well seeding density in a 96 well black walled plate (Corning). Cells were cultured in 100 μL DMEM (Gibco) plus 10% HIFBS and PenStrep overnight. Using a separate plate, serial dilutions were made of each compound in DMEM. 10 μL of each serial dilution was transferred into the experimental plate so that the final compound concentrations were 4.69, 9.38, 18.75, 37.5, 75, 150, or 300 μM and 1% DMSO solvent. Untreated control cells also received DMSO vehicle at 1% final concentration. Cells were cultured with and without test compounds for 48 hours and then 20 μL of Cell titer-blue reagent (Promega) was added to each well and to control wells containing media only to account for background. Cells were then incubated for 2 hours and fluorescence was read using Molecular Devices Spectra Max M5 (560_{Ex}/590_{Em}). Results were recorded

as percent viability determined by dividing the experimental values by the untreated controls and subtracting the background from cell-free wells.

Acknowledgements

Reproduced from *M. E. Lanning, W. Yu, J. L. Yap, J. Chauhan, L. Chen, E. Whiting, L. S. Pidugu, T. Atkinson, H. Bailey, W. Li, B.M. Roth, L. Hynicka, K. Chesko, E. A. Toth, P. Shapiro, A.D. MacKerell Jr., P.T. Wilder, and S. Fletcher; Structure-Based Design of N-Substituted 1-Hydroxy-4-sulfamoyl-2-naphthoates as Selective Inhibitors of the Mcl-1 Oncoprotein. European Journal of Medicinal Chemistry, 2016; 113, 273–292.* with permission from Elsevier Manson. Copyright © 2017 published by Elsevier Masson SAS. All rights reserved.

Chapter 3 Towards More Drug-Like Proteomimetics: Two-Faced Synthetic α -Helix Mimetics Based on a Purine Scaffold

3.1 Design and Strategy Towards the Purine Scaffold

Protein–protein interactions (PPIs) participate in pivotal roles in cell signaling pathways, and their dysregulations can lead to a wide range of pathologies, including cancer, cardiovascular and neurodegenerative diseases.^{2-3, 8, 191} In addition, PPIs featuring exogenous proteins are involved in the transmission of infectious diseases, such as HIV.⁷ Given the potential health benefits, it is no surprise that the disruption of PPIs by synthetic agents has rapidly become a major goal in contemporary medicinal chemistry.^{30, 192-194} The intensity with which these biological interfaces are being interrogated is likely fueled by the various successful approaches reported over the last decade, quashing the pessimism that this is too formidable a goal. In particular, there have been exciting advances in the realm of helix-mediated PPIs; the most notable examples of which are ABT-737⁶⁰ and the Nutlins,¹⁹⁵ which are low-molecular-weight, nanomolar inhibitors of the oncoproteins Bcl-xL and HDM2, respectively.

One strategy to disrupt helix-mediated PPIs is through synthetic α -helix mimetics.¹⁹⁶⁻¹⁹⁹ Traditionally, helix mimetics reproduce key functionality located on only one face of an α -helix, even though many α -helices that engage in PPIs utilize multiple faces to accomplish recognition of their target proteins.¹³ Most typically, the i , $i + 3/4$ and $i + 7$ hydrophobic side chains are emulated.¹⁹⁶⁻¹⁹⁹ A potential caveat with this strategy is that the resulting molecules are rather hydrophobic, particularly the pioneering terphenyls, with clogP values often around 5 or higher, which might result in poor solubilities and off-

target effects.⁴⁸ Also, the molecular weights (MW) of these compounds are commonly greater than 500. Thus, in at least two ways, some of the original helix mimetics contravene Lipinski's rules. The mimicry of multiple faces of an α -helix is expected to afford more potent agents that can better discriminate between protein surfaces through a richer recognition profile and may, therefore, provide a source of selectivity. Accordingly, towards the discovery of novel and potent Mcl-1 inhibitors, we recently described amphipathic α -helix mimetics based on a 1,2-diphenylacetylene scaffold.⁷⁶ Other groups have also developed two-faced, synthetic α -helix mimetics,^{54-55, 71, 200} although all of these designs suffer from lengthy syntheses.^{54-55, 71, 76, 200} As part of our group's continued interest in disrupting helix-mediated PPIs with small-molecule α -helix mimetics, we sought to discover more drug-like (MW < 500, clogP < 5) agents with therapeutic utility in which mimicry of two faces is once more accomplished, and in which the target molecules may be more readily accessed. At the same time, it is acknowledged that mimicry of just one face of an α -helix might afford inhibitors that exhibit polypharmacologies,²⁰¹⁻²⁰² hitting multiple targets as a more effective strategy to kill cancer cells, for example. In this latter scenario, a convenient means of installing a solubilizing group would be of utility in a location that has limited interference with the PPI, such as the opposing face to that emulated at the protein–protein interface. This would complement work by Rebek, Hamilton and Wilson who have described helix mimetics with a “wet” edge.²⁰³⁻²⁰⁵

Lim and colleagues have described single-faced helix mimetics based on a rigid pyrrolopyrimidine scaffold wherein side chains are projected from the 2, 6 and 7 positions.⁷⁸ Their molecules proved potent disrupters of the MDM2–p53 PPI, indicating that a flexible scaffold is not crucial for effective helix mimicry. We hypothesized that a

related 2,6,9-tri-substituted purine scaffold would permit mimicry of the i and $i + 3/4$ side chains on one face of the helix, and the $i + 2$ side chain (or simply a solubilizing group) on the opposing face, as depicted in **Figure 3.1A**. Mimicry of opposing faces of one turn of an α -helix in this way might afford potent and selective inhibitors that exhibit lower-molecular-weights than the terphenyls and their counterparts. Additionally, the purine scaffold is more hydrophilic than the terphenyl scaffold, which would serve to lower the clog P of the helix mimetic. Finally, elaboration of functionality introduced at the 2-position, such as a carbamate or a sulfonamide, might allow suitable emulation of both the $i + 3/4$ and the $i + 7$ side chains from the same position (**Figure 3.1B**).

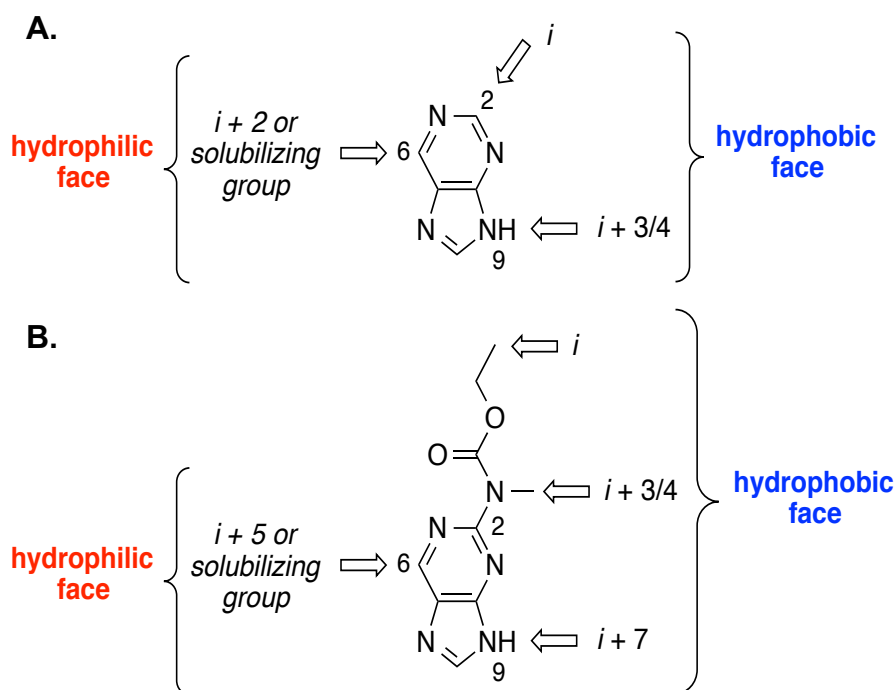


Figure 3.1: Substitution of the 2, 6 and 9 positions of the purine scaffold putatively permits mimicry of two faces of an α -helix.

To test our hypothesis, we designed molecules to inhibit the anti-apoptotic Bcl-2

protein Mcl-1, which, along with its relative Bcl-x_L, is overexpressed in a range of cancers, including pancreatic cancer and acute myeloid leukemia.^{4, 206} Mcl-1 seizes the BH3 α -helical domains of pro-apoptotic Bcl-2 family members, including Bak and Bim, through a hydrophobic crevice on its surface.⁴ Under normal conditions, the levels of anti- and pro-apoptotic Bcl-2 proteins are tightly regulated to maintain a healthy population of cells but in many cancers, the high levels of Mcl-1 and other anti-apoptotic proteins results in the neutralization of the pro-apoptotic proteins and, thus, tumorigenesis.⁴ Akin to the successful inhibition of Bcl-x_L and HDM2,^{29, 195-196, 207} it has been proposed that low-molecular-weight ligands that can mimic these BH3 α -helices should compete with Mcl-1 binding, freeing up the pro- apoptotic proteins to initiate the intrinsic apoptosis pathway, and, thereby, destroy the cancer cell.^{70, 162}

Alanine scanning mutagenesis has revealed that the key side chains of the Bak-BH3 α -helix that engage the anti- apoptotic Bcl-2 proteins include Val74, Leu78 (i), Ile81 (i + 3), Ile85 (i + 7), on one face, which bind the p1, p2, p3 and p4 pockets, respectively, and Asp83 (i + 5) on the other face, which binds Arg139 of Bcl-x_L and Arg263 of Mcl-1.^{4, 28} Since potent inhibitors have been fashioned by mimicking only three of the four hydrophobic residues,¹⁹⁶⁻¹⁹⁹ we designed amphipathic α -helix mimetics that reproduced the functionality of only Leu78, Ile81 and Ile85 on the hydrophobic face and Asp83 on the opposing face; these residues are highlighted in **Figure 3.2A**. In **Figure 3.2B**, the corresponding purine-based synthetic α -helix mimetic of the helix in **Figure 3.2A** is given. **Figure 3.2C** illustrates the Bak-BH3 α -helix overlaid with an MM2 energy-minimized conformation of the helix mimetic in **Figure 3.2B**; very good mimicry of the key side chains is observed. **Figure 3.2D** describes our simplified, two-faced α -helix mimetic

design, wherein R^1 and R^2 are intended to mimic the $i + 7$ and $i + 3$ side chains, respectively, and, to expedite compound synthesis, we fixed the Asp83 mimetic ($i + 5$) as CH_2COOH , and the carbamate group as a Boc group. This last constraint was anticipated to result in sub-optimal mimicry of Leu78 (i) but would greatly facilitate the synthetic chemistry.

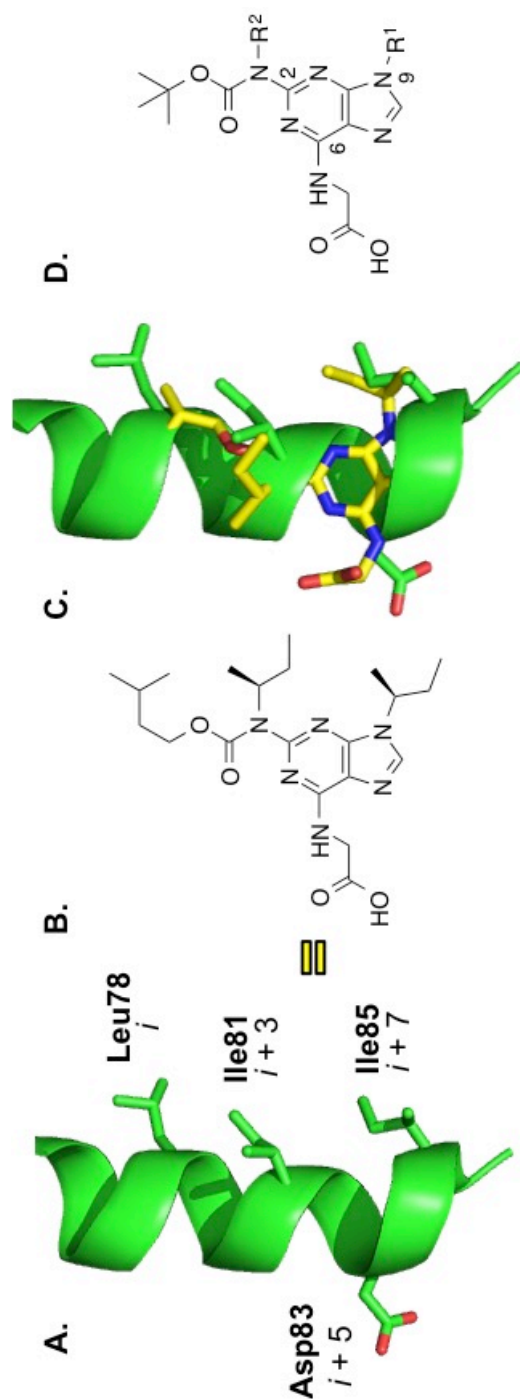


Figure 3.2: (A) Key residues of the Bak-BH3 α -helix. (B) A purine-based α -helix mimetic designed to imitate Leu78, Ile81, Ile85 and Asp83. (C) Superimposition of an MM2 energy-minimized conformation of the molecule in B on the Bak-BH3 α -helix. (D) Simplified Bak-BH3 α -helix mimetic where R^1 and R^2 are proposed to imitate the $i + 3$ and $i + 7$ side chains, respectively, whilst the Asp83 mimetic is fixed as CH_2COOH , and the Leu78 mimetic constrained as tert-butyl.

3.2 Results and Discussion

We have previously shown that N²-Boc-2-amino-6-chloro- purine (2) can be regioselectively alkylated at the N9 position under standard Mitsunobu conditions.^{79, 208} NB: In the preparation of 2, NaH as a dispersion in mineral oil gave capricious results, whereas dry NaH consistently drove complete Boc transfer from the N⁹ to the N² position. Therefore, as shown in **Figure 3.3**, to ensure projection of the R¹ (the i + 7 side chain of the Bak-BH3 α -helix) and CH₂COOH (i + 5) groups from opposite faces of the helix mimetic, 2 was condensed with alcohols R¹OH in the presence of DIAD and PPh₃. The resulting N⁹-alkylated products 3 were subjected to a second round of Mitsunobu chemistry using modified conditions (2.5 equiv. of R²OH, PPh₃ and DIAD, and gentle warming) to introduce the R² group (i + 3 mimetic). Finally, an S_NAr reaction with glycine installed the i + 5 mimetic on the opposite face of the scaffold, providing the target molecules 5 in five simple steps.

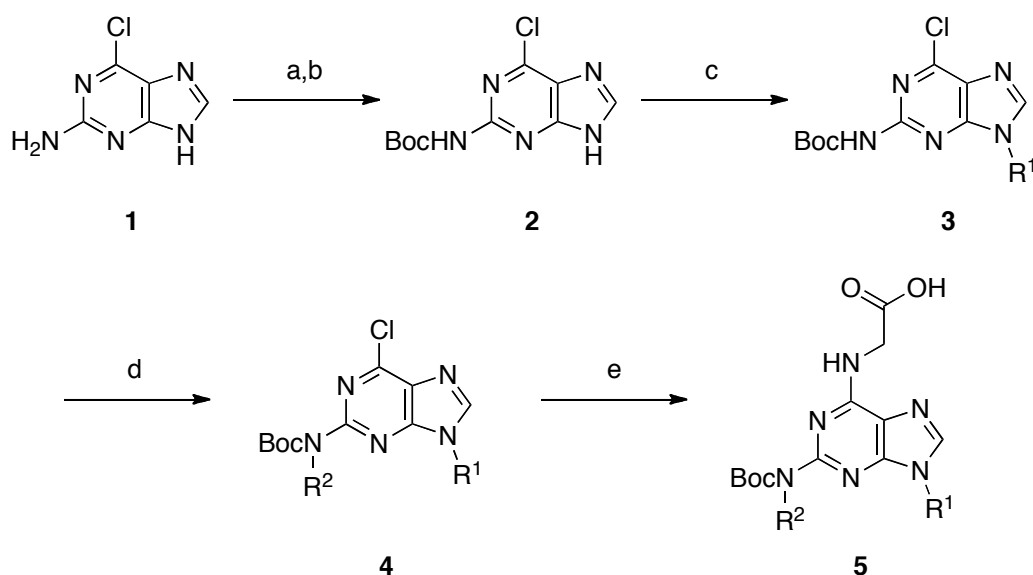
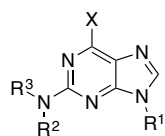


Figure 3.3: (a) Boc_2O , cat. DMAP, DMSO, 0 °C to RT; (b) NaH, THF, 0 °C to RT; (c) R^1OH , DIAD, PPh_3 , THF, RT; (d) R^2OH , DIAD, PPh_3 , THF, 35 °C; (e) glycine, K_2CO_3 , *i*PrOH, reflux.

Accordingly, a small library of amphipathic α -helix mimetics based on 5 was rapidly developed (**Table 3.1**) and then each library member was analyzed for its ability to disrupt the Mcl-1–Bak-BH3 PPI using a fluorescence anisotropy competition assay with a fluorescein-labeled Bak-BH3 peptide GQVGRQLAIIGDDINR, “FITC-Bak^{71–89}” (ESI[†]).¹⁶⁹ Unfortunately, only one compound, 5db, demonstrated appreciable activity with an estimated IC_{50} of 72.3 μM (**Figure 3.4**). Notably, the construction of a sufficiently hydrophobic face was required since there is a seven-fold variation in the estimated IC_{50} values for 5db ($\text{R}^2 = \text{benzyl}$: $\text{IC}_{50} = 72.3 \mu\text{M}$) and 5dc ($\text{R}^2 = \text{isobutyl}$: $\text{IC}_{50} = 472 \mu\text{M}$), and no activity for 5aa ($\text{R}^1 = \text{R}^2 = \text{isopropyl}$) or compound 7. Furthermore, deletion of the Boc group (6db) abrogated binding. Also of particular significance, the carboxylic acid at the *i* + 5 position was required for binding to Mcl-1 (4db exhibited no inhibitory activity).



Number	R ¹	R ²	R ³	X	MW (g/mol)	cLogD	K _I (μM) Mcl-1	K _I (μM) Bcl-x _L	K _I (μM) HDM2
5aa					392.5	-0.38	>250	>250	>350
5ba					454.5	1.13	>250	>250	>350
5cb					454.5	0.90	>250	>250	>350
5db					534.6	2.56	25.4 ± 6.6	55.7 ± 9.4	>350
5dc					504.6	2.30	245 ± 90	>250	>350
4db					501.1	5.52	>250	>250	>350
6db					438.5	0.36	>250	>250	>350
6db					227.6	-2.0	>250	>250	>350

Table 3.1: Binding affinities of purine-based, amphipathic α -helix mimetics to MCL-1, BCL-x_L, HDM2 that were prepared for this study

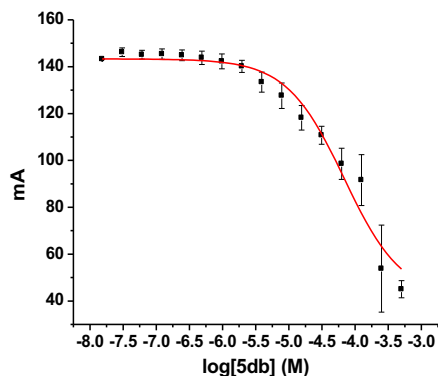


Figure 3.4: The FITC-BAK⁷¹⁻⁸⁹ was competed off Mcl-1¹⁷²⁻³²⁷ with 5db giving an estimated IC₅₀ of 72.3 ± 21.2 μM. Data are an average of biological triplicates and errors are standard deviations. mA = milli-anisotropy. An absolute anisotropy of 40 mA indicates complete competition. For further details, please see the Supporting Information.

Taken together, these data demonstrate that the appropriate functionalization of both faces of a purine scaffold furnished synthetic agents that are capable of recognition of Mcl-1. Although the MW of 5db is just over 500, its clog D at pH 7.4 (calculated using ACD Labs) is 2.56, which is considerably lower than those of analogous terphenyl-based helix mimetics (clogDs 7.22 (mono-acid), 5.27 (di-acid)). We anticipate that a structure–activity relationship (SAR) analysis of 5db will identify more potent Mcl-1 inhibitors that conform to Lipinski’s rules. More generally, these findings validate purine scaffolds as suit- able frameworks to achieve two-faced, α-helix mimicry.

The inhibitory profile of 5db was investigated further by interrogating the HDM2–p53 and Bcl-xL–Bak-BH3 PPIs using similar fluorescence anisotropy competition assays. In the latter case, the same Bak-BH3 peptide from the Mcl-1 experiments was utilized, whilst in the HDM2 experiments, a TAMRA-labeled p53 peptide SQETFSDLWLLPEN was employed (ESI†). Although no inhibition of HDM2 was observed, 5db weakly

inhibited Bcl-xL with an estimated IC_{50} of 201 μ M. Whilst the p53 helical peptide that binds HDM2 also presents a similar recognition pattern of amino acids (Phe19, Trp23, Leu26 on one face, and Asp21 on the other face),²⁰⁹ the naphthyl group (a good mimetic of Trp) of 5db, is at a terminus of the helix mimetic and so is improperly positioned to emulate Trp23. Moreover, Asp21 does not play a functional role in binding HDM2. Rather, the carboxylic acid of Asp21 forms a hydrogen bond with the hydroxyl of Thr18 within the p53 peptide to ensure it folds into the correct helical conformation to permit recognition of HDM2.²⁰⁹ Thus, appropriately-functionalized two-faced synthetic α -helix mimetics may, indeed, provide a source of selectivity over their single-faced counterparts.

To gain a better appreciation of the likely binding mode of 5db, as well as a possible explanation to the approximate 3-fold selectivity for Mcl-1 over Bcl-xL, we performed molecular docking simulations with GOLD. For this purpose, we used the crystal structure of Mcl-1 bound to the Bim-BH3 α -helix, which has a similar pattern of hydrophobic residues to Bak (Ile58, Leu62 (i), Ile65 (i + 3) and Phe69 (i + 7) on one face and Asp67 (i + 5) on the other (PDB ID: 2PQK)). For modelling experiments, the Bim-BH3 α -helix was first extracted to reveal the hydrophobic crevice binding site on the surface of Mcl-1. A high-scoring docking solution is given in **Figure 3.5A** with 5db shown in yellow, which is superimposed on the Bim-BH3 α -helix illustrated in green; key side chains of the helix are shown in stick format. It should be noted that the orientation of the molecule is anti-parallel to the original design. This finding may be due to the binding mode being driven by occupation of the p2 pocket by the large naphthylmethyl group, which, along with the salt bridge interaction with Arg263, is seen more clearly in **Figure 3.5B**. The side chains of Leu62 (Leu78 in Bak), Ile65 (Ile81) and Asp67 (Asp83) overlapped well with the

respective functionalities in 5db. As expected, the tert-butyl of the Boc group inadequately simulated the spatial orientation of the side chain of Phe69 (Ile85 in Bak, originally intended to mimic Leu78), clearly providing a focal point for the design of second-generation compounds. Interestingly, the accommodation of the naphthylmethyl moiety in the p2 pocket may explain the observed two-fold selectivity for Mcl-1 over Bcl-x_L since occupation of this pocket appears to be a determinant in Mcl-1 specificity.¹⁶² In closing, we would like to note that our work complements other research in the field of inhibiting helix-mediated PPIs.

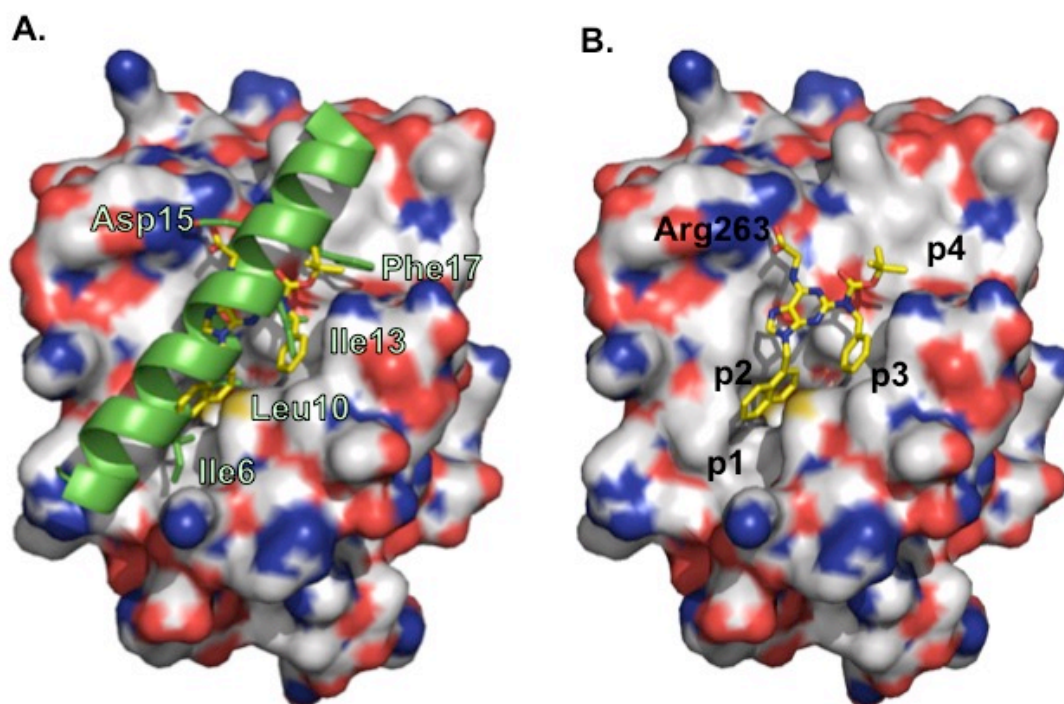


Figure 3.5: GOLD docking of 5db to Mcl-1 (PDB ID: 2PQK). Colored by atom type: grey = carbon, red = oxygen; blue = nitrogen; yellow = sulfur). A. Superimposition of 5db (yellow, colored by atom type) with the Bim-BH3 α -helix (green, key side chains shown in stick format, labeled in green). B. Predicted binding mode of 5db from A with BH3 α -helix removed: Arg263 and p1 – p4 subpockets on Mcl-1 labeled in black.

Particularly, occupation of the p2 pocket by the naphthylmethyl group of 5db

possibly explains the inverse selectivity of our purine-based helix mimetics for Mcl-1 over HDM2 for previously reported helix mimetics.²¹⁰ Also, a recently disclosed phenyl-piperazine-triazine-based helix mimetic demonstrates significantly greater selectivity for Mcl-1 over Bcl-x_L than that which we observed with our purines, although it is unclear if the groups mimicking the *i*, *i* + 3 and *i* + 7 side chains and/or the scaffold itself are responsible for this observation since only one compound was analyzed for selectivity.⁶⁸

3.3 Conclusions

In conclusion, 2,6,9-trisubstituted purines were proposed and then validated as two-faced, α -helix mimetics, permitting reasonable mimicry of the *i*, *i* + 3 and *i* + 7 side chains on one face and *i* + 5 on the opposing face of the Bak-BH3 α -helix. Alternatively, functionalization at the *i* + 5 position may simply be applied to install a solubilizing group opposite the decorated face. Computational modeling indicated that the non-flexible tert-butyl group incorporated to facilitate the synthetic chemistry may have compromised helix mimicry somewhat; more flexible carbamates and sulfonamides at the N2 position are predicted to remedy this undesired outcome. In the course of this research, a novel inhibitor of Mcl-1 was discovered. Efforts in our laboratory are now underway to optimize this compound through a SAR campaign, a goal that will be directly facilitated by the short and simple synthesis.

3.4 Experimental

3.4.1 Chemistry

General. Unless otherwise stated, all reaction were performed under an inert atmosphere

(N₂). Reagents and solvents were ACS grade, and purchased from Sigma- Aldrich, Alfa Aesar, Oakwood and TCI America. Anhydrous solvents were used as provided from Sigma-Aldrich. Reactions were monitored by thin-layer chromatography (TLC), visualizing with a UV lamp and/or KMnO₄ stain. Flash column chromatography was performed with silica gel 60 Å (70-230 mesh, Merck). ¹H and ¹³C NMR spectra were recorded on a Varian INOVA 400 MHz NMR spectrometer at 25 °C. Chemical shifts are reported in parts per million (ppm). Data for ¹H NMR are reported thus: chemical shift (δ ppm) (multiplicity, coupling constant (Hz), integration), where multiplicities are: s = singlet, d = doublet, t = triplet, m = multiplet. The residual solvent peak was used as an internal reference: CDCl₃ (δ_H 7.26; δ_C 77.21) and d₆-DMSO (δ_H 2.50; δ_C 39.51). Mass spectra were obtained on an Electrospray TOF (ESI-TOF) mass spectrometer (Bruker AmaZon X). All final molecules were deemed to be >95% pure by reversed-phased HPLC using a Waters 1525 analytical/preparative HPLC fitted with a C18 reversed- phase column (Atlantis T3: 4.6 mm x 150 mm) according to the following conditions with solvents (A) H₂O/0.1% TFA, (B) CH₃CN–H₂O, 9:1 with 0.1% TFA at 1 ml min⁻¹: (I) a gradient of 50% A to 100% B over 22 min; (II) an isocratic gradient of 100% B over 22 min. Data are presented as retention time (*t_R* (min)), purity (%), condition (I or II).

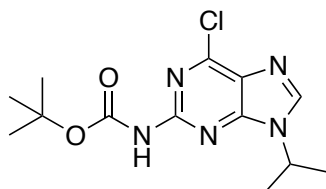
General Procedure A: Mitsunobu reaction at N9 position. *tert*-Butyl (6-chloro-9H-purin-2-yl)carbamate^{79, 208} (**2**; 1 eq) was dissolved in THF (0.07 M) at room temperature (RT). The requisite alcohol (1.1 eq) and PPh₃ (1.1 eq). Upon complete dissolution, DIAD (1.1 eq) was added dropwise. The reaction mixture was stirred for 1 h at RT, by which time

TLC indicated the reaction was complete (Hex/EtOAc, 1:3). The reaction mixture was concentrated to dryness. Some Ph₃P=O was triturated from the reaction mixture with Et₂O. The supernatant was dry-loaded onto silica gel, then purified by flash column chromatography, eluting with Hex/EtOAc, 1:3, to provide the *N*⁹-alkylated product.

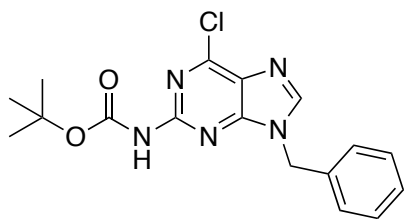
General Procedure B: Mitsunobu reaction at N2 position. The appropriate *N*⁹-alkylated product (**3**; 1 eq) was dissolved in THF (0.07 M) at 35 °C, followed by the requisite alcohol (1.1 eq) and PPh₃ (1.1 eq). As soon as the reaction mixture became homogeneous, DIAD (2.5 eq) was added dropwise. The reaction mixture was allowed to stir at 35 °C overnight. The next day, TLC indicated the reaction was complete (Hex/EtOAc, 2:3). The reaction mixture was concentrated to dryness. Some Ph₃P=O was triturated from the reaction mixture with Et₂O. The supernatant was dry-loaded onto silica gel, then purified by flash column chromatography, eluting with Hex/EtOAc, 2:3, to provide the *N*²-alkylated product.

General Procedure C: Nucleophilic aromatic substitution at C6 position. The appropriate *N*²,*N*⁹-dialkylated purine (**4**; 1 eq) was dissolved in *i*-PrOH (0.1 M). Glycine (5 eq) and K₂CO₃ (5 eq) were added, then the reaction mixture was heated at reflux for 3 d, by which time TLC indicated the reaction was complete (CH₂Cl₂/MeOH/AcOH, 92:7:1). The solvent was removed *in vacuo*. The residue was partitioned between water and Et₂O. The ethereal layer was collected, then the aqueous layer was extracted once again with Et₂O. The aqueous layer was carefully acidified to pH 5 with 0.1 M HCl, then diluted with sat. NaH₂PO₄. The product was extracted into EtOAc (x4). The pooled EtOAc

extractions were washed with water, brine, dried (Na_2SO_4), filtered and concentrated to yield a crude residue that was purified by silica gel flash column chromatography (eluent: $\text{CH}_2\text{Cl}_2/\text{MeOH}/\text{AcOH}$, 92:7:1) to furnish the final molecules **5**.

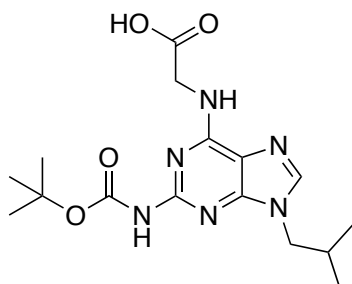


tert-Butyl (6-chloro-9-isopropyl-9H-purin-2-yl)carbamate (**3a**). General procedure A on a 2 mmol scale with isopropanol. White solid (468 mg, 75%); ^1H NMR (400 MHz, CDCl_3): δ 8.04 (s, 1H), 7.56 (s, 1H), 4.92-4.85 (q, $J=6.8$ Hz, 1H), 1.60 (d, $J=6.4$ Hz, 6H), 1.53 (s, 9H); ^{13}C NMR (100 MHz, CDCl_3): δ 152.4, 152.1, 151.0, 150.2, 141.9, 127.9, 81.5, 47.5, 28.2, 22.6; Calcd (M^+): 311.8, Found: 312.0 (M^+).

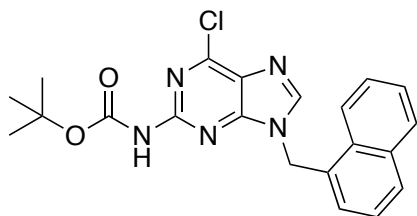


tert-Butyl (9-benzyl-6-chloro-9H-purin-2-yl)carbamate (**3b**). General procedure A on a 2

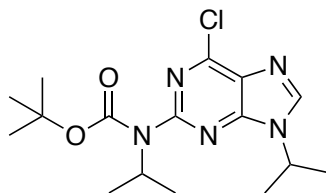
mmol scale with benzyl alcohol. White solid (575 mg, 80%): ^1H NMR (400 MHz, CDCl_3): δ 7.87 (s, 1H), 7.80 (s, 1H), 7.30-7.28 (m, 5H), 5.35 (s, 2H), 1.51 (s, 9H); ^{13}C NMR (100 MHz, CDCl_3): δ 152.9, 152.6, 151.2, 150.3, 143.9, 134.6, 129.1, 128.7, 128.2, 127.6, 81.6, 47.7, 28.2; Calcd (M^+): 359.1, Found: 360.2 ($[\text{M}+\text{H}]^+$).



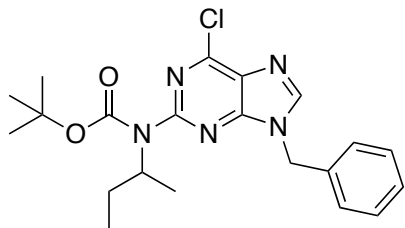
(2-((tert-Butoxycarbonyl)amino)-9-isobutyl-9H-purin-6-yl)glycine (**3c**). General procedure A on a 2 mmol scale with isobutanol. White solid (540 mg, 83%): ^1H NMR (400 MHz, CDCl_3): δ 7.91 (s, 1H), 7.46 (s, 1H), 4.02 (d, $J = 6.8$ Hz, 2H), 2.30-2.23 (m, 1H), 1.53 (s, 9H), 0.94 (d, $J = 7.2$ Hz, 6H); ^{13}C NMR (100 MHz, CDCl_3): δ 153.1, 152.3, 151.2, 150.2, 144.5, 127.8, 81.6, 51.4, 28.9, 28.2, 19.9; Calcd (M^+): 325.1, Found: 326.2 ($[\text{M}+\text{H}]^+$).



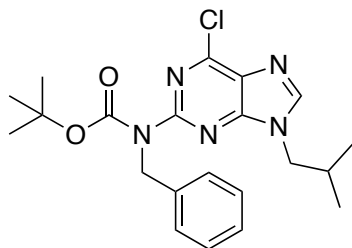
tert-Butyl (6-chloro-9-(naphthalen-1-ylmethyl)-9H-purin-2-yl)carbamate (**3d**). General procedure A on a 2 mmol scale with naphthalene-1-methanol. White solid (795 mg, 97%): ^1H NMR (400 MHz, d_6 -DMSO): δ 10.38 (s, 1H), 8.56 (s, 1H), 8.41 (d, $J = 7.6$ Hz, 1H), 7.97 (d, $J = 8$ Hz, 1H), 7.91 (d, $J = 8.4$ Hz, 1H), 7.63-7.55 (m, 2H), 7.46 (t, $J = 7.8$ Hz, 1H), 7.33 (d, $J = 7.2$ Hz, 1H), 5.89 (s, 2H), 1.45 (s, 9H); ^{13}C NMR (100 MHz, d_6 -DMSO): δ 153.4, 153.0, 151.3, 149.6, 146.6, 133.7, 132.1, 130.7, 129.1, 127.4, 127.1, 126.7, 126.5, 126.0, 123.8, 80.1, 79.6, 44.9, 28.4; Calcd (M^+): 409.1, Found: 410.2 ($[\text{M}+\text{H}]^+$).



tert-Butyl (6-chloro-9-isopropyl-9H-purin-2-yl)(isopropyl)carbamate (**4aa**). General procedure B on a 1 mmol scale with **3a** and isopropanol. Pale yellow gum, contaminated with DIAD- H_2 (350 mg, 99%): ^1H NMR (400 MHz, CDCl_3): δ 8.12 (s, 1H), 4.88-4.82 (m, 1H), 4.63-4.57 (m, 1H), 1.64 (d, $J = 7.2$ Hz, 6H), 1.42 (s, 9H), 1.30 (d, $J = 7.2$ Hz, 6H); ^{13}C NMR (100 MHz, CDCl_3): δ 153.9, 153.8, 151.9, 150.3, 142.9, 129.5, 80.8, 49.9, 48.1, 28.2, 22.4, 20.9; Calcd (M^+): 353.1, Found: 354.1 ($[\text{M}+\text{H}]^+$).

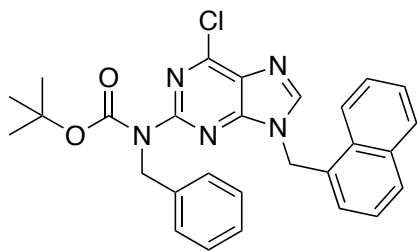


tert-Butyl (9-benzyl-6-chloro-9H-purin-2-yl)(sec-butyl)carbamate (4ba). General procedure B on a 1 mmol scale with **3b** and *sec*-butanol. Pale yellow gum, contaminated with DIAD-H₂ (362 mg, 87%): ¹H NMR (400 MHz, CDCl₃): δ 8.04 (s, 1H), 7.33-7.26 (m, 5H), 5.38 (s, 2H), 4.39-4.34 (m, 1H), 1.83-1.76 (m, 1H) 1.59-1.52 (m, 1H), 1.42 (s, 9H), 1.27 (d, *J* = 7.2 Hz, 3H), 0.94 (t, *J* = 8 Hz, 3H); ¹³C NMR (100 MHz, CDCl₃): δ 154.8, 154.2, 152.4, 150.4, 144.7, 134.6, 129.2, 128.8, 127.9, 80.9, 56.0, 47.9, 28.3, 28.2, 21.9, 18.9, 11.4; Calcd (M⁺): 415.2, Found: 416.2 ([M+H]⁺).



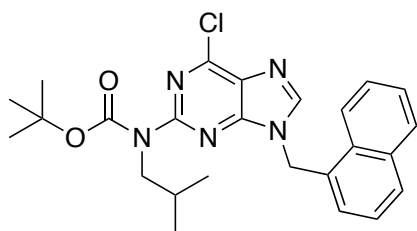
tert-Butyl benzyl(6-chloro-9-isobutyl-9H-purin-2-yl)carbamate (4cb). General procedure B on a 1 mmol scale with **3c** and benzyl alcohol. Pale yellow gum (345 mg, 83%): ¹H NMR (400 MHz, CDCl₃): δ 7.93 (s, 1H), 7.34 (d, *J* = 8.0 Hz, 2H), 7.24 (d, *J* = 7.2 Hz, 2H), 7.16 (t, *J* = 7.4 Hz, 1H), 5.15 (s, 2H), 3.94 (d, *J* = 8 Hz, 2H) 2.20-2.14 (m, 1H), 1.45 (s, 9H), 0.89 (d, *J* = 6.4 Hz, 6H); ¹³C NMR (100 MHz, CDCl₃): δ 155.1, 153.9, 152.3, 150.3, 144.9, 138.5, 128.2, 127.9, 127.5, 126.9, 81.9, 51.5 (2), 28.9, 28.1, 19.9; Calcd (M⁺): 415.2,

Found: 416.3 ($[M+H]^+$).



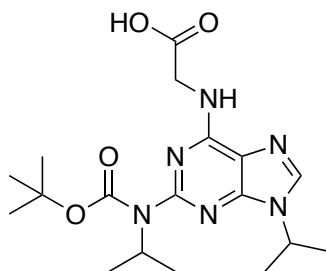
tert-Butyl benzyl(6-chloro-9-(naphthalen-1-ylmethyl)-9H-purin-2-yl)carbamate (**4db**).

General procedure B on a 1 mmol scale with **3e** and benzyl alcohol. Pale yellow gum (356 mg, 87%): ^1H NMR (400 MHz, d_6 -DMSO): δ 8.73 (s, 1H), 8.29-8.27 (m, 1H), 7.98- 7.96 (m, 1H), 7.91 (d, $J = 8.4$ Hz, 1H), 7.57-7.53 (m, 2H), 7.43 (t, $J = 7.8$ Hz, 1H), 7.29 (d, $J = 7.2$ Hz, 1H), 7.20-7.17 (m, 5H), 5.93 (s, 2H), 5.01 (s, 2H), 1.32 (s, 9H); ^{13}C NMR (100 MHz, d_6 -DMSO): δ 154.8, 153.8, 153.0, 149.1, 147.8, 138.6, 133.8, 131.7, 130.7, 129.2, 128.6, 128.0, 127.6, 127.4, 127.2, 126.9, 126.6, 125.9, 123.5, 81.6, 51.3, 45.2, 28.0; Calcd (M^+): 499.2, Found: 500.2 ($[M+H]^+$); $t_R = 9.64$ min (99.7%, II).



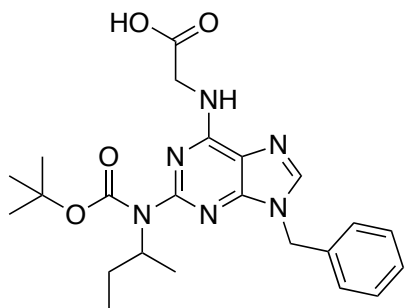
tert-Butyl (6-chloro-9-(naphthalen-1-ylmethyl)-9H-purin-2-yl)(isobutyl)carbamate (**4dc**).

General procedure B on a 1 mmol scale with **3d** and isobutanol. Pale yellow gum, contaminated with DIAD- H_2 after flash column chromatography. The material was used directly in the next step without further attempts of purification.



(2-((tert-Butoxycarbonyl)(isopropyl)amino)-9-isopropyl-9H-purin-6-yl)glycine (**5aa**).

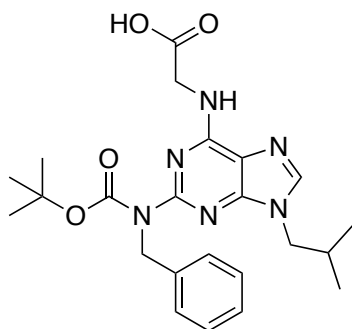
General procedure B on a 0.5 mmol scale with **4aa**. White solid (143 mg, 73%): ^1H NMR (400 MHz, d_6 -DMSO): δ 12.53 (s, 1H), 8.25 (s, 1H), 7.97 (s, 1H), 4.71-4.66 (m, 1H), 4.38-4.34 (m, 1H), 4.06 (d, $J = 4.8$ Hz, 2H), 1.53 (d, $J = 6$ Hz, 6H), 1.34 (s, 9H), 1.15 (d, $J = 6.4$ Hz, 6H); ^{13}C NMR (100 MHz, CDCl_3): δ 172.1, 154.8, 154.1, 153.6, 149.8, 139.9, 118.3, 79.3, 48.7, 47.1, 42.1, 28.4, 22.5, 21.1; mp = 178–182 °C; Calcd (M^+): 392.2, Found: 393.1 ($[\text{M}+\text{H}]^+$); $t_{\text{R}} = 12.4$ min (100%, I).



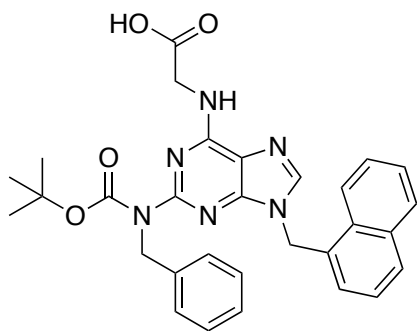
(9-Benzyl-2-((tert-butoxycarbonyl)(sec-butyl)amino)-9H-purin-6-yl)glycine (**5ba**).

General procedure B on a 0.5 mmol scale with **4ba**. White solid (150 mg, 66%): ^1H NMR (400 MHz, CDCl_3): δ 12.52 (s, 1H), 8.26 (s, 1H), 8.01 (s, 1H), 7.29-7.24 (m, 5H), 5.31 (s, 2H), 4.04-3.99 (m, 3H), 1.59-1.52 (m, 1H), 1.40-1.33 (m, 1H), 1.27 (s, 9H), 1.08 (d, $J = 6.4$ Hz, 3H), 0.85 (t, $J = 7.2$ Hz, 3H); ^{13}C NMR (100 MHz, CDCl_3): δ 171.9, 154.8, 154.5,

154.3, 150.2, 141.8, 137.5, 129.0, 128.2, 128.0, 117.7, 79.3, 54.7, 46.7, 42.0, 28.3, 28.1, 19.3, 11.7; mp = 197–200 °C; Calcd (M⁻): 454.2, Found: 353.3 ([M-Boc-H]⁻); *t*_R = 13.5 min (100%, I).

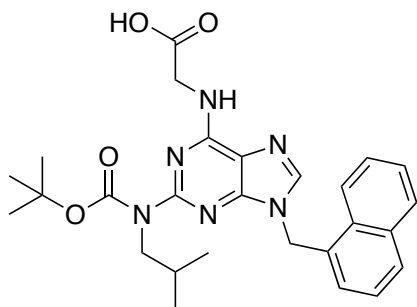


(2-(Benzyl(*tert*-butoxycarbonyl)amino)-9-isobutyl-9H-purin-6-yl)glycine (**5cb**). General procedure B on a 0.5 mmol scale with **4cb**. White solid (177 mg, 78%): ¹H NMR (400 MHz, *d*₆-DMSO): δ 12.55 (s, 1H), 8.09 (s, 1H), 8.00 (s, 1H), 7.32-7.18 (m, 5H), 4.92 (s, 2H), 4.07 (d, *J* = 5.6 Hz, 2H), 3.89 (d, *J* = 7.6 Hz, 2H), 2.19-2.15 (m, 1H), 1.38 (s, 9H), 0.83 (d, *J* = 6.8 Hz, 6H); ¹³C NMR (100 MHz, *d*₆-DMSO): δ 172.1, 155.2, 154.6, 150.4, 141.9 (2), 139.5, 128.4, 127.8, 127.0, 117.0, 80.3, 51.3, 50.5, 42.0, 28.7, 28.3, 20.1; mp = 168–171 °C; Calcd (M⁻): 454.2, Found: 353.3 ([M-Boc-H]⁻); *t*_R = 12.3 min (98.8%, I).



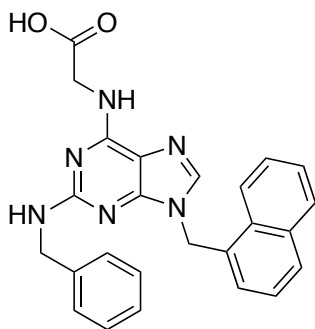
(2-(Benzyl(*tert*-butoxycarbonyl)amino)-9-(naphthalen-1-ylmethyl)-9H-purin-6-yl)glycine

(5db). General procedure B on a 0.5 mmol scale with **4db**. White solid (162 mg, 74%): ^1H NMR (400 MHz, d_6 -DMSO): δ 12.58 (s, 1H), 8.31 (d, $J = 7.2$ Hz, 1H), 8.19 (s, 1H), 8.12 (s, 1H), 7.97 (d, $J = 8$ Hz, 1H), 7.90 (d, $J = 8$ Hz, 1H), 7.57-7.54 (m, 2H), 7.45 (t, $J = 7.8$ Hz, 1H), 7.29 (d, $J = 7.2$ Hz, 2H), 7.24-7.18 (m, 4H), 5.81 (s, 2H), 4.96 (s, 2H), 4.10 (d, $J = 5.6$ Hz, 2H), 1.29 (s, 9H); ^{13}C NMR (100 MHz, d_6 -DMSO): δ 172.0, 155.5, 154.6, 154.5, 150.3, 141.6, 139.5, 133.8, 132.9, 130.8, 129.1, 128.9, 128.5, 127.7, 127.1, 127.0, 126.5, 126.3, 125.9, 123.6, 116.8, 80.4, 51.2, 44.2, 42.1, 28.2; mp = 194–197 °C (dec.); Calcd (M^-): 538.23, Found: 437.3 ($[\text{M-Boc-H}]^-$); $t_{\text{R}} = 16.3$ min (100%, I).



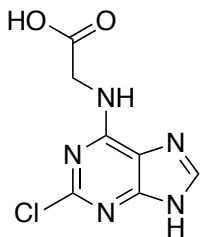
(2-((tert-Butoxycarbonyl)(isobutyl)amino)-9-(naphthalen-1-ylmethyl)-9H-purin-6-yl)glycine

(5dc). General procedure B on a 0.5 mmol scale with **4dc**. White solid (174 mg, 69%): ^1H NMR (400 MHz, d_6 -DMSO): δ 12.51 (s, 1H), 8.32-8.30 (m, 1H), 8.18 (s, 1H), 8.06 (s, 1H), 7.98-7.95 (m, 1H), 7.90 (d, $J = 7.6$ Hz, 1H), 7.57-7.54 (m, 2H), 7.45 (t, $J = 7.8$ Hz, 1H), 7.26 (d, $J = 6.8$ Hz, 1H), 5.81 (s, 2H), 4.06 (d, $J = 8$ Hz, 2H), 3.53 (d, $J = 6.8$ Hz, 2H), 1.81-1.77 (m, 1H), 1.28 (s, 9H), 0.77 (d, $J = 6$ Hz, 6H); ^{13}C NMR (100 MHz, d_6 -DMSO): δ 171.9, 155.9, 154.7, 151.2, 150.3, 141.6, 133.8, 132.9, 130.8, 129.1, 128.9, 127.1, 126.5, 126.4, 125.9, 123.6 (2), 79.7, 54.9, 44.2, 42.1, 28.2 (2), 20.3; mp = 170–173 °C (dec.); Calcd (M^-): 504.3, Found: 403.5 ($[\text{M}-\text{Boc}-\text{H}]^-$); $t_{\text{R}} = 15.7$ min (96.9%, I).



(2-(Benzylamino)-9-(naphthalen-1-ylmethyl)-9H-purin-6-yl)glycine **(6db)**. (2-

(*Benzyl(tert-butoxycarbonyl)amino*)-9-(*naphthalen-1-ylmethyl*)-9*H*-purin-6-yl)glycine (**5db**; 30 mg, 0.056 mmol, 1 eq) was dissolved in anhydrous CH₂Cl₂ (1 mL), then TFA (1 mL) was added. The reaction mixture was stirred for 1 h at RT, by which time TLC confirmed the reaction was complete. All solvent was removed *in vacuo*, and the residual TFA was azeotroped with CHCl₃ (x3). The residue was suspended in ether, then collected by vacuum filtration to yield the title compound as an off-white solid (25 mg, 92%): ¹H NMR (400 MHz, *d*₆-DMSO): δ 8.25 (d, *J* = 8 Hz, 1H), 7.98 (d, *J* = 8.8 Hz, 2H), 7.90 (d, *J* = 7.6 Hz, 1H), 7.58–7.53 (m, 2H), 7.43 (t, *J* = 7.6 Hz, 1H), 7.32 (d, *J* = 6.8 Hz, 3H), 7.27–7.19 (m, 4H), 5.72 (s, 2H), 4.46–4.08 (m, 6H); ¹³C NMR (100 MHz, *d*₆-DMSO): δ 171.2, 159.9, 159.6, 159.2, 156.7, 142.2, 140.2, 138.9, 133.8, 131.7, 130.7, 129.1, 128.6, 128.0, 127.2, 126.6, 126.0, 123.4, 117.7, 114.8, 45.5, 44.9, 42.5; *t*_R = 14.9 min (100%, I).



(2-Chloro-9*H*-purin-6-yl)glycine (**7**). 2,6-Dichloropurine (350 mg, 1.85 mmol, 1 eq) was dissolved in anhydrous DMSO (6 mL). Glycine *tert*-butyl ester. HCl (310 mg, 1.85 mmol, 1 eq) and DIPEA (967 μL, 5.55 mmol, 3 eq) were added to the reaction mixture, which was subsequently heated at 80 °C for 16 h. TLC confirmed the reaction was complete. Upon cooling to RT, ice-cold water was added. The resulting beige precipitate was collected by vacuum filtration, washing with copious ice-cold water, then dried under vacuum at 50 °C for 4 h to afford *tert*-butyl (2-chloro-9*H*-purin-6-yl)glycinate as a beige

solid (509 mg, 97%): ^1H NMR (400 MHz, d_6 -DMSO): δ ^1H NMR (400 MHz, d_6 -DMSO, 60 °C): δ 12.85 (s, 1H), 8.07 (s, 2H), 4.02 (s, 2H), 1.37 (s, 9H); ^{13}C NMR (100MHz, d_6 -DMSO, 60 °C): δ 168.5, 154.3, 152.2, 139.8, 117.2, 80.3, 42.6, 27.5. *tert*-Butyl (2-chloro-9H-purin-6-yl)glycinate (100 mg, 0.352 mmol) was suspended in anhydrous CH_2Cl_2 (3.5 mL), then TFA (3.5 mL) was added, which afforded complete dissolution of the *tert*-butyl ester. After stirring for 3 h at RT, TLC confirmed the reaction was complete. All solvent was removed *in vacuo*, and the residual TFA was azeotroped with CHCl_3 (x3). The residue was suspended in ether, then collected by vacuum filtration to yield the title compound as an off-white solid (76 mg, 95%): ^1H NMR (400 MHz, d_6 -DMSO): δ ^1H NMR (400 MHz, d_6 -DMSO, 60 °C): δ 8.07–7.97 (m, 2H), 4.10 (s, 2H); ^{13}C NMR (100MHz, d_6 -DMSO, 60 °C): δ 171.5, 155.0, 153.2, 140.6, 118.0, 42.4. $t_R = 1.87$ min (100%, II).

3.4.2 Biology

Materials. All chemical reagents were ACS grade or higher unless otherwise indicated. All buffers were passed through Chelex-100 (Bio-Rad, Hercules, CA) to remove trace metals. The D_2O , D_6 -DMSO, and $^{15}\text{NH}_4\text{Cl}$ were purchased from Cambridge Isotope Laboratories, Inc. (Andover, MA). All other chemicals were purchased from Sigma-Aldrich (St. Louis, MO).

Proteins. The pET30a expression vector (EMD Millipore, Billerica, MA) was used to express N-terminal His6-tagged Hdm2 N-terminal domain residues 1 to 155 (Hdm2¹⁻¹¹⁵) in HMS174 (DE3) cells (EMD Millipore). Briefly, the ^{15}N -labeled protein was purified

(>98% final) from inclusion bodies by initial solubilizing in 6 M guanidium chloride in PBS, pH 7.4, with 0.5 mM TCEP. The denatured protein was refolded by rapid dilution into 6-fold volume of PBS, pH 7.4, with 0.5 mM TCEP. The folded protein was then captured on Q-sepharose resin and eluted with a linear gradient of 0 to 2 M NaCl in 10 mM Na₃PO₄, pH 7.0, and 1 mM DTT. Then (NH₄)₂SO₄ powder was added to reach a final concentration of 0.8 M by slow addition over 30 minutes and stirring for an additional 30 minutes. The sample was added to a butyl sepharose column preconditioned with 0.8 M (NH₄)₂SO₄, 10 mM Na₃PO₄, pH 7.0, and 1 mM DTT buffer. The sample was eluted with a linear gradient of decreasing (NH₄)₂SO₄ to a final buffer of 10 mM Na₃PO₄, pH 7.0, and 1 mM DTT. The protein was concentrated using a 10,000 MWCO centrifugal filter concentrator (EMD Millipore) and the concentrate stored frozen in the same buffer. The pLM302 expression vector was constructed to produce His6- MBP (maltose binding protein) tagged recombinant human Mcl-1 residues 172 to 327 (Mcl-1¹⁷²⁻³²⁷) in HMS174 (DE3) cells (EMD Millipore) using either LB or minimal media supplemented with ¹⁵NH₄Cl to produce unlabeled or ¹⁵N-labeled Mcl-1, respectively. The tagged protein was initially purified from the crude cell lysate by IMAC chromatography (GE Healthcare Life Sciences), and after dialysis to remove the imidazole the affinity tag was cleaved using PreScission Protease (GE Healthcare Life Sciences). A Sephacryl S- 200 size exclusion column was used as a final purification step before the protein was concentrated with a 10,000 MWCO centrifugal filter concentrator (EMD Millipore). The concentrations of the proteins were determined using the Bio-Rad Protein Assay (Bio- Rad Inc., Hercules, CA) using BSA of a known concentration as the standard (Pierce). The purity of the protein was confirmed using SDS-PAGE analysis and NMR HSQC experiments were done to confirm

the protein was properly folded (data not shown).

Peptides. A 6-aminohexanoic acid linker was conjugated to the N-terminus of the Bak BH3 peptide (GQVGRQLAIIGDDINR), capped with fluorescein (on the amino group of the linker), and the peptide was amidated on the C-terminus to give FITC-Ahx-GQVGRQLAIIGDDINR-CONH₂, hereafter referred to as “FITC-Bak⁷¹⁻⁸⁹” (synthesized by Neo BioScience in >95% purity). The p53 peptides were derived from the N-terminal human p53, residues 15-29 (SQETFSDLWKLLPEN) with an amidated C-terminus with either an acetylated (p53¹⁵⁻²⁹) or TAMRA-labeled (TAMRA-p53¹⁵⁻²⁹) N-terminus. Each peptide was soluble and stored in H₂O at pH 7. The concentration of the stock solution of unlabeled peptides were determined by quantitative amino acid analysis (Biosynthesis Inc., Lewisville, TX), the concentration of FITC peptides was determined at pH 8.0 using the extinction coefficient for amide-linked FITC, $\epsilon_{494} = 68,000 \text{ cm}^{-1}\text{M}^{-1}$, and the concentration of the TAMRA peptide was determined using the extinction coefficient for TAMRA, $\epsilon_{547} = 65,000 \text{ cm}^{-1}\text{M}^{-1}$. All peptides were synthesized using solid-state peptide synthesis and their purity was determined to be >95% by high pressure liquid chromatography and mass spectrometry.

Fluorescence anisotropy experiments. Fluorescence anisotropy experiments were conducted using a PHERAstar FS (BMG Labtech) multimode microplate reader equipped with two PMTs for simultaneous measurements of the perpendicular and parallel fluorescence emission. In addition, the absolute anisotropy measurements were made on a Cary Eclipse Fluorescence Spectrophotometer (Agilent Technologies) equipped with automated polarizers.

The fluorescence anisotropy assays were performed in black polypropylene 384-well microplate (Costar) with a final volume of 20 μ L. Initially the affinity (K_D) of the FITC-Bak⁷¹⁻⁸⁹ peptide was determined by titrating either Mcl-1¹⁷²⁻³²⁷ or Bcl-xL²⁻²¹², into 10 nM FITC-Bak⁷¹⁻⁸⁹ peptide in 20 mM HEPES, pH 6.8, 50 mM NaCl, 3 mM DTT, 0.01% Triton X-100 and 5% DMSO at room temperature while monitoring the perpendicular and parallel fluorescence emission with a 485 nm excitation and 520 nm emission filters. The fluorescence anisotropy competition assay was performed using 100 nM Mcl-1¹⁷²⁻³²⁷ or 15 nM Bcl-xL²⁻²¹² in the same buffer (10 nM FITC-Bak⁷¹⁻⁸⁹ peptide in 20 mM HEPES, pH 6.8, 50 mM NaCl, 3 mM DTT, 0.01% Triton X-100 and 5% DMSO) with varying concentrations of either unlabeled peptide or experimental compounds.

Similarly, the affinity of TAMRA-p53¹⁵⁻²⁹ was determined by the titration of Hdm2¹⁻¹¹⁵ into 10 nM TAMRA-p53¹⁵⁻²⁹ peptide in PBS with 0.01% Triton X-100 and 5% DMSO at room temperature with a 544nm excitation and 590 nm emission filters. The fluorescence polarization assays (FPCA) were performed using 10 μ M Hdm2¹⁻¹¹⁵ in the same buffer (PBS with 0.01% Triton X-100 and 5% DMSO) with varying concentrations of unlabeled p53¹⁵⁻²⁹ peptide or experimental compounds.

The initial binding affinities (K_D) were determined by fitting the binding data to the Dose Response function in the Origin software (OriginLab, Northampton, MA): $y = A_1 + (A_2 - A_1) / (1 + 10^{(\text{LOG}x_0 - x)p})$ such that dynamic range = abs ($A_1 - A_2$) and the $K_D = 10^{\text{LOG}x_0}$. The IC₅₀ in the competition assays were determined by fitting the binding data to the One Site Competition function in the Origin software (OriginLab, Northampton, MA): $y = A_2$

$+ (A_1 - A_2) / (1 + 10^{(x - \log x)})$ such that dynamic range = $\text{abs}(A_1 - A_2)$ and the $IC_{50} = 10^{\wedge}(\log x_0)$. It has been shown that each of the proteins used here binds a single target peptide (1:1 stoichiometry) at the concentrations used in the competition assays.^{28, 211-212} Therefore, we are able to use an equation derived by Nikolovska-Coleska et al.¹⁷⁰ to calculate the K_d from the IC_{50} from the anisotropy competition assays. The affinity (K_d) of TAMRA-p53¹⁵⁻²⁹ for Hdm²¹⁻¹¹⁵ was determined to be $6.51 \pm 0.44 \mu\text{M}$, and the affinities of FITC-Bak⁷¹⁻⁸⁹ for Mcl-1¹⁷²⁻³²⁷ and Bcl-xL²⁻²¹² were determined to be $41.96 \pm 2.78 \text{ nM}$ and $6.67 \pm 0.05 \text{ nM}$, respectively, in the assay conditions used.

The quality and suitability of the fluorescence anisotropy competition assays were evaluated using the Z-factor developed by Zhang et al.²¹³ The Z-factor = $1 - (3SD_b + 3SD_f) / (|\mu_b - \mu_f|)$ where μ_b and μ_f are the mean anisotropy (mA) values of the bound and free probe, respectively, and SD_b and SD_f are the standard deviations of those values for bound and free probe, respectively. The Z-factor can be any value ≤ 1 , with a value of 1 being an ideal assay, ≥ 0.5 but < 1.0 being an excellent assay, and a value < 0.5 being unacceptable for our application.

A titration of MCL-1 into Bak (**Figure S1A**) shows that the interaction between the protein and ligand and give a $K_D = 41.96 \pm 2.78 \text{ nM}$. In **Figure S1B** a FITC labeled BAK was competed off a protein-ligand complex of Mcl-1/unlabeled truncated Bak (71-89).

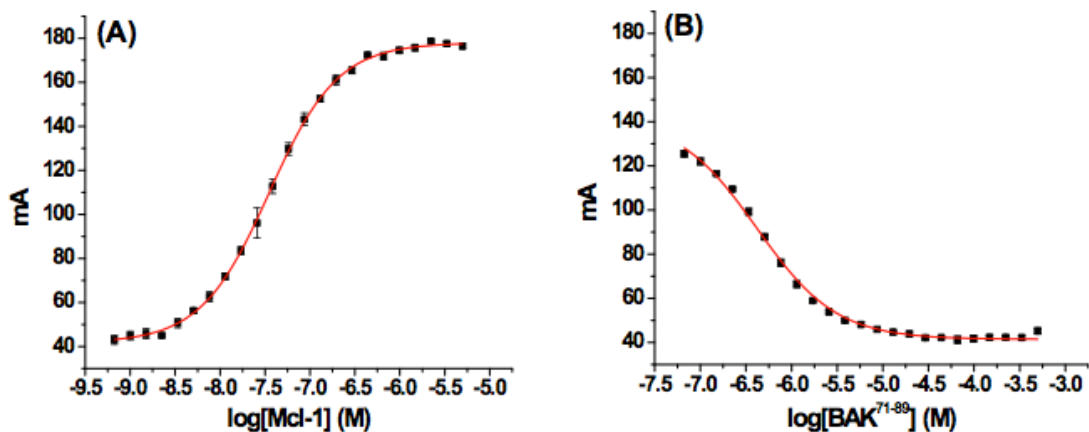


Figure S1. (A) Titration of Mcl-1¹⁷²⁻³²⁷ into 10 nM FITC-BAK⁷¹⁻⁸⁹ gives a K_D of 41.96 ± 2.78 nM with the free FITC-BAK peptide having an absolute anisotropy value of 41.4 ± 1.4 mA (this is the same as Mcl-1 assay b/c same peptide, buffer and conditions) and the Mcl-1 bound peptide 178.0 ± 1.4 mA. (B) The FITC-BAK⁷¹⁻⁸⁹ was competed off Mcl-1¹⁷²⁻³²⁷ with unlabeled BAK⁷¹⁻⁸⁹ peptide with an IC_{50} of 418.19 ± 37.77 nM giving a calculated K_D of 101.84 ± 12.37 nM. For this competition assay 60 nM Mcl-1¹⁷²⁻³²⁷ was used and gives an excellent Z-factor of 0.79 with a dynamic range of 86.96 ± 0.32 mA.

Using the same conditions as above, a FITC labeled BAK was competed off MCL-1 with either **5dc** (Figure S2A) or **5db** (Figure S2B). Molecule **5dc** was unable to compete off FITC-BAK peptide completely giving an observed $IC_{50} = 471.54 \pm 123.12$ μ M and **5db** gave an $IC_{50} = 72.17 \pm 21.21$ μ M.

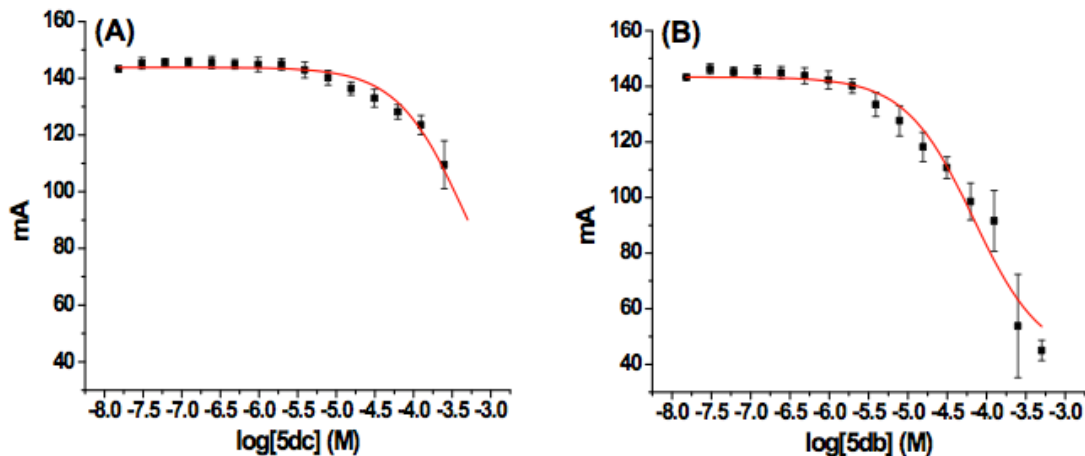


Figure S2. The FITC-BAK⁷¹⁻⁸⁹ was competed off Mcl-1¹⁷²⁻³²⁷ with (A) **5dc** or (B) **5db** giving an estimated IC₅₀ of 471.54 ± 123.12 μM and IC₅₀ 72.17 ± 21.21 μM, respectively. For all the competition assays used to test compounds, 100 nM Mcl-1¹⁷²⁻³²⁷ was used giving an excellent Z-factor of 0.82 with a dynamic range of 101.8 ± 2.85 mA.

A similar approach was used for the BCL-x_L protein and labeled FITC-BAK. The protein-ligand complex gave a K_D of 6.67 ± 0.05 nM (**Figure S3A**) with the free FITC-BAK having an absolute anisotropy of 41.4 ± 1.4 mA. Labeled FITC-BAK was competed off BCL-x_L with an unlabeled truncated BAK peptide (71-89) giving an IC₅₀ = 206.28 ± 14.77 nM and a calculated K_d = 57.17 ± 4.30 nM (**Figure S3B**).

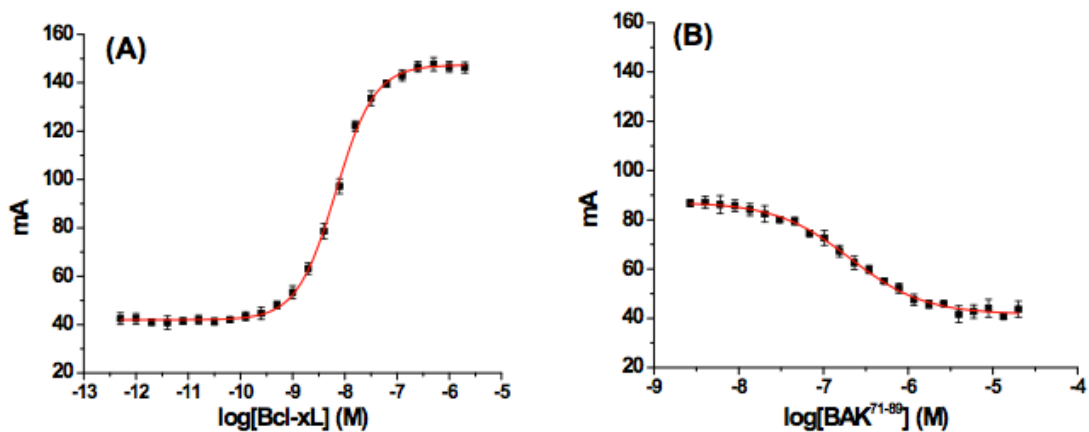


Figure S3. (A) Titration of Bcl-xL²⁻²¹² into 10 nM FITC-BAK⁷¹⁻⁸⁹ gives a K_D of 6.67 ± 0.05 nM with the free FITC-BAK peptide having an absolute anisotropy value of 41.4 ± 1.4 mA (this is the same for MCL-1 assay because it is the same peptide, buffer and conditions) and the Bcl-xL²⁻²¹² bound peptide 147.1 ± 1.4 mA. (B) The FITC-BAK⁷¹⁻⁸⁹ was competed off Bcl-xL²⁻²¹² with unlabeled BAK⁷¹⁻⁸⁹ peptide with an IC_{50} of 206.28 ± 14.77 nM giving a calculated K_d of 57.17 ± 4.30 nM. For this competition assay 15 nM Bcl-xL²⁻²¹² was used giving an excellent Z-factor of 0.91 with a dynamic range of 45.8 ± 0.6 mA.

Lastly, it was determined if molecules **5dc** and **5db** were able to inhibit BCL-x_L. Molecule **5dc** did not compete off the FITC-BAK peptide (**Figure S4A**), but molecule **5db** (**Figure S4B**) had weak inhibition of BCL-x_L giving an estimated $IC_{50} = 201.82 \pm 51.53$ μ M.

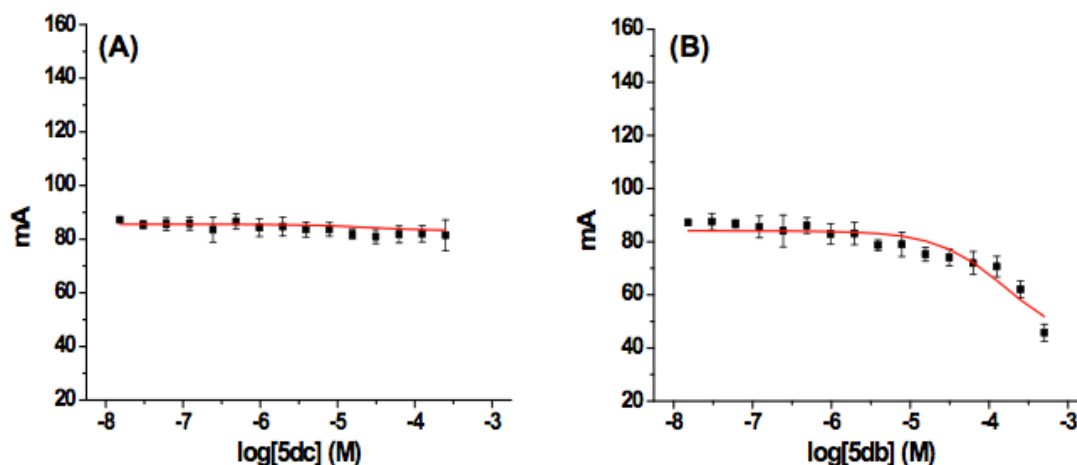


Figure S4. (A) **5dc** does not significantly compete with FITC-BAK⁷¹⁻⁸⁹ binding to Bcl-xL²⁻²¹². (B) **5db** weakly competed with an estimated IC₅₀ of $201.82 \pm 51.53 \mu\text{M}$. For all the competition assays used to test compounds, 15 nM Bcl-xL²⁻²¹² was used giving an excellent Z-factor of 0.91 with a dynamic range of $45.8 \pm 0.6 \text{ mA}$.

Acknowledgements

Reproduced from M.E. Lanning, P.T. Wilder, H. Bailey, B. Drennen, M., Cavalier, L. Chen, J.L. Yap, M. Raje, and S. Fletcher. Towards More Drug-like Proteomimetics: Two-Faced, Synthetic α -Helix Mimetics Based on a Purine Scaffold. *Organic & Biomolecular Chemistry*, 2015; 13: 8642-8648 with *permission from the Royal Society of Chemistry*.
 Copyright © 2015 Royal Society of Chemistry. All rights reserved.

Chapter 4 Azodicarbonyl Dimorpholide (ADDM): An Efficient, Versatile and Water-Soluble Mitsunobu Reagent

The Mitsunobu reaction, first reported by Oyo Mitsunobu in 1967, converts an alcohol (ROH) into a variety of other functional groups, such as esters and aryl ethers, through reaction with a pro-nucleophile (Nu-H) with inversion of the alcohol's stereocenter.²¹⁴⁻²¹⁶ More specifically, reaction of an azodicarboxylate, such as diethyl azodicarboxylate (DEAD, **Figure 4.1**) or diisopropyl azodicarboxylate (DIAD), with a phosphine, typically triphenylphosphine (PPh₃), generates a betaine intermediate that transforms the alcohol into a good leaving group, which is subsequently attacked by the now-deprotonated pro-nucleophile in an overall dehydrative coupling reaction. The requirement for the generation of the conjugate base of the pro-nucleophile imposes upon the reaction the “pK_a rule”, which states that the pK_a of the pro-nucleophile must be around 12 or below, otherwise alkylation of DEAD/DIAD results.²¹⁷ Beyond the traditional applications to functionalize carboxylic acids, phenols, imides and sulfonamides, all of which adhere to the pK_a rule, we have expanded the scope of the Mitsunobu reaction to include purine pro-nucleophiles.^{79, 208, 218} Moreover, we have further demonstrated the synthetic utility of this chemistry in the chemo- and regioselective *N*-anilide alkylations of benzodiazepine-2,5-diones.²¹⁹

Due to its mildness and versatility, the Mitsunobu reaction has gained wide acceptance in synthetic organic chemistry. However, the reaction is associated with one significant flaw: purification of the reaction mixture, as products can often be contaminated with azo, hydrazide and phosphine species from the co-reagents. In recent years, there have been reports of new Mitsunobu reagents (both azodicarboxylates and phosphines) devised

to facilitate purification, which include PPh₃ on resin and di-*tert*-butylazodicarboxylate.³ Given our continued interest in the Mitsunobu reaction, which we use routinely in the functionalization of our synthetic α -helix mimetics,²⁹ we, too, were interested in elaborating the toolbox of “purification-friendly” Mitsunobu reagents. To this end, we herein present azodicarbonyl dimorpholide (ADDM, **2**) as an effective and versatile Mitsunobu reagent, which, along with its reduced form ADDM-H₂, may be conveniently removed from the reaction mixture either by trituration with ether or by washing with water.

4.1 Azodicarbonyl Dimorpholide (ADDM)

ADDM is a useful reagent for the formation of disulfide bonds under aqueous conditions.²²⁰ Carrying the requisite azodicarbonyl functionality, ADDM would also appear to be a suitable reagent for the Mitsunobu reaction, but there is only a handful of such reports, and an analysis of its versatility in this reaction is lacking.²²¹⁻²²⁴ Given its excellent aqueous solubility, we considered that ADDM would greatly simplify Mitsunobu reaction purification, and so we embarked on a study to examine its scope in this reaction. ADDM is commercially available, but it is rather expensive. Alternatively, ADDM may be conveniently and cost-effectively prepared in a single, chromatography-free step by the dropwise addition of morpholine to a solution of DEAD in ether at 0 °C, as shown in **Figure 4.1**, in a modification of a previously-reported procedure.²²⁵

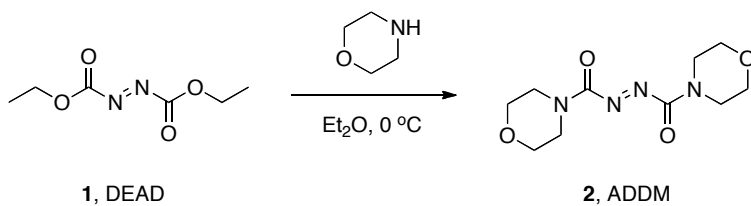


Figure 4.1: Reaction scheme to make ADDM from DEAD and morpholine.

4.2 Scope of ADDM: Results and Discussion

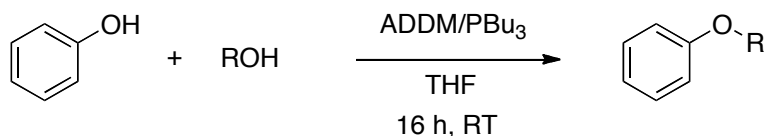
After some experimentation with phenol and 1-butanol, isopropanol and benzyl alcohol, we identified optimal conditions for the Mitsunobu reaction with ADDM: 1 equiv of phenol, and 2 equiv of each of the alcohol, ADDM and tri-*n*-butylphosphine (PBU₃) at room temperature (RT) for 16 h (**Table 4.1**).

Table 4.1: Alcohol substrate scope for Mitsunobu coupling to phenol with ADDM.^a

^aReaction conditions: phenol (0.5 mmol), ROH (1, 1.5 or 2 equiv) and tri-*n*-butylphosphine (1, 1.5 or 2 equiv) were dissolved in anhydrous THF (7 mL) at RT. After 2 min, ADDM (1, 1.5 or 2 equiv) was added in one portion. The reaction mixture was stirred at RT for 16 h under an inert atmosphere.

^bPhenol fixed at 0.5 mmol; all other reagents present as equal numbers of equivalents shown.

^cIsolated yield.



Entry	Alcohol	Equivalents ^b	Product	Yield (%) ^c
1		1		43
2		1		38
3		1		41
4		1.5		75
5		2		94

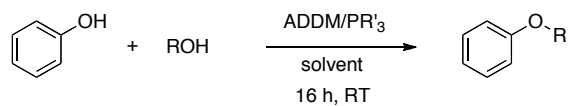
Close monitoring by TLC suggested that the benzyl alcohol reaction (2 equiv of all reagents relative to phenol) was complete within 6 h (~90% complete after 30 min. (isolated yield)), whereas the reaction with the less reactive isopropanol took around 6 h to reach approximately 90% completion (isolated yield) with no further change beyond 16 h. For these reasons, 16 h was selected as the optimum reaction time irrespective of the alcohol employed. A survey of solvents (entries 1–3, **Table 4.2**) traditionally used in the Mitsunobu reaction revealed that THF (0.07 M) was the solvent of choice. In terms of the phosphine co-reagent, we observed that PBu_3 consistently afforded higher yields than the less nucleophilic PPh_3 (compare entries 1 and 4). Using these optimized conditions, we

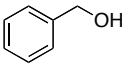
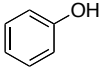
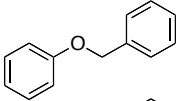
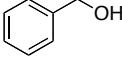
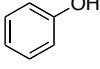
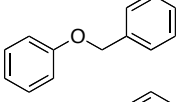
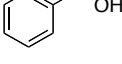
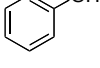
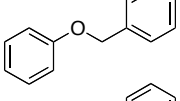
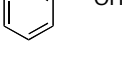
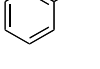
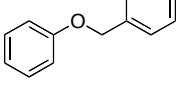

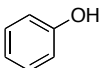
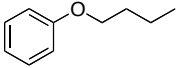
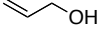
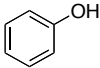
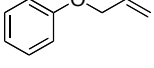
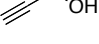
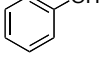
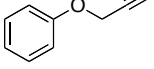
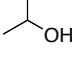
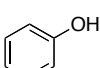
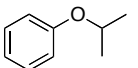
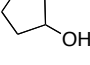
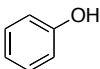
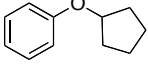
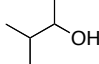
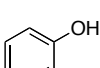
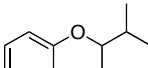
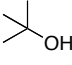
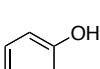
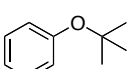
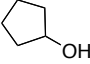
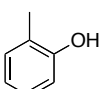
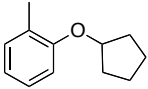
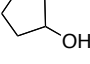
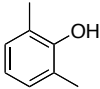
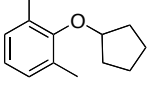
investigated the scope of the Mitsunobu reaction first with a range of alcohols. As is evident from **Table 4.2**, ADDM is effective in activating a variety of primary and secondary alcohols with yields of the expected phenol ethers in many cases in excess of 80%. The lower yields for the allyl and propargyl phenol ethers (entries 6 and 7) may be due to the volatilities of the products, whereas the moderate yield for 3-methyl-2-butanol is presumably due to steric hindrance. The reaction with *tert*-butanol did not proceed, as anticipated, due to spatial crowding around the tertiary alcohol carbon atom. Entries 9, 12 and 13 demonstrate that the Mitsunobu reaction with ADDM is compatible with hindered pro-nucleophiles, but increasing steric bulk results in progressively lower yields, as expected. Nevertheless, it is noteworthy that 2,6-dimethylphenol, in which the acidic OH is flanked by two bulky methyl groups, coupled to the secondary alcohol cyclopentanol with a yield of 62% (entry 13). In terms of reaction mixture purification, due to the greater polarities of ADDM and ADDM-H₂ relative to DIAD and DIAD-H₂, we found that these impurities could be easily removed by silica gel flash chromatography as they were readily separable from the target compounds. Alternatively, after concentration of the THF reaction solvent, ADDM/ADDM-H₂ could be triturated with ether, or extracted into water from CH₂Cl₂ or EtOAc, as anticipated, greatly facilitating purification and minimizing costs incurred with laborious column chromatography.

Table 4.2: Alcohol substrate scope for Mitsunobu coupling to phenol with ADDM.^a

^aReaction conditions:¹¹ phenol (0.5 mmol), ROH (1 mmol) and phosphine (1 mmol) were dissolved in anhydrous solvent (7 mL) at RT. After 2 min, ADDM (1 mmol) was added in one portion. The reaction mixture was stirred at RT for 16 h under an inert atmosphere.

^bIsolated yield.



Entry	Alcohol	Phenol	Phosphine	Solvent	Product	Yield (%) ^b
1			PBu ₃	THF		94
2			PBu ₃	CH ₂ Cl ₂		80
3			PBu ₃	toluene		87
4			PPh ₃	THF		82
5			PBu ₃	THF		89
6			PBu ₃	THF		65
7			PBu ₃	THF		66
8			PBu ₃	THF		82
9			PBu ₃	THF		86
10			PBu ₃	THF		51
11			PBu ₃	THF		NR
12			PBu ₃	THF		80
13			PBu ₃	THF		62

Next, we examined the scope of the ADDM-mediated Mitsunobu reaction with a range of pro-nucleophiles; our results are shown in **Table 4.3**. Benzoic acid, phenol, phthalimide and *N*-benzylbenzenesulfonamide²²⁶ all underwent condensations with benzyl alcohol with excellent isolated yields of the expected products in yields of >80%. Although the Mitsunobu reaction did not proceed with diethyl malonate, employing the more acidic di(2,2,2-trifluoroethyl) malonate²²⁷ afforded a 60% yield of a mixture of mono- and di-benzylated malonates.

NuH + c1ccc(CO)cc1 $\xrightarrow[\text{THF, 16 h, RT}]{\text{ADDM/PBu}_3}$ c1ccc(CNu)cc1

Entry	Pro-nucleophile (NuH)	Product	Yield (%) ^b
1	<chem>c1ccc(C(=O)O)cc1</chem>	<chem>c1ccc(C(=O)OCc2ccccc2)cc1</chem>	88
2	<chem>c1ccc(O)cc1</chem>	<chem>c1ccc(OCc2ccccc2)cc1</chem>	94
3	<chem>O=C1OC(=O)c2ccccc12</chem>	<chem>O=C1OC(=O)N(Cc2ccccc2)c3ccccc13</chem>	93
4	<chem>c1ccc(CNS(=O)(=O)c2ccccc2)cc1</chem>	<chem>c1ccc(CN(Cc2ccccc2)S(=O)(=O)c3ccccc3)cc1</chem>	82
5	<chem>CCOC(=O)CC(=O)OCC</chem>	<chem>CCOC(=O)C(Bc1ccccc1)C(=O)OCC</chem>	NR
6	<chem>CCOC(=O)CC(=O)OCC(F)(F)F</chem>	<chem>CCOC(=O)C(Bc1ccccc1)C(=O)OCC(F)(F)F</chem>	60 ^c

Table 4.3: Pro-nucleophile substrate scope for Mitsunobu coupling to benzyl alcohol with ADDM.^a

^aReaction conditions: pro-nucleophile (0.5 mmol), ROH (1 mmol) and PBu_3 (1 mmol) were dissolved in anhydrous THF (7 mL) at RT. After 2 min, ADDM (1 mmol) was added in one portion. The reaction mixture was stirred at RT for 16 h.

^bIsolated yield.

^cMixture of mono- and di-benzylated di(2,2,2-trifluoroethyl) malonate.

Since ADDM-H₂ has excellent solubility in water and limited solubility in ether, we reasoned that it should be readily separable from the reaction mixture and then recyclable by oxidation back to ADDM. To this end, we repeated the condensation of benzyl alcohol and phenol in THF with ADDM and PBU₃, and recovered about 60% of ADDM-H₂ by trituration with ether. Re-oxidation of ADDM-H₂ with silver (I) oxide (Ag₂O) delivered ADDM (**Figure 4.2**). The regenerated ADDM was utilized in another otherwise identical round of Mitsunobu chemistry with no detriment to the yield relative to fresh ADDM that was prepared from DEAD and morpholine.

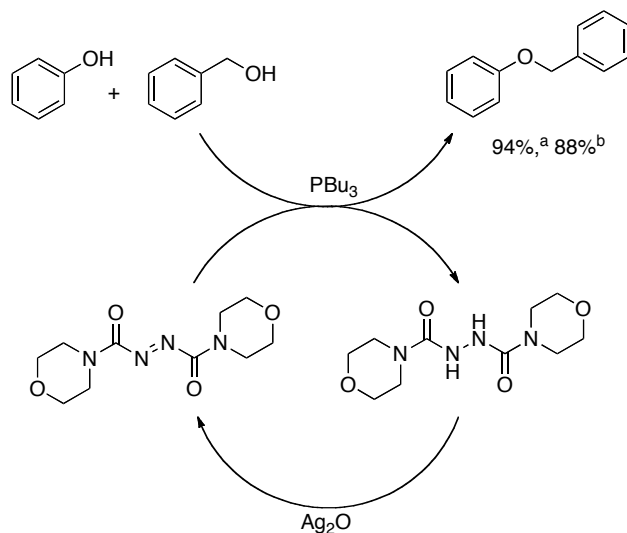


Figure 4.2: Yields for the Mitsunobu reaction with (a) ADDM prepared from DEAD and (b) recycled ADDM prepared by re-oxidation of ADDM-H₂.

Finally, we investigated whether a chromatography-free Mitsunobu reaction with ADDM would be possible. A mixture of 1 equiv of benzoic acid, 2 equiv of each of 1-butanol and ADDM, and 3 equiv of PPh₃ on resin in CH₂Cl₂ was gently agitated for 16 h at room temperature (**Figure 4.3**). TLC analysis of the reaction mixture confirmed all of the phenol had been consumed, and only one new UV-active species was generated. Filtration of the reaction mixture removed the PPh₃/PPh₃O on resin. After the filtrate had

been concentrated, the residue was resuspended in ether, and washed thoroughly with water to afford the product in >95% purity, as judged by ^1H NMR.

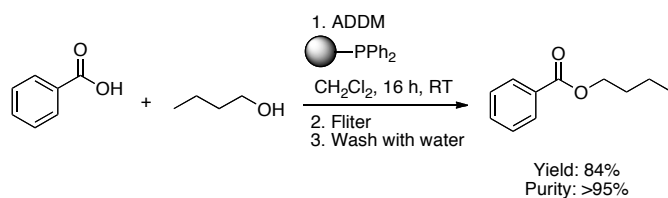


Figure 4.3: A chromatography-free Mitsunobu reaction.

4.3 Conclusions

In summary, we have demonstrated that commercially available ADDM is a versatile Mitsunobu reagent, facilitating the dehydrative couplings of a variety of primary and secondary alcohols with a diverse collection of pro-nucleophiles spanning a pK_a range from 5 to 12. Furthermore, the greater polarities of ADDM and ADDM-H₂, relative to the more traditional Mitsunobu reagent DIAD (and DIAD-H₂), results in simpler flash chromatographic purification. Alternatively, ADDM and ADDM-H₂ may be conveniently removed from the reaction mixture by trituration with ether, or by extraction into water. ADDM may be regenerated by brief treatment of recovered ADDM-H₂ with Ag₂O. By employing PPh₃ on resin, we also showed that ADDM allows for a chromatography-free Mitsunobu reaction.

4.4 Experimental

4.4.1 Chemistry

Synthesis of ADDM from DEAD: To a stirred solution of diethyl azodicarboxylate (40

wt% in toluene; 5 mL, 11.5 mmol, 1 equiv) in Et₂O (25 mL) at 0 °C was added a solution of morpholine (1.98 mL, 23 mmol, 2 equiv) in Et₂O (25 mL) over 3 h with a dropping funnel. The reaction mixture was stirred for a further 2 h whilst slowly warming to room temperature. The yellow-orange precipitate was collected by vacuum filtration, washed with cold Et₂O, and dried on the filter to furnish ADDM as a yellow-orange solid (1.62 g, 55% yield): δ_{H} (CDCl₃, 400 MHz) 3.61 (m, 4H, 2 CH₂), 3.74 (m, 8H, 4 CH₂), 3.83 (m, 4H, 2 CH₂).

General procedure: A solution of phenol (47 mg, 0.5 mmol, 1 equiv), benzyl alcohol (108 μ L, 1.0 mmol, 2 equiv) and PBu₃ (250 μ L, 1.0 mmol, 2 equiv) in anhydrous THF (7 mL) was stirred at RT for 5 min. ADDM (256.4 mg, 1.0 mmol, 2 equiv) was added in one portion. The reaction mixture was stirred at RT for 16 h. The solvent was concentrated under reduced pressure, and then the residue was adsorbed onto silica gel from CH₂Cl₂, and purified by flash column chromatography (eluent: Hex/EtOAc, 9:1) to give (benzyloxy)benzene as a colorless oil (92 mg, 94%): δ_{H} (CDCl₃, 400 MHz) 5.08 (s, 2H, CH₂), 7.28–7.49 (m, 10H, Ar).

Regeneration of ADDM: Trituration of the crude residue from an ADDM/PBu₃ Mitsunobu reaction afforded about 60% recovery of reduced ADDM, or “ADDM-H₂”. To a solution of ADDM-H₂ (235 mg, 0.910 mmol, 1 equiv) in MeOH (9 mL) was added silver (I) oxide (211 mg, 0.910 mmol, 1 equiv). The reaction mixture was stirred for 15 min, by which time it had turned a dark orange color, at which point it was dried with anhydrous MgSO₄, and then filtered. The filtrate was concentrated, resuspended in minimal acetonitrile, filtered and concentrated once more to deliver regenerated ADDM (133 mg, 60% yield).

Solid phase procedure: A solution of benzoic acid (122 mg, 1.0 mmol, 2 equiv), 1-butanol

(45.7 μL , 0.5 mmol, 1 equiv) and PPh_3 on resin (2.09 mmol/g, 1.0 mmol, 2 equiv) in anhydrous CH_2Cl_2 (7.5 mL) was stirred. Then, ADDM (256 mg, 1.0 mmol, 2 equiv) was added in one portion. The reaction mixture was stirred at RT overnight. The PPh_3 on resin was removed by filtration. The solvent was concentrated under reduced pressure. The residue was partitioned between ether and water, and then the ether layer was washed with 1M HCl, saturated NaHCO_3 , water (x 3), brine, dried (Na_2SO_4), filtered and concentrated to afford 1-butyl benzoate in >95% purity as a clear oil (78 mg, 88%): δ_{H} (CDCl_3 , 400 MHz) 0.90 (t, 3H, CH_3), 1.39 (m, 2H, CH_2CH_3), 1.67 (m, 2H, $\text{CH}_2\text{CH}_2\text{CH}_3$), 4.24 (t, 2H, OCH_2), 7.35 (t, $J = 7.4$ Hz, 2H, Ar), 7.46 (t, $J = 7.4$ Hz, 1H, Ar), 7.96 (d, $J = 7.4$ Hz, 2H, Ar).

Acknowledgements

Reproduced from *M.E. Lanning and S. Fletcher. Azodicarbonyl Dimorpholide (ADDM): An Effective, Versatile, and Water-Soluble Mitsunobu Reagent. Tetrahedron Letters 2013; 54: 4624-4628 with permission from Elsevier Ltd. Copyright © 2013 published by Elsevier Ltd.*

Chapter 5 Chromatography-Free Entry to Substituted Salicylonitriles: Mitsunobu-Triggered Domino Reactions of Salicylaldoximes

In connection with our research program into the development of inhibitors of the Mcl-1 oncoprotein,^{29, 70 162} we sought to replace the benzoic acid moiety of our drug molecules – whose interaction with Arg263 is crucial to the activity of the inhibitors – with alternative bioisosteres that might exhibit improved cell permeabilities. Towards this goal, it was speculated that salicylonitriles, or 2-hydroxybenzonitriles, bearing pK_{a} s of around 6.86,²²⁸ might prove remedial. In fact, Chen and colleagues have developed some Mcl-1 inhibitors that feature a 2-hydroxynicotinonitrile moiety wherein the *ortho* hydroxyl and cyano groups might together function as a bioisostere of a carboxylic acid.¹⁵⁸ More generally, since the nitrile moiety is a versatile functional group, salicylonitriles may provide access to more complex heterocyclic and pharmaceutically-relevant compounds, such as 3-aminobenzofurans,²²⁹ benzofuro[3,2-b]pyridines,²²⁹ benzofuro[3,2-b]quinolines,²³⁰ arylbenzofurodiazepin-6-ones²³¹ and pyrazines.²³² However, there are limited synthetic procedures in the literature towards the synthesis of substituted salicylonitriles.

One of the more traditional strategies to access salicylonitriles is the Rosenmund-von Braun reaction in which a 2-halophenol is treated with CuCN (Figure 5.1).²³³ A caveat of this approach is that very high temperatures (up to 200°C) are often required for effective displacement of the halogen by CN. A handful of approaches involve the corresponding salicylaldehyde. For example, substituted salicylonitriles can be prepared by treatment of the corresponding salicylaldehyde with hydroxylamine, although high temperatures, extended reaction times and microwave energy may be required to encourage dehydration

of the intermediate salicylaldoxime.²³⁴⁻²³⁸ The Kemp and Woodward method in which the salicylaldehyde is reacted with hydroxylamine *O*-sulfonic acid has been shown to lead to almost a three-fold greater amount of the undesired Beckmann rearrangement product *ortho*-hydroxyformanilide over the desired salicylonitrile.²³⁹ Recently, Anwar and Hansen introduced a one-pot procedure for the conversion of substituted phenols into substituted salicylonitriles, although this three-stage reaction requires reaction monitoring before progression to the next stage.²⁴⁰ Furthermore, in many of the procedures listed here, column chromatography is required in order to isolate the salicylonitrile. Herein, we demonstrate that substituted salicylonitriles can be readily and efficiently accessed from the corresponding salicylaldoximes by a one-pot, two-stage domino reaction initiated by Mitsunobu chemistry that occurs quickly at room temperature (RT) under essentially neutral conditions, wherein column chromatography is circumvented.

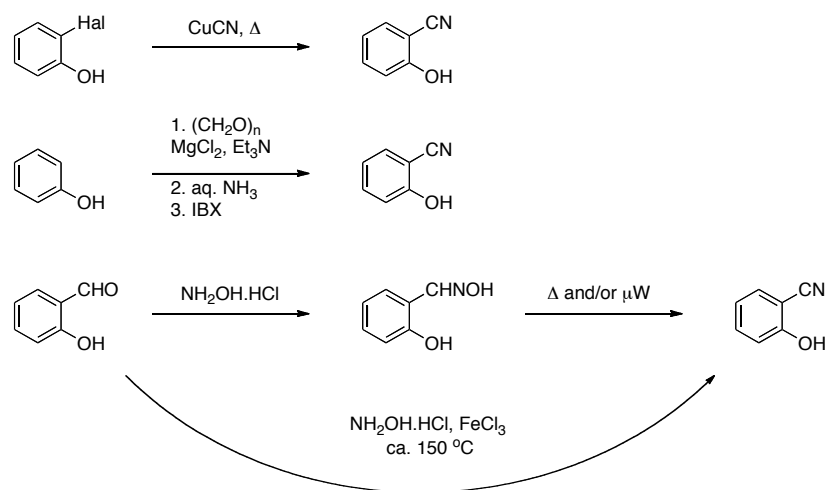


Figure 5.1: Existing methods to prepare salicylonitriles.

In addition to its more contemporary applications in the regioselective alkylation

of purines,^{79, 208, 218} benzodiazepin-2,5-diones²¹⁹ and 3-hydroxyisoxazoles,²⁴¹ the Mitsunobu reaction²¹⁷ has been utilized to effect cyclodehydrations of salicylaldoximes into 1,2-benzisoxazoles.²³⁹ Since 1,2-benzisoxazoles are prone to ring-opening reactions in the presence of a mild base, such as sodium acetate (Kemp elimination),²⁴²⁻²⁴³ we hypothesized that an excess of the Mitsunobu co-reagents would generate a surplus of the betaine intermediate whose basicity would initiate the Kemp elimination. Overall, this would amount to a cyclodehydration- β -elimination cascade reaction, furnishing the desired salicylonitrile from the corresponding salicylaldoxime in one pot.

5.1 Synthetic Strategy

To test our hypothesis, we subjected commercially available salicylaldoxime **1** (*(E)*-2-hydroxybenzaldehyde oxime) to 1.25 equiv of diisopropylazodicarboxylate (DIAD) and triphenylphosphine (PPh₃) in THF (**Table 5.1**). A concentration of 0.07 M was selected as we found this to be optimal in our earlier work on Mitsunobu chemistry.^{79, 208, 218-219, 241} TLC analysis of the reaction after 15 min revealed considerable starting material remaining along with a new, less polar product which we considered might be the 1,2-benzisoxazole **2**. Extending the reaction time to 1 h and then 16 h afforded no discernible reduction in remaining starting material. Silica gel column chromatography of the reaction mixture followed by ¹H NMR revealed that the solitary product generated was indeed **2**. We next repeated the reactions in CH₂Cl₂ and CH₃CN, and observed they were complete within 15 min, affording excellent yields of 1,2-benzisoxazole **2** in each case. ¹H NMR analysis of the crude mixtures of similar reactions that had been allowed to stand overnight demonstrated the emergence of salicylonitrile **3** (entries **5** and **6**, (δ_{H} C3-H (**2**) 8.90 ppm;

Reaction scheme: Salicylonitrile **1** reacts with DIAD and PPh₃ in a solvent at room temperature (RT) to produce salicylonitrile **3** and an intermediate **2**.

Entry	Equivalents	Solvent	Time	Ratio, ^b 2:3	Yield (3, %) ^c
1	1.25	THF	15 min	1:0	0
2	1.25	CH ₂ Cl ₂	15 min	>99:1	trace
3	1.25	CH ₃ CN	15 min	>99:1	trace
4	1.25	THF	16 h	9:1	5
5	1.25	CH ₂ Cl ₂	16 h	5:1	14
6	1.25	CH ₃ CN	16 h	5:1	16
7	2	CH ₂ Cl ₂	16 h	2:5	63
8	2.5	THF	1 h	5.5:1	20
9	2.5	CH ₂ Cl ₂	1 h	0:1	93
10	2.5	CH ₃ CN	1 h	0:1	97
11	1.25, 1.25	CH ₂ Cl ₂	1 h, 1 h	0:1	93

Table 5.1: Screening of reaction conditions.^a

^aThe salicylonitrile **1** (0.5 mmol, 1 equiv.) and PPh₃ were dissolved in the appropriate solvent (0.07 M) at RT under an inert (N₂) atmosphere. After 5 min, DIAD was added dropwise, then the reaction was allowed to stir at RT for the time stated; ^bdetermined by ¹H NMR analysis of crude material; ^cisolated yield.

δ_{H} OH (**3**) 11.1 ppm (*d*₆-DMSO)). Additional experiments revealed that 2.5 equiv of DIAD and PPh₃ were sufficient to convert all of salicylaldehyde **1** into salicylonitrile **3** in CH₂Cl₂ and CH₃CN within 1 h. To further investigate if the transformation of **1** into **3** occurred through **2** under Mitsunobu conditions, we again treated **1** with 1.25 equiv of DIAD and PPh₃ in CH₂Cl₂ (entry 11), which, after 1 h showed complete conversion to **2** and no evidence of **3**. Then, we introduced another 1.25 equiv of DIAD and PPh₃, and a TLC check of the reaction after an additional 1 h revealed **2** had been completely transformed into **3**.

Taken together, our findings suggest that, as hypothesized, treatment of salicylaldoxime **1** with an excess of the Mitsunobu reagents DIAD and PPh₃ triggers a domino reaction of a cyclodehydration to 1,2-benzisoxazole **2** followed by a ring-opening Kemp elimination to furnish salicylonitrile **3**. We note that (*E*)-benzaldehyde oxime underwent dehydration under these conditions to afford benzonitrile in an E2 elimination reaction, and so the phenolic hydroxyl of salicylaldoxime is sufficiently reactive and correctly positioned to intercept the activated oxime to deliver the observed 1,2-benzisoxazole intermediate. A plausible mechanism for this cascade reaction is proposed in **Figure 5.2**.

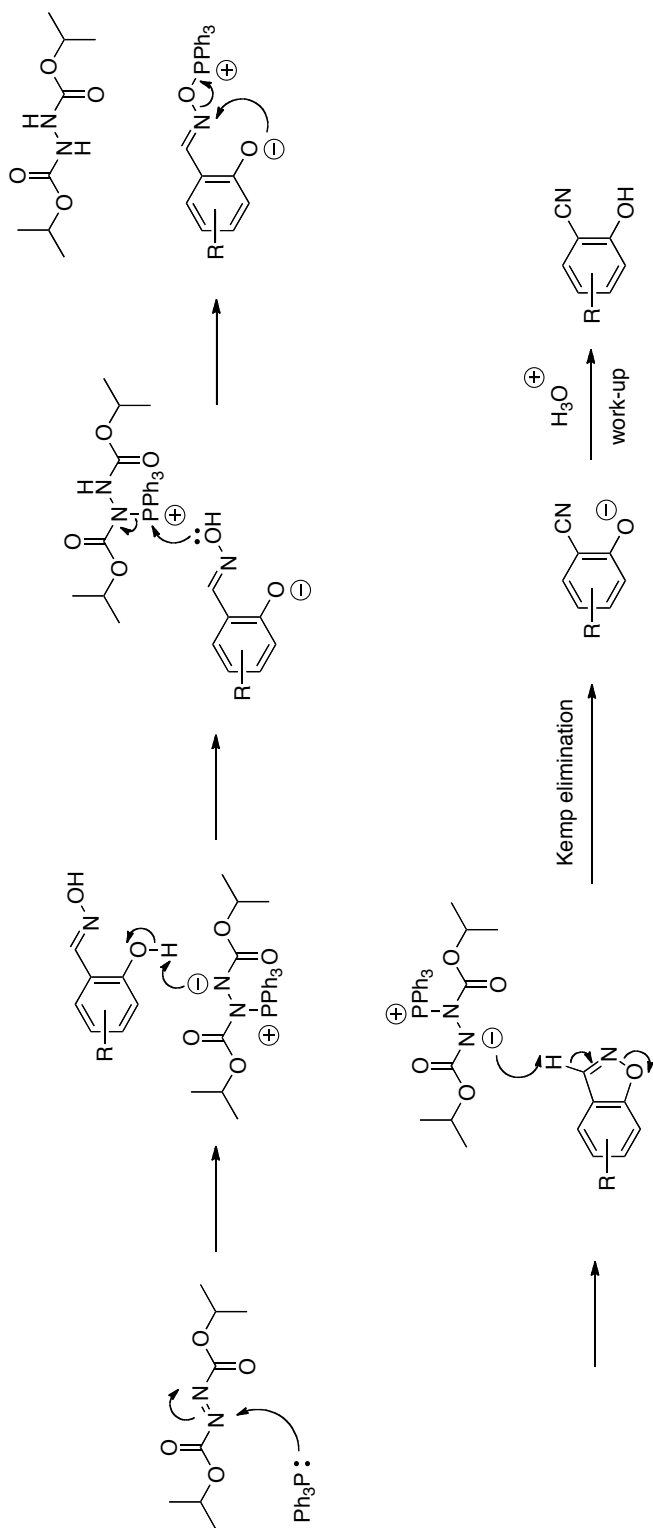
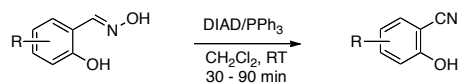


Figure 5.2: Proposed mechanism for the two step, one-pot conversion of salicylaldoximes to their corresponding salicylonitriles.

We next turned our attention to assessing the scope of this methodology, and our results are presented in Table 5.2. All salicylaldoximes substrates therein were prepared by treatment of the corresponding salicylaldehydes **1** with hydroxylamine according to a standard procedure described in the Experimental Section. Solitary products were detected in each case, which were presumed to be the desired (*E*)-isomers owing to similar oxime CH chemical shifts to that for unsubstituted salicylaldoxime (δ_{H} 8.17–8.54 versus 8.33) and that the corresponding oxime proton in (*Z*)-isomers is often around 1 ppm upfield (e.g. (*Z*)-*para*-methoxybenzaldehyde oxime: δ_{H} 7.25 vs. (*E*)-*para*-methoxybenzaldehyde: δ_{H} = 8.06²⁴⁴). Furthermore, the (*E*) geometry of salicylaldoximes is thermodynamically favored through the formation of intramolecular, hydrogen-bonded, six-membered rings between the phenol OH and the oxime N lone pair.²⁴⁵



Entry	Substrate	Product	Yield ^b (%)	Entry	Substrate	Product	Yield ^b (%)
1			93	8			87
2			95	9			85
3			92	10			89
4			90	11			92
5			87	12			97
6			94				
7			93				

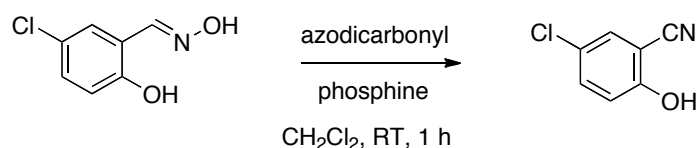
Table 5.2: Salicylaldoxime substrate scope.^a

^aThe salicylonitrile (0.5 mmol, 1 equiv.) and PPh_3 (1.25 mmol, 2.5 equiv.) were dissolved/suspended in CH_2Cl_2 (0.07 M) at RT under an inert (N_2) atmosphere. After 5 min, DIAD (1.25 mmol, 2.5 equiv.) was added dropwise. If not already so, the reaction became homogeneous within 30 s. The reaction was stirred until complete (30-90 min (TLC)); ^bisolated yield.

Mitsunobu reactions were performed using optimized conditions of 2.5 equiv of each of PPh_3 and DIAD in CH_2Cl_2 (0.07 M) at RT. Although CH_3CN provided a slightly higher yield of **3** (Table 5.1, entry 10), we elected to use CH_2Cl_2 as the reaction solvent since this would facilitate the work-up procedure. Some salicylaldoximes were not

completely soluble in CH₂Cl₂ (although all were in CH₃CN) but upon adding DIAD the reactions became homogeneous. In order to purify salicylonitriles **3**, we exploited their acidities ($pK_a \leq 7$). Upon completion (TLC; in all but one case, reactions were complete within 1 h at RT), each reaction mixture was subjected to a basic work-up (0.1 M NaOH), then the basic aqueous layer containing only the salicylonitrile was acidified with 1M HCl and re-extracted into CH₂Cl₂, avoiding the often-laborious column chromatography that is associated with Mitsunobu reactions. Electron-poor, electron-rich and electron-neutral salicylaldoximes were compatible with the reaction conditions and a range of functional groups was tolerated to afford excellent yields of the target salicylonitriles **3**. It should be noted that for entry 5, the work-up protocol was modified slightly to avoid saponification of the methyl ester: extraction into the aqueous layer was accomplished with 1M K₂CO₃ in lieu of 0.1 M NaOH.

In the event that a basic work-up of the target salicylonitrile is precluded due to sensitive functionality elsewhere in the molecule, silica gel flash column chromatography may be conducted. Conveniently, water-soluble azodicarbonyl species (ADDM = azodicarbonyl dimorpholide (both oxidized and reduced forms may be extracted readily into water;²⁴⁶ DMEAD = dimethoxyethylazodicarboxylate (the reduced form DMEAD-H₂ is removed readily into water²⁴⁷)) may be employed along with PPh₃ on resin with no detriment to the yield (**Table 5.3**).



Entry	Azodicarbonyl	Phosphine	Yield ^b (%)
1	DIAD	PPh ₃	95
2	ADDM	PPh ₃	95
3	DMEAD	PS-PPh ₃	94
4	ADDM	PS-PPh ₃	97

Table 5.3: Alternative azodicarbonyl and phosphine species.^a

^aThe salicylonitrile (0.5 mmol, 1 equiv.) and phosphine (1.25 mmol, 2.5 equiv.) were gently stirred in CH₂Cl₂ (0.07 M) at RT under an inert (N₂) atmosphere. After 5 min, the azodicarbonyl agent (1.25 mmol, 2.5 equiv.) was added at once; ^bisolated yield.

5.2 Conclusions

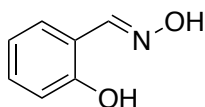
In conclusion, we have introduced a mild, swift and efficient technique to generate salicylonitriles from salicylaloximes using Mitsunobu chemistry. The transformation proceeds through the corresponding 1,2-benzisoxazole intermediates, which undergo the Kemp elimination *in situ*. The chemistry is general, proving effective with electron neutral, electron-rich and electron-poor salicylonitriles, and is compatible with a range of functional groups. Owing to their acidities (pK_as around 7 and below), the salicylonitriles may be isolated by simple acid-base work-ups, circumventing the need for column chromatography that often plagues Mitsunobu reactions. It is anticipated that the chemistry described herein will be readily adopted as the preferable means by which to synthesize salicylonitriles, given that DIAD and PPh₃ are cheap chemicals, and the purification protocol is fast, cost-effective and simple. In addition to their roles in the construction of

more complex chemical species, salicylonitriles may function as bioisosteres of carboxylic acids, and this is an active area of research within our laboratory.

5.3 Experimental

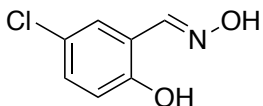
5.3.1 Chemistry

General. Anhydrous solvents were purchased and used as supplied. All reactions were conducted using oven-dried glassware and under an inert (N_2) atmosphere. Reactions were monitored by thin layer chromatography (TLC), visualizing with a UV lamp (254 nm) and $KMnO_4$ stain. Reactions purified by flash column chromatography were carried out with Merck 60 Å silica gel (230-400 mesh). NMR spectra were performed on a 400 MHz NMR spectrometer. Spectra were calibrated to residual solvent peaks: $CDCl_3$ (δ_H , 7.26; δ_C 77.21) and d_6 -DMSO (δ_H 2.50; δ_C 39.51). Coupling constants are expressed in Hz, and splitting patterns are denoted as follows: s, singlet; d, doublet; dd, doublet of doublets; m, multiplet. Melting points are uncorrected.



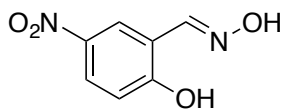
Salicylaldoxime synthesis. To a solution of the aldehyde (5 mmol) in EtOH (35 mL) was added $NH_2OH.HCl$ (25 mmol) and pyridine (10 mmol). The reaction mixture was heated at 60 °C for 3 h. TLC confirmed the reaction was complete. The reaction mixture was concentrated to *ca.* 10 mL, then partitioned between EtOAc (150 mL) and 1M HCl (50 mL). The EtOAc layer was washed again with 1M HCl (50 mL), water (2 x 50 mL), brine

(50 mL), dried (Na_2SO_4), filtered and concentrated to provide the oxime, which required no further purification. NOTE: Basic oxime **1h** was partitioned between EtOAc and water, with the EtOAc layer repeatedly (x5) washed with water to extract all of the pyridine.



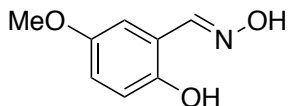
(*E*)-5-Chloro-2-hydroxybenzaldehyde oxime (**1a**).²⁴⁸ Yield = 832 mg, 97%; white solid.

Spectral data consistent with published data.



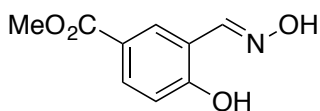
(*E*)-5-Nitro-2-hydroxybenzaldehyde oxime (**1b**).²⁴⁹ Yield = 892 mg, 98%; yellow solid.

Spectral data consistent with published data.

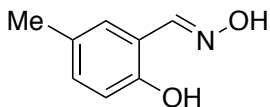


(*E*)-5-Methoxy-2-hydroxybenzaldehyde oxime (**1c**).²⁵⁰ Yield = 828 mg, 99%; white solid.

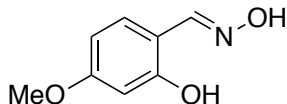
Spectral data consistent with published data.



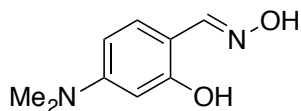
(*E*)-Methyl 4-hydroxy-3-((hydroxyimino)methyl)benzoate (**1d**) General procedure was modified: methyl 3-formyl-4-hydroxybenzoate (1.5 mmol), NH₂OH.HCl (1.2 eq), pyridine (1.5 eq) were stirred in MeOH (15 mL) overnight at room temperature. The reaction mixture was concentrated to *ca.* 5 mL then worked-up as per the general procedure. Yield = 278 mg, 95%; off-white solid; mp = 160–163 °C; IR (neat, cm⁻¹) 3337; ¹H NMR (400 MHz, d₆-DMSO) δ 11.46 (s, 1H) 10.92 (s, 1H), 8.36 (s, 1H), 8.17 (d, *J* = 1.6 Hz, 1H), 7.82 (dd, *J*₁ = 7.6 Hz, *J*₂ = 1.6 Hz, 1H), 6.98 (d, *J* = 8.4 Hz, 1H), 3.81 (s, 1H); ¹³C NMR (100 MHz, d₆-DMSO) δ 166.1, 160.3, 146.3, 132.0, 129.4, 121.2, 119.1, 116.7, 52.3; MS (ESI) *m/z* Calcd for C₉H₉NO₄ (M⁺): 195.1, Found: 196.2 (M+H⁺); Anal. Calcd for C₉H₉NO₄: C, 55.39; H, 4.65; N, 7.18. Found: C, 55.61; H, 4.57; N, 6.93.



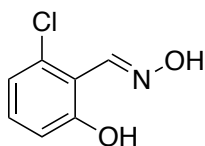
(*E*)-5-Methyl-2-hydroxybenzaldehyde oxime (**1e**).²⁵⁰ Yield = 726 mg, 95%; white solid. Spectral data consistent with published data.



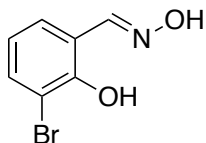
(*E*)-2-Hydroxy-4-methoxybenzaldehyde oxime (**1f**).²⁵¹ Yield = 819 mg, 98%; white solid. Spectral data consistent with published data.



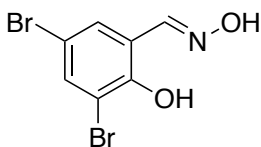
(E)-4-(Dimethylamino)-2-hydroxybenzaldehyde oxime (**1g**). Yield = 828 mg, 92%; light brown solid; mp = 150–154 °C; IR (neat, cm^{-1}) 3410; ^1H NMR (400 MHz, d_6 -DMSO) δ 10.83 (s, 1H), 10.05 (s, 1H), 8.17 (s, 1H), 7.18 (d, $J = 8.8$ Hz, 1H), 6.26 (dd, $J_1 = 8.8$ Hz, $J_2 = 1.6$ Hz, 1H), 6.14 (d, $J = 1.6$ Hz, 1H), 2.90 (s, 3H); ^{13}C NMR (100 MHz, d_6 -DMSO) δ 157.7, 152.1, 149.4, 129.8, 106.4, 104.2, 98.4, 39.7 (obsc); MS (ESI) m/z Calcd for $\text{C}_9\text{H}_{12}\text{N}_2\text{O}_2$ (M^+): 180.1, Found: 181.2 ($\text{M}+\text{H}^+$); Anal. Calcd for $\text{C}_9\text{H}_{12}\text{N}_2\text{O}_2$: C, 59.99; H, 6.71; N, 15.55. Found: C, 60.21; H, 6.76; N, 15.28.



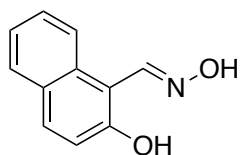
(E)-2-Chloro-6-hydroxybenzaldehyde oxime (**1h**). Yield = 838 mg, 98%; white solid; mp = 154–158 °C; IR (neat, cm^{-1}) 3347; ^1H NMR (400 MHz, d_6 -DMSO) δ 11.98 (s, 1H), 10.89 (s, 1H), 8.54 (s, 1H), 7.23 (t, $J = 8.2$ Hz, 1H), 6.97 (d, $J = 7.6$ Hz, 1H), 6.89 (d, $J = 8.8$ Hz, 1H); ^{13}C NMR (100 MHz, d_6 -DMSO) δ 158.2, 147.3, 132.7, 131.2, 120.5, 115.5, 114.7; MS (ESI) m/z Calcd for $\text{C}_7\text{H}_6\text{ClNO}_2$ (M^+): 171.0, Found: 172.1 ($\text{M}+\text{H}^+$); Anal. Calcd for $\text{C}_7\text{H}_6\text{ClNO}_2$: C, 49.00; H, 3.52; N, 8.16. Found: C, 49.26; H, 3.50; N, 7.91.



(E)-3-Bromo-2-hydroxybenzaldehyde oxime (**1i**).²⁵² Yield = 1.06 g, 99%; white solid; mp = 170–174 °C; IR (neat, cm⁻¹) 3407; ¹H NMR (400 MHz, d₆-DMSO); δ 11.79 (s, 1H), 10.93 (s, 1H), 8.41 (s, 1H), 7.55 (d, *J* = 7.2 Hz, 1H), 7.43 (d, *J* = 7.6 Hz, 1H), 6.86 (t, *J* = 7.8 Hz, 1H); ¹³C NMR (100 MHz, d₆-DMSO) δ 153.0, 149.9, 133.6, 129.3, 120.9, 119.1, 109.8; MS (ESI) *m/z* Calcd for C₇H₆BrNO₂ (M⁺): 215.0, Found: 216.1 (M+H⁺).



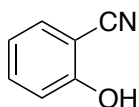
(E)-3,5-Dibromo-2-hydroxybenzaldehyde oxime (**1j**) Yield = 1.39 g, 95%; pinkish-grey solid; mp >200 °C; IR (neat, cm⁻¹) 3397; ¹H NMR (400 MHz, d₆-DMSO) δ 11.95 (s, 1H), 11.01 (s, 1H), 8.38 (s, 1H), 7.74 (d, *J* = 2.4 Hz, 1H), 7.65 (d, *J* = 2.4 Hz, 1H); ¹³C NMR (100 MHz, d₆-DMSO) δ 152.4, 148.5, 134.9, 131.1, 120.8, 111.1, 110.8; MS (ESI) *m/z* Calcd for C₇H₅Br₂NO₂ (M⁺): 292.9, Found: 293.9 (M+H⁺); Anal. Calcd for C₇H₅Br₂NO₂: C, 28.51; H, 1.71; N, 4.75. Found: C, 28.53; H, 1.49; N, 4.65.



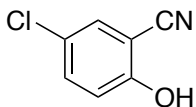
E-2-Hydroxy-1-naphthaldehyde oxime (**1k**).²⁵³ Yield = 916 mg, 98%; peach solid; mp = 160–164 °C; IR (neat, cm⁻¹) 3311; ¹H NMR (400 MHz, d₆-DMSO) δ 11.57 (s, 1H), 11.18 (s, 1H), 9.09 (s, 1H), 8.47 (d, *J* = 8.8 Hz, 1H), 7.85–7.82 (m, 2H), 7.50 (t, *J* = 7.6 Hz, 1H),

7.35 (t, $J = 7.4$ Hz), 7.21 (d, $J = 9.6$ Hz); ^{13}C NMR (100 MHz, d_6 -DMSO) δ 156.1, 147.6, 131.6, 131.4, 128.6, 127.4, 123.3, 122.6, 118.3, 108.6; MS (ESI) m/z Calcd for $\text{C}_{11}\text{H}_9\text{NO}_2$ (M^+): 187.1, Found: 188.2 ($\text{M}+\text{H}^+$).

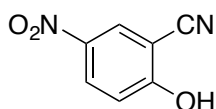
Salicylonitrile synthesis. To a solution of the appropriate salicylaldehyde (0.5 mmol, 1 eq) and PPh_3 (1.25 mmol, 2.5 eq) in anhydrous CH_2Cl_2 (7 mL) was added DIAD (1.25 mmol, 2.5 eq) dropwise at rt (if the salicylaldehyde was not already dissolved, the reaction became homogenous upon addition of DIAD). The reaction was stirred at rt under an inert atmosphere until completion (TLC). The reaction mixture was partitioned between further CH_2Cl_2 (100 mL) and 0.1N NaOH (50 mL). The aqueous layer was washed with CH_2Cl_2 (3 x 50 mL), then acidified with 1N HCl (10 mL). The acidic aqueous was then extracted into CH_2Cl_2 (2 x 50 mL). These organic extractions were combined, dried (Na_2SO_4), filtered and concentrated to provide the salicylonitrile, which needed no further purification.



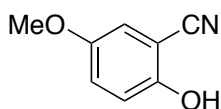
Salicylonitrile (3). Yield = 55 mg, 93%; white solid; mp = 96–99 °C; IR (neat, cm^{-1}) 3268, 2228; ^1H NMR (400 MHz, d_6 -DMSO) δ 11.05 (s, 1H), 7.57 (d, $J = 6.4$ Hz, 1H), 7.48 (t, $J = 7.4$ Hz, 1H), 7.01 (d, $J = 7.6$ Hz, 1H), 6.92 (t, $J = 7.4$ Hz, 1H); ^{13}C NMR (100 MHz, d_6 -DMSO) δ 160.2, 134.8, 133.3, 119.6, 117.1, 116.2, 98.9; MS (ESI) m/z Calcd for $\text{C}_7\text{H}_5\text{NO}$ (M^+): 119.0, Found: 142.0 ($\text{M}+\text{Na}^+$).



5-Chloro-2-hydroxybenzonitrile (3a).²⁴⁸ Yield = 73 mg, 95%; white solid; mp = 167–179 °C. IR (neat, cm^{-1}) 3230, 2239; ^1H NMR (400 MHz, d_6 -DMSO): d 11.38 (s, 1H), 7.73 (d, $J = 2.4$ Hz, 1H), 7.52 (dd, $J_1 = 8.8$ Hz, $J_2 = 2.4$ Hz, 1H), 7.01 (d, $J = 8.8$ Hz, 1H); ^{13}C NMR (100 MHz, d_6 -DMSO) δ 159.3, 134.6, 132.2, 122.7, 117.9, 115.7, 100.3; MS (ESI) m/z Calcd for $\text{C}_7\text{H}_4\text{ClNO}$ (M^+): 153.0, Found: 154.0 ($\text{M}+\text{H}^+$).

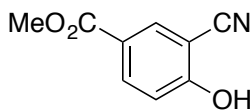


5-Nitro-2-hydroxybenzonitrile (3b).²⁴² Yield = 75 mg, 92%; pale yellow solid; mp >200 °C; IR (neat, cm^{-1}) 3144, 2254; ^1H NMR (400 MHz, d_6 -DMSO) δ 12.72 (bs, 1H), 8.59 (d, $J = 2.8$ Hz, 1H), 8.35 (dd, $J_1 = 9.4$ Hz, $J_2 = 2.6$ Hz, 1H), 7.16 (d, $J = 8.8$ Hz, 1H); ^{13}C NMR (100 MHz, d_6 -DMSO) δ 165.6, 139.3, 130.3, 130.1, 116.8, 115.1, 99.7; MS (ESI) m/z Calcd for $\text{C}_7\text{H}_4\text{N}_2\text{O}_3$ (M^+): 164.0, Found: 163.1 ($\text{M}-\text{H}^+$).

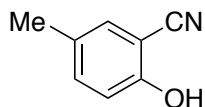


2-Hydroxy-5-methoxybenzonitrile (3c).²⁵⁴ Yield = 67 mg, 90%; white solid; mp = 133–136 °C; IR (neat, cm^{-1}) 3283, 2230; ^1H NMR (400 MHz, d_6 -DMSO) δ 10.53 (s, 1H), 7.15 (d, $J = 2.4$ Hz), 7.10 (dd, $J_1 = 9.6$ Hz, $J_2 = 3.2$ Hz, 1H), 6.93 (d, $J = 9.2$ Hz, 1H), 3.70 (s, 1H); ^{13}C NMR (100 MHz, d_6 -DMSO) δ 154.8, 152.2, 122.6, 117.8, 117.4, 116.3, 98.9, 56.2;

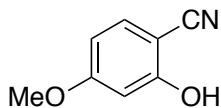
MS (ESI) m/z Calcd for $C_8H_7NO_2$ (M^+): 149.1, Found: 172.2 ($M+Na^+$).



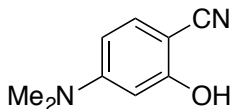
Methyl 3-cyano-4-hydroxybenzoate (3d).²⁵⁵ Extraction of the product into the aqueous layer was accomplished using 1 M K_2CO_3 in place of 0.1 M NaOH. NOTE: Care should be taken when the aqueous layer is acidified due to substantial effervescence. Yield = 77 mg, 87%; white solid; mp = 198–202 °C; IR (neat, cm^{-1}) 3154, 2249; 1H NMR (400 MHz, d_6 -DMSO) δ 12.08 (s, 1H), 8.12 (d, $J = 1.6$ Hz, 1H), 8.03 (dd, $J_1 = 9.6$ Hz, $J_2 = 2.4$ Hz, 1H), 7.10 (d, $J = 8.8$ Hz, 1H), 3.81 (s, 1H); ^{13}C NMR (100 MHz, d_6 -DMSO) δ 165.1, 164.4, 136.0, 135.4, 121.4, 116.9, 116.4, 99.8, 52.6 MS (ESI) m/z Calcd for $C_9H_7NO_3$ (M^+): 177.0, Found: 178.1 ($M+H^+$).



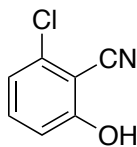
2-Hydroxy-5-methylbenzonitrile (3e).²⁵⁶ Yield = 63 mg, 94%; white solid; mp = 100–103 °C; IR (neat, cm^{-1}) 3241, 2233; 1H NMR (400 MHz, d_6 -DMSO) δ 10.76 (s, 1H), 7.37 (s, 1H), 7.28 (d, $J = 8.8$ Hz, 1H), 6.90 (d, $J = 8.4$ Hz, 1H), 2.20 (s, 1H); ^{13}C NMR (100 MHz, d_6 -DMSO) δ 158.0, 135.4, 132.7, 128.5, 117.1, 116.0, 98.4, 19.5; MS (ESI) m/z Calcd for C_8H_7NO (M^+): 133.1, Found: 156.1 ($M+Na^+$).



2-Hydroxy-4-methoxybenzonitrile (3f).²⁵⁷ Yield = 69 mg, 93%; white solid; mp = 176–179 °C; IR (neat, cm⁻¹) 3217, 2226; ¹H NMR (400 MHz, d₆-DMSO) δ 11.04 (s, 1H), 7.50 (d, *J* = 8.8 Hz, 1H), 6.53–6.50 (m, 2H), 3.76 (s, 1H); ¹³C NMR (100 MHz, d₆-DMSO) δ 164.0, 161.8, 134.4, 117.4, 106.7, 101.0, 91.2, 55.5; MS (ESI) *m/z* Calcd for C₈H₇NO₂ (M⁺): 149.1, Found: 150.1 (M+H⁺).

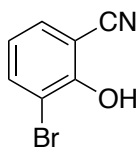


4-(Dimethylamino)-2-hydroxybenzonitrile (3g). Extraction of the product from the basic aqueous was accomplished through careful neutralization of the aqueous layer with 1M HCl, then mild acidification with saturated NH₄Cl. Yield = 71 mg, 87%; grey-brown solid; mp = 157–162 °C; IR (neat, cm⁻¹) 3217, 2207; ¹H NMR (400 MHz, d₆-DMSO) δ 10.49 (s, 1H), 7.28 (d, *J* = 8.8 Hz, 1H), 6.25 (dd, *J*₁ = 9.2 Hz, *J*₂ = 2.4 Hz, 1H), 6.14 (d, *J* = 1.6 Hz), 2.93 (s, 6H); ¹³C NMR (100 MHz, d₆-DMSO) δ 161.5, 154.5, 133.9, 119.1, 104.7, 97.8, 85.4, 39.9 (obsc); MS (ESI) *m/z* Calcd for C₉H₁₀N₂O (M⁺): 162.1, Found: 163.2 (M+H⁺). Anal. Calcd for C₉H₁₀N₂O: C, 66.65; H, 6.21; N, 17.27. Found: C, 66.17; H, 6.27; N, 16.88.

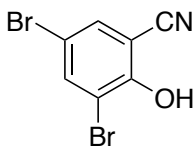


6-Chloro-2-hydroxybenzonitrile (3h).²⁵⁸ Yield = 65 mg, 85%; white solid; mp = 163–165 °C; IR (neat, cm⁻¹) 3247, 2242; ¹H NMR (400 MHz, d₆-DMSO); δ 11.65 (s, 1H), 7.49 (t,

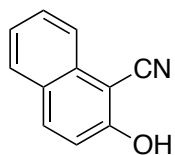
$J = 8.2$ Hz, 1H), 7.09 (d, $J = 8$ Hz, 1H), 6.98 (d, $J = 8.4$ Hz, 1H); ^{13}C NMR (100 MHz, $\text{d}_6\text{-DMSO}$) δ 162.0, 135.6, 135.3, 120.0, 114.9, 114.2, 100.0; MS (ESI) m/z Calcd for $\text{C}_7\text{H}_4\text{ClNO}$ (M^+): 153.0, Found: 176.1 ($\text{M}+\text{Na}^+$).



3-Bromo-2-hydroxybenzonitrile (3i).²⁴⁰ Yield = 88 mg, 89%; pale orange solid; mp = 119–123 °C; IR (neat, cm^{-1}) 3271, 2234; ^1H NMR (400 MHz, $\text{d}_6\text{-DMSO}$) δ 11.05 (bs, 1H), 7.84 (dd, $J_1 = 9.6$ Hz, $J_2 = 1.6$ Hz, 1H), 7.66 (dd, $J_1 = 8$ Hz, $J_2 = 1.6$ Hz, 1H), 6.93 (t, $J = 7.8$ Hz, 1H); ^{13}C NMR (100 MHz, $\text{d}_6\text{-DMSO}$) δ 156.2, 138.1, 132.9, 121.8, 116.2, 112.0, 102.3; MS (ESI) m/z Calcd for $\text{C}_7\text{H}_4\text{BrNO}$ (M^+): 197.0, Found: 220.1 ($\text{M}+\text{Na}^+$).



3,5-Dibromo-2-hydroxybenzonitrile (3j) Yield = 126 mg, 92%; white solid; mp = 172–176 °C; IR (neat, cm^{-1}) 3281, 2239; ^1H NMR (400 MHz, $\text{d}_6\text{-DMSO}$) δ 11.44 (bs, 1H), 8.07 (s, 1H), 7.94 (s, 1H); ^{13}C NMR (100 MHz, $\text{d}_6\text{-DMSO}$) δ 156.1, 139.9, 134.9, 115.1, 113.5, 111.2, 103.9; MS (ESI) m/z Calcd for $\text{C}_7\text{H}_3\text{Br}_2\text{NO}$ (M^+): 274.9, Found: 276.0 ($\text{M}+\text{H}^+$); Anal. Calcd for $\text{C}_7\text{H}_3\text{Br}_2\text{NO}$: C, 30.36; H, 1.09; N, 5.06. Found: C, 30.42; H, 0.91; N, 4.97.



2-Hydroxy-1-naphthonitrile (3k).²³⁴ Yield = 82 mg, 97%; white solid; mp = 156–159 °C; IR (neat, cm⁻¹) 3408, 2223; ¹H NMR (400 MHz, d₆-DMSO) δ 11.65 (s, 1H), 8.07, (d, *J* = 9.6 Hz, 1H) 7.92 (d, *J* = 8 Hz, 1H), 7.86 (d, *J* = 8.4 Hz, 1H), 7.65 (t, *J* = 7.6 Hz, 1H), 7.44 (t, *J* = 7.4 Hz, 1H), 7.28 (d, *J* = 9.6 Hz, 1H); ¹³C NMR (100 MHz, d₆-DMSO) δ 161.3, 135.1, 133.0, 129.1, 128.8, 127.0, 124.4, 122.7, 117.7, 116.0, 91.2; MS (ESI) *m/z* Calcd for C₁₁H₇NO (M⁺): 169.1, Found: 192.2 (M+Na⁺).

Acknowledgement

Reproduced with permission from *E. Whiting, M.E. Lanning, J.A. Scheenstra, and S. Fletcher. The Journal of Organic Chemistry, 2015, 80, 1229-1234. Copyright © 2015 American Chemical Society. Published by the American Chemical Society. All rights Reserved,*

Chapter 6 Ongoing and Future Synthetic α -Helix and BH3 Mimetics

6.1 Ongoing and Future Small Molecule BH3 Mimetics

6.1.1 Design Strategy for Acyl-sulfonamides based on a Naphthoic Acid Core

As previously described, we took inspiration from Fesik's³³ and Abbvie's⁶² work using fragment-based drug design to advance the MCL-1 field by discovering potent inhibitors. We merged part of each molecule to create a novel scaffold with low nanomolar inhibition based a 1-hydroxy-2-naphthoic acid scaffold.⁶⁴ While this scaffold afforded potent *in vitro* data, cell killing activity was several orders of magnitude worse, only in the low μ M range. We attributed this to the charged carboxylic acid unable to permeate the cell membrane, and therefore we made analogs of pro-drugs to circumvent this issue.

However, *in lieu* of using pro-drugs Fesik and colleagues published data on 2-indole-acylsulfonamides¹³⁰ as a follow up to their 2013 work.³³ They showed that by introducing an acyl-sulfonamides in place of a carboxylic acid, which added extra functionality to their molecules, they achieved picomolar inhibition *in vitro* with selectivity over BCL-x_L over 500 fold.¹³⁰ Abbvie has described an especially potent MCL-1 inhibitor (K_i : 0.454 nM) and stated that sub-nanomolar potencies *in vitro* are necessary to ensure on target activity in cellular assays.¹²⁷ With this new insight into requirements to target MCL-1 we developed a new strategy using our existing scaffold.

Therefore, our current work looks to increase affinities and selectivities towards MCL-1 *in vitro*, which we hypothesize will translate into improved cell activities. Nikolovska-Coleska and co-workers utilized a similar scaffold and achieved selectivity toward MCL-1.⁶⁵ We propose on the other hand to use our 1-hydroxy-2-naphthoic acid

scaffold, which presently is predicted to bind only the p2 pocket and Arg263 as a starting place and build into the p4 pocket. From the previously generated SILCS data (**Figure 6.1**) the carboxylic acid is in a perfect position to bridge into the p4 pocket. As seen, there is a hydrophobic FragMap in the p4 pocket that will accommodate an aryl or alkyl group. We chose to use acylsulfonamides, like several other research groups, which would provide a synthetic handle to link the p2 and p4 pocket, but retain the acidic functionality since the pKa of the sulfonamide is around 5.^{60, 127, 130, 259} The expansion into the p4 pocket gives the benefit of increasing potency in our molecules, by targeting more than the p2 pocket. While it is believed the p2 pocket dictates selectivity, the p4 pocket promotes greater affinity.

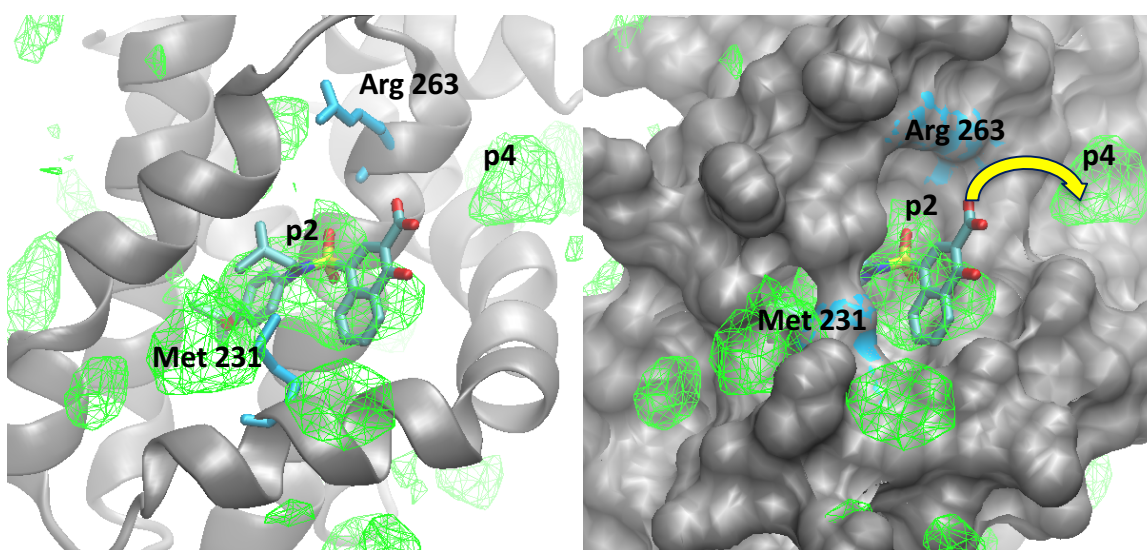


Figure 6.1: SILCS modeling of MCL-1 and compound **3ba** (blue). FragMaps (green) indicate areas of general hydrophobicity. Arg263 and Met231 are highlighted (cyan) to orient protein and show key interactions. PDBID: 4HW4.

The molecules chosen were based on our previously described library (**Chapter 2**) and therefore we chose 2 potent compounds and one that was newly synthesized (**Figure 6.2**). The parent molecules of **7b** and **7c** in **Figure 6.2A** have $K_i = 487$ nM and 31 nM respectively. We hypothesize that by adding the R³ groups will increase our affinity and

potency, which should translate into cell activity based on the work by Fesik, Abbvie, and Amgen.^{127-128, 130} The two examples for acyl sulfonamides (**Figure 6.2B**) were chosen based on their ability to reach the p4 pocket and that they have been widely used (left Nikolovska-Coleska, and Fesik, right Souers, Elmore et al.).^{33, 65, 94, 130-131, 133} This will yield the best chance to increase our potency to sub-nanomolar affinity.

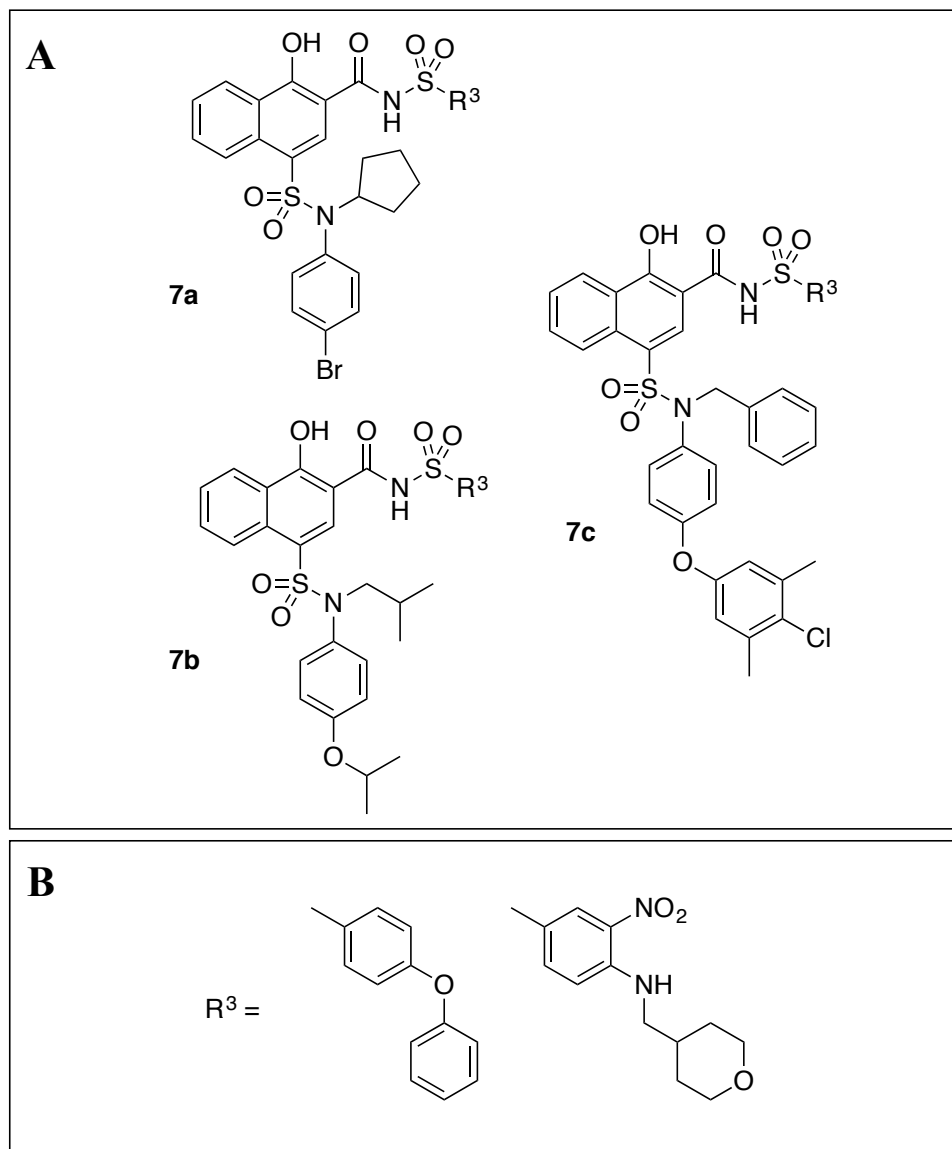


Figure 6.2: (A) Example of scaffolds being taken forward based on K_i from Chapter 2. (B) Example of acyl sulfonamide groups to target p4 pocket. (Right, sulfonamide Nikolovska-Coleska and co-workers utilized. Left, sulfonamide used by Abbvie in the development of ABT-199)^{65, 94}

6.1.2 Synthesis of Acyl-Sulfonamides

To furnish molecule **7** the synthesis from our first generation naphthoates has expanded to a six-step synthesis. As previously stated, 1-hydroxy-2-naphthoic acid (**1**) was chloro-sulfonylated at the 4 position to afford 4-sulfamoyl-1-hydroxy-2-naphthoic acid (**2**). Various anilines or secondary amines were coupled to **2** to furnish the parent compounds **3**. The parent compounds were bis-benzylated and subsequently the benzyl ester was saponified to yield compound **5**. Once the acid was exposed, multiple sulfonamides were coupled using EDCI and DMAP to generate the corresponding 1-hydroxy-protected acyl sulfonamides **6**. Finally, the 1-hydroxyl position was revealed to give the final compound **7**.

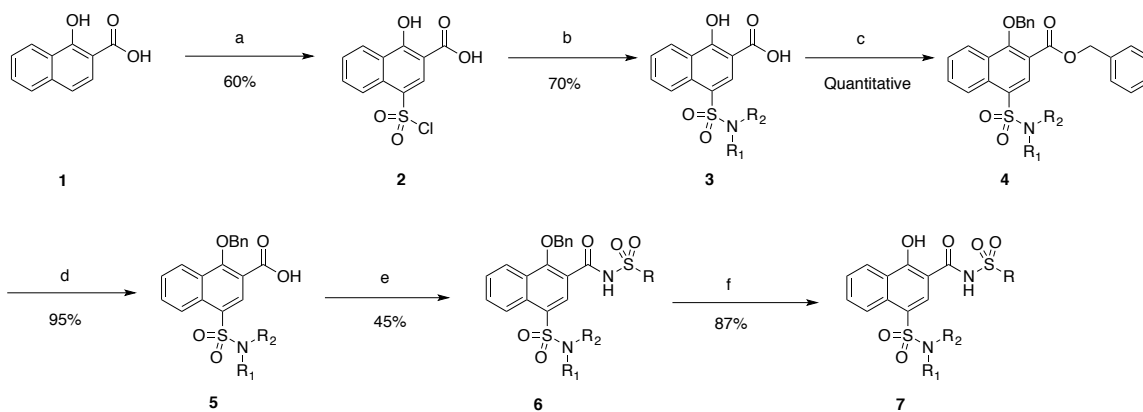


Figure 6.3: Synthetic scheme to acquire acyl-sulfonamides. (a) $ClSO_3H$, 0 °C, 30 min; (b) R_1NH_2/R_1R_2NH , pyridine, Acetone, 50 °C, o.n.; (c) $BnBr$; K_2CO_3 , DMF, 60 °C, o.n.; (d) $NaOH$, THF/ H_2O , 60 °C, o.n.; (e) RSO_2NH_2 , EDCI, DMAP, CH_2Cl_2 , rt, o.n.; (f) CH_2Cl_2/TFA , rt, 3d

To couple the acyl sulfonamide to the acid several conditions were tried and tested until the aforementioned conditions were found. First, we tried using isobutyl chloroformate and *N*-methylmorpholine (NMM) at -10 °C to activate our acid before adding in the sulfonamide and sodium hydride (NaH) and allowing the reaction to stir

overnight. Under these conditions, we were able to activate the acid, but the sulfonamide did not couple. After isolating what was thought to be the product it was confirmed that it was the activated acid, however all of the sulfonamide had apparently been consumed (TLC). Next we tried the coupling using EDCI.HCl, and DMAP at room temperature, overnight. Our first attempt, gave us a small amount of product, however after adjusting the equivalents used, we isolated the acyl sulfonamide product.

6.1.3 Future Directions

From what is proposed currently, this project is in early developmental stages. I would design one or two more acyl sulfonamides to use and then ask the CADD Center to model the requisite compounds to determine the best compounds to move forward with the synthesis. I think that the derivative based on compound **3bl** will be the most potent compound once the sulfonamides are coupled because of the nature of the p2 pocket^{33, 130}, which requires large hydrophobic groups for binding as in **3bl**. The p4 pocket has a hydrophobic FragMap to target, and if the original scaffold is not hydrophobic enough, I would predict the binding mode to flip depending on the sulfonamide used.

6.2 Ongoing and Future Synthetic α -Helix Mimetics

6.2.1 Design of Second-Generation Purines

There are several strategies to disrupt PPIs, such as structure or fragment-based drug design (**Chapter 1**), within these strategies there are sub-strategies: small molecule BH3 mimetics and synthetic α -helix mimetics.^{33, 59, 64, 76} The structure-based design of small molecule BH3 and synthetic α -helix mimetics are strategies our lab employs on the

BCL-2 family of proteins. In **Chapter 3**, we reported on a 2,6,9-tri-substituted purine scaffold that disrupts the Bak–MCL-1 protein–protein interaction with low μM inhibition.⁵⁹ When we designed our second-generation molecules, a SAR was performed to determine what was necessary from the scaffold and what could be modified; two scaffolds were taken forward as leads. The first retains the purine core, however, the 2N-Boc group was replaced with substituted phenylpiperazines (**Figure 6.4**). In an effort to increase the hydrophobic van der Waals interactions within the binding pocket and to increase the number of side chains mimicked, phenylpiperazines were used. In the hydrophobic pocket, our compounds could interact with Leu253, Leu 249, Met231, Phe228, and the carboxylic acid can interact with Arg263. Depending on what moiety is at the R¹ position, interactions with Phe270 in the p2 pocket will occur.

From a Gold docking simulation as mentioned in **Chapter 3**, the 9H substituent of the purine scaffold bound to the p2 pocket of MCL-1 and the N2 substituent bound in the p3 pocket (**Figure 3.5**, page 138). We hypothesized that this binding orientation occurred due to the large hydrophobic nature of the 9H and N2 moieties. To invert the binding mode; i.e. 9H bound towards the p4 pocket and N2 binds in the p2-p3 pocket we created a library of 2-substituted 6-chloro-2-(piperazin-1-yl)-9H-purine. As formerly reported, the Boc group is a poor mimetic of Leu78, but was utilized for rapid access to the library of compounds.⁵⁹ Replacing the Boc group with substituted piperazines allows for better access to the binding pocket of MCL-1 and more extensive mimicry of the Bak-BH3 helix and allow interaction with Leu 253, Leu 249, and Met231 in particular.

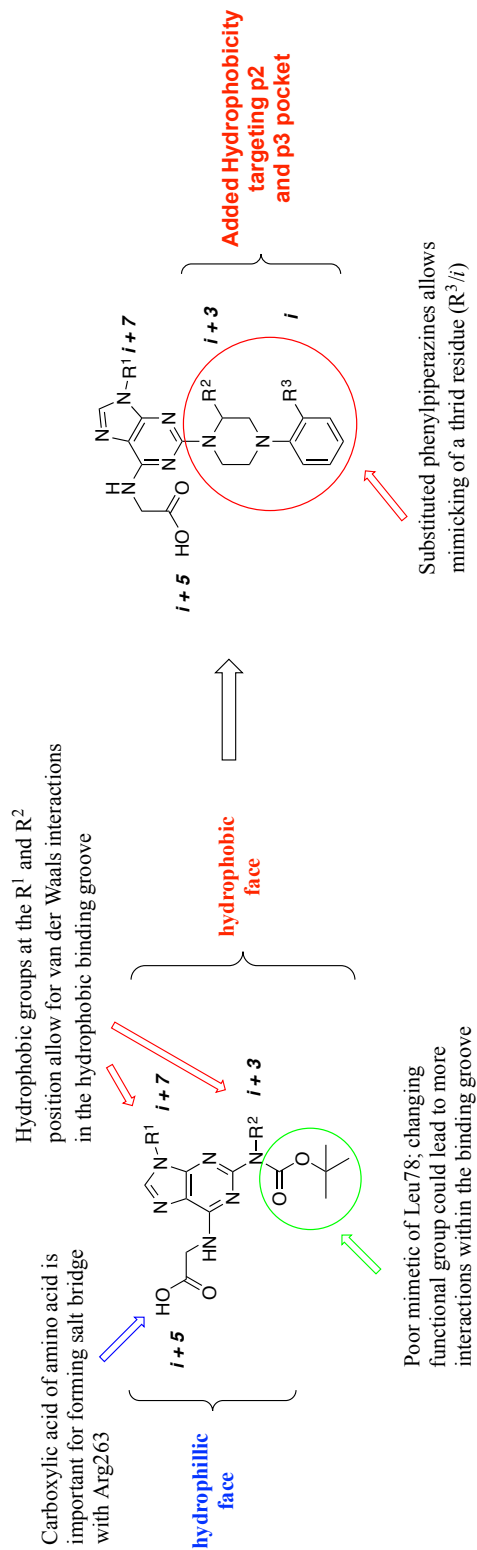


Figure 6.4: Schematic of moving from original purine scaffold to the second-generation purine scaffold utilizing substituted piperazines.

6.2.2 Synthesis of Purines

Final second-generation purine molecules were obtained in a short 4 step synthesis starting with 2,6-dichloropurine (**8**) which was alkylated by aryl-bromides. The products obtained were a mixture of N7 and N9 alkylation products. The two molecules were easily separated by thin layer chromatography (TLC) and were isolated using flash chromatography on a Biotage Isolera 1 in Hexanes/EtOAc 4:1. The N9 product eluted first and confirmed by NMR. Previous work from Fletcher and colleagues yielded a crystal structure of the N9 substituted product, which correlated to the NMR obtained.²⁰⁸ We compared our chemical shifts of the N9 and N7 products to the N9 chemical shifts obtained by Fletcher et al.^{79, 208} The N9 product (**9**) underwent a regioselective S_NAr at the 6-chloro position with glycine tert-butyl ester in n-BuOH at 60°C to give **10**. The subsequent S_NAr at the 2 position with substituted piperazines used different conditions to get the reaction to go to completion. Pyridine was used as the solvent, K₂CO₃ as the base at 180°C in a pressure vial furnished compound **11**. Deprotection of the tert-butyl ester revealed the carboxylic acid to yield the final molecule **12**.

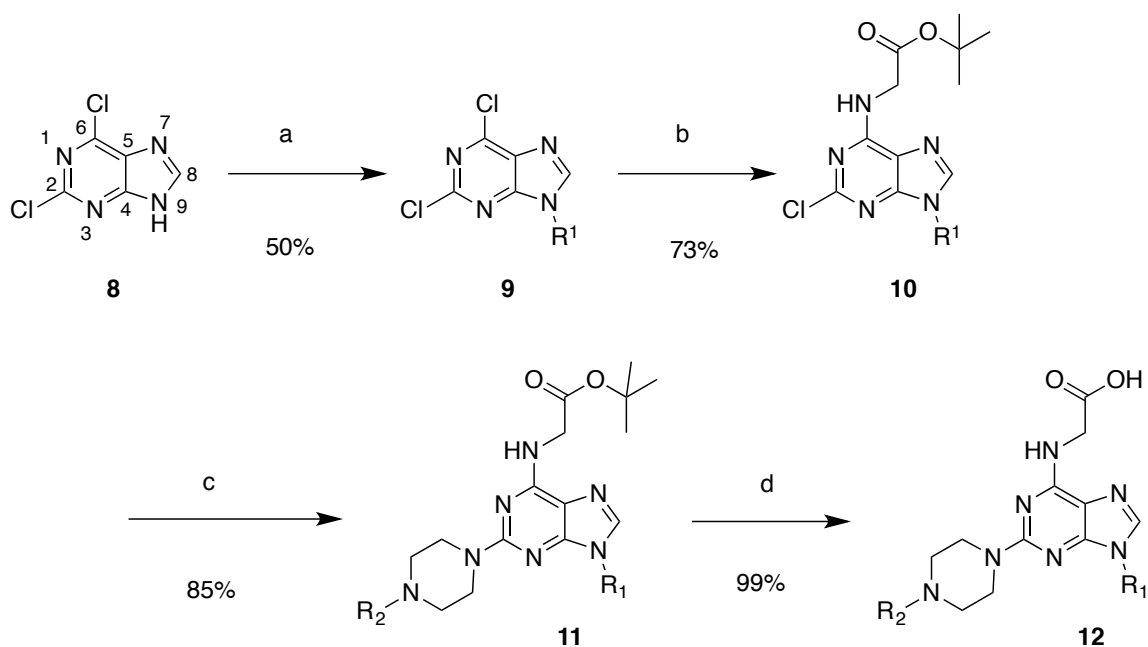


Figure 6.5: Synthesis of di-substituted (2-(piperazin-1-yl)-9H-purin-6-yl)glycine (a) Aryl-Br, K_2CO_3 , DMF, rt, 16 h; (b) *t*-Butyl glycine, K_2CO_3 , *n*-BuOH, 60°C, 12 h; (c) 1-substituted piperazines, K_2CO_3 , pyridine, 180°C, 18 h; (d) TFA/ CH_2Cl_2 , rt, 3 h.

6.2.3 Results and Discussion

To determine if our molecules would bind the MCL-1 protein, the SILCS method¹⁶⁴⁻¹⁶⁷ was used. As previously mentioned, SILCS FragMaps represent the 3D free energy functional group requirements for the numerous types of functional groups in and around the protein.⁶⁴ The FragMaps included contributions from solute-protein interactions and both solute and protein desolvation in the context of protein flexibility.¹⁶⁵⁻¹⁶⁶ In addition, to ensure that all regions accessible to solute atoms could be occupied by the studied ligands, the protein surface was defined based on SILCS exclusion maps.¹⁶⁸ Notably, the information content of SILCS may be used to qualitatively direct ligand design as well as to rapidly make quantitative estimates of relative ligand affinities.¹⁶⁶

Based on the molecular modeling simulations (**Figure 6.6**) for our purine based core second generation molecules, they bind anti-parallel to the first-generation molecules

described in **Chapter 3**, which was in accordance with the original design idea.⁵⁹ In **Figure 6.6B** the SILCS exclusion maps denote the flexibility of the protein, and clearly indicates the molecule interacting in the p1 and p2 pocket. While the binding pattern is not in the pockets we hypothesized (i.e. p2 and p4), the binding orientation with the substituted-piperazine pointing towards the p1 and “R¹” in the p2 pocket correlates to our original binding hypothesis in **Chapter 3**. With molecules binding the p1 and p2 pockets, the p4 pocket is open to expand into for future work.

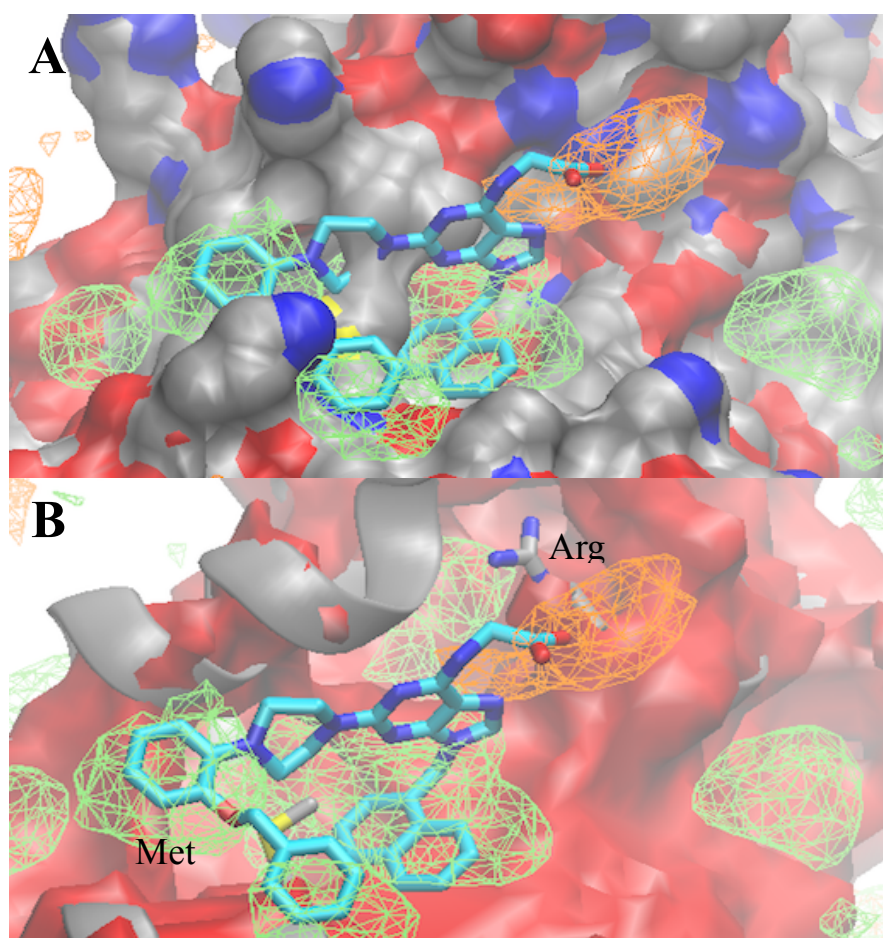
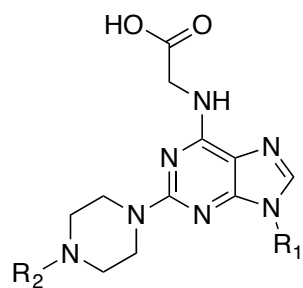


Figure 6.6: SILCS Molecular Modeling renderings of the binding orientation of compound 8. *A:* Surface representation of MCL-1 (silver) and compound 8 binding to the p2 and p1 pockets (cyan) *B:* Exclusion FragMap indicating protein flexibility around compound 8 FragMaps: Green represent general hydrophobic residues, Orange represents the functional group acetic acid. Silver represents carbon atoms, blue: nitrogens, and red: oxygens.

Our library of molecules were evaluated in the fluorescence polarization competition assay (FPCA). A FITC labeled Bak peptide was utilized to compete off of MCL-1. From the data collected, our molecules improved over 10-fold from our previously published data in **Chapter 3**. Compounds **1** and **2** had no affinity for MCL-1, although though for compound **2** this could be due to the benzyl group not reaching deep enough in the p2 pocket and the rigidity of the phenyl piperazine compared to the flexibility of subsequent compounds (**Table 6.1**). Compound **3** had a K_i of 10.5 μM , which could be due to the benzyl group not interacting to the degree that the naphthyl group interacts in the p2 pocket. Compound **6**, **7**, **8** have relatively similar K_i 's 1.3, 1.8, and 1.6 μM respectively. The improvement on the binding affinity of the naphthyl derivatives could be due to deep p2 pocket interaction and extension into the p1 pocket that our previous molecules did not make. Compound **6** has a slightly better K_i than **7** and **8**, and this could be due to the placement of the 4-bromo moiety on the 4-bromobenzene sulfonyl group that can reach further into the p1 pocket vs the 3-bromo moiety on compound **7**. The 2- Benzoxypyphenyl in compound **8** makes additional interactions with the p1 pocket that compounds **6** and **7** are unable to make.

Table 6.1: *Experimental FPCA data for second generation purines based on a 2,6-dichloropurine scaffold. K_i values determined by Nikolovska-Coleska equation from IC_{50} values.¹⁷⁰ Data represent the average of at least two independent assays; errors are standard deviations. NA, no activity.*



Compound	R ₁	R ₂	Mcl-1 K _i (μM)
1			NA
2			NA
3			10.5 ± 3.24
4			1.3 ± 0.19
5			NA
6			1.3 ± 0.15
7			1.8 ± 0.16
8			1.6 ± 0.14

6.2.4 Future Directions

Moving this project forward there are several things I would do to improve potency towards MCL-1 to get into the picomolar range. For the purine based scaffold, I would extend into the p4 pocket because as seen from the SILCS images, there is a lot of hydrophobic interactions, His265, Leu261, and Leu216, that are not being utilized. To reach the p4 pocket, synthesizing acyl sulfonamides or amides would allow for the Arg 263 interaction while bridging the gap to the p4 pocket. To maximize contacts with p1 pocket I would consider merging scaffolds, i.e, synthesis a 2-Benzoxo-4-bromophenylpiperazine with the naphthyl at the R¹ position.

Ultimately, for all future work, not just this project, obtaining crystal structures of how our lead binds MCL-1 or any of the anti-apoptotic proteins will be essential for future structure-based design. Having experimental data that can support our hypotheses and the molecular modeling data will definitively show us where we can modify our molecules to improve potency and affinity.

6.2.5 Design of Pyrrolopyrimidines

The other lead scaffold, based on a 4-chloro-7H-pyrrolopyrimidine, moves away from the polar core (**Figure 6.7**) towards a scaffold that may be better accommodated by the hydrophobic BH3-binding groove. The difference in clogP's goes from -0.22 for the purine core to a clogP of 0.41 for pyrrolopyrimidine. The 7N was removed from the purine scaffold to better abide to Lipinski's Rule of Five²⁶⁰, where the clogP of our molecules will be below five to increase chances of being cell permeable and orally bioavailable, the molecular weight of our proof of concept molecule is around 500 g/mol, it has less than 5

hydrogen bond donors and 10 hydrogen bond acceptors.²⁶⁰ Our previous work using a purine core were designed to bind the p2 and p4 pocket, but our molecules bound mostly in the p2 pocket according to molecular modeling.⁵⁹

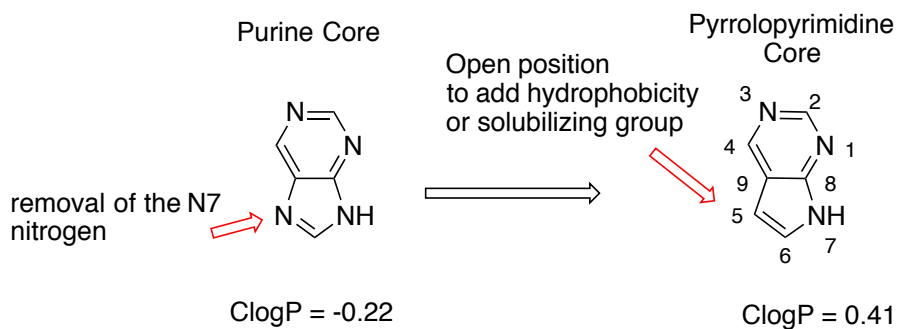


Figure 6.7: Transforming the purine core to a pyrrolopyrimidine core.

As previously mentioned in **Chapter 1**, a collaboration between Servier Laboratories and the University of Melbourne discovered a MCL-1 selective inhibitor; the lead molecule based on a thienopyrimidine core through a NMR fragment-based screen.⁶³ After a thorough SAR and x-ray crystallography, they determined, their best molecule bound MCL-1 in all four pockets; most notably deep in the p2, and high into the p4 pocket⁶³ (**Figure 6.8**). In cells, their compound bound with $<1\mu\text{M}$ to MM cell lines, chronic myeloid leukemia (CML), AML, and were potent in xenograft AML models.⁶³

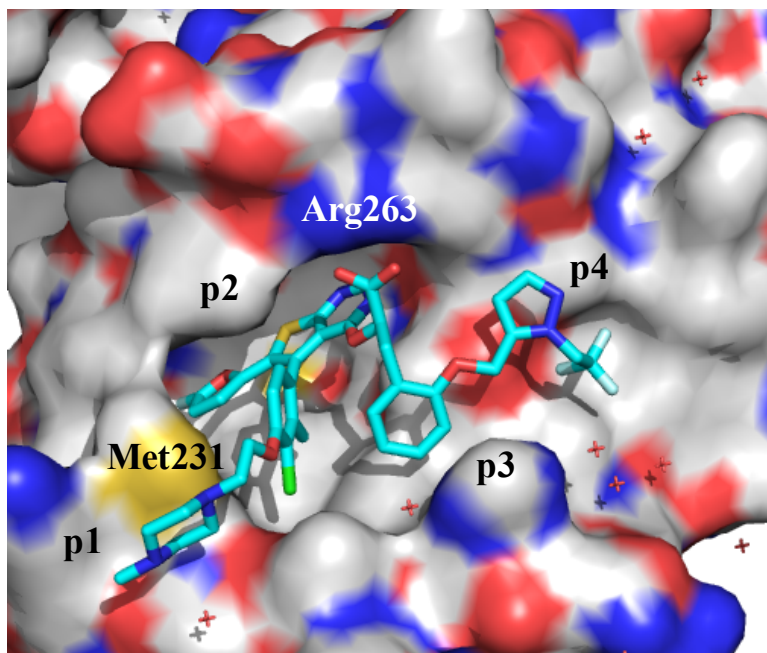


Figure 6.8: Servier Research Laboratories S63845 (cyan) molecule bound into MCL-1 (white = carbon, blue = basic, red = acid) PDBID: 5LOF.

To permit our molecules to reach both pockets, the p2, p4 and bind Arg263, we substituted the 4, 5, and 7 positions. (**Figure 6.9**). Based on how Servier's molecule bound the MCL-1 binding groove, we hypothesized that this substitution pattern would replicate the binding pattern of Servier's S63845 molecule.⁶³ Using substituted aryl groups at the 5 position connected to a solubilizing linker allows access to the p3 ledge and the hydrophobic p4 pocket. Functionalizing the 4 position will allow Arg263 to form a salt-bridge from the hydrophobic (aryl) amino acids. Finally, the 7H position will be functionalized with small hydrophobic (alkyl) groups to increase the van der Waals interactions.

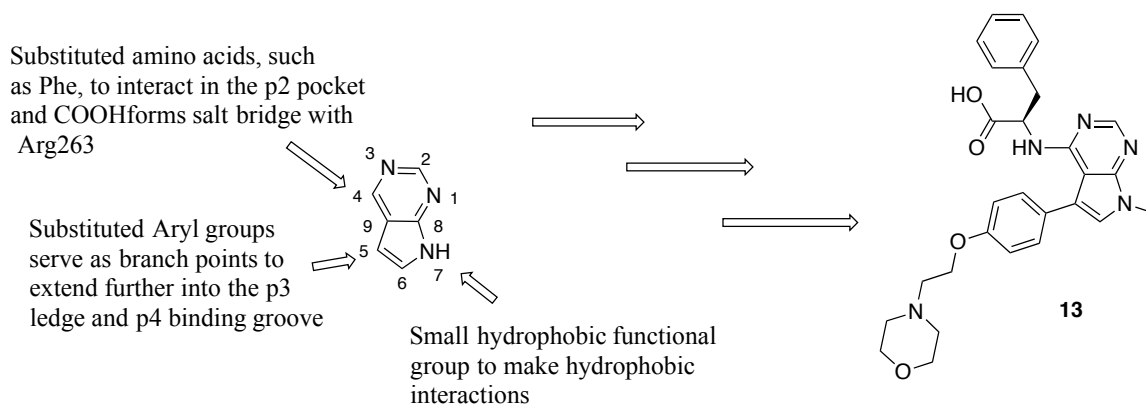


Figure 6.9: Schematic functionalizing pyrrolopyrimidine molecule at the 4, 5, and 7 positions to bind into the MCL-1 hydrophobic groove (left). Fully functionalized proof of concept scaffold (right).

To determine how our proof of concept molecule (**13**) will bind into MCL-1 initial docking studies using GOLD was used. An energy minimized structure using ChemDraw 3D was input into the GOLD docking simulations using 4HW2 protein and then the solutions were visualized in PYMol. To obtain the GOLD (Genetic Optimization for Ligand Docking) simulations, molecule **13** from ChemDraw was energy minimized using ChemDraw3D. Then the molecule was opened in ArgusLab to optimize the most favorable geometry. Protein 4HW2 (docking ready) with the natural ligand removed was loaded into Hermes and all hydrogen atoms were added. The binding site was defined by constraining the ligand to Arg263 in a 10 Å radius. The proof of concept ligand (**13**) was loaded into GOLD and the ligand flexibility and GA were set. The GA was set to maximum because only one ligand was being utilized. Finally, the GOLD simulation ran using 25 simulations.

Two of the highest docking solutions can be visualized in **Figure 6.10**. Compared to S63845 binding interaction with MCL-1 **Figure 6.10B** binds in a similar orientation. However, the compound in **Figure 6.10A** binds slightly differently with the pyrrolopyrimidine core binding in the upper p2 pocket and the Phe amino acid binding

deep in the p2 pocket with the morpholine moiety in the p4 pocket.

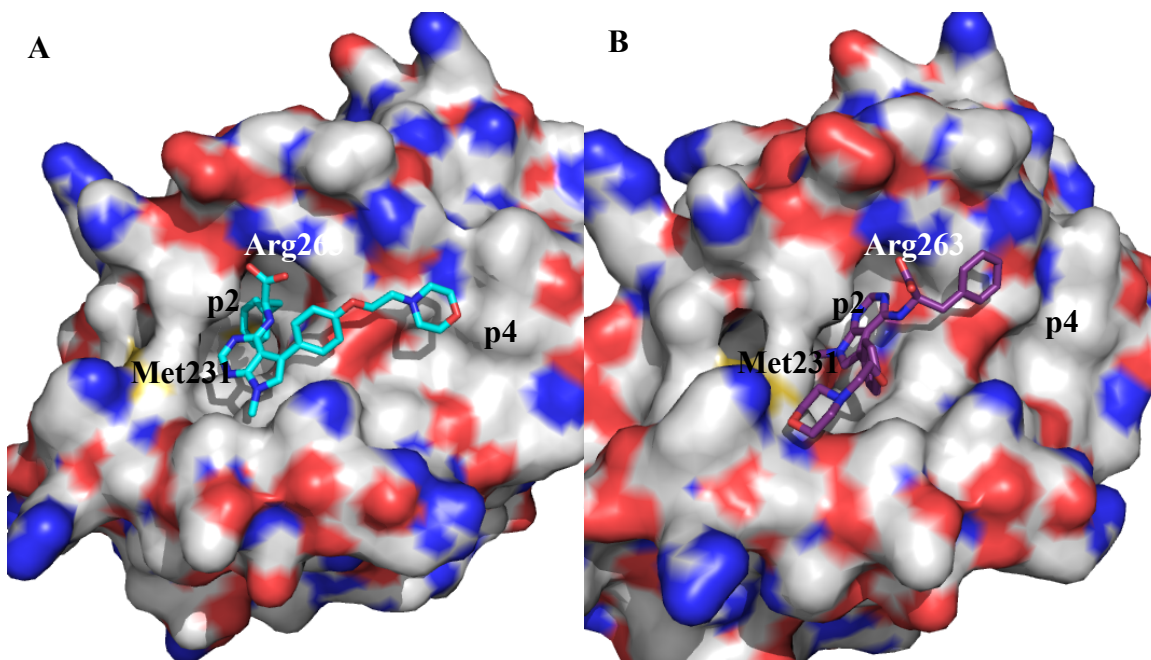


Figure 6.10: (A) MCL-1 bound to proof of concept molecule with one of the higher scoring Gold docking solutions. The acid connected to the 4C position interacts with Arg263 and the morpholine moiety extends into the p4 pocket. (B) Another higher scoring solution with the 7N pointing into the p2 pocket, the Phe acid forming a salt bridge with Arg263. PDBID: 4HW2. Molecule constrained to Arg263 in a 10Å radius.

6.2.6 Synthesis of Pyrrolopyrimidines

The tri-substituted pyrrolopyrimidines were achieved in a short 5 step synthesis. 4-Chloro-7H-pyrrolo{2,3-d}-pyrimidine was reacted in an electrophilic aromatic substitution (S_EAr) with *N*-Iodosuccinimide to furnish 4-chloro-5-iodo-7H-pyrrolopyrimidine (**15**). Compound **15** was directly alkylated using small alkyl groups or benzylic groups to yield **16**. Next, an S_NAr at the C4 position allows installation of protected hydrophobic amino acids to give **17**. Then 4-hydroxyboronic acid was coupled through a Suzuki reaction giving **18**. The 4-hydroxy on the phenyl ring was next alkylated using a two-carbon linker attached to a solubilizing group giving compound **19**. Finally, a saponification of **19** gave **20**, revealing the acid.

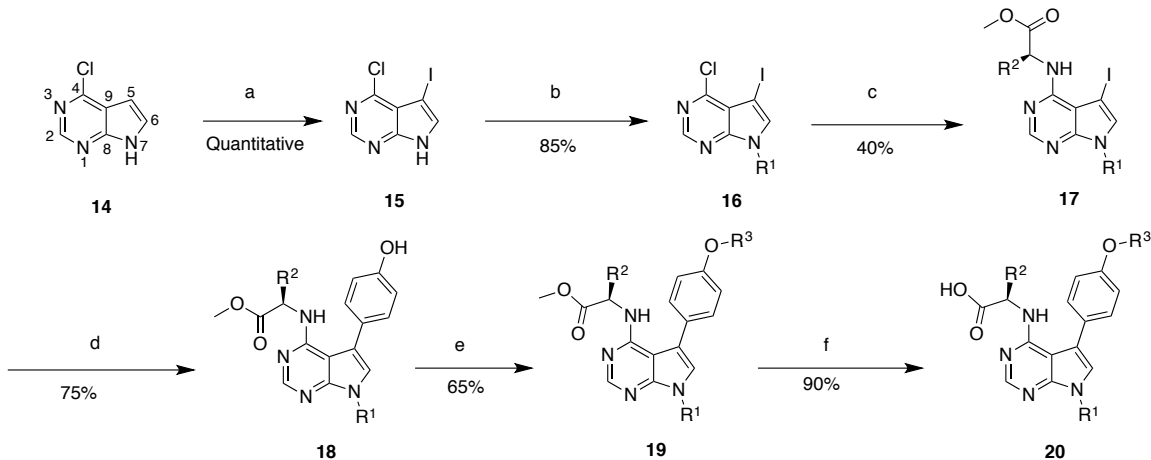


Figure 6.11: Synthesis of tri-substituted pyrrolopyrimidine: (a) NIS, DMF, rt, 16 h; (b) alkylation, K_2CO_3 , DMF, rt, 16 h; (c) protected amino acid, Et_3N , EtOH, DABCO 100°C, 2d; (d) Suzuki: 4-substituted-phenylboronic acid, CsF, tetrakis, DME/MeOH, 80°C, 18 h; (e) alkylation, K_2CO_3 , DMF, rt, 16 h; (f) $LiOH \cdot H_2O$, THF/MeOH/ H_2O , rt, 1-2 h.

After extensive discussion, it was decided that the R^1 position should be small or benzylic hydrophobic groups (i.e Me, or $CH_2(\text{Het-})\text{Ar}$) so as not to alter the position of the core in the binding pocket. The R^2 groups were selected from hydrophobic side chains of naturally occurring amino acids and finally the R^3 groups off the phenoxy were alkyl linkers ending with a solubilizing moiety (i.e. herein, morpholine).

6.2.7 Future Directions

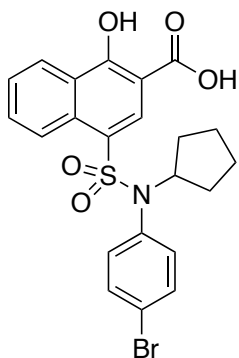
The pyrrolopyrimidines are still in early stages of development and a small library should be synthesized based on the proof-of-concept molecule. After designing a small library, I would utilize the CADD Center, specifically MD combined with SILCS to determine the optimal binding mode of these compounds. With the MD/SILCS data, functionalizing the scaffold will be easily visualized to see what can be accommodated by

the protein and what should be modified. After synthesis of the compounds they should be tested against the BCL-2 family to test for selectivity and affinity for the family. At this point, once the experimental data has been analyzed a determination about how to move forward can be made.

6.3 Experimental

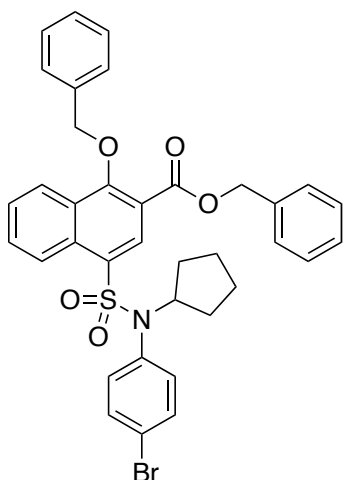
6.3.1 Chemistry

General. Anhydrous solvents were purchased and used as supplied. All reactions were conducted using oven-dried glassware and under an inert (N_2) atmosphere. Reactions were monitored by thin layer chromatography (TLC), visualizing with a UV lamp (254 nm) and $KMnO_4$ stain. Reactions purified by flash column chromatography were carried out with Merck 60 Å silica gel (230-400 mesh). NMR spectra were performed on a 400 MHz NMR spectrometer. Spectra were calibrated to residual solvent peaks: $CDCl_3$ (δ_H , 7.26; δ_C 77.21) and d_6 -DMSO (δ_H 2.50; δ_C 39.51). Coupling constants are expressed in Hz, and splitting patterns are denoted as follows: s, singlet; d, doublet; dd, doublet of doublets; m, multiplet.



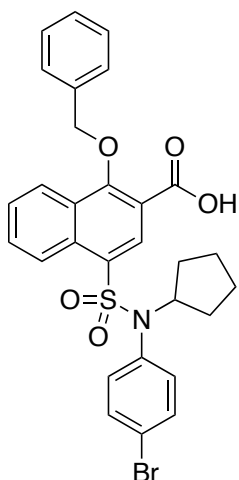
MEL-5-038 – 4-(*N*-(4-bromophenyl)-*N*-cyclopentylsulfamoyl)-1-hydroxy-2-naphthoic acid (**3a**).

4-Chlorosulfonyl-1-hydroxy-2-naphthoic acid (**2**) was coupled to 4-bromo-*N*-cyclopentylaniline according to general procedure A from **Chapter 2** on a 7 mmol scale to yield the title compound as a dark grey solid (2.3g, 64%): δ_{H} (400 MHz, d_6 -DMSO) δ_{H} 8.43 (dd, 2H, Ar, $J = 8.4$ Hz), 8.28 (s, 1H, Ar), 7.89 (t, 1H, Ar, $J = 7.8$ Hz), 7.74 (t, 1H, Ar, $J = 7.8$ Hz), 7.54 (d, 2H, Ar, $J = 8$ Hz), 6.93 (d, 2H, Ar, $J = 8$ Hz), 4.56-4.48 (m, 1H, $\text{NCH}(\text{CH}_2)_2$), 1.73-1.72 (m, 2H), 1.40-1.20 (m, 6H); δ_{C} (100 MHz, d_6 -DMSO) 172.1, 165.7, 135.0, 134.5, 132.5, 131.9, 131.5, 127.3, 125.7, 125.1, 124.7, 123.6, 122.4, 105.5, 60.0, 30.2, 22.5.



MEL-5-039 – *Benzyl 1-(benzyloxy)-4-(N-(4-bromophenyl)-N-cyclopentylsulfamoyl)-2-naphthoate (4a)*.

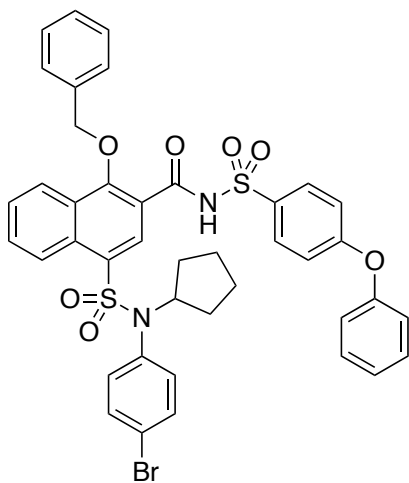
Compound (**3a**, 4 mmol, 1 eq) was dissolved in Acetone (0.3M) and K_2CO_3 (12 mmol, 3 eq) was added. Lastly, benzyl bromide (12 mmol, 3 eq) was added dropwise over 10 min. The reaction stirred at reflux overnight and TLCd the next day in 4:1 Hex/EtOAc. Upon completion, the acetone was concentrated to dryness and then taken up in di- H_2O (100 mL). The solution was partitioned with EtOAc (50 mL x 3). The organics were collected and washed with brine, then dried with Na_2SO_4 , filtered, and concentrated. The crude product was purified by flash column chromatography in 4:1 Hex/EtOAc, concentrated to give the title compound as a beige solid (93% yield): (δ_H (400 MHz, $CDCl_3$) δ_H 8.58 (d, 1H, Ar, $J = 8.4$ Hz), 8.56 (s, 1H, Ar), 8.32 (d, 2H, Ar, $J = 8.8$ Hz), 7.71 (t, 1H, Ar, $J = 7.8$ Hz), 7.60 (t, 1H, Ar, $J = 7.4$ Hz), 7.44-7.35 (m, 12H, Ar), 6.89 (d, 2H, Ar, $J = 8.8$ Hz), 5.40 (s, 2H, CH_2 Benzylic), 5.17 (s, 2H, CH_2 Benzylic), 4.65-4.57 (m, 1H, $NCH(CH_2)_2$), 1.83-1.81 (m, 2H), 1.57-1.40 (m, 4H), 1.31-1.26 (m, 2H); δ_C (100 MHz, d_6 -DMSO) 159.8, 156.3, 131.4, 130.7, 129.6, 129.3, 127.4, 127.3, 126.7, 125.7, 125.4, 125.0, 123.9, 123.8, 123.7, 123.5, 122.6, 120.7, 120.0, 118.1, 112.9, 73.6, 62.6, 55.6, 39.5, 25.4, 17.5.



MEL-5-041 – *1-(benzyloxy)-4-(N-(4-bromophenyl)-N-cyclopentylsulfamoyl)-2-naphthoic acid (5a)*

Compound (**4a**, 1.3 mmol, 1 eq, 850 mg) was dissolved in a mixture of THF/H₂O (3:1 mixture, 0.1M) and NaOH (5.1 mmol, 4 eq, 203 mg) was added. The reaction mixture stirred at 60°C for 2 d. The reaction was TLCd in CH₂Cl₂/MeOH/AcOH (92:7:1) to ensure completion. The reaction was quenched with H₂O (50 mL) and partitioned with EtOAc (25 mL x 3). The organics were collected and washed with brine, dried with Na₂SO₄, filtered, and concentrated. Crude product was columned by gravity chromatography using CH₂Cl₂/MeOH/AcOH (92:7:1). Product was collected, concentrated, and azeotroped (x4). Concentrate yielded title compound as a white solid in quantitative yield (736 mg): δ_{H} (400 MHz, *d*₆-DMSO) δ_{H} 13.59 (s, 1H, COOH), 8.47 (d, 1H, Ar, *J* = 8.8 Hz), 8.38 (s, 1H, Ar), 8.32 (d, 1H, Ar, *J* = 8 Hz), 7.87 (t, 1H, Ar, *J* = 7.4 Hz), 7.75 (t, 1H, Ar, *J* = 7.8 Hz), 7.56-7.52 (m, 4H, Ar), 7.44-7.38 (m, 3H, Ar) , 6.93 (d, 2H, Ar, *J* = 7.6 Hz), 5.27 (s, 2H, CH₂ Benzylic), 4.57-4.54 (m, 1H, NCH(CH₂)₂), 1.74 (m, 2H, CH(CH₂CH₂)₂), 1.44-1.21 (m, 6H, CH(CH₂CH₂)₂), δ_{C} (100 MHz, *d*₆-DMSO) 159.8, 156.3, 131.4, 130.7, 129.6,

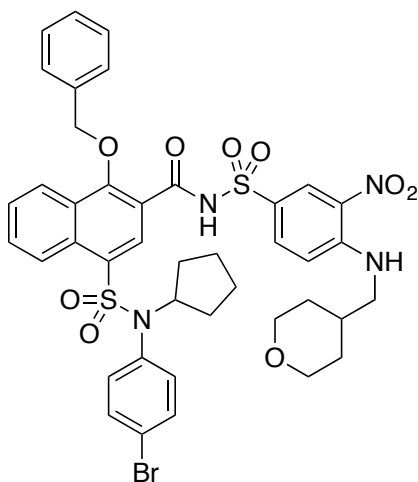
129.3, 127.4, 127.3, 126.7, 125.7, 125.4, 125.0, 123.9, 123.8, 123.7, 123.5, 122.6, 120.7, 120.0, 118.1, 112.9, 73.6, 62.6, 55.6, 39.5, 25.4, 17.5.



MEL-5-053 - *1-(benzyloxy)-4-(N-(4-bromophenyl)-N-cyclopentylsulfamoyl)-N-((4-phenoxyphenyl)sulfonyl)-2-naphthamide (6a)*

Compound (**5a**, 1 mmol, 1 eq, 600 mg) was dissolved in anhydrous CH₂Cl₂. EDCI·HCl (1.5 mmol, 1.5 eq, 300 mg) and requisite acyl sulfonamide (1.2 mmol, 1.2 eq, 310 mg) were added. Lastly, DMAP (2 mmol, 2 eq, 210 mg) was added and the reaction was allowed to stir at rt overnight. To ensure completion, the reaction was TLCd next day in CH₂Cl₂/MeOH/AcOH (92:7:1). The reaction was quenched with di-H₂O (60 mL) and partitioned with CH₂Cl₂ (40 mL). Organics were collected and washed with brine, dried with Na₂SO₄, filtered and concentrated. Crude product was columned by gravity chromatography using CH₂Cl₂/MeOH/AcOH (92:7:1). Product was collected, concentrated, and azeotroped (x4). Concentrate yielded title compound as a light pink solid (536 mg, 64%): δ_H (400 MHz, CDCl₃) δ_H 10.34 (s, 1H, NH), 8.66 (s, 1H, Ar), 8.57 (d, 1H, Ar, *J* = 8 Hz), 8.30 (d, 1H, Ar, *J* = 7.6 Hz), 8.01 (d, 2H, Ar, *J* = 8 Hz), 7.76-7.69 (m,

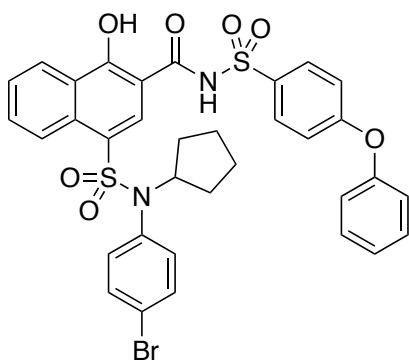
2H, Ar), 7.47-7.39 (m, 9H, Ar), 7.24 (s, 1H, Ar), 7.08 (d, 2H, Ar, $J = 8$ Hz), 7.02 (d, 2H, Ar, $J = 8.4$ Hz), 6.94 (d, 2H, Ar, $J = 8$ Hz), 5.21 (s, 2H, $\text{CH}_2(\text{CH})_2$), 4.55-4.51 (m, 1H, $\text{CH}(\text{CH}_2)_2$), 1.83 (s, 2H, CHCH_2CH_2), 1.45 (m, 4H, xxx), 1.27 (s, 2H, xxx); δ_{C} (100 MHz, CDCl_3) 162.9, 161.0, 158.8, 154.6, 134.2, 134.0, 133.6, 132.9, 132.2, 131.5, 131.1, 130.8, 130.7, 130.2, 129.7, 129.2, 128.9, 128.4, 128.1, 126.2, 125.3, 124.2, 123.0, 120.6, 119.1, 117.1, 80.3, 60.5, 30.1, 29.7, 22.3.



MEL-5-054 - 1-(benzyloxy)-4-(((4-bromophenyl)(cyclopentyl)amino)thio)-N-((3-nitro-4-(((tetrahydro-2H-pyran-4-yl)methyl)amino)phenyl)sulfonyl)-2-naphthamide (**6b**).

Compound (**5b**, 1 mmol, 1 eq, 600 mg) was dissolved in anhydrous CH_2Cl_2 . EDCI·HCl (1.5 mmol, 1.5 eq, 300 mg) and requisite acyl sulfonamide (1.2 mmol, 1.2 eq, 310 mg) were added. Lastly, DMAP (2 mmol, 2 eq, 210 mg) was added and the reaction was allowed to stir at rt overnight. To ensure completion, the reaction was TLCd next day in $\text{CH}_2\text{Cl}_2/\text{MeOH}/\text{AcOH}$ (92:7:1). The reaction was quenched with di- H_2O (60 mL) and partitioned with CH_2Cl_2 (40 mL). Organics were collected and washed with brine, dried with Na_2SO_4 , filtered and concentrated. Crude product was columned by gravity

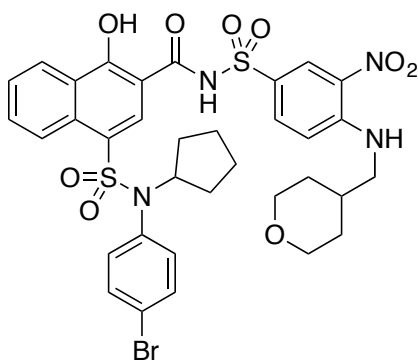
chromatography using CH₂Cl₂/MeOH/AcOH (92:7:1). Product was collected, concentrated, and azeotroped (x4). Concentrate yielded title compound as a light yellow solid (536 mg, 64%): δ_{H} (400 MHz, CDCl₃) δ_{H} 10.35 (s, 1H, NH), 8.84 (s, 1H, Ar), 8.65 (s, 1H, Ar), 8.57 (d, 2H, Ar, $J = 6.4$ Hz), 8.32 (d, 1H, Ar, $J = 8$ Hz), 8.15 (d, 1H, Ar, $J = 9.6$ Hz), 7.78-7.71 (m, 2H, Ar), 7.49 (s, 5H, Ar), 7.39 (d, 1H, Ar, $J = 7.6$ Hz), 6.94 (t, 3H, Ar, $J = 7.8$ Hz), 5.23 (s, 2H, CH₂(CH)₂), 4.55-4.52 (m, 1H, CH Cp), 4.03 (d, 2H, NHCH(CH₂)₂ Cy, $J = 7.6$ Hz), 1.83 (s, 4H, CH(CH₂CH₂)₂ Cp), 1.6 (s, 4H, CH(CH₂CH₂)₂ Cp), 1.46-1.26 (m, 8H, -(CH₂)₂-O--(CH₂)₂CH-).



MEL-5-055 - 4-(((4-bromophenyl)(cyclopentyl)amino)thio)-1-hydroxy-N-((3-nitro-4-phenoxyphenyl)sulfonyl)-2-naphthamide (7a).

Compound (**6a**, .1 mmol, 1 eq, 81 mg) was dissolved in a 1:1 mixture of TFA/Toluene (1 mL: 1 mL). The reaction mixture stirred for 3 d at room temperature. TLCd to ensure completion in CH₂Cl₂/MeOH/AcOH (92:7:1). Solvent was concentrated and then taken up in 1 M HCl (30 mL) and partitioned with EtOAc (15 mL). Organics were combined and washed with brine, then dried with Na₂SO₄, filtered and concentrated to give the title compound as a light purple solid in quantitative yield (72 mg): δ_{H} (400 MHz, *d*₆-DMSO) δ_{H} 13.13 (s, 1H, OH)8.40 (s, 2H, Ar), 8.29 (d, 1H, Ar, $J = 8.8$ Hz), 7.96 (d, 2H, Ar, $J = 8.8$

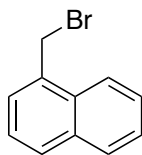
Hz), 7.75 (t, 1H, Ar, $J = 7.4$ Hz), 7.61 (t, 2H, Ar, $J = 7.4$ Hz), 7.53 (d, 2H, Ar, $J = 8$ Hz), 7.45 (t, 2H, Ar, $J = 7.6$ Hz), 7.25 (d, 1H, Ar, $J = 6.8$ Hz), 7.13 (d, 3H, Ar, $J = 7.2$ Hz), 7.07 (d, 2H, Ar, $J = 8.8$ Hz), 6.97 (d, 2H, Ar, $J = 7.6$ Hz), 4.40-4.32 (m, 1H, $\text{CH}(\text{CH}_2)_2$), 1.63 (s, 2H, CHCH_2CH_2), 1.33-1.13 (m, 6H, piperazine),; δ_{C} (100 MHz, d_6 -DMSO) 168.2, 167.0, 160.7, 155.4, 136.5, 135.4, 134.4, 132.8, 132.4, 131.3, 130.8, 130.3, 129.4, 128.9, 128.8, 127.2, 126.3, 125.2, 125.1, 124.9, 122.1, 120.5, 117.4, 109.2, 59.8, 30.1, 22.4.



MEL-5-056 - 4-(((4-bromophenyl)(cyclopentyl)amino)thio)-1-hydroxy-N-((3-nitro-4-((tetrahydro-2H-pyran-4-yl)methyl)amino)phenyl)sulfonyl)-2-naphthamide (**7b**).

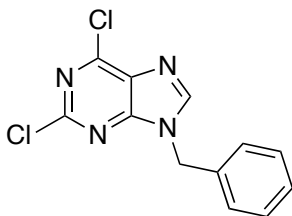
Compound (**6b**, .1 mmol, 1 eq, 81 mg) was dissolved in a 1:1 mixture of TFA/Toluene (1 mL: 1 mL). The reaction mixture stirred for 3 d at room temperature. TLCd to ensure completion in $\text{CH}_2\text{Cl}_2/\text{MeOH}/\text{AcOH}$ (92:7:1). Solvent was concentrated and then taken up in 1 M HCl (30 mL) and partitioned with EtOAc (15 mL). Organics were combined and washed with brine, then dried with Na_2SO_4 , filtered and concentrated to give the title compound as a light purple solid in quantitative yield (72 mg): δ_{H} (400 MHz, d_6 -DMSO) δ_{H} 8.16 (s, 1H, Ar), 8.12 (s, 1H, Ar), 7.92 (dd, 2H, Ar, $J_1 = 19.6$ Hz, $J_2 = 7.2$ Hz), 7.51 (d, 1H, Ar, $J = 8.4$ Hz), 7.29 (t, 1H, Ar, $J = 7.4$ Hz), 7.08 (d, 2H, Ar, $J = 8$ Hz), 6.76 (d, 1H, Ar, $J = 8.8$ Hz), 6.52 (d, 2H, Ar, $J = 7.6$ Hz), 3.97-3.93 (m, 1H, CH Cp), 3.40 (d, 2H,

NHCH(CH₂)₂ Cy, $J = 9.6$ Hz), 1.83 (s, 4H, CH(CH₂CH₂)₂ Cp), 1.6 (s, 4H, CH(CH₂CH₂)₂ Cp), 1.00-0.82 (m, 8H, -(CH₂)₂-O--(CH₂)₂CH-).



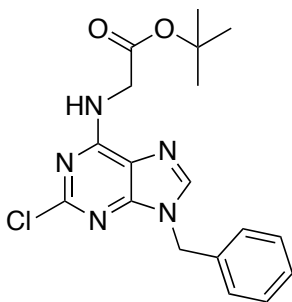
MEL-3-052 – *1-(bromomethyl)naphthalene*.

1-naphthalene methanol (12.7 mmol, 1 eq) was dissolved in anhydrous CH₂Cl₂ (0.2 M) and cooled to 0 °C. PBr₃ (13.9 mmol, 1.1 eq) was added dropwise maintaining temperature and finally 1 drop of pyridine was added. The reaction mixture stirred overnight warming up to room temperature (RT). TLC (2:1 Hexanes/EtOAc) indicated the reaction had gone to completion and was diluted further with CH₂Cl₂. Organics were washed with di-H₂O, brine, dried (Na₂SO₄), filtered, and concentrated *in vacuo* it afforded the title compound as a clear yellow oil in quantitative yield. δ_{H} (400 MHz, CDCl₃) δ_{H} 8.19 (d, 1H, Ar, $J = 8.4$ Hz), 7.89 (dd, 2H, Ar, $J_1 = 19.6$ Hz, $J_2 = 8.4$ Hz), 7.65 (t, 1H, Ar, $J = 7.4$ Hz), 7.56 (d, 2H, Ar, $J = 4.4$ Hz), 7.43 (t, 1H, Ar, $J = 7.4$ Hz), 4.98 (s, 2H, CH₂ Benzylic); δ_{C} (100 MHz, CDCl₃) 134.0, 133.3, 131.1, 129.8, 128.9, 127.8, 126.7, 126.3, 125.4, 123.8, 31.8.



MEL-3-138 – *9-benzyl-2,6-dichloro-9H-purine (9a)*.

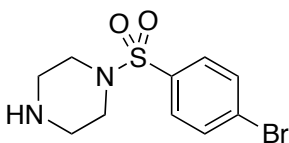
2,6-dichloro-9*H*-purine (**8**, 15.9 mmol, 3 g, 1 eq) was dissolved in DMF (0.2 M) and K₂CO₃ (47.6 mmol, 6.58 g, 3 eq) was added to the stirring reaction at 0 °C. After 1 h, benzyl bromide (31.7 mmol, 3.8 mL, 2 eq) was added dropwise over 20 mins maintaining 0 °C and stirred overnight warming up to room temperature (rt). The reaction was TLCd (1:2 Hexanes/EtOAc) to check for completion. The reaction was quenched with deionized H₂O (100 mL) and partitioned with EtOAc (50 mL x 3). The organic were washed with H₂O (150 mL x 3), brine and then dried (Na₂SO₄), filtered and concentrated. This afforded the *N*-9 and *N*-7 tautomers, which were separated using FCC (1:2 Hexanes/EtOAc) to isolate the *N*-9 as a white solid in 50% yield. δ_{H} (400 MHz, CDCl₃) δ_{H} 8.06 (s, 1H, Ar), 7.39 (d, 2H, Ar, *J* = 5.6 Hz), 7.31 (d, 2H, Ar, *J* = 8 Hz), 5.42 (s, 2H, CH₂); δ_{C} (100 MHz, CDCl₃) 145.5, 133.9, 129.4, 129.1, 128.1, 48.0. Calcd (M⁺): 278.0, Found: 279.0 ([M+H]⁺)



MEL-3-139 – *tert-butyl (9-benzyl-2-chloro-9*H*-purin-6-yl)glycinate (10a)*.

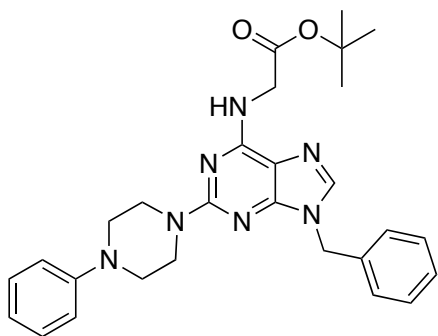
Compound **9a** (1.8 mmol, 500 mg, 1 eq) was dissolved in n-BuOH (0.2 M) and *tert*-butyl glycine (2 mmol, 270 μ L, 1.1 eq, as the free base) was added dropwise. Lastly, K₂CO₃ (2.7 mmol, 371 mg, 1.5 eq) was added and the reaction stirred at 60 °C overnight. Completion was confirmed by TLC (1:1 Hexane/EtOAc). The reaction was quenched with deionized H₂O and extracted with EtOAc (20 mL x 3). Combined organics were washed NaHCO₃(aq), brine, dried (Na₂SO₄), filtered and concentrated to afford **10a** as a beige solid

in a quantitative yield. δ_{H} (400 MHz, CDCl_3) δ_{H} 7.68 (s, 1H, Ar), 7.37-7.31 (m, 3H, Ar), 7.26 (d, 2H, Ar, $J = 3.2$ Hz), 6.57 (s, 1H, NH), 5.31 (s, 2H, CH_2 benzylic), 4.28 (s, 2H, NHCH_2), 1.49 (s, 9H, $\text{C}(\text{CH}_3)_3$); δ_{C} (100 MHz, CDCl_3) 168.7, 154.7, 140.2, 138.4, 135.1, 129.1, 128.5, 128.3, 127.9, 118.4, 82.4, 47.3, 43.2, 28.0. Calcd (M^+): 373.1, Found: 374.1 ($[\text{M}+\text{H}]^+$)



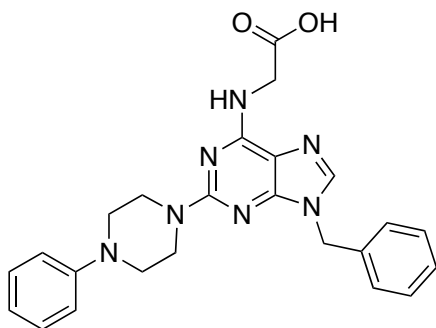
MEL-3-140 – *1-((4-bromophenyl)sulfonyl)piperazine*.

4-bromobenzenesulfonyl chloride (10 mmol, 5.17 g, 1 eq) was added in one portion to a solution of piperazine (60 mmol, 2.26 g, 6 eq) in CH_2Cl_2 (100 mL, 0.1 M.) at 0 °C. The reaction mixture stirred for 30 mins maintaining temperature and a TLC in $\text{CH}_2\text{Cl}_2/\text{MeOH}/\text{NH}_4\text{OH}$ (92:7:1) confirmed completion. The reaction was diluted with CH_2Cl_2 (100 mL) and washed with $\text{NaHCO}_3(\text{aq})$ (100 mL x 3), brine (100 mL), dried (Na_2SO_4), filtered and concentrated to give the title compound in quantitative yield as a yellow solid. δ_{H} (400 MHz, CDCl_3) δ_{H} 7.67 (d, 2H, Ar, $J = 8.4$ Hz), 7.60 (d, 2H, Ar, $J = 8.8$ Hz), 2.97 (d, 4H, piperazine, $J = 4.4$ Hz), 2.92 (d, 4H, piperazine, $J = 5.2$ Hz) 1.67 (s, 1H, NH piperazine); δ_{C} (100 MHz, CDCl_3) 134.5, 132.3, 129.2, 127.9, 46.8, 45.2.



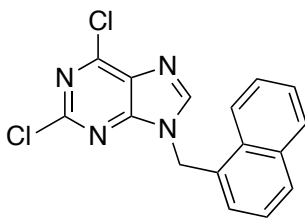
MEL-3-145 – *tert-butyl (9-benzyl-2-(4-phenylpiperazin-1-yl)-9H-purin-6-yl)glycinate (11a).*

Compound **10a** (0.5 mmol, 200 mg, 1 eq) was dissolved in pyridine (0.08 M). 1-Phenylpiperazine (2.5 mmol, 410 μ L, 5 eq) and K_2CO_3 (3.8 mmol, 555 mg, 7.5 eq) were added to a pressure reaction vessel. The reaction was heated to 180 $^{\circ}C$ and stirred overnight. Completion was confirmed by TLC in $CH_2Cl_2/5\%$ MeOH. The reaction mixture was diluted with CH_2Cl_2 and washed with di- H_2O (100 mL x 3), brine (50 mL), dried (Na_2SO_4), filtered and concentrated. The crude product was purified by FCC using $CH_2Cl_2/EtOAc$ (1:1) to afford **11a** as a white solid in 90% yield. δ_H (400 MHz, $CDCl_3$) δ_H 7.48 (s, 1H, Ar), 7.36-7.28 (m, 6H, Ar), 6.99 (d, 2H, Ar, $J = 8.8$ Hz), 6.89 (t, 1H, Ar, $J = 7$ Hz), 6.18 (s, 1H, $NHCH_2$), 5.23 (s, 2H, CH_2 benzylic), 4.25 (s, 2H, $NHCH_2$), 3.99 (s, 4H, $N(CH_2)_2$), 3.25 (s, 4H, $N(CH_2)_2$), 1.49 (s, 9H, $C(CH_3)_3$); δ_C (100 MHz, $CDCl_3$) compound decomposed; unable to get carbon.



MEL-3-146 – (9-benzyl-2-(4-phenylpiperazin-1-yl)-9H-purin-6-yl)glycine (**12a**).

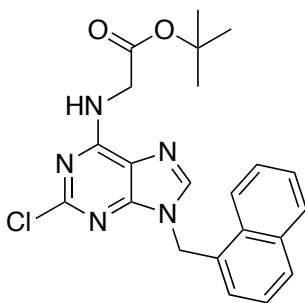
Compound **11a** (0.2 mmol, 100 mg, 1 eq) was suspended in 500 μ L of CH_2Cl_2 . TFA (500 μ L) was added dropwise and the reaction mixture stirred for 1 hr. After 1 hr, TLC in $\text{CH}_2\text{Cl}_2/\text{MeOH}/\text{AcOH}$ (92:7:1) indicated completion. The mixture was concentrated to dryness and azeotroped with CHCl_3 (x5) to afford the TFA salt crude product. Gravity column chromatography afforded **12a** as a grey solid in 85% yield. δ_{H} (400 MHz, d_6 -DMSO) δ_{H} 8.56 (s, 1H, Ar), 7.42-7.26 (m, 8H, Ar), 7.08 (d, 2H, Ar, $J = 8$ Hz), 6.89 (t, 1H, Ar, $J = 7$ Hz), 5.36 (s, 2H, CH_2 benzylic), 4.12 (s, 2H, NHCH_2), 3.88 (s, 4H, $\text{N}(\text{CH}_2)_2$), 3.23(s, 4H, $\text{N}(\text{CH}_2)_2$).



MEL-3-149 – 2,6-dichloro-9-(naphthalen-1-ylmethyl)-9H-purine (**9b**).

2,6-dichloro-9H-purine **8** (5.3 mmol, 1 g, 1 eq) was dissolved in DMF (0.2 M) and K_2CO_3 (15.9 mmol, 2.2 g, 3 eq) was added to the stirring reaction at 0 $^\circ\text{C}$. After 1 h, 1-(bromomethyl)naphthalene (10.6 mmol, 2.3g, 2 eq) was added portionwise over 20 mins maintaining 0 $^\circ\text{C}$ and stirred overnight warming up to room temperature. The reaction was

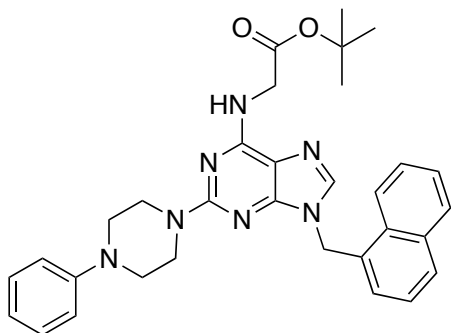
TLCd (1:2 Hexanes/EtOAc) to check for completion. The reaction was quenched with deionized H₂O (100 mL) and partitioned with EtOAc (50 mL x 3). The organics were washed with H₂O (150 mL x 3), brine and then dried (Na₂SO₄), filtered and concentrated. This afforded the *N*-9 and *N*-7 tautomers, which were separated using FCC (1:2 Hexanes/EtOAc) to isolate the *N*-9 as a white solid in 50% yield. δ_{H} (400 MHz, CDCl₃) δ_{H} 7.93-7.84 (m, 4H, Ar), 7.54-7.47 (m, 3H, Ar), 7.42 (d, 1H, Ar, $J = 7.2$ Hz), 5.83 (s, 2H, CH₂ benzylic); δ_{C} (100 MHz, CDCl₃) 153.1, 151.9, 145.5, 133.9, 130.9, 130.4, 129.2, 128.9, 127.8, 127.6, 127.2, 126.6, 125.4, 122.3, 45.9. Calcd (M⁺): 328.0, Found: 329.0 ([M+H]⁺)



MEL-3-151 – *tert-butyl (2-chloro-9-(naphthalen-1-ylmethyl)-9H-purin-6-yl)glycinate (10b)*.

Compound **9b** (1.5 mmol, 500 mg, 1 eq) was dissolved in n-BuOH (0.2 M) and *tert*-butyl glycine (1.7 mmol, 230 μ L 1.1 eq, as the free base) was added dropwise. Lastly, K₂CO₃ (2.3 mmol, 315 mg, 1.5 eq) was added and the reaction stirred at 60 °C overnight. Completion was confirmed by TLC (2:1 Hexane/EtOAc). The reaction was quenched with deionized H₂O and extracted with EtOAc (20 mL x 3). Combined organics were washed NaHCO₃(aq), brine, dried (Na₂SO₄), filtered and concentrated to afford **10b** as a white solid in a 60 % yield. δ_{H} (400 MHz, CDCl₃) δ_{H} 7.91-7.89 (s/m, 3H, Ar), 7.53-7.44 (m, 4H, Ar),

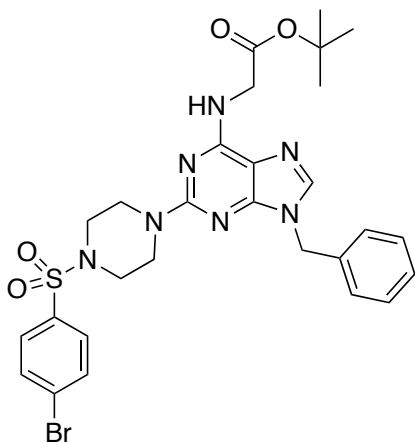
7.36 (d, 1H, Ar, $J = 7.2$ Hz), 7.42 (d, 1H, Ar, $J = 7.2$ Hz), 6.54 (s, 1H, NHCH_2) 5.75 (s, 2H, CH_2 benzylic), 4.29 (s, 2H, NHCH_2), 1.49 (s, 9H, $\text{C}(\text{CH}_3)_3$); δ_{C} (100 MHz, CDCl_3) 168.8, 154.8, 154.4, 140.2, 133.9, 130.9, 130.1, 129.7, 128.9, 127.3, 127.2, 126.4, 125.3, 122.7, 118.4, 82.4, 45.3, 43.2, 29.7, 28.0. Calcd (M^+): 423.1, Found: 424.1 ($[\text{M}+\text{H}]^+$)



MEL-3-154 – *tert-butyl (2-chloro-9-(naphthalen-1-ylmethyl)-2-(4-phenylpiperazin-1-yl)-9H-purin-6-yl)glycinate (11b)*.

Compound **10b** (0.47 mmol, 200 mg, 1 eq) was dissolved in pyridine (0.08 M). 1-Phenylpiperazine (2.4 mmol, 360 μL , 5 eq) and K_2CO_3 (3.5 mmol, 489 mg, 7.5 eq) were added to a pressure reaction vessel. The reaction was heated to 180 $^\circ\text{C}$ and stirred overnight. Completion was confirmed by TLC in CH_2Cl_2 / 5% MeOH. The reaction mixture was diluted with CH_2Cl_2 and washed with di- H_2O (100 mL x 3), brine (50 mL), dried (Na_2SO_4), filtered and concentrated. The crude product was purified by FCC using CH_2Cl_2 /EtOAc (1:1) to afford **11b** as a white solid in 97% yield. δ_{H} (400 MHz, CDCl_3) δ_{H} 8.11 (s, 1H, Ar), 7.90-7.85 (m, 2H, Ar), 7.53-7.50 (m, 2H, Ar), 7.45 (t, 1H, Ar, $J = 8$ Hz), 7.37 (d, 1H, Ar, $J = 7.2$ Hz), 7.30 (t, 2H, Ar, $J = 7.8$ Hz), 7.00 (d, 2H, Ar, $J = 8$ Hz), 6.96-6.88 (m, 2H, Ar), 6.15 (s, 1H, NHCH_2) 5.67 (s, 2H, CH_2 benzylic), 4.24 (s, 2H, NHCH_2), 4.02 (t, 4H, $\text{N}(\text{CH}_2)_2$, $J = 4.6$ Hz), 3.27 (t, 4H, $\text{N}(\text{CH}_2)_2$, $J = 4.8$ Hz), 1.49 (s, 9H, $\text{C}(\text{CH}_3)_3$); δ_{C} (100

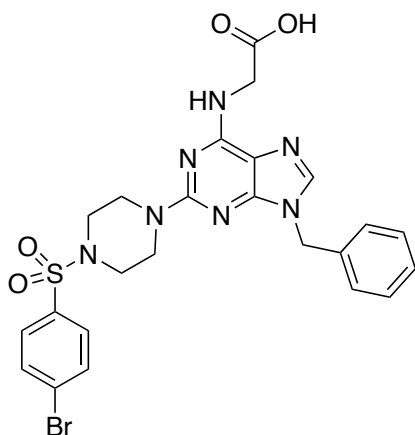
MHz, CDCl₃) 169.4, 160.7, 153.9, 151.5, 137.1, 133.8, 131.4, 131.0, 129.3, 129.2, 128.9, 127.0, 126.9, 126.2, 125.4, 123.1, 120.9, 120.0, 117.1, 116.5, 81.8, 50.7, 49.5, 45.6, 44.5, 39.9, 28.1. Calcd (M⁺): 549.3, Found: 550.3 ([M+H]⁺)



MEL-3-156 – *tert-butyl (9-benzyl-2-((4-(4-bromophenyl)sulfonyl)piperazin-1-yl)-9H-purin-6-yl)glycinate (11aa)*.

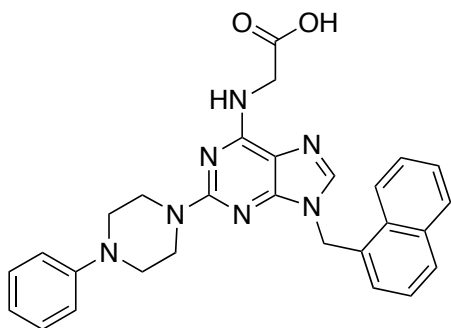
Compound **10a** (1.3 mmol, 500 mg, 1 eq) was dissolved in pyridine (0.08 M). 1-((4-bromophenyl)sulfonyl)piperazine (6.7 mmol, 2 g, 5 eq) and K₂CO₃ (10 mmol, 1.4 g, 7.5 eq) were added to a pressure reaction vessel. The reaction was heated to 180 °C and stirred overnight. Completion was confirmed by TLC in CH₂Cl₂/ 5% MeOH. The reaction mixture was diluted with CH₂Cl₂ and washed with di-H₂O (100 mL x 3), brine (50 mL), dried (Na₂SO₄), filtered and concentrated. The crude product was purified by FCC using CH₂Cl₂/EtOAc (1:1) to afford **11aa** as a white solid in 90% yield. δ_H (400 MHz, CDCl₃) δ_H 7.64 (ABq, 4H, Ar, *J*_A = 8.4 Hz, *J*_B = 7.6 Hz), 7.44 (s, 1H, Ar), 7.31 (d, 3H, Ar, *J* = 5.6 Hz), 7.22 (d, 2H, Ar, *J* = 7.2 Hz), 6.00 (s, 1H, NHCH₂) 5.17 (s, 2H, CH₂ benzylic), 4.15 (s, 2H, NHCH₂), 3.92 (s, 4H, N(CH₂)₂), 3.04 (s, 4H, N(CH₂)₂), 1.46 (s, 9H, C(CH₃)₃); δ_C (100

MHz, CDCl₃) 169.3, 158.2, 153.9, 137.3, 136.1, 134.5, 132.4, 129.2, 128.8, 128.1, 128.0, 127.8, 113.5, 81.8, 46.6, 45.9, 43.7, 28.1. Calcd (M⁺): 641.1, Found: 642.2 ([M+H]⁺)



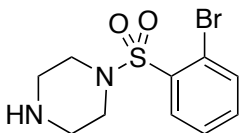
BD-1-091 – (9-benzyl-2-(4-((4-bromophenyl)sulfonyl)piperazin-1-yl)-9H-purin-6-yl)glycine (**12aa**).

Compound **11aa** (0.36 mmol, 200 mg, 1 eq) was suspended in 500 μ L of CH₂Cl₂. TFA (500 μ L) was added dropwise and the reaction mixture stirred for 1 hr. After 1 hr, TLC in CH₂Cl₂/MeOH/AcOH (92:7:1) indicated completion. The mixture was concentrated to dryness and azeotroped with CHCl₃ (x5) to afford the TFA salt crude product. Gravity column chromatography afforded **12aa** as a white solid in quantitative yield. δ_{H} (400 MHz, *d*₆-DMSO) δ_{H} 8.33 (s, 1H, Ar), 7.91 (s, 1H, Ar), 7.84 (d, 2H, Ar, *J* = 7.6 Hz), 7.67 (d, 2H, Ar, *J* = 8.4 Hz), 7.32 (s, 6H, Ar), 5.25 (s, 2H, CH₂ benzylic), 4.02 (s, 2H, NHCH₂), 3.80 (s, 4H, N(CH₂)₂), 2.91 (s, 4H, N(CH₂)₂); δ_{C} (100 MHz, *d*₆-DMSO) 171.9, 158.4, 153.4, 150.9, 138.4, 136.9, 134.5, 132.9, 129.9, 129.0, 128.4, 128.3, 127.8, 122.9, 110.6, 46.8, 45.8, 43.7, 42.5. Calcd (M⁺): 585.1, Found: 586.1 ([M+H]⁺)



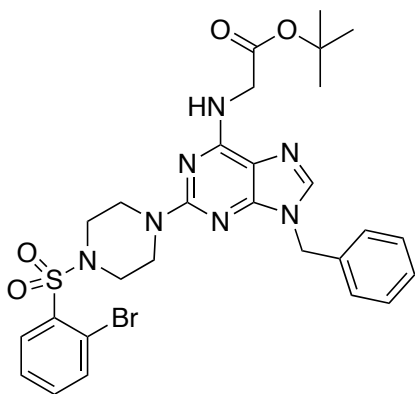
MEL-3-157 – (9-(naphthalen-1-ylmethyl)-2-(4-phenylpiperazin-1-yl)-9H-purin-6-yl)glycine (**12b**).

Compound **11b** (0.36 mmol, 200 mg, 1 eq) was suspended in 500 μL of CH_2Cl_2 . TFA (500 μL) was added dropwise and the reaction mixture stirred for 1 hr. After 1 hr, TLC in $\text{CH}_2\text{Cl}_2/\text{MeOH}/\text{AcOH}$ (92:7:1) indicated completion. The mixture was concentrated to dryness and azeotroped with CHCl_3 (x5) to afford the TFA salt crude product. Gravity column chromatography afforded **12b** as a brown solid in 90% yield. δ_{H} (400 MHz, CDCl_3) δ_{H} 8.41 (d, 1H, Ar, $J = 8$ Hz), 7.98 (d, 1H, Ar, $J = 7.6$ Hz), 7.91 (d, 2H, Ar, $J = 8.8$ Hz), 7.75 (s, 1H, NHCH_2), 7.63-7.55 (m, 2H, Ar), 7.49 (t, 1H, Ar, $J = 7.4$ Hz), 7.34 (d, 1H, Ar, $J = 6.8$ Hz), 7.24 (t, 2H, Ar, $J = 7$ Hz), 6.99 (d, 2H, Ar, $J = 8$ Hz), 6.80 (t, 1H, Ar, $J = 7.4$ Hz), 5.73 (s, 2H, CH_2 benzylic), 4.03 (s, 2H, NHCH_2), 3.84 (s, 4H, $\text{N}(\text{CH}_2)_2$), 3.16 (s, 4H, $\text{N}(\text{CH}_2)_2$); δ_{C} (100 MHz, CDCl_3) 172.4, 158.8, 151.6, 138.7, 133.7, 133.3, 130.9, 129.4, 129.0, 128.8, 127.0, 126.5, 125.9, 123.9, 119.5, 116.2, 70.6, 48.7, 44.4, 43.9, 28.8, 13.2. Calcd (M^+): 493.2, Found: 494.2 ($[\text{M}+\text{H}]^+$)



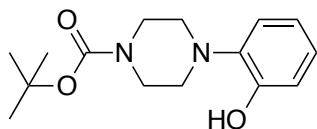
MEL-3-169 – *1-((2-bromophenyl)sulfonyl)piperazine*.

2-bromobenzenesulfonyl chloride (19.6 mmol, 5g, 1 eq) was added in one portion to a solution of piperazine (117.4 mmol, 10.1g, 6 eq) in CH₂Cl₂ (100 mL, 0.1 M.) at 0 °C. The reaction mixture stirred for 30 mins maintaining temperature and a TLC in CH₂Cl₂/MeOH/NH₄OH (92:7:1) confirmed completion. The reaction was diluted with CH₂Cl₂ (100 mL) and washed with NaHCO₃(aq) (100 mL x 3), brine (100 mL), dried (Na₂SO₄), filtered and concentrated to give the title compound in quantitative yield as a white solid. δ_{H} (400 MHz, CDCl₃) δ_{H} 7.98 (d, 1H, Ar, $J = 7.6$ Hz), 7.67 (d, 1H, Ar, $J = 8$ Hz), 7.41-7.32 (m, 2H, Ar), 3.18 (t, 4H, piperazine, $J = 4.8$ Hz), 2.82 (t, 4H, piperazine, $J = 4.6$ Hz) 1.66 (s, 1H, NH piperazine); δ_{C} (100 MHz, CDCl₃) 137.3, 135.8, 133.7, 132.2, 127.5, 120.3, 46.5, 45.5. Calcd (M⁺): 304.0, Found: 305.0 ([M+H]⁺)



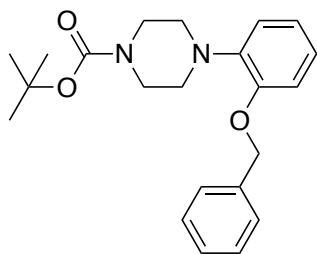
MEL-3-171 – *tert-butyl (9-benzyl-2-(4-((2-bromophenyl)sulfonyl)piperazin-1-yl)-9H-purin-6-yl)glycinate (11ab)*.

Compound **10a** (1.3 mmol, 500 mg, 1 eq) was dissolved in pyridine (0.08 M). 1-((2-bromophenyl)sulfonyl)piperazine (6.7 mmol, 2 g, 5 eq) and K_2CO_3 (10 mmol, 1.4 g, 7.5 eq) were added to a pressure reaction vessel. The reaction was heated to 180 °C and stirred overnight. Completion was confirmed by TLC in CH_2Cl_2 / 5% MeOH. The reaction mixture was diluted with CH_2Cl_2 and washed with di- H_2O (100 mL x 3), brine (50 mL), dried (Na_2SO_4), filtered and concentrated. The crude product was purified by FCC using CH_2Cl_2 /EtOAc (1:1) to afford **11ab** as a white solid in 90% yield. δ_H (400 MHz, $CDCl_3$) δ_H 8.09 (d, 1H, Ar, $J = 7.2$ Hz), 7.74 (d, 1H, Ar, $J = 7.6$ Hz), 7.47-7.43 (m, 2H, Ar), 7.39 (t, 1H, Ar, $J = 7$ Hz), 7.34-7.24 (m, 6H, Ar), 6.17 (s, 1H, Ar), 5.18 (s, 2H, \underline{CH}_2 benzylic), 4.17 (s, 2H, $NH\underline{CH}_2$), 3.89 (s, 4H, $N(\underline{CH}_2)_2$), 3.34 (s, 4H, $N(\underline{CH}_2)_2$), 1.46 (s, 9H, $C(CH_3)_3$); δ_C (100 MHz, $CDCl_3$) 169.4, 154.0, 137.5, 136.2, 135.9, 133.7, 132.3, 128.8, 128.1, 127.8, 127.5, 120.4, 81.8, 46.6, 45.6, 44.2, 28.1. Calcd (M^+): 641.1, Found: 642.1 ($[M+H]^+$)



MEL-3-173 – *tert-butyl 4-(2-hydroxyphenyl)piperazine-1-carboxylate*.

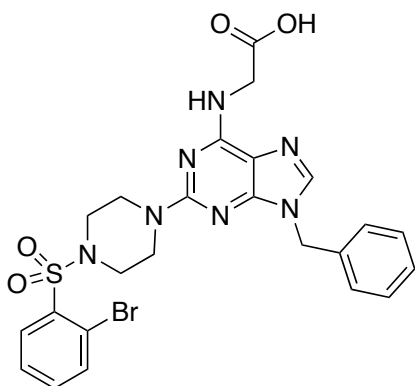
1-(2-hydroxyphenyl)piperazine (8.4 mmol, 1.5 g, 1 eq) was dissolved in a 1:1 mixture of dioxane/THF (56 mL). NaHCO₃ (11.8 mmol, 990 mg, 1.4 eq) was added as a solution in di-H₂O (28 mL) and lastly, (Boc)₂O (10.1 mmol, 2.2 g, 1.2 eq) was added in one portion to the reaction mixture. The reaction stirred overnight at room temperature (RT) and completion was confirmed by TLC in CH₂Cl₂/MeOH/NH₄OH (92:7:1). The reaction mixture was quenched with 1M HCl and extracted with CH₂Cl₂ (100 mL x 2). The combined organics were washed with brine, dried (Na₂SO₄), filtered and concentrated in vacuo to afford the title compound (2.2 g) as a white solid in 95 % yield. δ_H (400 MHz, CDCl₃) δ_H 7.13 (m, 2H, Ar), 6.95 (d, 1H, Ar, *J* = 7.2 Hz), 6.86 (t, 1H, Ar, *J* = 7.2 Hz), 3.59 (t, 4H, piperazine, *J* = 4.8 Hz), 2.83 (s, 4H, piperazine) 1.48 (s, 9H, C(CH₃)₃); δ_C (100 MHz, CDCl₃) 154.7, 151.2, 126.8, 121.3, 120.2, 114.4, 80.1, 67.0, 52.4, 28.3, 27.4.



MEL-3-175 – *tert-butyl 4-(2-(benzyloxy)phenyl)piperazine-1-carboxylate*.

MEL-3-173 (3.6 mmol, 1 g, 1 eq) was dissolved in DMF (0.1M). K₂CO₃ (8.6 mmol, 1.2 g, 2.4 eq) was added and benzyl bromide (4.3 mmol, 513 μL, 1.2 eq) was added dropwise over 5 mins. The reaction mixture stirred at room temperature overnight. Completion was

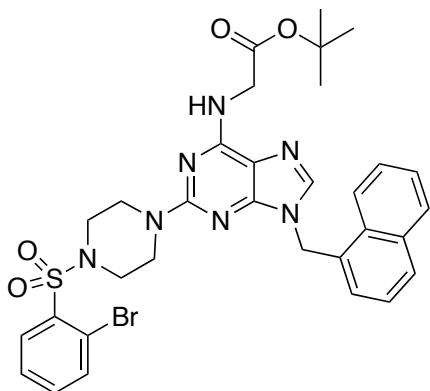
confirmed by TLC (2:1 Hexanes/EtOAc) and the reaction was quenched with di-H₂O and extracted with EtOAc (50 mL x 3). Combined organics were washed with di-H₂O (100 mL x3), brine, dried (Na₂SO₄), filtered and concentrated under vacuum. The crude product was columned by FCC in 2:1 Hexanes/EtOAc to afford the title compound as a white solid in 98% yield.



MEL-3-176 – (9-benzyl-2-(4-((2-bromophenyl)sulfonyl)piperazin-1-yl)-9H-purin-6-yl)glycine (**12ab**).

Compound **11ab** (0.23 mmol, 150 mg, 1 eq) was suspended in 500 μ L of CH₂Cl₂. TFA (500 μ L) was added dropwise and the reaction mixture stirred for 1 hr. After 1 hr, TLC in CH₂Cl₂/MeOH/AcOH (92:7:1) indicated completion. The mixture was concentrated to dryness and azeotroped with CHCl₃ (x5) to afford the TFA salt crude product. Gravity column chromatography afforded **12ab** as a white solid in 99% yield. δ_{H} (400 MHz, *d*₆-DMSO) δ_{H} 12.42 (bs, 1H, COOH), 8.02 (d, 1H, Ar, *J* = 7.2 Hz), 7.94 (s, 1H, Ar), 7.89 (d, 1H, Ar, *J* = 6.8 Hz), 7.78 (s, 1H, Ar), 7.62-7.57 (m, 2H, Ar), 7.31 (s, 5H, Ar), 5.21 (s, 2H, CH₂ benzylic), 3.98 (s, 2H, NHCH₂), 3.77 (s, 4H, N(CH₂)₂), 3.21 (s, 4H, N(CH₂)₂); δ_{C} (100 MHz, *d*₆-DMSO) 172.3, 158.3, 154.4, 138.7, 137.7, 137.3, 136.3, 135.0, 132.2, 129.0,

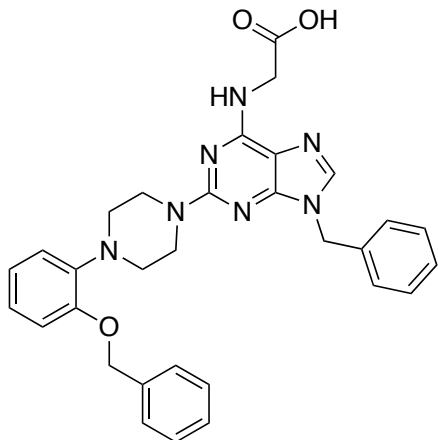
128.8, 128.2, 128.1, 119.9, 46.3, 45.5, 44.3, 42.4. Calcd (M^+): 585.1, Found: 586.1
($[M+H]^+$)



MEL-3-178 – *tert-butyl (2-(4-((2-bromophenyl)sulfonyl)piperazin-1-yl)-9-(naphthalen-1-ylmethyl)-9H-purin-6-yl)glycinate (11bb)*.

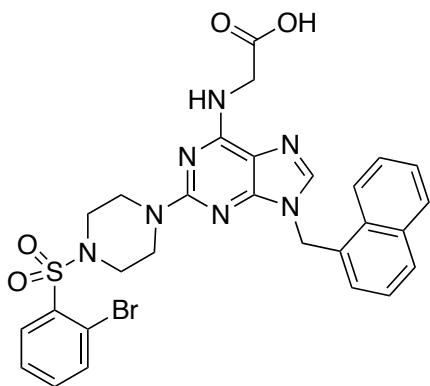
Compound **10b** (1.3 mmol, 500 mg, 1 eq) was dissolved in pyridine (0.08 M). 1-((2-bromophenyl)sulfonyl)piperazine (6.7 mmol, 2 g, 5 eq) and K_2CO_3 (10 mmol, 1.4 g, 7.5 eq) were added to a pressure reaction vessel. The reaction was heated to 180 °C and stirred overnight. Completion was confirmed by TLC in CH_2Cl_2 / 5% MeOH. The reaction mixture was diluted with CH_2Cl_2 and washed with di- H_2O (100 mL x 3), brine (50 mL), dried (Na_2SO_4), filtered and concentrated. The crude product was purified by FCC using CH_2Cl_2 /EtOAc (1:1) to afford **11bb** as a white solid in 90% yield. δ_H (400 MHz, d_6 -DMSO) δ_H 8.10 (d, 1H, Ar, $J = 8$ Hz), 8.00 (d, 1H, Ar, $J = 8$ Hz), 7.88 (t, 2H, Ar, $J = 9$ Hz), 7.75 (d, 1H, Ar, $J = 7.6$ Hz), 7.53-7.29 (m, 6H, Ar), 6.48 (s, 1H, Ar), 5.53 (s, 2H, \underline{CH}_2 benzylic), 4.16 (s, 2H, $NH\underline{CH}_2$), 3.95 (s, 4H, $N(\underline{CH}_2)_2$), 3.36 (s, 4H, $N(\underline{CH}_2)_2$), 1.46 (s, 9H, $C(CH_3)_3$); δ_C (100 MHz, $CDCl_3$) 169.1, 137.4, 135.9, 133.8, 133.7, 132.3, 120.9, 129.5, 128.9, 127.5, 127.1, 127.0, 126.2, 125.3, 122.9, 120.4, 81.8, 45.6, 44.7, 44.2, 28.0. Calcd

(M⁺): 691.2, Found: 692.2 ([M+H]⁺)



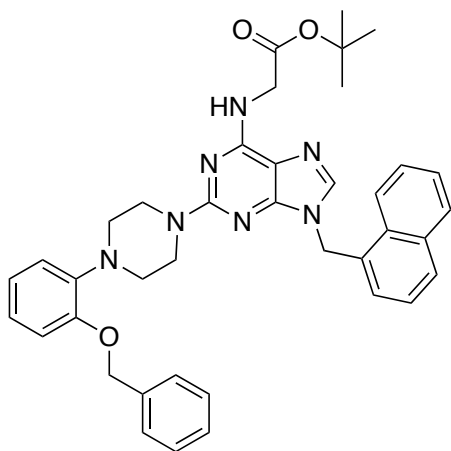
MEL-3-181 – (9-benzyl-2-(4-(2-(benzyloxy)phenyl)piperazin-1-yl)-9H-purin-6-yl)glycine (**12ac**).

Compound **11ac** (0.05 mmol, 30 mg, 1 eq) was suspended in 250 μ L of CH₂Cl₂. TFA (250 μ L) was added dropwise and the reaction mixture stirred for 1 hr. After 1 hr, TLC in CH₂Cl₂/MeOH/AcOH (92:7:1) indicated completion. The mixture was concentrated to dryness and azeotroped with CHCl₃ (x5) to afford the TFA salt crude product. Gravity column chromatography afforded **12ac** as a yellow solid in 88% yield. δ_{H} (400 MHz, *d*₆-DMSO) δ_{H} 12.45 (bs, 1H, COOH), 7.92 (s, 1H, Ar), 7.69(s, 1H, NHCH₂), 7.52 (d, 2H, Ar, *J* = 6.8 Hz), 7.42 (t, 2H, Ar, *J* = 7.4 Hz), 7.34-7.29 (m, 7H, Ar), 7.05 (d, 1H, Ar, *J* = 7.6 Hz), 6.99-6.90 (m, 3H, Ar), 5.25 (s, 2H, CH₂ benzylic), 5.16 (s, 2H, CH₂ benzylic), 4.02 (s, 2H, NHCH₂), 3.81 (s, 4H, N(CH₂)₂), 3.04 (s, 4H, N(CH₂)₂); δ_{C} (100 MHz, *d*₆-DMSO) 172.4, 158.9, 154.5, 151.5, 142.2, 138.5, 137.9, 129.0, 128.8, 128.1, 128.0, 127.4, 123.0, 121.7, 118.8, 114.1, 69.9, 50.6, 46.1, 44.8, 42.4.



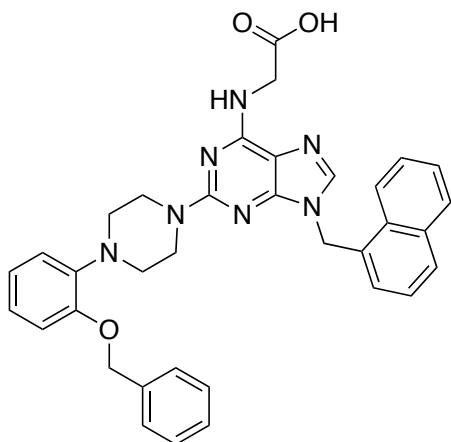
MEL-3-182 – (2-(4-((2-bromophenyl)sulfonyl)piperazin-1-yl)-9-(naphthalen-1-ylmethyl)-9H-purin-6-yl)glycine (**12bb**).

Compound **11bb** (0.31 mmol, 200 mg, 1 eq) was suspended in 500 μ L of CH_2Cl_2 . TFA (500 μ L) was added dropwise and the reaction mixture stirred for 1 hr. After 1 hr, TLC in $\text{CH}_2\text{Cl}_2/\text{MeOH}/\text{AcOH}$ (92:7:1) indicated completion. The mixture was concentrated to dryness and azeotroped with CHCl_3 (x5) to afford the TFA salt crude product. Gravity column chromatography afforded **12bb** as a light orange solid in 93% yield. δ_{H} (400 MHz, d_6 -DMSO) δ_{H} 8.36-8.33 (m, 1H, Ar), 8.01 (d, 1H, Ar, $J = 8$ Hz), 7.96 (t, 1H, Ar, $J = 4.8$ Hz), 7.91-7.88 (m, 3H, Ar), 7.74 (s, 1H, NHCH_2), 7.64-7.53 (s, 4H, Ar), 7.46 (t, 1H, Ar, $J = 7.4$ Hz), 7.33 (d, 1H, Ar, $J = 6.4$ Hz), 5.70 (s, 2H, CH_2 benzylic), 3.96 (s, 2H, NHCH_2), 3.77 (s, 4H, $\text{N}(\text{CH}_2)_2$), 3.19 (s, 4H, $\text{N}(\text{CH}_2)_2$).



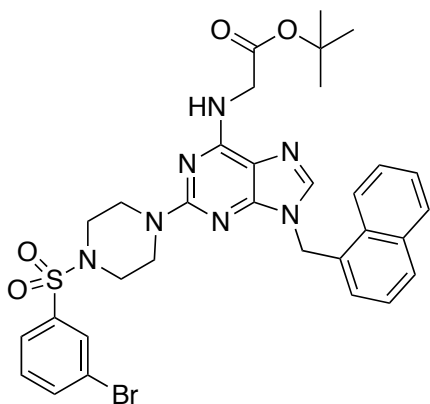
MEL-4-008 – *tert-butyl (2-(4-(2-(benzyloxy)phenyl)piperazin-1-yl)-9-(naphthalen-1-ylmethyl)-9H-purin-6-yl)glycinate (11bc).*

Compound **10b** (0.59 mmol, 250 mg, 1 eq) was dissolved in pyridine (0.08 M). 1-(2-(benzyloxy)phenyl)piperazine (2.9 mmol, 1.1 g, 5 eq) and K_2CO_3 (4.4 mmol, 611 mg, 7.5 eq) were added to a pressure reaction vessel. The reaction was heated to 180 °C and stirred overnight. Completion was confirmed by TLC in CH_2Cl_2 / 5% MeOH. The reaction mixture was diluted with CH_2Cl_2 and washed with di- H_2O (100 mL x 3), brine (50 mL), dried (Na_2SO_4), filtered and concentrated. The crude product was purified by FCC using CH_2Cl_2 /EtOAc (1:1) to afford **11bc** (384 mg) as a beige solid in 99% yield. δ_H (400 MHz, d_6 -DMSO) δ_H 8.13 (d, 1H, Ar, $J = 9.6$ Hz), 7.90-7.85 (m, 2H, Ar), 7.50 (d, 4H, Ar, $J = 8$ Hz), 7.48-7.31 (m, 7H, Ar), 7.00 (s, 5H, Ar), 6.06 (s, 1H, $NHCH_2$), 5.67 (s, 2H, CH_2 benzylic), 5.18 (s, 2H, CH_2 benzylic), 4.24 (s, 2H, $NHCH_2$), 4.03 (s, 4H, $N(CH_2)_2$), 3.21 (s, 4H, $N(CH_2)_2$), 1.48 (s, 9H, $C(CH_3)_3$); δ_C (100 MHz, d_6 -DMSO) 169.5, 153.9, 151.5, 148.2, 137.3, 137.0, 133.8, 131.6, 131.1, 129.2, 128.8, 128.5, 127.9, 127.7, 127.1, 127.0, 126.9, 126.2, 125.7, 123.5, 123.2, 122.9, 121.6, 118.6, 113.4, 81.7, 79.6, 70.3, 50.8, 44.8, 44.5, 40.3, 28.1. Calcd (M^+): 655.3, Found: 656.3 ($[M+H]^+$)



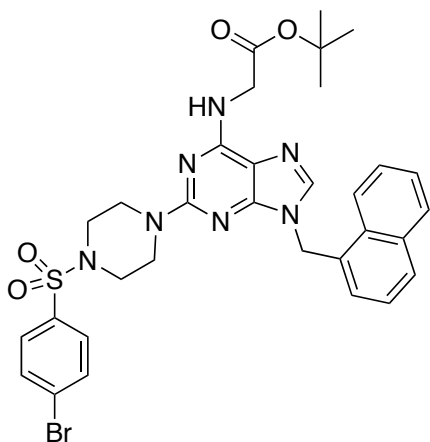
MEL-4-013 – (2-(4-(2-(benzyloxy)phenyl)piperazin-1-yl)-9-(naphthalen-1-ylmethyl)-9H-purin-6-yl)glycine (**12bc**).

Compound **11bc** (0.53 mmol, 350 mg, 1 eq) was suspended in 750 μ L of CH_2Cl_2 . TFA (750 μ L) was added dropwise and the reaction mixture stirred for 1 hr. After 1 hr, TLC in $\text{CH}_2\text{Cl}_2/\text{MeOH}/\text{AcOH}$ (92:7:1) indicated completion. The mixture was concentrated to dryness and azeotroped with CHCl_3 (x5) to afford the TFA salt crude product. Gravity column chromatography afforded **12bc** as a light brown solid in 97% yield. δ_{H} (400 MHz, d_6 -DMSO) δ_{H} 8.41 (d, 1H, Ar, $J = 5.6$ Hz), 7.98-7.96 (m, 1H, Ar), 7.90 (d, 2H, Ar, $J = 12$ Hz), 7.72 (s, 1H, NHCH_2), 7.57-7.46 (m, 5H, Ar), 7.42 (t, 2H, Ar, $J = 7.4$ Hz), 7.34 (d, 2H, Ar, $J = 8.4$ Hz), 7.05 (d, 1H, Ar, $J = 7.6$ Hz), 6.99-6.90 (m, 3H, Ar), 5.73 (s, 2H, CH_2 benzylic), 5.15 (s, 2H, CH_2 benzylic), 4.03 (s, 2H, NHCH_2), 3.82 (s, 4H, $\text{N}(\text{CH}_2)_2$), 3.03 (s, 4H, $\text{N}(\text{CH}_2)_2$); δ_{C} (100 MHz, d_6 -DMSO) 183.2, 177.2, 163.6, 159.2, 156.3, 146.9, 143.4, 142.7, 138.5, 138.1, 135.7, 133.8, 133.6, 132.8, 132.2, 131.7, 131.4, 131.2, 130.7, 128.7, 127.8, 126.5, 123.6, 118.8, 74.7, 55.4, 49.6, 48.6, 47.1. Calcd (M^+): 599.3, Found: 600.3 ($[\text{M}+\text{H}]^+$)



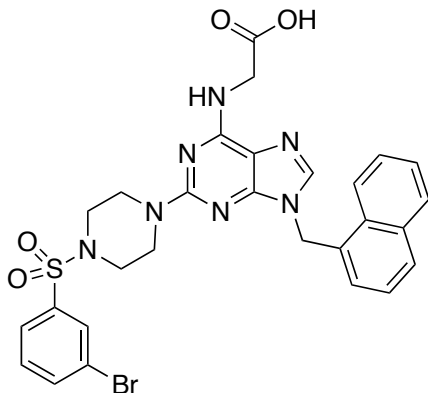
MEL-4-019 – *tert-butyl (2-(4-((3-bromophenyl)sulfonyl)piperazin-1-yl)-9-(naphthalen-1-ylmethyl)-9H-purin-6-yl)glycinate (11bd)*.

Compound **10b** (1.2 mmol, 500 mg, 1 eq) was dissolved in pyridine (0.08 M). 1-((3-bromophenyl)sulfonyl)piperazine (5.9 mmol, 1.8 g, 5 eq) and K_2CO_3 (8.8 mmol, 1.2 g, 7.5 eq) were added to a pressure reaction vessel. The reaction was heated to 180 °C and stirred overnight. Completion was confirmed by TLC in CH_2Cl_2 / 5% MeOH. The reaction mixture was diluted with CH_2Cl_2 and washed with di- H_2O (100 mL x 3), brine (50 mL), dried (Na_2SO_4), filtered and concentrated. The crude product was purified by FCC using CH_2Cl_2 /EtOAc (1:1) to afford **11bd** as a white solid in 90% yield. δ_H (400 MHz, $CDCl_3$) δ_H 8.34 (d, 1H, Ar, $J = 7.6$ Hz), 7.99-7.86 (m, 6H, Ar), 7.74 (d, 1H, Ar, $J = 6.8$ Hz), 3.82 (s, 6H), 2.91 (s, 4H, $N(CH_2)_2$), 1.39 (s, 9H, $C(CH_3)_3$); δ_C (100 MHz, $CDCl_3$) 200.3, 169.1, 162.9, 151.5, 136.0, 133.8, 130.9, 130.6, 130.5, 129.5, 128.9, 127.1, 127.0, 126.2, 125.4, 123.2, 122.8, 81.8, 45.9, 44.7, 44.5, 43.7, 28.1. Calcd (M^+): 691.2, Found: 692.2 ($[M+H]^+$)



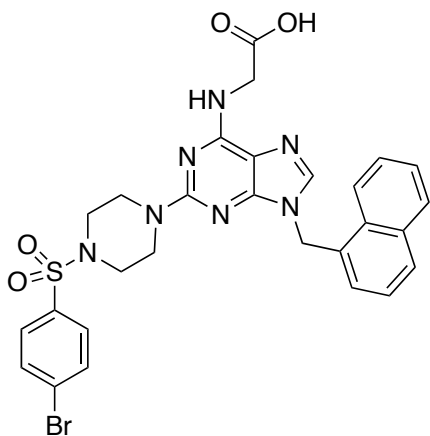
MEL-4-020 – *tert-butyl (2-(4-((4-bromophenyl)sulfonyl)piperazin-1-yl)-9-(naphthalen-1-ylmethyl)-9H-purin-6-yl)glycinate (11ba)*.

Compound **10b** (1.2 mmol, 500 mg, 1 eq) was dissolved in pyridine (0.08 M). 1-((4-bromophenyl)sulfonyl)piperazine (5.9 mmol, 2 g, 5 eq) and K_2CO_3 (8.9 mmol, 1.2 g, 7.5 eq) were added to a pressure reaction vessel. The reaction was heated to 180 °C and stirred overnight. Completion was confirmed by TLC in CH_2Cl_2 / 5% MeOH. The reaction mixture was diluted with CH_2Cl_2 and washed with di- H_2O (100 mL x 3), brine (50 mL), dried (Na_2SO_4), filtered and concentrated. The crude product was purified by FCC using CH_2Cl_2 /EtOAc (1:1) to afford **11ba** as a white solid in 90% yield. δ_H (400 MHz, d_6 -DMSO) δ_H 8.34 (d, 1H, Ar, $J = 6.4$ Hz), 7.98 (d, 1H, Ar, $J = 7.6$ Hz), 7.93-7.85 (m, 5H, Ar), 7.66 (d, 2H, Ar, $J = 7.6$ Hz), 7.59-7.53 (m, 2H, Ar), 7.47 (t, 1H, Ar, $J = 7.8$ Hz), 7.31 (d, 1H, Ar, $J = 7.2$ Hz), 5.68 (s, 2H, $\underline{CH_2}$ benzylic), 3.91 (s, 2H, $NH\underline{CH_2}$), 3.81 (s, 4H, $N(\underline{CH_2})_2$), 2.88 (s, 4H, $N(\underline{CH_2})_2$), 1.38 (s, 9H, $C(CH_3)_3$); δ_C (100 MHz, $CDCl_3$) 169.2, 153.8, 136.9, 134.5, 133.8, 132.4, 131.0, 130.9, 129.4, 129.2, 128.9, 128.0, 127.0, 126.9, 126.2, 125.3, 122.9, 81.8, 45.9, 44.6, 43.7, 28.1. Calcd (M^+): 691.2, Found: 693.2 ($[M+H]^+$)



MEL-4-022 – (2-(4-((3-bromophenyl)sulfonyl)piperazin-1-yl)-9-(naphthalen-1-ylmethyl)-9H-purin-6-yl)glycine (**12bd**).

Compound **11bd** (0.51 mmol, 350 mg, 1 eq) was suspended in 1 mL of CH₂Cl₂. TFA (1 mL) was added dropwise and the reaction mixture stirred for 1 hr. After 1 hr, TLC in CH₂Cl₂/MeOH/AcOH (92:7:1) indicated completion. The mixture was concentrated to dryness and azeotroped with CHCl₃ (x5) to afford the TFA salt crude product. Gravity column chromatography afforded **12bd** as a beige solid in 99% yield. δ_{H} (400 MHz, *d*₆-DMSO) δ_{H} 8.34-8.30 (m, 2H, Ar), 7.96 (d, 1H, Ar, *J* = 8 Hz), 7.90-7.88 (m, 4H, Ar), 7.75 (d, 2H, Ar, *J* = 7.6 Hz), 7.60-7.50 (m, 3H, Ar), 7.46 (t, 1H, Ar, *J* = 8 Hz), 7.32 (d, 1H, Ar, *J* = 7.2 Hz), 5.68 (s, 2H, CH₂ benzylic), 3.96 (s, 2H, NHCH₂), 3.81 (s, 4H, N(CH₂)₂), 2.92 (s, 4H, N(CH₂)₂); δ_{C} (100 MHz, *d*₆-DMSO) 177.0, 162.7, 159.2, 156.1, 143.6, 142.1, 141.4, 138.5, 137.9, 136.9, 135.6, 134.9, 133.7, 133.6, 131.8, 131.7, 131.5, 131.2, 130.7, 128.6, 127.7, 118.4, 50.7, 48.6, 48.4, 47.2.



MEL-4-023 – (2-(4-((4-bromophenyl)sulfonyl)piperazin-1-yl)-9-(naphthalen-1-ylmethyl)-9H-purin-6-yl)glycine (**12ba**).

Compound **11ba** (0.51 mmol, 350 mg, 1 eq) was suspended in 1 mL of CH₂Cl₂. TFA (1 mL) was added dropwise and the reaction mixture stirred for 1 hr. After 1 hr, TLC in CH₂Cl₂/MeOH/AcOH (92:7:1) indicated completion. The mixture was concentrated to dryness and azeotroped with CHCl₃ (x5) to afford the TFA salt crude product. Gravity column chromatography afforded **12ba** as an off white solid in quantitative yield. δ_{H} (400 MHz, *d*₆-DMSO) δ_{H} 12.35 (s, 1H, COOH), 8.32 (d, 1H, Ar, *J* = 8.8 Hz), 7.97 (d, 1H, Ar, *J* = 8 Hz), 7.90 (d, 2H, Ar, *J* = 4.8 Hz), 7.84 (d, 2H, Ar, *J* = 8.4 Hz), 7.77 (s, 1H, NHCH₂), 7.67 (d, 2H, Ar, *J* = 8.4 Hz), 7.59-7.50 (m, 2H, Ar), 7.46 (t, 1H, Ar, *J* = 7.6 Hz), 7.32 (d, 1H, Ar, *J* = 7.2 Hz), 5.68 (s, 2H, CH₂ benzylic), 3.97 (s, 2H, NHCH₂, *J* = 4.8 Hz), 3.79 (s, 4H, N(CH₂)₂), 2.88 (s, 4H, N(CH₂)₂), 1.38 (s, 9H, C(CH₃)₃); δ_{C} (100 MHz, *d*₆-DMSO) 177.0, 176.7, 162.8, 159.2, 143.6, 139.3, 138.5, 137.9, 137.7, 135.6, 134.7, 133.8, 133.6, 132.6, 131.7, 131.6, 131.2, 130.7, 128.6, 85.9, 50.6, 48.6, 48.4, 47.1.

6.3.2 Biology

General. All chemical reagents were ACS grade or higher unless otherwise indicated. All buffers were passed through Chelex-100 (Bio-Rad, Hercules, CA) to remove trace metals. The D₂O, d₆-DMSO, and ¹⁵NH₄Cl were purchased from Cambridge Isotope Laboratories, Inc. (Andover, MA).

Protein Production

A His6-MBP tagged recombinant human Mcl-1 residues 172 to 327 was produced in *E. coli* in either LB or minimal media supplemented with ¹⁵NH₄Cl to produce unlabeled or ¹⁵N-labeled Mcl-1. The tagged protein was initially purified from the crude cell lysate by IMAC chromatography (GE Healthcare Life Sciences), and after dialysis to remove the imidazole the affinity tag was cleaved using PreScission Protease (GE Healthcare Life Sciences). A Sephacryl S-200 size exclusion column was used as a final purification step before the protein was concentrated with a 10,000 MWCO centrifugal filter concentrator (Millipore). The protein purity was shown to be >98% by Coomassie Brilliant Blue (Bio-Rad) stained SDS-PAGE gel and the final concentration was determined using the Bradford protein assay (Bio-Rad) with BSA standards (Pierce).

Peptide

A 6-aminohexanoic acid linker was conjugated to the N-terminus of the Bak BH3 peptide (GQVGRQLAIIGDDINR), capped with fluorescein (on the amino group of the linker), and the peptide was amidated on the C-terminus to give FITC-Ahx-GQVGRQLAIIGDDINR-CONH₂, hereafter referred to as “FITC-Bak” (synthesized by Neo BioScience in >95% purity).

Fluorescence polarization experiments

Fluorescence polarization experiments were conducted using a BMG PHERAstar FS multimode microplate reader equipped with two PMTs for simultaneous measurements of the perpendicular and parallel fluorescence emission. The assays were performed in black polypropylene 384-well microplate (Costar) with a final volume of 20 μ L. Initially the affinity (K_D) of the FITC-Bak peptide was determined by titrating Mcl-1¹⁷²⁻³²⁷ into 10 nM FITC-Bak peptide in 20 mM HEPES, pH 6.8, 50 mM NaCl, 3 mM DTT, 0.01% Triton X-100 and 5% DMSO at room temperature while monitoring the perpendicular and parallel fluorescence emission with a 485 nm excitation and 520 nm emission filters. The fluorescence polarization competition assay (FPCA) was performed using 100 nM Mcl-1¹⁷²⁻³²⁷ in the same buffer (thus, 15 nM FITC-Bak) with varying concentrations of either unlabeled peptide or experimental. Regression analysis was carried out using Origin (OriginLab, Northampton, MA) to fit the data to the Hill equation (1) to determine the initial binding affinity (K_D) and the IC_{50} in the FPCA. For the fluorescence polarization competition titrations, an equation derived by Nikolovska-Coleska et al.¹⁷⁰ was used to calculate the K_i from the IC_{50} data.⁴⁹ The affinity of FITC-Bak for Mcl-1¹⁷²⁻³²⁷ was determined to be 33.8 ± 0.50 nM in the assay conditions used.

Chapter 7 References

1. Fletcher, S.; Hamilton, A. D., Protein surface recognition and proteomimetics: mimics of protein surface structure and function. *Cur Opin Chem Biol* **2005**, *9* (6), 632-8.
2. Nibbe, R. K.; Chowdhury, S. A.; Koyuturk, M.; Ewing, R.; Chance, M. R., Protein-protein interaction networks and subnetworks in the biology of disease. *Wiley Interdiscip Rev Syst Biol Med* **2011**, *3* (3), 357-67.
3. Smith, M. C.; Gestwicki, J. E., Features of protein-protein interactions that translate into potent inhibitors: topology, surface area and affinity. *Expert Rev Mol Med* **2012**, *14*, e16.
4. Lessene, G.; Czabotar, P. E.; Colman, P. M., BCL-2 family antagonists for cancer therapy. *Nat Rev Drug Discov* **2008**, *7* (12), 989-1000.
5. Knight, J. D.; Miranker, A. D., Phospholipid catalysis of diabetic amyloid assembly. *J Mol Biol* **2004**, *341* (5), 1175-87.
6. Al-Quobaili, F.; Montenarh, M., Pancreatic duodenal homeobox factor-1 and diabetes mellitus type 2 (review). *Int J Mol Med* **2008**, *21* (4), 399-404.
7. Mori, M.; Manetti, F.; Botta, M., Targeting protein-protein and protein-nucleic acid interactions for anti-HIV therapy. *Curr Pharm Des* **2011**, *17* (33), 3713-28.
8. Blazer, L. L.; Neubig, R. R., Small molecule protein-protein interaction inhibitors as CNS therapeutic agents: current progress and future hurdles. *Neuropsychopharmacology* **2009**, *34* (1), 126-41.
9. Scott, D. E.; Bayly, A. R.; Abell, C.; Skidmore, J., Small molecules, big targets: drug discovery faces the protein-protein interaction challenge. *Nat Rev Drug Discov* **2016**, *15* (8), 533-50.
10. Arkin, M. R.; Wells, J. A., Small-molecule inhibitors of protein-protein interactions: progressing towards the dream. *Nat Rev Drug Discov* **2004**, *3* (4), 301-17.
11. Arkin, M. R.; Tang, Y.; Wells, J. A., Small-molecule inhibitors of protein-protein interactions: progressing toward the reality. *Chem Biol* **2014**, *21* (9), 1102-14.
12. Bogan, A. A.; Thorn, K. S., Anatomy of hot spots in protein interfaces. *J Mol Biol* **1998**, *280* (1), 1-9.
13. Bullock, B. N.; Jochim, A. L.; Arora, P. S., Assessing helical protein interfaces for inhibitor design. *J Am Chem Soc* **2011**, *133* (36), 14220-3.
14. Cabezas, E.; Satterthwait, A. C., The Hydrogen Bond Mimic Approach: Solid Phase Synthesis of a Peptide Stabilized as an α -Helix with a Hydrazone Link. *J Am Chem*

Soc **1999**, *121*, 3862-3875.

15. Chapman, R. N.; Dimartino, G.; Arora, P. S., A highly stable short alpha-helix constrained by a main-chain hydrogen-bond surrogate. *J Am Chem Soc* **2004**, *126* (39), 12252-3.
16. Youle, R. J.; Strasser, A., The BCL-2 protein family: opposing activities that mediate cell death. *Nat Rev Mol Biol* **2008**, *9* (1), 47-59.
17. Opferman, J. T., Attacking cancer's Achilles heel: antagonism of anti-apoptotic BCL-2 family members. *FEBS J* **2016**, *283* (14), 2661-75.
18. Fesik, S. W., Promoting apoptosis as a strategy for cancer drug discovery. *Nat Rev Cancer* **2005**, *5* (11), 876-85.
19. Petros, A. M.; Olejniczak, E. T.; Fesik, S. W., Structural biology of the Bcl-2 family of proteins. *Biochim Biophys Acta* **2004**, *1644* (2-3), 83-94.
20. Sarosiek, K. A.; Letai, A., Directly targeting the mitochondrial pathway of apoptosis for cancer therapy using BH3 mimetics - recent successes, current challenges and future promise. *FEBS J* **2016**, *283* (19), 3523-3533.
21. Yap, J. L.; Chen, L.; Lanning, M. E.; Fletcher, S., Expanding the Cancer Arsenal with Targeted Therapies: Disarmament of the Antiapoptotic Bcl-2 Proteins by Small Molecules. *J Med Chem* **2017**, *60* (3), 821-838.
22. Czabotar, P. E.; Lessene, G.; Strasser, A.; Adams, J. M., Control of apoptosis by the BCL-2 protein family: implications for physiology and therapy. *Nat Rev Mol Cell Biol* **2014**, *15* (1), 49-63.
23. Gross, A.; McDonnell, J. M.; Korsmeyer, S. J., BCL-2 Family Members and the Mitochondria in Apoptosis. *Genes Dev* **1999**, *13*, 1899-1911.
24. Tait, S. W.; Green, D. R., Mitochondrial regulation of cell death. *Cold Spring Harb Perspect Biol* **2013**, *5* (9).
25. Youle, R. J., Cell biology. Cellular demolition and the rules of engagement. *Science* **2007**, *315* (5813), 776-7.
26. Willis, S. N.; Fletcher, J. I.; Kaufmann, T.; van Delft, M. F.; Chen, L.; Czabotar, P. E.; Ierino, H.; Lee, E. F.; Fairlie, W. D.; Bouillet, P.; Strasser, A.; Kluck, R. M.; Adams, J. M.; Huang, D. C., Apoptosis initiated when BH3 ligands engage multiple Bcl-2 homologs, not Bax or Bak. *Science* **2007**, *315* (5813), 856-9.
27. Rautureau, G. J.; Day, C. L.; Hinds, M. G., Intrinsically disordered proteins in bcl-2 regulated apoptosis. *Int J Mol Sci* **2010**, *11* (4), 1808-24.
28. Sattler, M.; Liang, H.; Nettesheim, D. G.; Meadows, R. P.; Harlan, J. E.; Eberstadt,

M.; Yoon, H. S.; Shuker, S. B.; Chang, B. S.; Minn, A. J.; Thompson, C. B.; Fesik, S. W., Structure of Bcl-xL-Bak Peptide Complex: Recognition Between Regulators of Apoptosis. *Science* **1997**, *275*.

29. Yap, J. L.; Cao, X.; Vanommeslaeghe, K.; Jung, K. Y.; Peddaboina, C.; Wilder, P. T.; Nan, A.; MacKerell, A. D., Jr.; Smythe, W. R.; Fletcher, S., Relaxation of the rigid backbone of an oligoamide-foldamer-based alpha-helix mimetic: identification of potent Bcl-xL inhibitors. *Org Biomol Chem* **2012**, *10* (15), 2928-33.

30. Fletcher, S.; Hamilton, A. D., Targeting protein-protein interactions by rational design: mimicry of protein surfaces. *J R Soc* **2006**, *3* (7), 215-33.

31. Lee, E. F.; Czabotar, P. E.; van Delft, M. F.; Michalak, E. M.; Boyle, M. J.; Willis, S. N.; Puthalakath, H.; Bouillet, P.; Colman, P. M.; Huang, D. C.; Fairlie, W. D., A novel BH3 ligand that selectively targets Mcl-1 reveals that apoptosis can proceed without Mcl-1 degradation. *J Cell Biol* **2008**, *180* (2), 341-55.

32. Zhang, Z.; Li, X.; Song, T.; Zhao, Y.; Feng, Y., An anthraquinone scaffold for putative, two-face Bim BH3 alpha-helix mimic. *J Med Chem* **2012**, *55* (23), 10735-41.

33. Friberg, A.; Vigil, D.; Zhao, B.; Daniels, R. N.; Burke, J. P.; Garcia-Barrantes, P. M.; Camper, D.; Chauder, B. A.; Lee, T.; Olejniczak, E. T.; Fesik, S. W., Discovery of potent myeloid cell leukemia 1 (Mcl-1) inhibitors using fragment-based methods and structure-based design. *J Med Chem* **2013**, *56* (1), 15-30.

34. Lee, E. F.; Czabotar, P. E.; Smith, B. J.; Deshayes, K.; Zobel, K.; Colman, P. M.; Fairlie, W. D., Crystal structure of ABT-737 complexed with Bcl-xL: implications for selectivity of antagonists of the Bcl-2 family. *Cell Death Differ* **2007**, *14* (9), 1711-3.

35. Lee, E. F.; Czabotar, P. E.; Yang, H.; Sleebs, B. E.; Lessene, G.; Colman, P. M.; Smith, B. J.; Fairlie, W. D., Conformational changes in Bcl-2 pro-survival proteins determine their capacity to bind ligands. *J Biol Chem* **2009**, *284* (44), 30508-17.

36. Henchey, L. K.; Porter, J. R.; Ghosh, I.; Arora, P. S., High specificity in protein recognition by hydrogen-bond-surrogate alpha-helices: selective inhibition of the p53/MDM2 complex. *ChemBioChem* **2010**, *11* (15), 2104-7.

37. Walensky, L. D.; Kung, A. L.; Escher, I.; Malia, T. J.; Barbuto, S.; Wright, R. D.; Wagner, G.; Verdine, G. L.; Korsmeyer, S. J., Activation of apoptosis in vivo by a hydrocarbon-stapled BH3 helix. *Science* **2004**, *305* (5689), 1466-70.

38. Blackwell, H. E.; Grubbs, R. H., Highly Efficient Synthesis of Covalently Cross-Linked Peptide Helices by Ring-Closing Metathesis. *Angew Chem, Int Ed* **1998**, *37* (23), 3281-3284.

39. Bouvier, M.; Taylor, J. W., Probing the functional conformation of neuropeptide Y through the design and study of cyclic analogues. *J Med Chem* **1992**, *35* (6), 1145-55.

40. Jackson, D. Y.; King, D. S.; Chmielewski, J.; Singh, S.; Schultz, P. G., General Approach to the Synthesis of Short Alpha-Helical Peptides. *J Am Chem Soc* **1991**, *113*, 9391-9392.
41. Marqusee, S.; Baldwin, R. L., Helix stabilization by Glu...Lys⁺ salt bridges in short peptides of de novo design. *Proc Natl Acad Sci USA* **1987**, *84* (24), 8898-902.
42. Kawamoto, S. A.; Coleska, A.; Ran, X.; Yi, H.; Yang, C. Y.; Wang, S., Design of triazole-stapled BCL9 alpha-helical peptides to target the beta-catenin/B-cell CLL/lymphoma 9 (BCL9) protein-protein interaction. *J Med Chem* **2012**, *55* (3), 1137-46.
43. Cao, X.; Yap, J. L.; Newell-Rogers, M. K.; Peddaboina, C.; Jiang, W.; Papaconstantinou, H. T.; Jupiter, D.; Rai, A.; Jung, K. Y.; Tubin, R. P.; Yu, W.; Vanommeslaeghe, K.; Wilder, P. T.; MacKerell, A. D., Jr.; Fletcher, S.; Smythe, W. R., The Novel BH3 α -Helix Mimetic JY-1-106 induces apoptosis in a subset of cancer cells (lung cancer, colon cancer and mesothelioma) by disrupting Bcl-xL and Mcl-1 protein-protein interactions with Bak. *Mol Cancer* **2013**, *12*, 42-.
44. Kazi, A.; Sun, J.; Doi, K.; Sung, S. S.; Takahashi, Y.; Yin, H.; Rodriguez, J. M.; Becerril, J.; Berndt, N.; Hamilton, A. D.; Wang, H. G.; Sebti, S. M., The BH3 alpha-helical mimic BH3-M6 disrupts Bcl-X(L), Bcl-2, and MCL-1 protein-protein interactions with Bax, Bak, Bad, or Bim and induces apoptosis in a Bax- and Bim-dependent manner. *J Biol Chem* **2011**, *286* (11), 9382-92.
45. Horwell, D. C.; Howson, W.; Nolan, W. P.; Ratcliffe, G. S.; Rees, D. C.; Willems, H. M. G., The Design of Dipeptide Helical Mimetics, Part I: the Synthesis of 1,6-Disubstituted Indanes. *Tetrahedron* **1995**, *51*, 203-216.
46. Horwell, D. C.; Howson, W.; Ratcliffe, G. S.; Willems, H. M., The design of dipeptide helical mimetics: the synthesis, tachykinin receptor affinity and conformational analysis of 1,1,6-trisubstituted indanes. *Bioorg Med Chem* **1996**, *4* (1), 33-42.
47. Orner, B. P.; Ernst, J. T.; Hamilton, A. D., Toward Proteomimetics: Terphenyl Derivatives as Structural and Functional Mimics of Extended Regions of an α -Helix. *J Am Chem Soc* **2001**, *123*, 5382-5383.
48. Kutzki, O.; Park, H. S.; Ernst, J. T.; Orner, B. P.; Yin, H.; Hamilton, A. D., Development of a Potent Bcl-xL Antagonist Based on α -Helix Mimicry. *J Am Chem Soc* **2002**, *124*, 11838-11839.
49. Davis, J. M.; Truong, A.; Hamilton, A. D., Synthesis of a 2,3';6',3"-terpyridine scaffold as an alpha-helix mimetic. *Org Lett* **2005**, *7* (24), 5405-8.
50. Ernst, J. T.; Becerril, J.; Park, H. S.; Yin, H.; Hamilton, A. D., Design and application of an alpha-helix-mimetic scaffold based on an oligoamide-foldamer strategy: antagonism of the Bak BH3/Bcl-xL complex. *Angew Chem, Int Ed* **2003**, *42* (5), 535-9.
51. Yin, H.; Hamilton, A. D., Terephthalamide derivatives as mimetics of the helical

region of Bak peptide target Bcl-xL protein. *Bioorg Med Chem Lett* **2004**, *14* (6), 1375-9.

52. Yin, H.; Lee, G.; Sedey, K. A.; Kutzki, O.; Park, H. S.; Orner, B. P.; Ernst, J. T.; Wang, H.-G.; Sebt, S. M.; Hamilton, A. D., Terphenyl-Based Bak BH3 α -Helical Proteomimetics as Low-Molecular-Weight Antagonists of Bcl-xL. *J Am Chem Soc* **2005**, *127*, 10191-10196.

53. Rodriguez, J. M.; Ross, N. T.; Katt, W. P.; Dhar, D.; Lee, G. I.; Hamilton, A. D., Structure and function of benzoylurea-derived α -helix mimetics targeting the Bcl-x(L)/Bak binding interface. *ChemMedChem* **2009**, *4* (4), 649-56.

54. Thompson, S.; Hamilton, A. D., Amphiphilic α -helix mimetics based on a benzoylurea scaffold. *OrgBiomol Chem* **2012**, *10* (30), 5780-2.

55. Thompson, S.; Vallinayagam, R.; Adler, M. J.; Scott, R. T. W.; Hamilton, A. D., Double-sided α -helix mimetics. *Tetrahedron* **2012**, *68* (23), 4501-4505.

56. Adler, M. J.; Hamilton, A. D., Oligophenylaminones as scaffolds for α -helix mimicry. *J Org Chem* **2011**, *76* (17), 7040-7.

57. Adler, M. J.; Scott, R. T.; Hamilton, A. D., Enaminone-based mimics of extended and hydrophilic α -helices. *Chem* **2012**, *18* (41), 12974-7.

58. Jung, K. Y.; Vanommeslaeghe, K.; Lanning, M. E.; Yap, J. L.; Gordon, C.; Wilder, P. T.; MacKerell, A. D., Jr.; Fletcher, S., Amphipathic α -Helix Mimetics Based on a 1,2-Diphenylacetylene Scaffold. *Org Lett* **2013**, *15* (13), 3234- 3237.

59. Lanning, M. E.; Wilder, P. T.; Bailey, H.; Drennen, B.; Cavalier, M.; Chen, L.; Yap, J. L.; Raje, M.; Fletcher, S., Towards more drug-like proteomimetics: two-faced, synthetic α -helix mimetics based on a purine scaffold. *Org Biomol Chem* **2015**, *13* (32), 8642-6.

60. Oltersdorf, T.; Elmore, S. W.; Shoemaker, A. R.; Armstrong, R. C.; Augeri, D. J.; Belli, B. A.; Bruncko, M.; Deckwerth, T. L.; Dinges, J.; Hajduk, P. J.; Joseph, M. K.; Kitada, S.; Korsmeyer, S. J.; Kunzer, A. R.; Letai, A.; Li, C.; Mitten, M. J.; Nettlesheim, D. G.; Ng, S.; Nimmer, P. M.; O'Connor, J. M.; Oleksijew, A.; Petros, A. M.; Reed, J. C.; Shen, W.; Tahir, S. K.; Thompson, C. B.; Tomaselli, K. J.; Wang, B.; Wendt, M. D.; Zhang, H.; Fesik, S. W.; Rosenberg, S. H., An inhibitor of Bcl-2 family proteins induces regression of solid tumours. *Nature* **2005**, *435* (7042), 677-81.

61. Lessene, G.; Czabotar, P. E.; Sleebs, B. E.; Zobel, K.; Lowes, K. N.; Adams, J. M.; Baell, J. B.; Colman, P. M.; Deshayes, K.; Fairbrother, W. J.; Flygare, J. A.; Gibbons, P.; Kersten, W. J.; Kulasegaram, S.; Moss, R. M.; Parisot, J. P.; Smith, B. J.; Street, I. P.; Yang, H.; Huang, D. C.; Watson, K. G., Structure-guided design of a selective BCL-X(L) inhibitor. *Nat Chem Biol* **2013**, *9* (6), 390-7.

62. Petros, A. M.; Swann, S. L.; Song, D.; Swinger, K.; Park, C.; Zhang, H.; Wendt, M. D.; Kunzer, A. R.; Souers, A. J.; Sun, C., Fragment-based discovery of potent inhibitors

of the anti-apoptotic MCL-1 protein. *Bioorg Med Chem Lett* **2014**, *24* (6), 1484-8.

63. Kotschy, A.; Szlavik, Z.; Murray, J.; Davidson, J.; Maragno, A. L.; Le Toumelin-Braizat, G.; Chanrion, M.; Kelly, G. L.; Gong, J. N.; Moujalled, D. M.; Bruno, A.; Csekei, M.; Paczal, A.; Szabo, Z. B.; Sipos, S.; Radics, G.; Proszenyak, A.; Balint, B.; Ondi, L.; Blasko, G.; Robertson, A.; Surgenor, A.; Dokurno, P.; Chen, I.; Matassova, N.; Smith, J.; Pedder, C.; Graham, C.; Studeny, A.; Lysiak-Auvity, G.; Girard, A. M.; Grave, F.; Segal, D.; Riffkin, C. D.; Pomilio, G.; Galbraith, L. C.; Aubrey, B. J.; Brennan, M. S.; Herold, M. J.; Chang, C.; Guasconi, G.; Cauquil, N.; Melchiorre, F.; Guigal-Stephan, N.; Lockhart, B.; Colland, F.; Hickman, J. A.; Roberts, A. W.; Huang, D. C.; Wei, A. H.; Strasser, A.; Lessene, G.; Geneste, O., The MCL1 inhibitor S63845 is tolerable and effective in diverse cancer models. *Nature* **2016**, *538* (7626), 477-482.

64. Lanning, M. E.; Yu, W.; Yap, J. L.; Chauhan, J.; Chen, L.; Whiting, E.; Pidugu, L. S.; Atkinson, T.; Bailey, H.; Li, W.; Roth, B. M.; Hynicka, L.; Chesko, K.; Toth, E. A.; Shapiro, P.; MacKerell, A. D.; Wilder, P. T.; Fletcher, S., Structure-Based Design of N-Substituted 1-Hydroxy-4-sulfamoyl-2-naphthoates as Selective Inhibitors of the Mcl-1 Oncoprotein. *Eur J Med Chem* **2016**.

65. Abulwerdi, F. A.; Liao, C.; Mady, A. S.; Gavin, J.; Shen, C.; Cierpicki, T.; Stuckey, J. A.; Showalter, H. D.; Nikolovska-Coleska, Z., 3-Substituted-N-(4-Hydroxynaphthalen-1-yl)arylsulfonamides as a Novel Class of Selective Mcl-1 Inhibitors: Structure-Based Design, Synthesis, SAR, and Biological Evaluation. *J Med Chem* **2014**, *57* (10), 4111-33.

66. Cummings, M. D.; Schubert, C.; Parks, D. J.; Calvo, R. R.; LaFrance, L. V.; Lattanze, J.; Milkiewicz, K. L.; Lu, T., Substituted 1,4-benzodiazepine-2,5-diones as alpha-helix mimetic antagonists of the HDM2-p53 protein-protein interaction. *Chem Bio Drug Des* **2006**, *67* (3), 201-5.

67. Chen, L.; Jung, K.-Y.; Fletcher, S., Amphipathic A-Helix Mimetics Based on a 1,4-Disubstituted-2,3,4,5-Tetrahydro-1H-Benzo[E][1,4]Diazepine: Inhibition of the Mcl-1 Oncoprotein. In *Proceedings of the 249th ACS National Meeting & Exposition, Denver, CO, USA, 22-26 March 2015*. **2015**.

68. Moon, H.; Lee, W. S.; Oh, M.; Lee, H.; Lee, J. H.; Im, W.; Lim, H. S., Design, solid-phase synthesis, and evaluation of a phenyl-piperazine-triazine scaffold as alpha-helix mimetics. *ACS Comb Sci* **2014**, *16* (12), 695-701.

69. Zhao, Y.; Aguilar, A.; Bernard, D.; Wang, S., Small-molecule inhibitors of the MDM2-p53 protein-protein interaction (MDM2 Inhibitors) in clinical trials for cancer treatment. *J Med Chem* **2015**, *58* (3), 1038-52.

70. Cao, X.; Yap, J. L.; Newell-Rogers, M. K.; Peddaboina, C.; Jiang, W.; Papaconstantinou, H. T.; Jupiter, D.; Rai, A.; Jung, K. Y.; Tubin, R. P.; Yu, W.; Vanommeslaeghe, K.; Wilder, P. T.; MacKerell, A. D., Jr.; Fletcher, S.; Smythe, R. W., The novel BH3 alpha-helix mimetic JY-1-106 induces apoptosis in a subset of cancer cells (lung cancer, colon cancer and mesothelioma) by disrupting Bcl-xL and Mcl-1 protein-protein interactions with Bak. *Mol Cancer* **2013**, *12* (1), 42.

71. Marimganti, S.; Cheemala, M. N.; Ahn, J.-M., Novel Amphiphilic α -Helix Mimetics Based on a Bis-benzamide Scaffold. *Org Lett* **2009**, *11* (19), 4418-4421.
72. Kemp, D. S.; Li, Z. Q., 2-Amino-2'-carboxydiphenylacetylenes as beta-turn mimetics. Synthesis and conformational properties. *Tetrahedron Lett* **1995**, *36*.
73. Kemp, D. S.; Li, Z. Q., A short beta-sheet containing proline nucleated by a 2,2'-substituted tolan beta-turn mimetic. *Tetrahedron Lett* **1995**, *36*, 4179-4180.
74. Spivey, A. C.; McKendrick, J.; Srikanan, R., Solid-Phase Synthesis of an A-B Loop Mimetic of the CE3 Domain of Human IgE: Macrocyclization by Sonogashira Coupling. *J Org Chem* **2003**, *68*, 1843-1851.
75. Lingard, H.; Han, J. T.; Thompson, A. L.; Leung, I. K.; Scott, R. T.; Thompson, S.; Hamilton, A. D., Diphenylacetylene-linked peptide strands induce bidirectional beta-sheet formation. *Angew Chem, Int Ed* **2014**, *53* (14), 3650-3.
76. Jung, K. Y.; Vanommeslaeghe, K.; Lanning, M. E.; Yap, J. L.; Gordon, C.; Wilder, P. T.; MacKerell, A. D., Jr.; Fletcher, S., Amphipathic alpha-helix mimetics based on a 1,2-diphenylacetylene scaffold. *Org Lett* **2013**, *15* (13), 3234-7.
77. Li, X.; Wang, Z.; Feng, Y.; Song, T.; Su, P.; Chen, C.; Chai, G.; Yang, Y.; Zhang, Z., Two-face, two-turn α -helix mimetics based on a cross-acridine scaffold: Analogues of the Bim BH3 domain. *ChemBioChem* **2014**, *15*, 1280-1285.
78. Lee, J. H.; Zhang, Q.; Jo, S.; Chai, S. C.; Oh, M.; Im, W.; Lu, H.; Lim, H. S., Novel pyrrolopyrimidine-based alpha-helix mimetics: cell-permeable inhibitors of protein-protein interactions. *J Am Chem Soc* **2011**, *133* (4), 676-9.
79. Fletcher, S.; Shahani, V. M.; Gunning, P. T., Facile and efficient access to 2,6,9-tri-substituted purines through sequential N9, N2 Mitsunobu reactions. *Tetrahedron Lett* **2009**, *50* (29), 4258-4261.
80. Ripka, W. C.; De Lucca, G. V.; Bach II, A. C.; Pottorf, R. S.; Blaney, J. M., Protein β -turn mimetics I. Design, synthesis, and evaluation in model cyclic peptides. *Tetrahedron* **1993**, *49* (17), 3593-3608.
81. Bayly, A. R.; White, A. J. P.; Spivey, A. C., Design and Synthesis of a Prototype Scaffold for Five-Residue α -Helix Mimetics. *Eur J Org Chem* **2013**, *2013* (25), 5566-5569.
82. Tanaka, Y.; Aikawa, K.; Nishida, G.; Homma, M.; Sogabe, S.; Igaki, S.; Hayano, Y.; Sameshima, T.; Miyahisa, I.; Kawamoto, T.; Tawada, M.; Imai, Y.; Inazuka, M.; Cho, N.; Imaeda, Y.; Ishikawa, T., Discovery of potent Mcl-1/Bcl-xL dual inhibitors by using a hybridization strategy based on structural analysis of target proteins. *J Med Chem* **2013**, *56* (23), 9635-45.
83. Wendt, M. D.; Shen, W.; Kunzer, A.; McCellan, W. J.; Bruncko, M.; Oost, T. K.; Ding, H.; Joseph, M. K.; Zhang, H.; Nimmer, P. M.; Ng, S.; Shoemaker, A. R.; Petros, A. M.; Oleksijew, A.; Marsh, K.; Bauch, J.; Oltersdorf, T.; Belli, B. A.; Martineau, D.; Fesik,

S. W.; Rosenberg, S. H.; Elmore, S. W., Discovery and Structure-Activity Relationship of Antagonists of B-Cell Lymphoma 2 Family Proteins with Chemopotential Activity in Vitro and in Vivo. *J Med Chem* **2006**, *49*, 1165-1181.

84. Park, C.; Bruncko, M.; Adickes, J.; Bauch, J.; Ding, H.; Kunzer, A.; Marsh, K. C.; Nimmer, P.; Shoemaker, A. R.; Song, X.; Tahir, S. K.; Tse, C.; Wang, X.; Wendt, M. D.; Yang, X.; Zhang, H.; Fesik, S. W.; Rosenberg, S. H.; Elmore, S. W., Discovery of an Orally Bioavailable Small Molecule Inhibitor of Prosurvival B-Cell Lymphoma 2 Proteins. *J Med Chem* **2008**, *51*, 6902-6915.

85. Tahir, S. K.; Yang, X.; Anderson, M. G.; Morgan-Lappe, S. E.; Sarthy, A. V.; Chen, J.; Warner, R. B.; Ng, S. C.; Fesik, S. W.; Elmore, S. W.; Rosenberg, S. H.; Tse, C., Influence of Bcl-2 family members on the cellular response of small-cell lung cancer cell lines to ABT-737. *Cancer Res* **2007**, *67* (3), 1176-83.

86. Konopleva, M.; Contractor, R.; Tsao, T.; Samudio, I.; Ruvolo, P. P.; Kitada, S.; Deng, X.; Zhai, D.; Shi, Y. X.; Sneed, T.; Verhaegen, M.; Soengas, M.; Ruvolo, V. R.; McQueen, T.; Schober, W. D.; Watt, J. C.; Jiffar, T.; Ling, X.; Marini, F. C.; Harris, D.; Dietrich, M.; Estrov, Z.; McCubrey, J.; May, W. S.; Reed, J. C.; Andreeff, M., Mechanisms of apoptosis sensitivity and resistance to the BH3 mimetic ABT-737 in acute myeloid leukemia. *Cancer Cell* **2006**, *10* (5), 375-88.

87. van Delft, M. F.; Wei, A. H.; Mason, K. D.; Vandenberg, C. J.; Chen, L.; Czabotar, P. E.; Willis, S. N.; Scott, C. L.; Day, C. L.; Cory, S.; Adams, J. M.; Roberts, A. W.; Huang, D. C., The BH3 mimetic ABT-737 targets selective Bcl-2 proteins and efficiently induces apoptosis via Bak/Bax if Mcl-1 is neutralized. *Cancer Cell* **2006**, *10* (5), 389-99.

88. Tse, C.; Shoemaker, A. R.; Adickes, J.; Anderson, M. G.; Chen, J.; Jin, S.; Johnson, E. F.; Marsh, K. C.; Mitten, M. J.; Nimmer, P.; Roberts, L.; Tahir, S. K.; Xiao, Y.; Yang, X.; Zhang, H.; Fesik, S.; Rosenberg, S. H.; Elmore, S. W., ABT-263: a potent and orally bioavailable Bcl-2 family inhibitor. *Cancer Res* **2008**, *68* (9), 3421-8.

89. Vogler, M.; Dinsdale, D.; Dyer, M. J.; Cohen, G. M., Bcl-2 inhibitors: small molecules with a big impact on cancer therapy. *Cell Death Differ* **2009**, *16* (3), 360-7.

90. Rudin, C. M.; Hann, C. L.; Garon, E. B.; Ribeiro de Oliveira, M.; Bonomi, P. D.; Camidge, D. R.; Chu, Q.; Giaccone, G.; Khaira, D.; Ramalingam, S. S.; Ranson, M. R.; Dive, C.; McKeegan, E. M.; Chyla, B. J.; Dowell, B. L.; Chakravarty, A.; Nolan, C. E.; Rudersdorf, N.; Busman, T. A.; Mabry, M. H.; Krivoshik, A. P.; Humerickhouse, R. A.; Shapiro, G. I.; Gandhi, L., Phase II Study of Single-Agent Navitoclax (ABT-263) and Biomarker Corelates in Patients with Relapsed Small Cell Lung Cancer. *Clin Cancer Res* **2012**, *18*, 909-916.

91. Gandhi, L.; Camidge, D. R.; Ribeiro de Oliveira, M.; Bonomi, P.; Gandara, D.; Khaira, D.; Hann, C. L.; McKeegan, E. M.; Litvinovich, E.; Hemken, P. M.; Dive, C.; Enschede, S. H.; Nolan, C.; Chiu, Y. L.; Busman, T.; Xiong, H.; Krivoshik, A. P.; Humerickhouse, R.; Shapiro, G. I.; Rudin, C. M., Phase I study of Navitoclax (ABT-263), a novel Bcl-2 family inhibitor, in patients with small-cell lung cancer and other solid

tumors. *J Clin Oncol* **2011**, *29* (7), 909-16.

92. Mason, K. D.; Carpinelli, M. R.; Fletcher, J. I.; Collinge, J. E.; Hilton, A. A.; Ellis, S.; Kelly, P. N.; Ekert, P. G.; Metcalf, D.; Roberts, A. W.; Huang, D. C.; Kile, B. T., Programmed anuclear cell death delimits platelet life span. *Cell* **2007**, *128* (6), 1173-86.

93. Zhang, H.; Nimmer, P. M.; Tahir, S. K.; Chen, J.; Fryer, R. M.; Hahn, K. R.; Iciek, L. A.; Morgan, S. J.; Nasarre, M. C.; Nelson, R.; Preusser, L. C.; Reinhart, G. A.; Smith, M. L.; Rosenberg, S. H.; Elmore, S. W.; Tse, C., Bcl-2 family proteins are essential for platelet survival. *Cell Death Differ* **2007**, *14* (5), 943-51.

94. Souers, A. J.; Levenson, J. D.; Boghaert, E. R.; Ackler, S. L.; Catron, N. D.; Chen, J.; Dayton, B. D.; Ding, H.; Enschede, S. H.; Fairbrother, W. J.; Huang, D. C.; Hymowitz, S. G.; Jin, S.; Khaw, S. L.; Kovar, P. J.; Lam, L. T.; Lee, J.; Maecker, H. L.; Marsh, K. C.; Mason, K. D.; Mitten, M. J.; Nimmer, P. M.; Oleksijew, A.; Park, C. H.; Park, C. M.; Phillips, D. C.; Roberts, A. W.; Sampath, D.; Seymour, J. F.; Smith, M. L.; Sullivan, G. M.; Tahir, S. K.; Tse, C.; Wendt, M. D.; Xiao, Y.; Xue, J. C.; Zhang, H.; Humerickhouse, R. A.; Rosenberg, S. H.; Elmore, S. W., ABT-199, a potent and selective BCL-2 inhibitor, achieves antitumor activity while sparing platelets. *Nat Med* **2013**, *19* (2), 202-8.

95. Rogers, K. A.; Byrd, J. C., Venetoclax Adds a New Arrow Targeting Relapsed CLL to the Quiver. *Cancer Cell* **2016**, *29* (1), 3-4.

96. Vandenberg, C. J.; Cory, S., ABT-199, a new Bcl-2-specific BH3 mimetic, has in vivo efficacy against aggressive Myc-driven mouse lymphomas without provoking thrombocytopenia. *Blood* **2013**, *121* (12), 2285-8.

97. Levenson, J. D.; Phillips, D. C.; Mitten, M. J.; Boghaert, E. R.; Diaz, D.; Tahir, S. K.; Belmont, L. D.; Nimmer, P.; Xiao, Y.; Ma, X. M.; Lowes, K. N.; Kovar, P.; Chen, J.; Jin, S.; Smith, M.; Xue, J.; Zhang, H.; Oleksijew, A.; Magoc, T. J.; Vaidya, K. S.; Albert, D. H.; Tarrant, J. M.; La, N.; Wang, L.; Tao, Z. F.; Wendt, M. D.; Sampath, D.; Rosenberg, S. H.; Tse, C.; DC, S. H.; Fairbrother, W. J.; Elmore, S. W.; Souers, A. J., Exploiting selective BCL-2 family inhibitors to dissect cell survival dependencies and define improved strategies for cancer therapy. *Science Transl Med* **2015**, *7* (279), 279ra40.

98. Mehrpour, M.; Codogno, P.; Chen, Q., Gossypol: from contraceptive for men to antitumoral activity. *Gastro Hepat* **2009**, *2*, 51-55.

99. Kitada, S.; Leone, M.; Sareth, S., Discovery, Characterization, and Structure-Activity-Relationship Studies of Proapoptotic Polyphenols Targeting B-Cell Lymphocyte/Leukemia-2 Proteins. *J Med Chem* **2003**, *46*, 4259-4264.

100. Xu, L.; Yang, D.; Wang, S., (-)-Gossypol enhances response to radiation therapy and results in tumor regression of human prostate cancer. *Am Assoc Cancer Res* **2005**, *4*, 267-275.

101. Zhang, M.; Liu, H.; Guo, R., Molecular mechanism of gossypol-induced cell growth inhibition and cell death of HT-29 human colon carcinoma cells. *Biochem Pharm* **2003**,

66, 93-103.

102. Oliver, C. L.; Miranda, M. B.; Shangary, S.; Land, S.; Wang, S.; Johnson, D. E., (-)-Gossypol acts directly on the mitochondria to overcome Bcl-2- and Bcl-X(L)-mediated apoptosis resistance. *Mol Cancer Ther* **2005**, *4* (1), 23-31.

103. Mohammad, R. M.; Wang, S.; Aboukameel, A.; Chen, B.; Wu, X.; Chen, J.; Al-Katib, A., Preclinical studies of a nonpeptidic small-molecule inhibitor of Bcl-2 and Bcl-X(L) [(-)-gossypol] against diffuse large cell lymphoma. *Mol Cancer Ther* **2005**, *4* (1), 13-21.

104. Wolter, K. G.; Wang, S. J.; Henson, B. S.; Wang, S.; Griffith, K. A.; Kumar, B.; Chen, J.; Carey, T. E.; Bradford, C. R.; D'Silva, N. J., (-)-gossypol inhibits growth and promotes apoptosis of human head and neck squamous cell carcinoma in vivo. *Neoplasia* **2006**, *8* (3), 163-72.

105. Zaidi, R.; Hadi, S. M., Complexes involving gossypol, DNA and Cu(II). *Biochem Int* **1992**, *28* (6), 1135-43.

106. Balakrishnan, K.; Wierda, W. G.; Keating, M. J.; Gandhi, V., Gossypol, a BH3 mimetic, induces apoptosis in chronic lymphocytic leukemia cells. *Blood* **2008**, *112* (5), 1971-80.

107. Pang, X.; Wu, Y.; Wu, Y.; Lu, B.; Chen, J.; Wang, J.; Yi, Z.; Qu, W.; Liu, M., (-)-Gossypol suppresses the growth of human prostate cancer xenografts via modulating VEGF signaling-mediated angiogenesis. *Mol Cancer Ther* **2011**, *10* (5), 795-805.

108. Bajwa, N.; Liao, C.; Nikolovska-Coleska, Z., Inhibitors of the anti-apoptotic Bcl-2 proteins: a patent review. *Expert Opin Ther Pat* **2012**, *22* (1), 37-55.

109. Mi, J. X.; Wang, G. F.; Wang, H. B.; Sun, X. Q.; Ni, X. Y.; Zhang, X. W.; Tang, J. M.; Yang, D. J., Synergistic antitumoral activity and induction of apoptosis by novel pan Bcl-2 proteins inhibitor apogossypolone with adriamycin in human hepatocellular carcinoma. *Acta Pharmacol Sin* **2008**, *29* (12), 1467-77.

110. Hu, Z. Y.; Zhu, X. F.; Zhong, Z. D.; Sun, J.; Wang, J.; Yang, D.; Zeng, Y. X., ApoG2, a novel inhibitor of antiapoptotic Bcl-2 family proteins, induces apoptosis and suppresses tumor growth in nasopharyngeal carcinoma xenografts. *Int J Cancer* **2008**, *123* (10), 2418-29.

111. Sun, Y.; Wu, J.; Aboukameel, A.; Banerjee, S.; Arnold, A. A.; Chen, J.; Nikolovska-Coleska, Z.; Lin, Y.; Ling, X.; Yang, D.; Wang, S.; Al-Katib, A.; Mohammad, R. M., Apogossypolone, a nonpeptidic small molecule inhibitor targeting Bcl-2 family proteins, effectively inhibits growth of diffuse large cell lymphoma cells in vitro and in vivo. *Cancer Biol Ther* **2008**, *7* (9), 1418-26.

112. Kitada, S.; Kress, C. L.; Krajewska, M.; Jia, L.; Pellecchia, M.; Reed, J. C., Bcl-2 antagonist apogossypol (NSC736630) displays single-agent activity in Bcl-2-transgenic

mice and has superior efficacy with less toxicity compared with gossypol (NSC19048). *Blood* **2008**, *111* (6), 3211-9.

113. Wang, G.; Nikolovska-Coleska, Z.; Yang, C. Y.; Wang, R.; Tang, G.; Guo, J.; Shangary, S.; Qiu, S.; Gao, W.; Yang, D.; Meagher, J.; Stuckey, J.; Krajewski, K.; Jiang, S.; Roller, P. P.; Abaan, H. O.; Tomita, Y.; Wang, S., Structure-based design of potent small-molecule inhibitors of anti-apoptotic Bcl-2 proteins. *J Med Chem* **2006**, *49* (21), 6139-42.

114. Zhai, D.; Jin, C.; Satterthwait, A. C.; Reed, J. C., Comparison of chemical inhibitors of antiapoptotic Bcl-2-family proteins. *Cell Death Differ* **2006**, *13* (8), 1419-21.

115. Perez-Galan, P.; Roue, G.; Villamor, N.; Campo, E.; Colomer, D., The BH3-mimetic GX15-070 synergizes with bortezomib in mantle cell lymphoma by enhancing Noxa-mediated activation of Bak. *Blood* **2007**, *109* (10), 4441-9.

116. Li, J.; Viallet, J.; Haura, E. B., A small molecule pan-Bcl-2 family inhibitor, GX15-070, induces apoptosis and enhances cisplatin-induced apoptosis in non-small cell lung cancer cells. *Cancer Chemother Pharmacol* **2008**, *61* (3), 525-34.

117. Trudel, S.; Li, Z. H.; Rauw, J.; Tiedemann, R. E.; Wen, X. Y.; Stewart, A. K., Preclinical studies of the pan-Bcl inhibitor obatoclax (GX015-070) in multiple myeloma. *Blood* **2007**, *109* (12), 5430-8.

118. Konopleva, M.; Watt, J.; Contractor, R.; Tsao, T.; Harris, D.; Estrov, Z.; Bornmann, W.; Kantarjian, H.; Viallet, J.; Samudio, I.; Andreeff, M., Mechanisms of antileukemic activity of the novel Bcl-2 homology domain-3 mimetic GX15-070 (obatoclax). *Cancer Res* **2008**, *68* (9), 3413-20.

119. Vogler, M.; Weber, K.; Dinsdale, D.; Schmitz, I.; Schulze-Osthoff, K.; Dyer, M. J.; Cohen, G. M., Different forms of cell death induced by putative BCL2 inhibitors. *Cell Death Differ* **2009**, *16* (7), 1030-9.

120. Schimmer, A. D.; O'Brien, S.; Kantarjian, H.; Brandwein, J.; Cheson, B. D.; Minden, M. D.; Yee, K.; Ravandi, F.; Giles, F.; Schuh, A.; Gupta, V.; Andreeff, M.; Koller, C.; Chang, H.; Kamel-Reid, S.; Berger, M.; Viallet, J.; Borthakur, G., A phase I study of the pan bcl-2 family inhibitor obatoclax mesylate in patients with advanced hematologic malignancies. *Clin Cancer Res* **2008**, *14* (24), 8295-301.

121. Paik, P. K.; Rudin, C. M.; Brown, A.; Rizvi, N. A.; Takebe, N.; Travis, W.; James, L.; Ginsberg, M. S.; Juergens, R.; Markus, S.; Tyson, L.; Subzwari, S.; Kris, M. G.; Krug, L. M., A phase I study of obatoclax mesylate, a Bcl-2 antagonist, plus topotecan in solid tumor malignancies. *Cancer Chemother Pharmacol* **2010**, *66* (6), 1079-85.

122. Vogler, M., Targeting BCL2-Proteins for the Treatment of Solid Tumours. *Adv Med* **2014**, *2014*, 943648.

123. Wertz, I. E.; Kusam, S.; Lam, C.; Okamoto, T.; Sandoval, W.; Anderson, D. J.;

Helgason, E.; Ernst, J. A.; Eby, M.; Liu, J.; Belmont, L. D.; Kaminker, J. S.; O'Rourke, K. M.; Pujara, K.; Kohli, P. B.; Johnson, A. R.; Chiu, M. L.; Lill, J. R.; Jackson, P. K.; Fairbrother, W. J.; Seshagiri, S.; Ludlam, M. J.; Leong, K. G.; Dueber, E. C.; Maecker, H.; Huang, D. C.; Dixit, V. M., Sensitivity to antitubulin chemotherapeutics is regulated by MCL1 and FBW7. *Nature* **2011**, *471* (7336), 110-4.

124. Beroukhi, R.; Mermel, C. H.; Porter, D.; Wei, G.; Raychaudhuri, S.; Donovan, J.; Barretina, J.; Boehm, J. S.; Dobson, J.; Urashima, M.; Mc Henry, K. T.; Pinchback, R. M.; Ligon, A. H.; Cho, Y. J.; Haery, L.; Greulich, H.; Reich, M.; Winckler, W.; Lawrence, M. S.; Weir, B. A.; Tanaka, K. E.; Chiang, D. Y.; Bass, A. J.; Loo, A.; Hoffman, C.; Prensner, J.; Liefeld, T.; Gao, Q.; Yecies, D.; Signoretti, S.; Maher, E.; Kaye, F. J.; Sasaki, H.; Tepper, J. E.; Fletcher, J. A.; Taberero, J.; Baselga, J.; Tsao, M. S.; Demichelis, F.; Rubin, M. A.; Janne, P. A.; Daly, M. J.; Nucera, C.; Levine, R. L.; Ebert, B. L.; Gabriel, S.; Rustgi, A. K.; Antonescu, C. R.; Ladanyi, M.; Letai, A.; Garraway, L. A.; Loda, M.; Beer, D. G.; True, L. D.; Okamoto, A.; Pomeroy, S. L.; Singer, S.; Golub, T. R.; Lander, E. S.; Getz, G.; Sellers, W. R.; Meyerson, M., The landscape of somatic copy-number alteration across human cancers. *Nature* **2010**, *463* (7283), 899-905.

125. Wei, G.; Margolin, A. A.; Haery, L.; Brown, E.; Cucolo, L.; Julian, B.; Shehata, S.; Kung, A. L.; Beroukhi, R.; Golub, T. R., Chemical genomics identifies small-molecule MCL1 repressors and BCL-xL as a predictor of MCL1 dependency. *Cancer Cell* **2012**, *21* (4), 547-62.

126. Petros, A. M.; Dinges, J.; Augeri, D. J.; Baumeister, S. A.; Betebenner, D. A.; Bures, M. G.; Elmore, S. W.; Hajduk, P. J.; Joseph, M. K.; Landis, S. K.; Nettlesheim, D. G.; Rosenberg, S. H.; Shen, W.; Thomas, S.; Wang, X.; Zanze, I.; Zhang, H.; Fesik, S. W., Discovery of a potent inhibitor of the antiapoptotic protein Bcl-xL from NMR and parallel synthesis. *J Med Chem* **2006**, *49* (2), 656-63.

127. Levenson, J. D.; Zhang, H.; Chen, J.; Tahir, S. K.; Phillips, D. C.; Xue, J.; Nimmer, P.; Jin, S.; Smith, M.; Xiao, Y.; Kovar, P.; Tanaka, A.; Bruncko, M.; Sheppard, G. S.; Wang, L.; Gierke, S.; Kategaya, L.; Anderson, D. J.; Wong, C.; Eastham-Anderson, J.; Ludlam, M. J.; Sampath, D.; Fairbrother, W. J.; Wertz, I.; Rosenberg, S. H.; Tse, C.; Elmore, S. W.; Souers, A. J., Potent and selective small-molecule MCL-1 inhibitors demonstrate on-target cancer cell killing activity as single agents and in combination with ABT-263 (navitoclax). *Cell Death Dis* **2015**, *6*, e1590.

128. Bruncko, M.; Wang, L.; Sheppard, G. S.; Phillips, D. C.; Tahir, S. K.; Xue, J.; Erickson, S.; Fidanze, S.; Fry, E.; Hasvold, L.; Jenkins, G. J.; Jin, S.; Judge, R. A.; Kovar, P. J.; Madar, D.; Nimmer, P.; Park, C.; Petros, A. M.; Rosenberg, S. H.; Smith, M. L.; Song, X.; Sun, C.; Tao, Z. F.; Wang, X.; Xiao, Y.; Zhang, H.; Tse, C.; Levenson, J. D.; Elmore, S. W.; Souers, A. J., Structure-Guided Design of a Series of MCL-1 Inhibitors with High Affinity and Selectivity. *J Med Chem* **2015**, *58* (5), 2180-94.

129. Bruncko, M.; Wang, L.; Sheppard, G. S.; Phillips, D. C.; Tahir, S. K.; Xue, J.; Erickson, S.; Fidanze, S.; Fry, E.; Hasvold, L.; Jenkins, G. J.; Jin, S.; Judge, R. A.; Kovar, P. J.; Madar, D.; Nimmer, P.; Park, C.; Petros, A. M.; Rosenberg, S. H.; Smith, M. L.;

Song, X.; Sun, C.; Tao, Z. F.; Wang, X.; Xiao, Y.; Zhang, H.; Tse, C.; Levenson, J. D.; Elmore, S. W.; Souers, A. J., Correction to Structure-Guided Design of a Series of MCL-1 Inhibitors with High Affinity and Selectivity. *J Med Chem* **2015**, *58* (9), 4089.

130. Pelz, N. F.; Bian, Z.; Zhao, B.; Shaw, S.; Tarr, J. C.; Belmar, J.; Gregg, C.; Camper, D. V.; Goodwin, C. M.; Arnold, A. L.; Sensintaffar, J. L.; Friberg, A.; Rossanese, O. W.; Lee, T.; Olejniczak, E. T.; Fesik, S. W., Discovery of 2-Indole-acylsulfonamide Myeloid Cell Leukemia 1 (Mcl-1) Inhibitors Using Fragment-Based Methods. *J Med Chem* **2016**, *59* (5), 2054-66.

131. Lee, T.; Bian, Z.; Zhao, B.; Hogdal, L. J.; Sensintaffar, J. L.; Goodwin, C. M.; Belmar, J.; Shaw, S.; Tarr, J. C.; Veerasamy, N.; Matulis, S. M.; Koss, B.; Fischer, M. A.; Arnold, A. L.; Camper, D. V.; Browning, C. F.; Rossanese, O. W.; Budhraj, A.; Opferman, J.; Boise, L. H.; Savona, M. R.; Letai, A.; Olejniczak, E. T.; Fesik, S. W., Discovery and biological characterization of potent myeloid cell leukemia-1 inhibitors. *FEBS Lett* **2017**, *591* (1), 240-251.

132. Burke, J. P.; Bian, Z.; Shaw, S.; Zhao, B.; Goodwin, C. M.; Belmar, J.; Browning, C. F.; Vigil, D.; Friberg, A.; Camper, D. V.; Rossanese, O. W.; Lee, T.; Olejniczak, E. T.; Fesik, S. W., Discovery of tricyclic indoles that potently inhibit Mcl-1 using fragment-based methods and structure-based design. *J Med Chem* **2015**, *58* (9), 3794-805.

133. Abulwerdi, F.; Liao, C.; Liu, M.; Azmi, A. S.; Aboukameel, A.; Mady, A. S.; Gulappa, T.; Cierpicki, T.; Owens, S.; Zhang, T.; Sun, D.; Stuckey, J. A.; Mohammad, R. M.; Nikolovska-Coleska, Z., A novel small-molecule inhibitor of mcl-1 blocks pancreatic cancer growth in vitro and in vivo. *Mol Cancer Ther* **2014**, *13* (3), 565-75.

134. Chen, L.; Fletcher, S., Mcl-1 inhibitors: a patent review. *Expert Opin Ther Pat* **2017**, *27* (2), 163-178.

135. Koehler, M. F.; Bergeron, P.; Choo, E. F.; Lau, K.; Ndubaku, C.; Dudley, D.; Gibbons, P.; Sleebs, B. E.; Rye, C. S.; Nikolakopoulos, G.; Bui, C.; Kulasegaram, S.; Kersten, W. J.; Smith, B. J.; Czabotar, P. E.; Colman, P. M.; Huang, D. C.; Baell, J. B.; Watson, K. G.; Hasvold, L.; Tao, Z. F.; Wang, L.; Souers, A. J.; Elmore, S. W.; Flygare, J. A.; Fairbrother, W. J.; Lessene, G., Structure-Guided Rescaffolding of Selective Antagonists of BCL-XL. *ACS Med Chem Lett* **2014**, *5* (6), 662-7.

136. Weber, G., Polarization of the fluorescence of macromolecules I. Theory and experimental method. *Biochem J* **1952**, *51*, 145-155.

137. Jameson, D. M.; Mocz, G., Fluorescence polarization/anisotropy approaches to study protein-ligand interactions: Effects of errors and uncertainties. *Methods Mol Biol* **2005**, *305*, 301-322.

138. Jameson, D. M.; Sawyer, W. H., Fluorescence anisotropy applied to biomolecular interactions. *Methods Enzym* **1995**, *246*, 283-300.

139. Jameson, D. M.; Seifried, S. E., Quantification of protein-protein interactions using

fluorescence polarization. *Methods* **1999**, *19*, 222-233.

140. Jameson, D. M., Introduction to Fluorescence. *CRC Press* **2014**, 75-100.

141. Adams, J. M.; Cory, S., The Bcl-2 apoptotic switch in cancer development and therapy. *Oncogene* **2007**, *26* (9), 1324-37.

142. Wang, S., The promise of cancer therapeutics targeting the TNF-related apoptosis-inducing ligand and TRAIL receptor pathway. *Oncogene* **2008**, *27* (48), 6207-15.

143. Billard, C., BH3 mimetics: status of the field and new developments. *MolCancer Ther* **2013**, *12* (9), 1691-700.

144. Wilson, W. H.; O'Connor, O. A.; Czuczman, M. S.; LaCasce, A. S.; Gerecitano, J. F.; Leonard, J. P.; Tulpule, A.; Dunleavy, K.; Xiong, H.; Chiu, Y. L.; Cui, Y.; Busman, T.; Elmore, S. W.; Rosenberg, S. H.; Krivoschik, A. P.; Enschede, S. H.; Humerickhouse, R. A., Navitoclax, a targeted high-affinity inhibitor of BCL-2, in lymphoid malignancies: a phase 1 dose-escalation study of safety, pharmacokinetics, pharmacodynamics, and antitumour activity. *Lancet Oncol* **2010**, *11* (12), 1149-59.

145. Roberts, A. W.; Seymour, J. F.; Brown, J. R.; Wierda, W. G.; Kipps, T. J.; Khaw, S. L.; Carney, D. A.; He, S. Z.; Huang, D. C.; Xiong, H.; Cui, Y.; Busman, T. A.; McKeegan, E. M.; Krivoschik, A. P.; Enschede, S. H.; Humerickhouse, R., Substantial susceptibility of chronic lymphocytic leukemia to BCL2 inhibition: results of a phase I study of navitoclax in patients with relapsed or refractory disease. *J Clin Oncol* **2012**, *30* (5), 488-96.

146. Warr, M. R.; Shore, G. C., Unique biology of Mcl-1: therapeutic opportunities in cancer. *Curr Mol Med* **2008**, *8* (2), 138-47.

147. Backus, H. H.; van Riel, J. M.; van Groeningen, C. J.; Vos, W.; Dukers, D. F.; Bloemena, E.; Wouters, D.; Pinedo, H. M.; Peters, G. J., Rb, Mcl-1 and p53 Expression Correlate with Clinical Outcome in Patients with Liver Metastases from Colorectal Cancer. *Ann Oncol* **2001**, *12*, 779-785.

148. Song, L.; Coppola, D.; Livingston, S.; Cress, D.; Haura, E. B., Mcl-1 regulates survival and sensitivity to diverse apoptotic stimuli in human non-small cell lung cancer cells. *Cancer Biol Ther* **2005**, *4* (3), 267-76.

149. Ding, Q.; He, X.; Xia, W.; Hsu, J. M.; Chen, C. T.; Li, L. Y.; Lee, D. F.; Yang, J. Y.; Xie, X.; Liu, J. C.; Hung, M. C., Myeloid cell leukemia-1 inversely correlates with glycogen synthase kinase-3beta activity and associates with poor prognosis in human breast cancer. *Cancer Res* **2007**, *67* (10), 4564-71.

150. Y, M.; R, H.; M, W.; JU, L.; T, K.; K, F.; S, T.; S, N.; R, D.; M, K.; Y, S.; M, I., Immunohistochemical Analysis of Bcl-2, Bak, Bcl-x, and Mcl-1 Expression in pancreatic Cancers. *Oncology* **1998**, *56*, 73-82.

151. Zhang, T.; Zhao, C.; Luo, L.; Zhao, H.; Cheng, J.; Xu, F., The expression of Mcl-1 in human cervical cancer and its clinical significance. *Med Oncol* **2012**, *29* (3), 1985-91.
152. Brotin, E.; Meryet-Figuere, M.; Simonin, K.; Duval, R. E.; Villedieu, M.; Leroy-Dudal, J.; Saison-Behmoaras, E.; Gauduchon, P.; Denoyelle, C.; Poulain, L., Bcl-XL and MCL-1 constitute pertinent targets in ovarian carcinoma and their concomitant inhibition is sufficient to induce apoptosis. *Int J Cancer* **2010**, *126* (4), 885-95.
153. Glaser, S. P.; Lee, E. F.; Trounson, E.; Bouillet, P.; Wei, A.; Fairlie, W. D.; Izon, D. J.; Zuber, J.; Rappaport, A. R.; Herold, M. J.; Alexander, W. S.; Lowe, S. W.; Robb, L.; Strasser, A., Anti-apoptotic Mcl-1 is essential for the development and sustained growth of acute myeloid leukemia. *Genes Dev* **2012**, *26* (2), 120-5.
154. Wenzel, S. S.; Grau, M.; Mavis, C.; Hailfinger, S.; Wolf, A.; Madle, H.; Deeb, G.; Dorken, B.; Thome, M.; Lenz, P.; Dirnhofner, S.; Hernandez-Ilizaliturri, F. J.; Tzankov, A.; Lenz, G., MCL1 is deregulated in subgroups of diffuse large B-cell lymphoma. *Leukemia* **2013**, *27* (6), 1381-90.
155. Chen, S.; Dai, Y.; Harada, H.; Dent, P.; Grant, S., Mcl-1 down-regulation potentiates ABT-737 lethality by cooperatively inducing Bak activation and Bax translocation. *Cancer Res* **2007**, *67* (2), 782-91.
156. Wei, S. H.; Dong, K.; Lin, F.; Wang, X.; Li, B.; Shen, J. J.; Zhang, Q.; Wang, R.; Zhang, H. Z., Inducing apoptosis and enhancing chemosensitivity to gemcitabine via RNA interference targeting Mcl-1 gene in pancreatic carcinoma cell. *Cancer Chemother Pharmacol* **2008**, *62* (6), 1055-64.
157. Cohen, N. A.; Stewart, M. L.; Gavathiotis, E.; Tepper, J. L.; Bruekner, S. R.; Koss, B.; Opferman, J. T.; Walensky, L. D., A competitive stapled peptide screen identifies a selective small molecule that overcomes MCL-1-dependent leukemia cell survival. *Chem Biol* **2012**, *19* (9), 1175-86.
158. Zhang, Z.; Liu, C.; Li, X.; Song, T.; Wu, Z.; Liang, X.; Zhao, Y.; Shen, X.; Chen, H., Fragment-based design, synthesis, and biological evaluation of N-substituted-5-(4-isopropylthiophenyl)-2-hydroxynicotinamide derivatives as novel Mcl-1 inhibitors. *Eur J Med Chem* **2013**, *60*, 410-20.
159. Zhang, Z.; Song, T.; Li, X.; Wu, Z.; Feng, Y.; Xie, F.; Liu, C.; Qin, J.; Chen, H., Novel soluble myeloid cell leukemia sequence 1 (Mcl-1) inhibitor (E,E)-2-(benzylaminocarbonyl)-3-styrylacrylonitrile (4g) developed using a fragment-based approach. *Eur J Med Chem* **2013**, *59*, 141-9.
160. Ding, X.; Li, Y.; Lv, L.; Zhou, M.; Han, L.; Zhang, Z.; Ba, Q.; Li, J.; Wang, H.; Liu, H.; Wang, R., De novo design, synthesis and evaluation of benzylpiperazine derivatives as highly selective binders of Mcl-1. *ChemMedChem* **2013**, *8* (12), 1986-2014.
161. Richard, D. J.; Lena, R.; Bannister, T.; Blake, N.; Pierceall, W. E.; Carlson, N. E.; Keller, C. E.; Koenig, M.; He, Y.; Minond, D.; Mishra, J.; Cameron, M.; Spicer, T.;

- Hodder, P.; Cardone, M. H., Hydroxyquinoline-derived compounds and analoguing of selective Mcl-1 inhibitors using a functional biomarker. *Bioorg Med Chem* **2013**, *21* (21), 6642-9.
162. Chen, L.; Lanning, M. E.; Fletcher, S., Small Molecule Inhibitors of the Mcl-1 Oncoprotein. *Austin J Anal Pharm Chem* **2014**, *1* (3).
163. Murayama, R. S., K.; Kawakami, S. Polymerizable Monomer, Polymeric Compound, Charge Control Agent Containing the Polymeric Compound, and Developer Bearing Member and Toner Which Contain the Charge Control Agent.
164. Guvench, O.; MacKerell, A. D., Jr., Computational fragment-based binding site identification by ligand competitive saturation. *PLoS Comput Biol* **2009**, *5* (7), e1000435.
165. Raman, E. P.; Yu, W.; Guvench, O.; Mackerell, A. D., Reproducing crystal binding modes of ligand functional groups using Site-Identification by Ligand Competitive Saturation (SILCS) simulations. *J Chem Inf Model* **2011**, *51* (4), 877-96.
166. Raman, E. P.; Yu, W.; Lakkaraju, S. K.; MacKerell, A. D., Jr., Inclusion of multiple fragment types in the site identification by ligand competitive saturation (SILCS) approach. *J Chem Inf Model* **2013**, *53* (12), 3384-98.
167. Yu, W.; Lakkaraju, S. K.; Raman, E. P.; MacKerell, A. D., Jr., Site-Identification by Ligand Competitive Saturation (SILCS) assisted pharmacophore modeling. *J Comput Aided Mol Des* **2014**, *28* (5), 491-507.
168. Yu, W.; Lakkaraju, S. K.; Raman, E. P.; Fang, L.; MacKerell, A. D., Jr., Pharmacophore Modeling Using Site-Identification by Ligand Competitive Saturation (SILCS) with Multiple Probe Molecules. *J Chem Inf Model* **2015**, *55* (2), 407-20.
169. Zhang, H.; Nimmer, P.; Rosenberg, S. H.; Ng, S.; Joseph, M. K., Development of a High-Throughput Fluorescence Polarization Assay for Bcl-xL. *Anal Biochem* **2002**, *307*, 70-75.
170. Nikolovska-Coleska, Z.; Wang, R.; Fang, X.; Pan, H.; Tomita, Y.; Li, P.; Roller, P. P.; Krajewski, K.; Saito, N. G.; Stuckey, J. A.; Wang, S., Development and optimization of a binding assay for the XIAP BIR3 domain using fluorescence polarization. *Anal Biochem* **2004**, *332* (2), 261-73.
171. Pearlman, D. A.; Charifson, P. S., Are free energy calculations useful in practice? A comparison with rapid scoring functions for the p38 MAP kinase protein system. *J Med Chem* **2001**, *44* (21), 3417-23.
172. Yang, C. Y.; Wang, S., Analysis of Flexibility and Hotspots in Bcl-xL and Mcl-1 Proteins for the Design of Selective Small-Molecule Inhibitors. *ACS Med Chem Lett* **2012**, *3* (4), 308-12.
173. McKee, C. S.; Hill, D. S.; Redfern, C. P.; Armstrong, J. L.; Lovat, P. E., Oncogenic

BRAF signalling increases Mcl-1 expression in cutaneous metastatic melanoma. *Exp Dermatol* **2013**, *22* (11), 767-9.

174. Wang, H.; Chauhan, J.; Hu, A.; Pendleton, K.; Yap, J. L.; Sabato, P. E.; Jones, J. W.; Perri, M.; Yu, J.; Cione, E.; Kane, M. A.; Fletcher, S.; Prochownik, E. V., Disruption of Myc-Max heterodimerization with improved cell-penetrating analogs of the small molecule 10074-G5. *Oncotarget* **2013**, *4* (6), 936-47.

175. Word, J. M.; Lovell, S. C.; Richardson, J. S.; Richardson, D. C., Asparagine and glutamine: using hydrogen atom contacts in the choice of side-chain amide orientation. *J Mol Biol* **1999**, *285* (4), 1735-47.

176. Van Der Spoel, D.; Lindahl, E.; Hess, B.; Groenhof, G.; Mark, A. E.; Berendsen, H. J., GROMACS: fast, flexible, and free. *J Comput Chem* **2005**, *26* (16), 1701-18.

177. Best, R. B.; Zhu, X.; Shim, J.; Lopes, P. E.; Mittal, J.; Feig, M.; Mackerell, A. D., Jr., Optimization of the additive CHARMM all-atom protein force field targeting improved sampling of the backbone phi, psi and side-chain chi(1) and chi(2) dihedral angles. *J Chem Theory Comput* **2012**, *8* (9), 3257-3273.

178. Vanommeslaeghe, K.; Hatcher, E.; Acharya, C.; Kundu, S.; Zhong, S.; Shim, J.; Darian, E.; Guvench, O.; Lopes, P.; Vorobyov, I.; Mackerell, A. D., Jr., CHARMM general force field: A force field for drug-like molecules compatible with the CHARMM all-atom additive biological force fields. *J Comput Chem* **2010**, *31* (4), 671-90.

179. Yu, W.; He, X.; Vanommeslaeghe, K.; MacKerell, A. D., Jr., Extension of the CHARMM General Force Field to sulfonyl-containing compounds and its utility in biomolecular simulations. *J Comput Chem* **2012**, *33* (31), 2451-68.

180. Jorgensen, W. L.; Chandrasekhar, J.; Madura, J. D.; Impey, R. W.; Klein, M. L., Comparison of simple potential functions for simulating liquid water. *J Chem Phys* **1983**, *79*, 926-935.

181. Molecular Operating Environment (MOE), V., Chemical ; Computing Group Inc., M., Canada, 2012.

182. Percec, V.; Okita, S.; Wang, J. H., Synthesis of aromatic polyethers by scholl reaction. vi. aromatic polyethers by cation-radical polymerization of 4,4'-, 3,3'-, and 2,2'-bis(1-naphthoxy)biphenyls and of 1,3-bis(1-naphthoxy)benzene. *Macromolecules* **1992**, *25*, 64-74.

183. Szajnman, S. H.; Yan, W.; Bailey, B. N.; Docampo, R.; Elhalem, E.; Rodriguez, J. B., Design and synthesis of aryloxyethyl thiocyanate derivatives as potent inhibitors of Trypanosoma cruzi proliferation. *J Med Chem* **2000**, *43* (9), 1826-40.

184. Raiford, L. C.; Thiessen, G. W.; Wernert, I. J., Some derivatives of diphenyl ether. *J Am Chem Soc* **1930**, *52*, 1205-1209.

185. Marion, D.; Driscoll, P. C.; Kay, L. E.; Wingfield, P. T.; Bax, A.; Gronenborn, A. M.; Clore, G. M., Overcoming the overlap problem in the assignment of ^1H NMR spectra of larger proteins by use of three-dimensional heteronuclear ^1H - ^{15}N Hartmann-Hahn-multiple quantum coherence and nuclear Overhauser-multiple quantum coherence spectroscopy: application to interleukin 1 beta. *Biochem* **1989**, *28* (15), 6150-6.
186. Bax, A.; Ikura, M., An efficient 3D NMR technique for correlating the proton and ^{15}N backbone amide resonances with the alpha-carbon of the preceding residue in uniformly $^{15}\text{N}/^{13}\text{C}$ enriched proteins. *J Biomol NMR* **1991**, *1* (1), 99-104.
187. Delaglio, F.; Grzesiek, S.; Vuister, G. W.; Zhu, G.; Pfeifer, J.; Bax, A., NMRPipe: a multidimensional spectral processing system based on UNIX pipes. *J Biomol NMR* **1995**, *6* (3), 277-93.
188. Edison, A. S.; Abildgaard, F.; Westler, W. M.; Mooberry, E. S.; Markley, J. L., Practical introduction to theory and implementation of multinuclear, multidimensional nuclear magnetic resonance experiments. *Methods Enzym* **1994**, *239*, 3-79.
189. Spera, S.; Ikura, M.; Bax, A., Measurement of the exchange rates of rapidly exchanging amide protons: application to the study of calmodulin and its complex with a myosin light chain kinase fragment. *J Biomol NMR* **1991**, *1* (2), 155-65.
190. Mori, S.; Abeygunawardana, C.; Johnson, M. O.; van Zijl, P. C., Improved sensitivity of HSQC spectra of exchanging protons at short interscan delays using a new fast HSQC (FHSQC) detection scheme that avoids water saturation. *J Magn Reson B* **1995**, *108* (1), 94-8.
191. Lee, L. C.; Maurice, D. H.; Baillie, G. S., Targeting protein-protein interactions within the cyclic AMP signaling system as a therapeutic strategy for cardiovascular disease. *Future Med Chem* **2013**, *5* (4), 451-64.
192. Falchi, F.; Caporuscio, F.; Recanatini, M., Structure-based design of small-molecule protein-protein interaction modulators: the story so far. *FutureMed Chem* **2014**, *6* (3), 343-57.
193. Silvian, L.; Enyedy, I.; Kumaravel, G., Inhibitors of protein-protein interactions: new methodologies to tackle this challenge. *Drug Discov Today Technol* **2013**, *10* (4), e509-15.
194. London, N.; Raveh, B.; Schueler-Furman, O., Druggable protein-protein interactions--from hot spots to hot segments. *Curr Opin Chem Biol* **2013**, *17* (6), 952-9.
195. Vassilev, L. T.; Vu, B. T.; Graves, B.; Carvajal, D.; Podlaski, F.; Filipovic, Z.; Kong, N.; Kammlott, U.; Lukacs, C.; Klein, C.; Fotouhi, N.; Liu, E. A., In vivo activation of the p53 pathway by small-molecule antagonists of MDM2. *Science* **2004**, *303* (5659), 844-8.
196. Davis, J. M.; Tsou, L. K.; Hamilton, A. D., Synthetic non-peptide mimetics of

alpha-helices. *Chem Soc Rev* **2007**, 36 (2), 326-34.

197. Cummings, C. G.; Hamilton, A. D., Disrupting protein-protein interactions with non-peptidic, small molecule alpha-helix mimetics. *Curr Opin Chem Biol* **2010**, 14 (3), 341-346.

198. Azzarito, V.; Long, K.; Murphy, N. S.; Wilson, A. J., Inhibition of alpha-helix-mediated protein-protein interactions using designed molecules. *Nat Chem* **2013**, 5 (3), 161-73.

199. Lanning, M. E.; Fletcher, S., Recapitulating the alpha-helix: nonpeptidic, low-molecular-weight ligands for the modulation of helix-mediated protein-protein interactions. *Future Med Chem* **2013**, 5 (18), 2157-74.

200. Jayatunga, M. K.; Thompson, S.; Hamilton, A. D., alpha-Helix mimetics: outwards and upwards. *Bioorg Med Chem Lett* **2014**, 24 (3), 717-24.

201. Yin, H.; Lee, G. I.; Sedey, K. A.; Kutzki, O.; Park, H. S.; Orner, B. P.; Ernst, J. T.; Wang, H. G.; Sebti, S. M.; Hamilton, A. D., Terphenyl-Based Bak BH3 alpha-helical proteomimetics as low-molecular-weight antagonists of Bcl-xL. *J Am Chem Soc* **2005**, 127 (29), 10191-10196.

202. Barnard, A.; Long, K.; Martin, H. L.; Miles, J. A.; Edwards, T. A.; Tomlinson, D. C.; Macdonald, A.; Wilson, A. J., Selective and Potent Proteomimetic Inhibitors of Intracellular Protein-Protein Interactions. *Angew Chem Weinheim Bergstr Ger* **2015**, 127 (10), 3003-3008.

203. Volonterio, A.; Moisan, L.; Rebek, J., Jr., Synthesis of pyridazine-based scaffolds as alpha-helix mimetics. *Org Lett* **2007**, 9 (19), 3733-6.

204. Cummings, C. G.; Ross, N. T.; Katt, W. P.; Hamilton, A. D., Synthesis and biological evaluation of a 5-6-5 imidazole-phenyl-thiazole based alpha-helix mimetic. *Org Lett* **2009**, 11 (1), 25-8.

205. Prabhakaran, P.; Barnard, A.; Murphy, N. S.; Kilner, C. A.; Edwards, T. A.; Wilson, A. J., Aromatic Oligoamide Foldamers with a "Wet Edge" as Inhibitors of the α -Helix-Mediated p53-hDM2 Protein-Protein Interaction. *Eur J Org Chem* **2013**, 2013 (17), 3504-3512.

206. Bose, P.; Grant, S., Mcl-1 as a Therapeutic Target in Acute Myelogenous Leukemia (AML). *Leuk Res Rep* **2013**, 2 (1), 12-14.

207. Plante, J. P.; Burnley, T.; Malkova, B.; Webb, M. E.; Warriner, S. L.; Edwards, T. A.; Wilson, A. J., Oligobenzamide proteomimetic inhibitors of the p53-hDM2 protein-protein interaction. *Chem Commun* **2009**, (34), 5091-3.

208. Fletcher, S.; Shahani, V. M.; Lough, A. J.; Gunning, P. T., Concise access to N9-mono-, N2-mono- and N2,N9-di-substituted guanines via efficient Mitsunobu reactions.

Tetrahedron **2010**, *66* (25), 4621-4632.

209. Kussie, P. H.; Gorina, S.; Marechal, V.; Elenbaas, B.; Moreau, J.; Levine, A. J.; Pavletich, N. P., Structure of the MDM2 oncoprotein bound to the p53 tumor suppressor transactivation domain. *Science* **1996**, *274* (5289), 948-53.

210. Azzarito, V.; Miles, J. A.; Fisher, J.; Edwards, T. A.; Warriner, S. L.; Wilson, A. J., Stereocontrolled protein surface recognition using chiral oligoamide proteomimetic foldamers. *Chem Sci* **2015**, *6* (4), 2434-2443.

211. Czabotar, P. E.; Lee, E. F.; Thompson, G. V.; Wardak, A. Z.; Fairlie, W. D.; Colman, P. M., Mutation to Bax beyond the BH3 domain disrupts interactions with pro-survival proteins and promotes apoptosis. *J Biol Chem* **2011**, *286* (9), 7123-31.

212. Popowicz, G. M.; Czarna, A.; Holak, T. A., Structure of the human Mdmx protein bound to the p53 tumor suppressor transactivation domain. *Cell Cycle* **2008**, *7* (15), 2441-3.

213. Zhang, J. H.; Chung, T. D. Y.; Oldenburg, K. R., A Simple Statistical Parameter for Use in Evaluation and Validation of High Throughput Screening Assays. *J Biomol Screen* **1999**, *4* (2), 67-73.

214. Mitsunobu, O., The use of diethyl azodicarboxylate and triphenylphosphine in synthesis and transformation of natural products. *Synthesis* **1981**, *1*, 1-28.

215. Mitsunobu, O.; Eguchi, M., Preparation of carboxylic esters and phosphoric esters by the activation of alcohols. *Bull Chem Soc Jpn* **1971**, *44*, 3427-3430.

216. Mitsunobu, O.; Yamada, M.; Mukaiyama, T., Preparation of esters of phosphoric acid by the reaction of trivalent phosphorus compounds with diethyl azodicarboxylate in the presence of alcohols. *Bull Chem Soc Jpn* **1967**, *40*, 935-939.

217. Swamy, K. C.; Kumar, N. N.; Balaraman, E.; Kumar, K. V., Mitsunobu and related reactions: advances and applications. *Chem Rev* **2009**, *109* (6), 2551-651.

218. Fletcher, S., Regioselective alkylation of the exocyclic nitrogen of adenine and adenosine by the Mitsunobu reaction. *Tetrahedron Lett* **2010**, *51* (22), 2948-2950.

219. Jung, K.-Y.; Fletcher, S., Fine-tuning the chemo- and regioselective alkylation of 1,4-benzodiazepines: further applications of the Mitsunobu reaction. *Med Chem Commun* **2012**, *3*, 1160.

220. Moroder, L.; Gobbo, M.; Becker, G.; Wunsch, E., Synthesis of thiol-functionalized N-acetylmuramyl peptide congeners suitable for their conjugation to target molecules. *Biol Chem Hoppe Seyler* **1989**, *370* (4), 365-75.

221. Parsons, P. J.; Charles, M. D.; Harvey, D. M.; Sumoreeah, L. R.; Shell, A.; Spoor, B.; Gill, A. L.; Smith, S., A general approach to galanthamine ring system. *Tetrahedron*

Lett **2001**, *42*, 2209-2011.

222. Bell, R.; Beswick, P. J.; Gosmini, R. L. M.; Hamlett, C. C. F.; King, N. P.; Patel, V. K., Phenylalkanoic acid and phenyloxyalkanoic acid derivatives as hppar activators. *PCT Int Appl* 2004000315 **2003**.

223. Beswick, P. J.; Hamlett, C. C. F.; Patel, V. K.; Sierra, M. L.; Ramsden, N. G., Furan and thiophene derivatives that activate human peroxisome proliferator activated receptors. *PCT Int Appl* 2002092590 **2002**.

224. Wuensch, E., Synthese des vermuteten Nervenwachstumsfaktor-Aktivzentrums. *Monatsh Chem* **1985**, *116*, 505-524.

225. Bose, A. K.; Manhasd, M. S.; Saha, P.; Hedge, V. R., Stereospecific cyclization of β -hydroxy aryl amides to β -lactams. *Can J Chem* **1984**, *62*, 2498-2505.

226. Fletcher, S.; Cummings, C. G.; Rivas, K.; Katt, W. P.; Horney, C.; Buckner, F. S.; Chakrabarti, D.; Sebti, S. M.; Gelb, M. H.; Van Voorhis, W. C.; Hamilton, A. D., Potent, Plasmodium-selective farnesyltransferase inhibitors that arrest the growth of malaria parasites: structure-activity relationships of ethylenediamine-analogue scaffolds and homology model validation. *J Med Chem* **2008**, *51* (17), 5176-97.

227. Takacs, J. M.; Xu, Z.; Jiang, X. T.; Leonov, A. P.; Theriot, G. C., Carbon nucleophiles in the Mitsunobu reaction. Mono- and dialkylation of bis(2,2,2-trifluoroethyl) malonates. *Org Lett* **2002**, *4* (22), 3843-5.

228. Haynes, W. M., Ed, CRC Press: Boca Raton, FL. *CRC Handbook of Chemistry and Physics* **2014-2015**, *95th ed*.

229. Mederski, W. W.; Osswald, M.; Dorsch, D.; Christadler, M.; Schmitges, C. J.; Wilm, C., Benzofuro[3,2-b]pyridines as mixed ET(A)/ET(B) and selective ET(B) endothelin receptor antagonists. *Bioorg Med Chem Lett* **1999**, *9* (4), 619-22.

230. Radl, S.; Konvicka, P.; Vachal, P., A new approach to the synthesis of benzofuro[3,2-b]quinolines, benzothieno[3,2-b]quinolines and indolo[3,2-b]quinolines. *J Heterocycl Chem* **2000**, *37*, 855-862.

231. Viti, G.; Giannotti, D.; Nannicini, R.; Ricci, R.; Pestellini, V., Synthesis of new arylbenzofurodiazepin-6-ones. *J Heterocycl Chem* **1990**, *27*, 1369-1375.

232. Taylor, E. C.; Pont, J. L.; Warner, J. C., Heterodienophilic intramolecular diels-alder reactions of 1,2,4 triazines. : Synthesis of novel polycyclic condensed pyrazines and lumazines. *Tetrahedron* **1987**, *43*, 5159-5168.

233. von Braun, J.; Manz, G., Fluoranthen und seine Derivate. III. Mitteilung. *Justus Liebigs Ann Chem* **1931**, *488*, 111-126.

234. Aspinall, H. C.; Beckingham, O.; Farrar, M. D.; Greeves, N.; Thomas, C. D., A

- general and convenient route to oxazolyl ligands. *Tetrahedron Lett* **2011**, *52*, 5120-5123.
235. Chakraborti, A. K.; Kaur, G., One-pot synthesis of nitriles from aldehydes under microwave irradiation: influence of the medium and mode of microwave irradiation on product formation. *Tetrahedron* **1999**, *55*, 13265-13268.
236. Supsana, P.; Liaskopoulos, T.; Tsoungas, P. G.; Varvounis, G., DMF-Catalysed Thermal Dehydration of Aldoximes: A Convenient Access to Functionalized Aliphatic and Aromatic Nitriles. *Synlett* **2007**, *17*, 2671-2674.
237. Tamilselvan, T.; Basavaraju, Y. B.; Sampathkumar, E.; Murugesan, R., Cobalt(II) catalyzed dehydration of aldoximes: A highly efficient practical procedure for the synthesis of nitriles. *Catal Commun* **2009**, *10*, 716-719.
238. Ghosh, P.; Subba, R., FeCl₃ mediated one-pot route to nitriles. *Tetrahedron Lett* **2013**, *54*, 4885-4887.
239. Poissonnet, G., A Simple and Convenient Synthesis of 1,2-Benzoxazoles Via Intramolecular Mitsunobu Reaction from Salicylaldoximes and Orthohydroxyarylketoimes. *Synth Commun* **1997**, *27*, 3839-3846.
240. Anwar, H. F.; Hansen, T. V., A one-pot synthesis of substituted salicylnitriles. *Tetrahedron Lett* **2008**, *49*, 4443-4445.
241. Chen, L.; Fletcher, S., O-Alkylation of 3-hydroxyisoxazoles predominates under Mitsunobu conditions. *Tetrahedron Lett* **2014**, *55* (10), 1693-1696.
242. Casey, M. L.; Kemp, D. S.; Paul, K. G.; Cox, D. D., Physical organic chemistry of benzisoxazoles. I. Mechanism of the base-catalyzed decomposition of benzisoxazoles. *J Org Chem* **1973**, *38*, 2294-2301.
243. Kemp, D. S.; Cox, D. D.; Paul, K. G., Physical organic chemistry of benzisoxazoles. IV. Origins and catalytic nature of the solvent rate acceleration for the decarboxylation of 3-carboxybenzisoxazoles. *J Am Chem Soc* **1975**, *97*, 7312-7318.
244. Owston, N. A.; Parker, A. J.; Williams, J. M. J., Iridium-Catalyzed Conversion of Alcohols into Amides via Oximes. *Org Lett* **2007**, *9*, 73-75.
245. Wood, P. A.; Forgan, R. S.; Henderson, D.; Parsons, S.; Pidcock, E.; Tasker, P. A.; Warren, J. E., Effect of pressure on the crystal structure of salicylaldoxime-I, and the structure of salicylaldoxime-II at 5.93 GPa. *Acta Crystallogr Sect B* **2006**, *62*, 1099-1111.
246. Lanning, M. E.; Fletcher, S., Azodicarbonyl dimorpholide (ADDM): an effective, versatile, and water-soluble Mitsunobu reagent. *Tetrahedron Lett* **2013**, *54* (35), 4624-4628.
247. Hagiya, K.; Muramoto, N.; Misaki, T.; Sugimura, T., DMEAD: a new dialkyl azodicarboxylate for the Mitsunobu reaction. *Tetrahedron* **2009**, *65*, 6109-6114.

248. Bonomi, P.; Servant, A.; Resmini, M., Modulation of imprinting efficiency in nanogels with catalytic activity in the Kemp elimination. *J Mol Recognit* **2012**, *25*, 352-360.
249. Stokker, G., Preparation of 1,2-benzisoxazoles from salicylaldoximes via trichloroacetyl isocyanate. *J Org Chem* **1983**, *48*, 2613-2615.
250. Aldred, R.; Johnston, R.; Levin, D.; Neilan, J., Magnesium-mediated ortho-specific formylation and formaldoximation of phenols. *J Chem Soc, Perkin Trans* **1994**, *1*, 1823-1831.
251. Gigant, N.; Claveau, E.; Bouyssou, P.; Gillaizeau, I., Diversity-Oriented Synthesis of Polycyclic Diazinic Scaffolds. *Org Lett* **2012**, *14*, 844-847.
252. Forgan, R. S.; Roach, B. D.; Wood, P. A.; White, F. J.; Campbell, J.; Henderson, D. K.; Kamenetzky, E.; McAllister, F. E.; Parsons, S.; Pidcock, E.; Richardson, P.; Swart, R. M.; Tasker, P. A., Using the outer coordination sphere to tune the strength of metal extractants. *InorgChem* **2011**, *50* (10), 4515-22.
253. Guo, Z.; Li, L.; Liu, G.; Dong, J., 1-(Hydroxy-imino-meth-yl)-2-naphthol. *Acta Crystallogr Sect E Struct Rep Online* **2008**, *64* (Pt 3), o568.
254. Shinoda, J., The constitution of gentisin. *J Chem Soc* **1927**, 1983-1985.
255. Madsen, P.; Ling, A.; Plewe, M.; Sams, C. K.; Knudsen, L. B.; Sidelmann, U. G.; Ynddal, L.; Brand, C. L.; Andersen, B.; Murphy, D.; Teng, M.; Truesdale, L.; Kiel, D.; May, J.; Kuki, A.; Shi, S.; Johnson, M. D.; Teston, K. A.; Feng, J.; Lakis, J.; Anderes, K.; Gregor, V.; Lau, J., Optimization of alkylidene hydrazide based human glucagon receptor antagonists. Discovery of the highly potent and orally available 3-cyano-4-hydroxybenzoic acid [1-(2,3,5,6-tetramethylbenzyl)-1H-indol-4-ylmethylene]hydrazide. *J Med Chem* **2002**, *45* (26), 5755-75.
256. Collin, M. J.; Hatton, P. M.; Sternhell, S., An N.M.R. investigation of ground state polarisation of some substituted aromatic systems. *Aust J Chem* **1992**, *45*, 1119-1134.
257. Magano, J.; Chen, M. H.; Clark, J. D.; Nussbaumer, T., 2-(Diethylamino)ethanethiol, a new reagent for the odorless deprotection of aromatic methyl ethers. *J Org Chem* **2006**, *71* (18), 7103-5.
258. Minutolo, F.; Bellini, R.; Bertini, S.; Carboni, I.; Lapucci, A.; Pistolesi, L.; Prota, G.; Rapposelli, S.; Solati, F.; Tuccinardi, T.; Martinelli, A.; Stossi, F.; Carlson, K. E.; Katzenellenbogen, B. S.; Katzenellenbogen, J. A.; Macchia, M., Monoaryl-substituted salicylaldoximes as ligands for estrogen receptor beta. *J Med Chem* **2008**, *51* (5), 1344-51.
259. Rega, M. F.; Wu, B.; Wei, J.; Zhang, Z.; Cellitti, J. F.; Pellecchia, M., SAR by interligand nuclear overhauser effects (ILOEs) based discovery of acylsulfonamide compounds active against Bcl-x(L) and Mcl-1. *J Med Chem* **2011**, *54* (17), 6000-13.

260. Lipinski, C. A.; Lombardo, F.; Dominy, B. W.; Feeny, P. J., Experimental and computational approaches to estimate solubility and permeability in drug discovery and development settings. *Adv Drug Deliv Rev* **1997**, *23*, 3-25.